A study of the mechanisms of milling-induced enhancement of solubility and dissolution rate of poorly soluble drugs

Amjad Hussain

Leicester School of Pharmacy, De Montfort University

February 2015

PhD Thesis

In partial fulfilment of the requirements for the degree of

Doctor of Philosophy

Submitted to

De Montfort University

Declaration

I, Amjad Hussain, confirm that the content presented in this thesis is of my own work. I confirm that the information derived from other sources has been indicated accordingly in this thesis.

Abstract

Milling and co-milling are well known techniques that have potential to enhance the solubility and/or dissolution rate of poorly soluble drugs. There are broadly two aims for this project. The first was to develop an understanding of how individual and combination of techniques may be used to explore the impact of milling on particle characteristics (including phase changes, fractures and change in particle size) as a function of milling time/speed, for a range of single powder materials. Anhydrous (lactose, sucrose), monohydrate (lactose) and dihydrate (trehalose) excipients and a poorly soluble drug (ibuprofen), were chosen as model substrates. Each material was micronized by ball-milling (for various time durations and milling speeds) and then characterized by a range of techniques, specifically, SEM, DSC, TGA, THz and dielectric spectroscopy. The second aim of the project was to investigate the impact of milling and co-milling on the solubility and dissolution rate of ibuprofen after co-milling with a variety of excipients (polymer and surfactants).

The principle findings of this programme of work can be summarized as follows: i) ball milling of lactose monohydrate produces nano-structured systems with a mixture of damaged crystals and amorphous phase, that can be characterised by dielectric relaxation spectroscopy (DRS), ii) THz spectroscopy provides estimates for residual crystallinity in lactose monohydrate that were much lower than the estimates from the thermal techniques. Such estimates of residual crystallinity are considered to be more reliable given the fact that the spectroscopic measurement characterizes the material in its native state, whereas thermal techniques require a heating process, which tend to induce de-vitrification and mutarotation of lactose. In case of anhydrous materials, while there was agreement between thermal and THz techniques at long milling times, it was shown that the THz technique was susceptible to moisture absorption and crystallization at short milling times, iii) In the molecular dynamics of milled sugars studied by DRS, the structural relaxation is not visible in the vicinity of glass transition, however the secondary relaxation (β) process is equally capable and provided molecular dynamics in term of activation energy changes. The activation energies of beta process of both lactose and sucrose are least affected by milling time, but the higher activation energies for sucrose as compared with lactose show that sucrose has lower propensity to re-crystallize than lactose during post milling storage, iv) Ibuprofen can be assayed by UV-method in the presence of interfering (in absorption) substance by applying multivariate method involving the calculation of concentration factors and v) Co-milling with soluplus has increased the in the solubility of ibuprofen by ~20% and dissolution rate ~50% in 30 min, while these values are ~5% and 30%, respectively in case of co-milling with HPMC.

Table of Contents

List of Figures

List of Tables

List of Abbreviations

APIs	Active pharmaceutical ingredients
BCS	Biopharmaceutics classification system
USP	United states pharmacopoeia
B.P	British pharmacopoeia
EP	European pharmacopeia
HLB	Hydrophilic lipophilic balance
T_g	Glass transition temperature
DSC	Differential Scanning Calorimetry
TGA	Thermogravimetric analysis
HPLC	High performance liquid chromatography
THz	Terahertz Spectroscopy
THz-TDS	Terahertz time domain spectroscopy
TPS	Terahertz Pulsed Spectroscopy
DVS	Dynamic Vapour Sorption
NIR	Near Infrared
PXRD	Powdered X-ray Diffraction
BDS	Broadband Dielectric Spectroscopy
DRS	Dielectric Relaxation Spectroscopy
PLS	Partial Least Square
SEM	Scanning Electron Microscopy
BET	Brunaer Emmet Teller
MT-DSC	Modulated Temperature Differential Scanning Calorimetry
IGC	Inverse Gas Chromatography
PSD	Particle size distribution
LMH	Lactose monohydrate (alpha)
β-LA	Anhydrous lactose (beta)
PEG	Polyethylene glycol

CMC	Critical Micellisation concentration
DE	Dissolution efficiency
MDT	Mean Dissolution Time
Q30min	Percentage drug released in 30min of dissolution
MCC	Microcrystalline Cellulose
HPMC	Hydroxy-propyl methyl cellulose
PVP	Polyvinyl pyrrolidone
PDI	Dry powder inhalers
nm	Nanometre
mm	millimetre
µm	micrometre
fs	Femtosecond
τ (tau)	Relaxation time
E_a	Activation energy

Acknowledgements

All praises to Almighty Allah, the most beneficent, the most merciful, who bestowed me with all best abilities to complete this thesis and all respects are for His Holy Prophet Hazrat Muhammad (Peace be upon him) for enlightening my conscious with the essence of faith in Allah.

Foremost, I would like to express my sincere gratitude to my supervisor, Dr. Geoff Smith. His passion on research, motivation, enthusiasm and broad insight inspired me. His guidance and motivation were remained available for me in all the time of research and writing for this thesis. As a result, my research was smooth and gratifying for me. I could not have imagined having a better advisor and mentors for my PhD study and afterward.

I would extend a special thanks to my co-supervisor, Dr Irina Ermolina, local supervisor, Dr. Nadeem Irfan Bukhari and technical advisor of my PhD, Dr. Karrar A.Khan for their continuous support of my PhD research. I also acknowledge their patience, motivation, enthusiasm, and immense knowledge. Their guidance helped me in all the time of research and writing of this thesis. I also thank Dr. Mobashar Ahmed Butt, Dean and Principal University College of Pharmacy and Dr. Khalid Hussain for their encouragement and guidance.

I offer my sincere thanks to Mr. Eugene Polygalov, Senior Research Fellow in the Pharmaceutical Technologies group at De Montfort University, and Nicholas Pedge, Associate Principal Scientist, AstraZeneca, Macclesfield, UK for their valuable discussion on dielectric data analysis and chemometric analysis of the THz result. I am also thankful to Surface Measurement Systems Ltd., London, UK for DVS and IGC measurements, AstraZeneca Macclesfield, UK for particle size measurement, University of Nottingham, UK for BET measurements and BASF, UK for providing Soluplus and Lutrol for this study.

I thank Dr Richard Webster and his technical team (Angela and Ian), Zahoor-ul Haq and his team (Nasmin, Rachel, Unmesh, Blenda) for their generous support during my experimental work at DMU. Special thanks to Steve for his quick responses for filling the nitrogen cylinders. Also the support of laboratory staff from University College of Pharmacy, University of the Punjab, Pakistan, Shahzad, Abrar, Javaid, Khalid and Zahid during my research is highly appreciated.

I thank my fellow lab mates: Alex, Joseph, Kazem, Amee, Ning, Shi, and Yan for the stimulating discussions, motivating and helping gestures to meet deadlines of my research work. My gratitude for my friends Abid, Ali, Zahid and Kashif for making me feel UK as my home town and Tayyab, Nasir, and Ejaz for their rejoicing and caring company. A special thanks for my best friend Muhammad Sohail Arshad and his family for all support and encouragements during my PhD.

My deepest gratitude goes to my family members especially my parents for their love and support throughout my life. I would also extend thanks to my siblings, my spouse, Sadia and daughters, Elaaf and Azwa for their prayers and sacrifices during this work which kept me motivated to undertake my research and for their patient to wait for the completion of my PhD.

Last, but not the least, I am indebted to University of the Punjab, Lahore for grant of scholarship for my research work.

Amjad Hussain

Publications/Conference Posters

Publications

1. "Quantification of Residual Crystallinity of Ball Milled, Commercially Available, Anhydrous β-lactose by Differential Scanning Calorimetry and Terahertz Spectroscopy" Journal of Thermal Analysis and Calorimetry **(doi.org/10.1007/s10973-015-4469-4).**

2. "Quantification of Residual Crystallinity in Ball Milled Commercially Sourced Lactose Monohydrate by Thermo-analytical Techniques and Terahertz Spectroscopy" European Journal of Pharmaceutics and Biopharmaceutics **(doi.org/10.1016/j.ejpb.2015.02.026)**.

3. "Study of Molecular Dynamics of Amorphous Phase in Milled Anhydrous Sugars (Lactose and Sucrose) by Dielectric Relaxation Spectroscopy" Molecular Pharmaceutics (near submission).

4. "Study of milling and co-milling: Techniques for the improvement of solubility and dissolution rate for poor soluble drug – Ibuprofen" European Journal of Pharmaceutical Sciences (near submission).

Conference Posters (attached as Appendices X - XIV)

1. "Surface percolation of protons a probe for the creation of crystal defects in lactose monohydrate following short milling times" APS UK PharmSci 2012, the Science of Medicines, East Midland Conference Centre, Nottingham UK, 12 - 14 September 2012. **This poster was also selected for Podium Presentation**

2. "A study of the amorphization of lactose monohydrate following extended milling times Poster Presentation". APS UK PharmSci 2012, the Science of Medicines, East Midland Conference Centre, Nottingham UK, 12 - 14 September 2012.

3. "Milling and Co-milling with various excipients for the improvement of intrinsic dissolution rate of Ibuprofen". APS UK PharmSci 2013, the Science of Medicines, Heriot Watt University, Edinburgh Scotland UK, 1 - 3 September 2013.

4. "Quantification of Residual Crystallinity of Ball Milled Anhydrous lactose using DSC and Terahertz Spectroscopy". 11th European Symposium of Thermal Analysis and Calorimetry, Dipoli Congress Centre, Espoo Finland 17 - 21 August 2014.

5. "Study of Changes in Crystallinity of Ball Milled Mefenamic Acid using Terahertz Pulsed Spectroscopy". APS UK PharmSci 2013, the Science of Medicines, Weston Auditorium Hertfordshire University, Hatfield UK, 8 - 10 September 2014.

1 Introduction

1.1 The Issues Related with Poor Solubility of New Drugs

In recent years, the majority of newly discovered active pharmaceutical ingredients (APIs) have poor aqueous solubility owing to their lipophilic nature (Venkatramana M.Rao, 2009). Approximately 40% of the marketed oral immediate-release drugs belong to the class that are practically insoluble (Lipinski et al., 2001). Many of the APIs even do not enter into the clinical development phase because of their poor aqueous solubility which may be compensated by adding high doses in the formulations which in turn leads to non-reliable efficacy, poor stability, higher side effects and increased cost (Koltzenburg, 2011).

The aqueous solubility of a drug is one of the critical factors that influences the extent of drug absorption after administration and is directly related to its bioavailability. The absorption of drug across the membrane occurs by the way of passive or active diffusion or by the way of facilitated transport (Ganong and Barrett, 2005). For absorption to take place by passive transport (the major route of absorption), the drug needs to be in solution form at the absorption site from where the diffusion of drug molecules takes place down a concentration gradient. The trans-membrane diffusion of a drug substance can be described by Fick's law given as Equation 1.1.

$$\frac{dc}{dt} = \frac{J}{(C_s - C_t)} \qquad \textbf{Equation 1.1}$$

where 'dc/dt' is the rate of diffusion, 'J' is the unidirectional flux and 'C_s-C_t' is the difference in concentration from the mucosal to the serosal side of the intestinal epithelium.

Classification of drugs based on their aqueous solubility: Biopharmaceutics Classification System (BCS) is a system according to which the APIs are classified into four categories based on their aqueous solubility and intestinal permeability. According to this system; Class I contains drugs with high solubility and high permeability, Class II, includes the drugs with low solubility and high permeability, Class III, the drugs exhibiting high solubility and low permeability and Class IV, the drugs showing low solubility and low permeability (Amidon et al., 1995). The Class II drugs are approximately 70% of all newly discovered drugs; therefore these are the matter of special interest to the formulation scientists to develop strategies for the improvement of their aqueous solubility.

1.2 The Solubility Phenomenon/The Mechanism of Solution formation

When a crystalline solid (solute) is placed in the solvent, the solute molecules break away from the surface and enter into the cavities formed within the solvent molecules (Figure 1.1). This mixing is dependent on the relative affinities of solute and solvent molecules for themselves and with each other, and is affected by the temperature and pH of the solvent medium. The rate at which these solute molecules enter the bulk of the solvent is higher at the start of the process but at a certain point this becomes equal to the rate of re-deposition (*i.e.* a dynamic equilibrium is established). The concentration of solute in the solvent at dynamic equilibrium is known as the solubility.

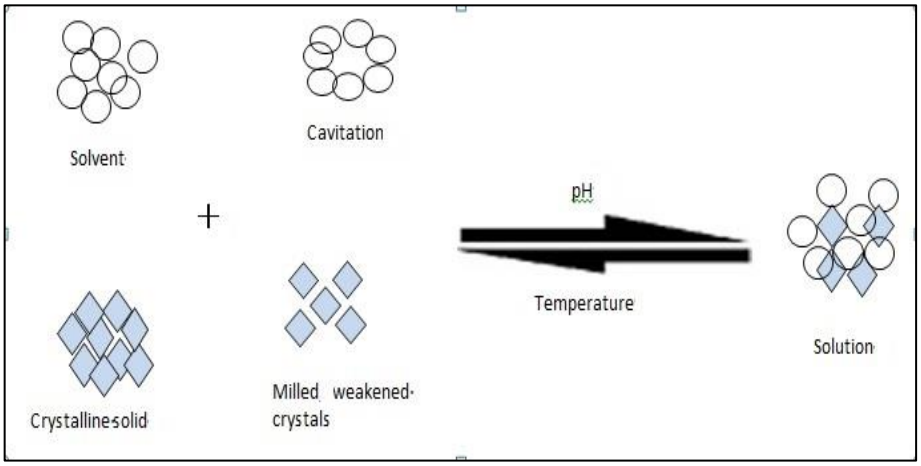

Figure 1.1: Diagrammatic representation of the mechanism of solution formation of a crystalline solid in the aqueous medium, adopted from (Qiu et al., 2009).

Thus, the solubility is a thermodynamic constant which depends on the energetics of the crystal lattice (*i.e.* the bonding energies which define the melting point) and the balance between solute-solute and solute-solvent (solvation) interactions in the solution state. The solute solvent interactions may be changed through the cohesive and adhesive forces of the solvent. Therefore, the solubility is the intrinsic property of the material and is not affected until the properties of material (polymorphic transformation, salt formation and amorphization) or the solvent properties (pH, co-solvency, addition of surfactant) are changed. The terms solubility enhancement anywhere used in literature is therefore a misnomer in our opinion as there is only an apparent change in the equilibrium solubility, once the solution reaches the equilibrium it cannot take any more solute.

In contrast, the rate at which the solute dissolves *i.e.* dissolution rate is a kinetic process, which is influenced by the features of the material such as the particle size distribution

(surface to volume ratio), surface tension (which influences the wettability of the surface) and the equilibrium thermodynamic solubility. It is important to note that in the case of an amorphous solid, it is possible to supersaturate the solution (*i.e.* exceed the thermodynamic equilibrium solubility limit) for a short time until the system has time for equilibrium to be restored (and the drug precipitates from solution).

The solubility is usually expressed in the concentration units such as percentage on weight or volume basis, mole fraction, molarity, molality, parts. According to USP the chemical substances have been classified into seven categories based on their aqueous solubility profiles as described in Table 1.1.

Table 1.1: Categories of drugs based on USP solubility definition (Stegemann et al., 2007)

	Parts of Solvent Required for 1 Part of Solute	Solubility range (mg ml^{-1})	Solubility assigned (mg ml^{-1})
Very soluble	Less than 1	>1000	1000
Freely soluble	From 1 to 10	100-1000	100
Soluble	From 10 to 30	33-100	33
Sparingly soluble	From 30 to 100	10-33	10
Slightly soluble	From 100 to 1,000	1-10	1
Very slightly soluble	From 1,000 to 10,000	0.1-1	0.1
Practically insoluble, or Insoluble	Greater than or equal to 10,000	<0.1	0.01

1.2.1 Thermodynamics of Solution Formation

The overall tendency of the solute molecules to break away from the solid and to exist instead in the solution state can be explained in terms of free energy changes. In part, the free energy change on dissolving a crystalline substance is related to the change in the overall enthalpy that arises from the net formation and breaking of individual bonds of the solute and solvent and in part from the net entropy change that occurs when an ordered crystalline solid is disrupted and the solute is solvated (Qiu et al., 2009).

Some of these terms used to describe the thermodynamics of solution are now described in detail here.

The **Enthalpy (ΔH)** of a pure component is the energy of a system at constant pressure while the enthalpy of solution of two components (the solute and solvent) is the difference between the sum of enthalpies of solute, solvent and of the mixture and can be described by Equation 1.2.

$$\Delta \mathbf{H_{solution}} = \Delta \mathbf{H_{mixture}} - (\Delta \mathbf{H_{solute}} + \Delta \mathbf{H_{solvent}}) \qquad \textbf{Equation 1.2}$$

where ΔH represents the enthalpies of solute, solvent and their mixture. The solution formation is favoured if $\Delta H_{solution}$ is negative, which is known as the excess enthalpy and is liberated as heat on mixing the two components (*i.e.* the process is exothermic).

The **Entropy (S)** of a system is the measure of randomness/disorder of its components. The entropy of a mixture depends on the number of ways (the degrees of freedom) in which the solute and solvent molecules can exist as pure forms and in the mixture. This can be described by Equation 1.3

$$\Delta \mathbf{S} = \mathbf{R} \ln \left[\frac{\Omega_{\mathbf{solution}}}{\Omega_{\mathbf{solute}} + \Omega_{\mathbf{solvent}}} \right] \qquad \textbf{Equation 1.3}$$

where 'Ω' represents the number of ways a molecule is present itself in the system. Generally $\Omega_{solution}$ is always greater than Ω_{solute}+$\Omega_{solvent}$, as the molecules have more freedom to move in solvent and as a consequence 'ΔS' is generally positive (*i.e.* there is increased disorder in the mixture compared to the disorder within the individual pure components). Therefore, favorable processes have a decrease in enthalpy (–ΔH) and/or an increase in entropy (+*ΔS*) and vice versa for unfavorable process

Free energy (ΔG) of the solution combines the effects of enthalpy (ΔH) and entropy (ΔS) and can be described by the Gibb's equation (Equation 1.4).

$$\Delta \mathbf{G} = \Delta \mathbf{H} - \mathbf{T}.\Delta \mathbf{S} \qquad \textbf{Equation 1.4}$$

where 'T' is the temperature measured on the Kelvin scale. Thus, the solution formation will be favourable only when the free energy is negative. Often there are the activation energy barriers to overcome before 'a process' may occur. The activation energy barrier in the case of the dissolution process is the energy required to disrupt (melt) the crystalline material. Once 'melted' then the interaction with the solvent may occur, which forms new bonds and releases energy. As described earlier, the net enthalpy change is a function of the energy required to disrupt the crystal (the molar heat of fusion) and the energy release when the solute interacts with the solvent (*i.e.* the enthalpy of solvation). Again, as intimated earlier, these enthalpy terms should not be considered in isolation of the impact of the changes in entropy that occur when an ordered solid is disrupted and the solute is free to mix with the solvent molecules. The transition from the ordered state to the disordered (dissolved state) inevitably results in a dramatic increase in the number of microstates and hence the entropy

of the system. Whilst this is favourable and one of the driving forces of the process, there is also a contribution from the ordering of the solvent around the solute (the process of solvation) which reduces the number of possible microstates (and hence reduces the entropy). On balance it is the sum of all such contributions to both the enthalpy and the entropy which defines whether the net free energy change is positive or negative.

1.2.2 Relationship of Solubility and Crystallinity of the Solids

The solubility of the crystalline solids is described by Van't Hoff equation (Equation 1.5).

$$-\mathbf{logX} = \frac{\mathbf{\Delta H_m}}{\mathbf{2.303R}}\left[\frac{\mathbf{T_0 - T}}{\mathbf{T\ T_0}}\right] + \mathbf{log\gamma} \qquad \textbf{Equation 1.5}$$

where, 'X' is the solubility of solute in mole fraction, 'ΔH_m' is the heat of melting, 'T_0' is the melting point of solute taken in degrees Kelvin, 'T' is the absolute temperature of the solution, and 'γ' is the activity coefficient which represents the intermolecular forces to be overcome to bring the solute in the solution. Stronger the solute-solute interaction, higher will be the value of 'γ'. Therefore the solubility is mainly affected by the crystallinity and temperature of the solvent. However there are many other factors including salinity, pH, dissolved organic matter and co-solvents that can also affect the solubility of a solid.

1.2.3 The Difference between Solubility and Dissolution

Where the solubility is an equilibrium phenomenon (as described in Section 1.2), the dissolution is a dynamic process and is measured as a rate. Dissolution can be thus defined as the rate at which the equilibrium between solute and solution is reached under the given conditions of temperature and pH.

1.3 Mechanism of Dissolution

The basic mechanism of the dissolution process is the convective diffusion with a simultaneous solvation process. When a drug is added in the dissolution medium, an aqueous boundary layer (ABL) is formed at solid-liquid interface (Figure 1.2), which is the rate limiting step for dissolution. The concentration of drug in this layer is equal to the solubility of the drug and the linear concentration gradient that is also equal to solubility divided by thickness of this layer (Avdeef et al., 2007). There are several physicochemical factors which control the dissolution rate of a drug and these can be described by the Noyes-Whitney equation (Equation 1.6).

$$\frac{dc}{dt} = \frac{AD}{h}(C_s - C_t) \qquad \text{Equation 1.6}$$

where 'dc/dt' is the rate at which a given substance dissolves in the medium, 'A' is the effective surface area of the substance available to dissolution medium, 'D' is the diffusion coefficient of the substance, 'C_s' is the solubility of the substance in the given dissolution medium, 'C_t' is the drug concentration in the medium at time 't' and 'h' represents the thickness of the ABL surrounding the surface of the dissolving substance. Therefore, increasing the surface area of particles can be a key for enhancing the dissolution rate of poorly soluble drugs.

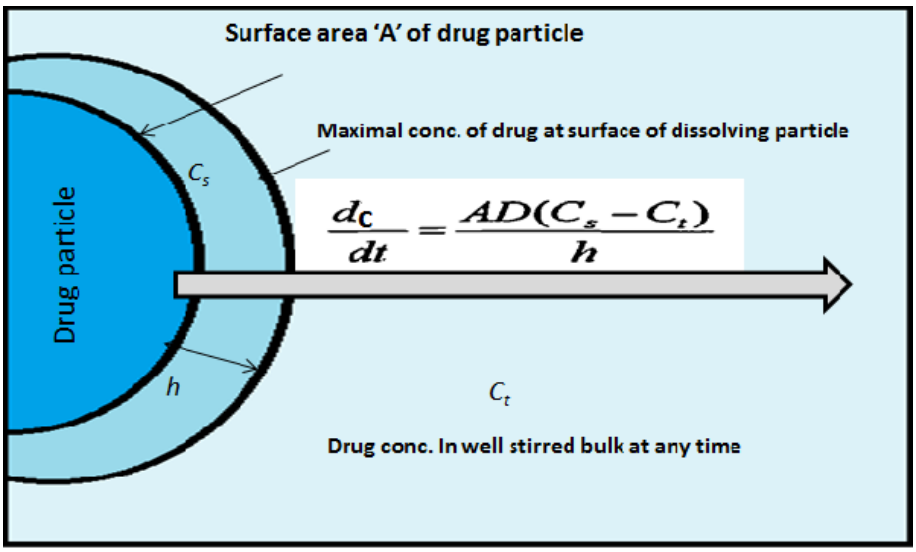

Figure 1.2: Diagrammatic representation of the dissolution process showing the Noyes Whitney equation and the movement of drug molecules from the surface of particle (boundary layer) into the bulk of solvent as indicated by the arrow head, adopted from (Avdeef et al., 2007).

1.4 Addressing the Problem of Poor Solubility

The development of new strategies to deal with the poor solubility of drugs is a challenge for formulation scientists as ~95% of the newly discovered drugs belong to BCS class II and IV (70% and 25% respectively). The techniques commonly employed for the improvement of solubility and/or dissolution rate of these drug categories are; salt formation (Tao et al., 2009), solid dispersion (Serajuddin†, 1999), polymorphism and co-crystals (Blagden et al., 2007), complex formation (Rawat and Jain, 2004), amorphization (Murdande et al., 2011), size reduction by milling (Kawabata et al., 2011) and co-milling (Bahl and Bogner, 2008, Vogt et al., 2008b). Among these methodologies, the process of milling is the more versatile method for the improvement of solubility and/or dissolution rate owing to its applications in size reduction, amorphization (based on the nature of material and time of milling), crystal

modification *i.e.* co-crystal formation (Vishweshwar et al., 2005) and preparation of solid dispersion by milling with other materials (Arnum, 2010, Barzegar-Jalali et al., 2010). Therefore, the milling can improve the solubility and/or dissolution rate of drugs by multiple mechanisms. It may also provide additional opportunity *e.g.* the incorporation of an excipient that helps in the stabilization of amorphous phase (Watanabe et al., 2002).

A literature summary of different techniques used for the improvement of solubility and/or dissolution rate has been given in Table 1.2 along with descriptions of the proposed mechanisms of such enhancement and advantages and disadvantages of each method.

Table 1.2: Summary of techniques used in literature for the enhancement of solubility and/or dissolution rate of poorly soluble drugs.

Technique	Mechanisms for the increase in dissolution and/or solubility	Advantages	Disadvantages
Co-solvency (Vemula et al., 2010)	combined solvent action of water and other miscible solvent	Simple and quick method	Toxicity of solvents. Precipitation/chemical stability
Liposome and Emulsions (Mohammed et al., 2004)	Solubilization within lipid membrane Emulsion droplets readily cross membrane	Improved tolerability	QC testing complicated Limited applications
Macro-emulsion (Humberstone and Charman, 1997)	Self-emulsifying drug delivery systems (SEDDS)	Easy to manufacture No dust formation	Drug loading is low Interaction with food in GIT Complicated filling in soft gels
Micro-emulsion (Krishnaiah, 2010)	Lipid base drug delivery system (LBDDS)	Easy to manufacture No interaction with food.	Poor tolerability (synthetic surfactants)
Solid dispersion (Biswal et al., 2008)	Amorphous drug is stabilized in hydrophilic polymer matrix	Potential to carry as final dosage form	Unsuitable for thermolabile compounds
Inclusion complex with Cyclodextrin (Baboota et al., 2005)	The exposed surface is hydrophilic while the interior lipophilic	Improved stability Excellent solubility	Pharmacokinetics of APIs altered Toxicity of cyclodextrins
Milling (Elamin et al., 1994)	Increased surface area Amorphous phase that has lower enthalpy	Simple and versatile Drug stabilization by excipients (co-milling)	Particle aggregation Stability problems due to amorphization
Co-crystals (Shiraki et al., 2008)	The lattice energy increase as the co-former makes the weak bond with drug	Easy to prepare Improved physical properties of API	Not applicable to all drugs Stability problem
Micelle formation (Kim et al., 2010)	Surfactant core is lipophilic while outer side is hydrophilic	Straightforward and scalable	QC testing complicated
Spray drying (Sahoo et al., 2011)	Partial amorphization during spray drying	Quick and Versatile method	Toxic solvents. Process is sophisticated and costly
Miscellaneous	Supercritical fluid process (Perrut et al., 2005), Liquisolid techniques (Javadzadeh et al., 2007), Microwave (Maurya et al., 2010), 3D Macro-porous Silica (Hu et al., 2011), Micro-porous silica (Mehanna et al., 2011), Porous starch (Wu et al., 2011), Precipitation (Zhang et al., 2009), pH Adjustment (Vemula et al., 2010)		

1.5 Milling of Solids – A Technique for Size Reduction

Size reduction by milling is often called as micronization due to the fact that this process is considered to generate the particles in the size range of a few microns or less. Invariably, the rationale for micronization is to increase the dissolution rate especially for the sparingly soluble drugs due to the significant increase in surface area (Mosharraf and Nyström, 1995). The aim of milling is to achieve the desired particle size without degrading the material and in the shortest time (Colombo et al., 2009). Furthermore, the particle size is also important as it controls the sedimentation and flocculation rates in suspensions (Chikhalia et al., 2006), demonstrates the therapeutic efficacy of dry powder inhalers (DPIs) (Pilcer and Amighi, 2010) and is responsible for the flowability and content uniformity in solid dosage forms (Mackin et al., 2002a).

1.5.1 Types of Milling

There are two major categories of milling based on the choice of milling medium, either liquid or air; *i.e.* wet milling and dry milling, respectively. In both of these methodologies, size reduction occurs by the collision of particles with each other and with the surfaces of milling chambers or balls. In wet milling the shearing of liquid and cavitation produced in the medium during milling provides an additional energy, therefore results in more effective size reduction, with the potential to produce particles in the nano-size range, as compared to the dry milling which usually produces micro-particles. Wet milling which involves, the milling of particles suspended in the liquid medium (slurry or dispersion depending on the amount of medium used) is advantageous for heat sensitive materials. However the development of static charge on the particles surface, interactions with the solvent and the dependence of the process on speed, density of slurry and temperature, make it a difficult process to control.

On the other hand, dry milling is a versatile technique that is commonly used in the processing of solid dosage forms. The disadvantages of dry milling includes; the powder build in the milling containers and the heat degradation of the sensitive materials (Fisher, 2007).

Among dry milling there are a variety of techniques available but the ball milling and air jet milling are the most commonly used in the pharmaceutical industry (Rasenack and Müller,

2004). Milling in an air jet mill has been reported to produce 1-5 µm particles and is usually employed for the production of powdered drugs for pulmonary delivery (Saleem and Smyth, 2010), while ball milling is probably the most aggressive size reduction technique, capable of creating even the sub-micron sized particles (Branham et al., 2012, Plakkot et al., 2011) and can be used for size reduction and amorphization.

There are two major types of ball mills; planetary (a multiple ball mill) and vibratory (usually a single ball mill). The planetary ball mill applies attrition/grinding force while the vibratory mill grinds the particles by high velocity impacts of ball against the walls of milling jar. Therefore, the planetary ball mill is used for size reduction (usually micron-sized particles) and mixing of materials (except when used for long milling times it can generate an amorphous phase). On the other hand the vibratory mill is usually employed for size reduction (nano-particles) and for smashing the surfaces/crystal lattice to create a totally disordered amorphous phase (Singh and Lillard Jr, 2009) . However, a careful control of size of balls, feed size, speed and milling time is required in order to get the desired output without destroying the API (Peltonen and Hirvonen, 2010).

1.5.2 Mechanism of Particle Breakage in Vibratory Ball Mill/ Energetics of Milling

During, milling in a vibratory ball mill, the high velocity collisions of the ball against the wall of the mill (Figure 1.3) provide impact, shear and attrition forces together that serve to reduce the particle size (Chen et al., 2004).

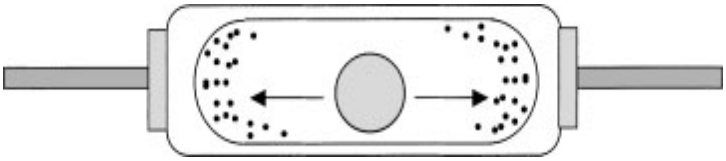

Figure 1.3: Cylinder of ball mill showing the 'to and fro' *i.e.* vibratory movement of the ball that impacts on the opposite walls to reduce the particle size, taken from (Chen et al., 2004).

According to the Griffith theory (Equation 1.7), solid particles have structural weaknesses (flaws) that may develop into cracks under applied stress (Parrott, 1987) and the size reduction of particles occurs through crack propagation.

$$\mathbf{T} = \sqrt{\frac{\mathbf{Y}.\in}{\mathbf{c}}} \qquad \textbf{Equation 1.7}$$

where ‘T’ is the tensile strength, ‘Y’ is young’s modulus, ‘∈’ is the surface energy and ‘c’ is critical crack length for the fracture. When the moving ball of the mill impacts the particle surface, it either fragments (if the scale length of crack exceeds of the critical length of fracture) or dissipates the absorbed energy to cause defects within the crystal lattice and thus increases the number and density of cracks.

The energy dissipated by the particles can be best illustrated by the stress-strain curve (Figure 1.5); which describes the impact of the stress applied to the particles on the resultant strain (*i.e.* displacement). Hooke’s law describes that, at low stress the strain increases proportionally to the applied stress (as depicted by the initial portion of the curve in Figure 1.4). As the stress is increased, the relationship between strain and stress becomes non-linear at a point, which is called ‘*yield point*’. This point is a measure of the resistance of a material to the permanent or plastic deformation. An increase in stress beyond this point results into a region of irreversible plastic deformation which eventually causes the fragmentation of the solid at fracture point (Ghadiri and Zhang, 2002).

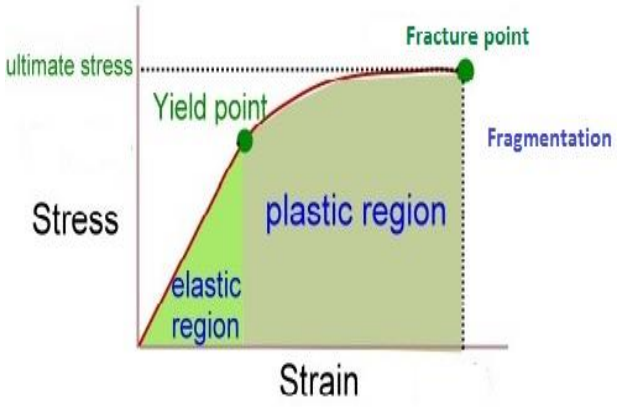

Figure 1.4: Stress-strain curve as taken from (Nordin and Frankel, 2001). The initial linear part of the curve represents the elastic region, followed by a non-linear plastic region and finally the fragmentation of the particles at fracture point.

If the process of milling is extended beyond few minutes, in addition to the above changes, the collisions of the balls with the walls of the mill can also increase the temperature (Chieng et al., 2006). This increased temperature may further contribute to the phase disruption of the crystal lattice and is partly responsible for the creation of amorphous domains.

1.5.3 Effect of Milling on the Solubility of Pharmaceuticals

The process of milling causes many changes in the crystalline solids. These changes range from size reduction, alteration of phase *e.g.* disorder in the crystal structure through the introduction of defects (thus increasing the surface area) and a complete modification of phase *i.e.* polymorphic transition and/or amorphization. Such changes can increase the transient (non-equilibrium) solubility (by lowering the melting point) and dissolution rate (by increasing surface area), and ultimately increase the bioavailability of a drug (Dudognon et al., 2006).

The increase in solubility on milling is not always linked with the lowering of melting point or increase in surface area; it has been shown in a milling study on griseofulvin that the solubility increases on milling even when the melting temperature or surface area of the particles remains unchanged. The reasons for this enhancement are; the increase in surface free energy and the reduction in the heat of solution that results from the disordering of the solid structure (Elamin et al., 1994). Another study involving a hydrophilic material has shown that the solubility (apparent) increases as the surface damage caused by milling increases. This is demonstrated in Figure 1.5 which shows that the amount of material needed to reach the saturation decreases as the surface damage increases (Mosharraf et al., 1999).

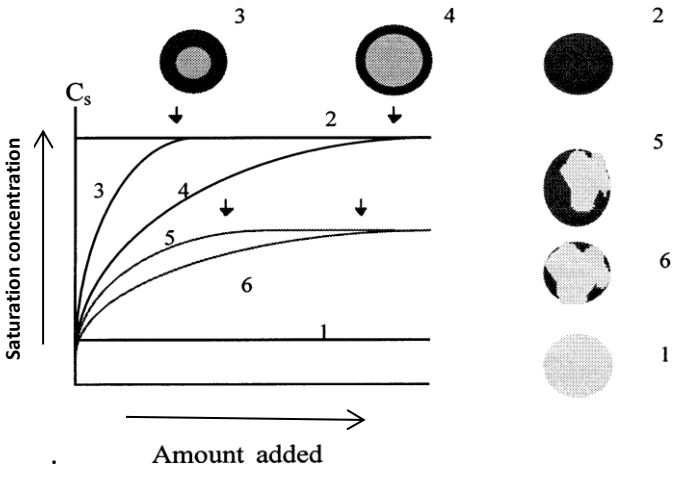

Figure 1.5: An illustration showing the amount of solute required to reach the saturation decrease as the surfaces are damaged from fully crystalline (1), partially damaged (3, 4, 5 and 6) to fully disordered (2), taken from (Mosharraf et al., 1999).

In case of hydrophobic material, wettability of particle surface by the solvent is also necessary to initiate the solubility process (Buckton et al., 1988). Therefore, there is a

requirement for the addition of excipient(s) during milling (*i.e.* co-milling) in order to improve the solubility of such materials.

1.5.4 Un-desired Effects of Milling

Despite certain applications, advantages and the favourable changes, the process of milling is not without disadvantages. The un-desirable effects of milling include:

i. The instability of the amorphous phase, which tend to de-vitrify over time (especially at higher temperature and humidity conditions).
ii. The development of charge on the surface of milled particles that leads to aggregation, which in turn results in an overall decrease in the specific surface area.
iii. Degradation of thermo-labile drugs by heat generated during the milling process.
iv. Polymorphic transformation that may affect the solubility or stability.

1.6 Co-milling – A Technique for Process Optimization

The term co-milling refers to the milling of a drug in the presence of excipient(s). It has been shown to be a simple, efficient and economical process that does not require any sophisticated equipment. It is also environment friendly as it does not involve the use of any organic solvent (Friedrich et al., 2005), as in the case of wet milling or solid dispersions (prepared by solvent evaporation method). Co-milling combines the advantages of particle size reduction and amorphization of milling with the additional benefits of improved solubilization/micellization provided by the co-milled excipient. Furthermore it can also overcome the disadvantages of milling *i.e.* i) minimize agglomeration by the surface coverage of charged particles, ii) stabilise the amorphous phase and iii) reduce the mechanical/thermal degradation of drugs by moderating the effect of heat (Lin et al., 2010) as demonstrated in Figure 1.6.

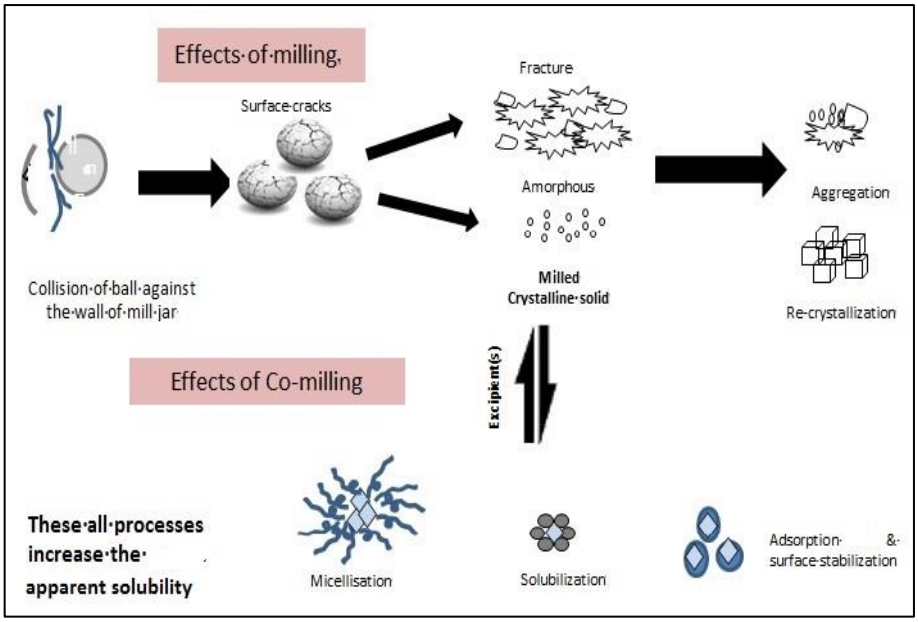

Figure 1.6: Graphical representation of the changes that occur on milling and co-milling of a solid and the effect of these on the solution kinetics. The added excipient in co-milling exerts its action by solubilization/micellization or the stabilization of the amorphous phase or by preventing the aggregation of particles, adopted from (Lin et al., 2010).

In literature, the technique of co-milling has been used for the enhancement of solubility and dissolution rate of poorly soluble drugs such as chordiazepoxide (Nokhodchi et al., 2007), indomethacin (Watanabe et al., 2003) , piroxicam (Al-Hamidi et al., 2012), nimodipine (Murali Mohan Babu et al., 2002) carbamazepine (Al-Hamidi et al., 2010), and gliclazide (Barzegar-Jalali et al., 2010). Co-milling has also been used for improving the processing properties of different drugs (Chattoraj et al., 2011, Shakhtshneider et al., 1996), and for the stabilization of amorphous powders, which are prone to heat degradation (Watanabe et al., 2003). A summary of the recent literature on co-milling describing the type of excipient, mill type and proposed mechanism for the improvement of solubility and dissolution rate, is given in Table 1.3.

Table 1.3: Summary of applications of co-milling given in literature for improving the solubility and dissolution rate of drugs.

Drug/Reference	Excipient used	Type of mill used	Proposed mechanism for increase in dissolution/solubility
Nimodipine (Murali Mohan Babu et al., 2002)	Gum Karaya	Ceramic mortar	Reduction in crystallinity of drug
Carbamazepine (Al-Hamidi et al., 2010)	Glucosamine	Planetary ball mill	Polymorphic transformation, Reduction in crystallinity, Effect of hydrophilic carrier, decrease in particle size
Piroxicam (Al-Hamidi et al., 2012)	Glucosamine	Planetary ball mill	Polymorphic transition
Fenofibrate (Vogt et al., 2008a)	PVP,LMH,SLS	Air jet mill	Facilitate de-aggregation, Increase dispersibility
Salbutamol sulphate (Balani et al., 2010b)	PVP	Planetary ball mill	Hydrogen bonding, Increased dispersibility, Amorphization and Stabilization of amorphous
Salbutamol sulphate (Balani et al., 2010a)	PVP, LMH, Mg. Stearate,	Planetary Ball mill	Amorphization, Stabilization of this amorphous
Accelofenac (Vadher et al., 2009)	Neusiline US2	Rolling jar mill	Increased Hydrogen bonding, Particle size reduction, Amorphization
Albendazole, Danzole, Felodipine, EMD (Vogt et al., 2008b)	LMH, Starch, PVP, HPMC	Air jet mill	Excipient and drug specific supersaturation(PVP, HPMC), No particle size reduction, No changes in crystallinity
Gliclazide (Barzegar-Jalali et al., 2010)	PVP, MCC	Vibration ball mill	Improved wettability, de-aggregation by the carriers, Particle size reduction, Decrease in crystallinity
Meloxicam (Kürti et al., 2011)	PVP,PEG	Planetary mono-mil	Particle size reduction (Nano-particles) Amorphization
Indomethacin (Bahl and Bogner, 2008)	Silicates	Rolling jar mill	The presence of silicic acid and ions (Mg2+ and Al3+) in dissolution media, Amorphization
Indomethacin (Watanabe et al., 2002)	SiO2, Talc, Mg. Hydroxide	Vibration ball mill	Amorphization Stabilization of amorphous phase
Pranlukast (Wongmekiat et al., 2003)	Cyclodextrin	Vibration ball mill	Generation of fine particles
Glybuzole (Otsuka et al., 1998)	Surfactant (SLS etc)	Planetary ball mill	Solubilization by the surfactant Amorphization
Nifedipine (Sugimoto et al., 1998)	PEG-HPMC	Vibratory ball mill	Enhanced wettability, particle size reduction
Raloxifen (Garg et al., 2009)	Plasodone, PVP	Ball mill	Surface erosion, Particle size reduction Reduction in crystallinity on co-milling
Raloxifene (Jagadish et al., 2010)	Super-disintegrants	Planetary ball mill	Reduction in crystallinity, Reduction in particle size
Gabapentine (Lin et al., 2010)	Mannitol, Starch, Magnesium stearate	Oscillatory ball mill	Stabilization of polymorphs
Oxaprozin (Maestrelli et al., 2011)	β-cyclodextrin, chitosan	Ball mill	Powerful solid-state interactions
Ciprofloxacin (Xianwen Li, 2007)	HPMC	Mortar & Pestle	Hydrogen bonding
Naproxen–Cimetidine (Morten Allesø,2009)	-	Oscillatory ball mill	Solid-state interaction between the imidazole ring of cimetidine and the carboxylic acid moiety of naproxen
Budesonide (Dudognon et al., 2006)	Excipient having high Tg- Alpha lactose	**B**all mill	Formation of glass solution that increase Tg of the blend and so stabilize the vitreous phase.
Ibuprofen (Mallick et al., 2008b)	Aluminium hydroxide	Ball mill	Solid state interaction with AlOH2
Ibuprofen (Han et al., 2011)	Hydrophilic nano-silica, PVP	Fluid energy mill (FEM)	Surface modification, de-aggregation Improved wettability, Increased surface area

1.7 Gap in the Knowledge/Opportunities for New Techniques

The generally accepted mechanisms responsible for the improvement of solubility and dissolution rate by milling and co-milling include:

i. Crystal damage and particle size reduction which increases the surface area and hence the dissolution rate.
ii. Conversion of the drug to its amorphous phase that has greater surface area and reduced energy for solution formation.
iii. Solubilization by surface active excipients which reduces the negative entropy change that is normally associated with attempts to dissolve hydrophobic drugs.
iv. Prevention of aggregation and improvement of dispersibility of the drug by the added excipient.
v. Improved wettability of drug by the wicking action provided by the added excipient.

Among these, the first two (*i.e.* size reduction and amorphization) are the effects of milling where as others are principally the effects of added excipient during co-milling. The improvement in solubility and dissolution occur largely as a consequence of the two factors; first, the significant increase in surface area that is usually linked with the reduction in particle size and second is the disorder in the crystal lattice (resulting in a partly or wholly amorphous phase) which requires less energy to disperse the solute into the solvent phase. However, much less is known about the contribution of the other physical characteristics of individual particles *e.g.* internal cracks/fissures developed on milling that may provide an enormous surface area for the penetration of a solvent during dissolution and may also compromise the stability of the material by enhancing moisture uptake during the post milling storage.

Nitrogen adsorption studies are usually employed for the measurement of specific surface areas of particles, including those cracks/defects that are either on or connected to the external faces of the particles (Westermarck et al., 1998). However, this technique cannot measure the internalized cracks of milled materials due to the inability of the probe (*i.e.* nitrogen gas) to penetrate the micro scale pores. Nor can this method be used for crystal hydrates given the fact that the evacuation of the sample chamber results in desorption of the water of crystallization and the creation of new surfaces that are then explored by the

BET gas probe. Such limitations in quantifying the specific surface area of the milled materials, warrants the need for some new techniques.

One novel element of this work (Chapter 2) is to explore the use of dielectric spectroscopy as a supplementary method for characterising the surface properties of the materials. Feldman's work on porous materials has shown that the features of the hydration surface of internal pores in term of micro-clusters of water may be estimated from dielectric relaxation spectroscopy (DRS) measurements of **percolation phenomenon** (Gutina et al., 2003). In percolation, the surface moisture provides the charge carriers (protons) to percolate over the surface of the solid to provide an assessment of the fractal dimension of the percolation pathways and the porosity of the solid (Feldman et al., 2006). These studies thus provide an opportunity for measuring milling-induced defects as the probe of the dielectric method (*i.e.* water/proton) is relatively small and can penetrate through these internalized surfaces.

Previous work at De Montfort University (Ermolina and Smith, 2011) on percolation phenomenon in lactose monohydrate and in the mixtures of crystalline material with amorphous freeze-dried lactose has shown that there are two dielectric processes that are broadly relevant to the interfacial properties of ball-milled particles; the first is the percolation of protons across hard surfaces of the original particles or the fragments of particles (that have simply fractured across fault lines within the particle) and the second is the classic dielectric relaxation of amorphous phase. In the case of the first process, it may be expected that the size reduction of a material on ball milling results in a reduction in the percolation path for proton diffusion (associated with decreased particle size) but that the associated creation of amorphous domains effectively increases the effective scale length for charge percolation owing to the propagation of the protons within the 'soft surfaces' of particles. In the case of the second process, the creation of amorphous surface domains, on otherwise crystalline particles, give rise to the classic dielectric relaxation of amorphous phase but modulated by the fact that the material is 'contained' or confined within a nano-scale surface volume.

The second novel aspect of this work is the application of dielectric spectroscopy for the characterization of properties of the amorphous phase that is generated on milling (This is also covered in Chapter 2). The characterization of this amorphous phase is necessary in

order to optimize its advantage (in the improvement of solubility and dissolution) and to understand the risk of its stability (as it has tendency to de-vitrify).

The third, novel aspect of this work involves the investigation of techniques for the **quantification** of crystallinity/amorphicity at various milling times and frequencies (Chapter 3). Given the importance of the amorphization phases to the ease by which the saturated solubility may be achieved then it is essential that techniques are available for the assessment of the extent of amorphization so that the pharmaceutical manufacturing process may be controlled. Ideally techniques should be available which are adaptable for in-line process measurements on the outflow from the mill so that adjustments may be made to the process in real time. THz spectroscopy, was shown to be such potential technique.

The quantification of crystallinity/amorphicity in milled materials is very challenging because of the presence of crystallite seeds for de-vitrification and the enormous surface area linked with the defected crystals or amorphous phase that readily adsorbs moisture from the environment and tends to de-vitrify in time. Another problem encountered during milling is the creation of moisture (internal/external), which then drives the de-vitrification of amorphous phase during post milling storage. The common techniques used for quantification of this amorphous content *i.e.* DSC, further accelerates the de-vitrification by heat during the analysis. There are few, if any techniques which can measure the native/inherent amorphous phase in the materials, which exists immediately post milling and least influenced by moisture/temperature induced de-vitrification.

The recent studies involving the use of Terahertz pulsed spectroscopy (TPS) in the crystallization phenomenon (Sibik et al., 2014, McIntosh et al., 2013) and quantification of crystallinity by of freeze-dried amino acids and sucrose by De Montfort University group (Darkwah et al., 2013, Ermolina et al., 2014) draw our attention to use this technique for the quantification of changes in crystallinity in milled materials. Although not explored in this thesis, the opportunity to use a spectroscopy such as terahertz for the in-line process monitoring is self-evident.

Once the amorphous content has been quantified, it is necessary to look at the effect of milling time and energy inputs on the **dynamics** of amorphous phase which will reflect the stability of this phase. This is very important step as the stability of a product during shelf life will depends on the behaviour of amorphous phase.

The fourth novel aspect of this work is to use dielectric spectroscopy for the first time in the assessment of the dynamics of the amorphous phase in the milled material (Chapter 4).

There are a range of techniques available for the analysis of molecular dynamics and thus stability of the amorphous phase. Parameters such as the structural relaxation time, enthalpy relaxation and/or fragility index (obtained from DSC or isothermal micro-calorimetry techniques) have been used to provide certain measures of molecular mobility, which have some relationship with the stability of the amorphous phase (Liu et al., 2002, Pokharkar et al., 2006, Graeser et al., 2009). More recently, studies by dielectric spectroscopy have shown that the structural relaxation (in terms of the characteristics of the α-relaxation) reflects a level of molecular mobility that appears to underpin the de-vitrification (and hence instability) of system containing amorphous phase (Kolodziejczyk et al., 2013, Rodrigues et al., 2013, Sailaja et al., 2013, Wojnarowska et al., 2013, Kothari et al., 2014).

In the final novel aspect of this work, the opportunity for using some new surfactants in **co-milling** with a poorly soluble drug, ibuprofen is explored with the aim of enhancing its solubility and dissolution rate in order to demonstrate the methodologies developed for the analysis of milled materials (Chapter 5).

1.8 Aim of this Work

The aim of this work is to develop the analytical methodologies to explain the physical and molecular mechanisms responsible for the milling induced improvement of solubility and/or dissolution rate of poorly soluble drugs, and the application of co-milling technique to sustain/overcome the effects of milling that contribute to the solubility and/or dissolution rate improvement.

1.9 Objectives

1. To appreciate, a theoretical background of the issue of poor solubility of drugs in formulation, milling induced changes affecting the solubility and dissolution rate of such drugs and how the co-milling can contribute to sustain these changes.
2. To develop a qualitative analytical methodology for studying the impact of milling on generation of internalized surfaces which contributes to the specific surface and facilitates the dissolution of milled particles. Particle characteristics (including phase

change, damage to crystal habit and change in size) as a function of milling time/energy input, would be determined with the routinely used techniques (for comparison) and relatively new techniques *i.e.* dielectric relaxation spectroscopy. This technique can measure the newly created hydration surfaces by the percolation of protons.

3. To develop analytical methodologies for quantitative estimation of the impact of milling on crystallinity. The changes in crystallinity of ball milled materials are estimated by; i) the changes in weight linked with desorption of the water of crystallization as estimated from TGA results of hydrated material, ii) changes in enthalpies of melting and crystallization from DSC data or iii) changes in the areas of the absorption peaks in THz spectra.
4. To develop analytical methodologies for studying the molecular dynamics of amorphous phase in milled pharmaceutical materials which might then provide an understanding of relative stability of the amorphous phase. The DSC profile of milled samples would reflect the changes in glass transition temperature, crystallization and melting enthalpies. In dielectric relaxation spectroscopy, the amorphous surface domains created, on otherwise crystalline particles, by milling can give rise to the classical dielectric relaxation of amorphous phase and can be described in term of secondary relaxation below glass transition temperature (T_g) and the structural relaxation above T_g.
5. To develop the method of analysis of a drug in the presence of excipients by Ultraviolet (UV) spectroscopy. The interference of excipient in the UV absorbance of drug (if any) would be determined and corrected or excluded.
6. To evaluate the effect of co-milling with selected excipient on the solubility and/or dissolution rate of poorly soluble drug. The drug and selected excipients would be milled together and the resultant mixture is analysed for solubility and dissolution rate.
7. To establish the mechanism of solubility and dissolution improvement keeping in views the effect of milling (analytical methodologies developed in first 3 sections) and the added excipient. The comparison of solubility and/or dissolution rate of milled drug, its physical and co-milled mixtures with that of un-milled drug would provide the information about the effect of milling the drug alone or with excipient(s).

1.10 Characteristics and Rationale for the Selection of Drug and Excipients

1.10.1 Ibuprofen

Ibuprofen, a non-steroidal anti-inflammatory drug is categorized in BCS Class II. This drug was selected as a model drug in the present study on the basis of its easy availability, simple and well established assay method (both spectrophotometric and HPLC) and less risks involved in its handling, etc.

Chemically ibuprofen is *2-(4-(2-methylpropyl) phenyl) propionic acid* (Figure 1.7a) that form dimer in the molecular packing (Figure 1.7b).

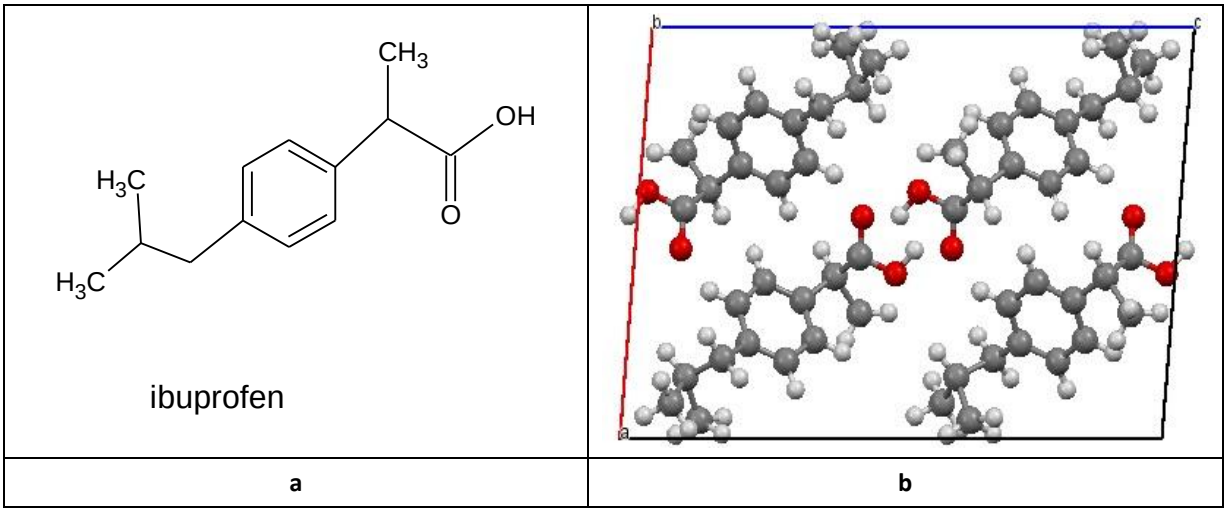

a	b

Figure 1.7: a) Structural formula of ibuprofen b) molecular packing of ibuprofen (viewed on 'b' axis) showing hydrogen bonding and functional groups (red) for dimer formation.

According to BP 2011, ibuprofen is a white or almost white crystalline powder having acicular shaped crystals with high cohesion tendency therefore it has poor flowability (Aly Nada, 2005). Ibuprofen is practically water insoluble, freely soluble in methanol, acetone, and methylene chloride. It also dissolves in dilute solutions of alkali hydroxides and carbonates. Its melting point is 75 °C – 78 °C, the absorption maxima at 221 nm, 264 nm and 272 nm a and log-P 3.83 (calculated), and 3.50 (experimental).

1.10.2 Candidate Excipients

The commonly used sugars were selected to study the effects of milling on their physical and thermodynamic properties, while the surfactants/solubilizers and polymers were employed in the co-milling study.

1.10.2.1 Sugars

Three sugars, including anhydrous (sucrose and lactose), monohydrate (lactose) and dihydrate (trehalose) were used in this study. The reasons for selecting these include; these are stable sugars, have a wide range of applications in pharmacy and are with known safety data. These sugars have a diverse milling behaviour and therefore are ideal compounds in the studies aimed to demonstrate the milling induced changes like the present one. The study of these sugars is also important to demonstrate the effect of crystalline water during the process of milling.

Lactose is a disaccharide formed from the condensation of galactose and glucose linked through a β,1-4 glycosidic linkage (Figure 1.8). Its main use is as a diluent in tablet formulations (Pilcer and Amighi, 2010). Lactose is an ideal material for the demonstration of milling induced changes like reduction in particle size, increase in surface area, amorphization etc. The different forms of lactose (monohydrate, anhydrous) have entirely different milling behaviour, presenting it as a further useful material for milling studies.

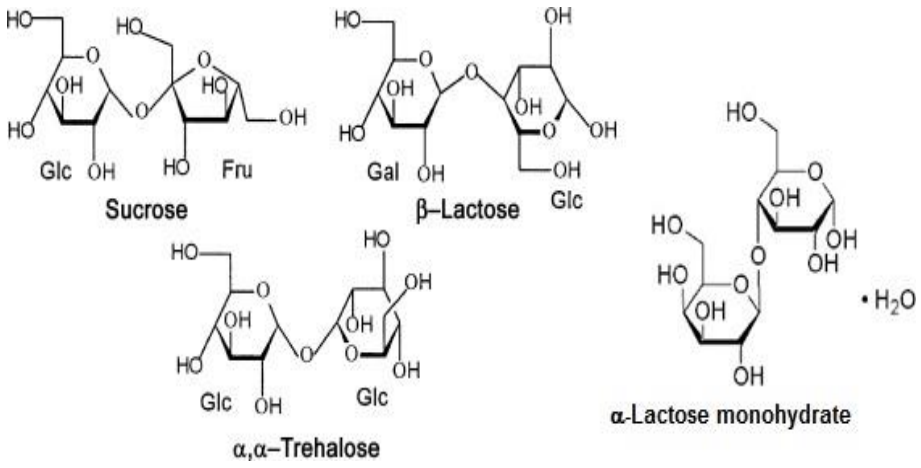

Figure 1.8: Molecular structures of sucrose, beta lactose, trehalose and alpha lactose monohydrate, taken from google images.

The melting point of anhydrous α-Lactose is 223 °C, of α-Lactose monohydrate 202 °C and of β-Lactose 252 °C (Raymond C Rowe, 2003). The commercially available forms alpha or beta lactose always contains some percentage of beta or alpha anomer as impurity.

Sucrose in a disaccharide that consists of glucose and fructose units linked through a α,1-2 glycosidic linkage (Figure 1.9). The milling of sucrose has shown that it is a brittle material having the breakage extent proportional to the square of the impact velocity. The breakage

of this sugar is influenced by the particle size of initial feed. Sucrose shows a greater extent of breakage as compared to the lactose (Yang et al., 2007).

Trehalose is a disaccharides of α-glucose formed by an α,α-1,1-glucoside bond between the two units (Figure 1.9). It occurs as anhydrous and dihydrate form and mainly used as cryo-protectants of biological drugs during freeze drying process (Crowe et al., 1996, Patist and Zoerb, 2005). The milling of anhydrous trehalose induces a direct transformation from crystal to glass phase and used as a popular of way producing the amorphous state (Willart et al., 2001). The milling of dihydrate form does not amorphize it rather converts it to a structurally invariant form. These behaviours are ascribed to the plasticizing effect of the structural water which decreases the glass transition temperature below the milling temperature (Willart et al., 2010).

1.10.3 Surfactants/Solubilizers

1.10.3.1 Lutrol F-68®

Lutrol® is also known as Poloxamer-188, Pluronic and Lutrol F-68. Poloxamers are the block co-polymeric non-ionic surfactant consisting of Polyoxyethylene-(PoE-) and Polyoxypropylene-(PoP-) units (a = *ca*. 79, b = *ca*. 28) as shown in Figure 1.9. The number 188 is derived from 18 (molecular weight of PoP part 18x100=1800), 8 (percentage weight of EO part, 8x10=80) while, F-68 is derived from 6 (molecular weight 6x1000=6000), 8 (percent weight of EO part, 8x10=80 (Quadir, 2005).

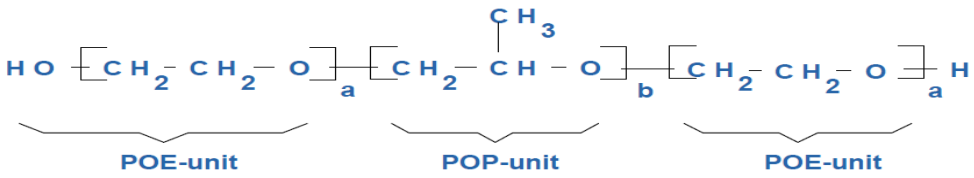

Figure 1.9: Molecular Structure of Lutrol F-68, taken from (Quadir, 2005) .

Lutrol F-68 occurs as white micro-beads or prilled granules with an average particle size 150 µm and a specific faint odor. Its melting point is 52 °C, hydrophilic lipophilic balance (HLB) value 29 and the bulk density ~ 1055 Kg m^{-3}. It is freely soluble in water and ethanol. Its molecular weight is ~ 9000 dalton and enthalpy of melting is 121 J g^{-1}.

Lutrol has been categorized as dispersing agent, emulsifying and solubilizing agent and widely used (5-10% by weight) for these properties as well as a wetting and plasticizing

agent (Raymond C Rowe, 2003). The minimum aggregation concentration for Lutrol F-68 is ~ 6.0 µmol L^{-1} (*i.e.* 0.054 mg ml^{-1}).

Solubilization Action of Lutrol®: The hydrophobic portion of a poloxamer is responsible for its solubilization action. In water, the molecules arrange themselves in an 'umbrella like' configuration (Figure 1.10) that incorporate the drug inside (Quadir, 2005).

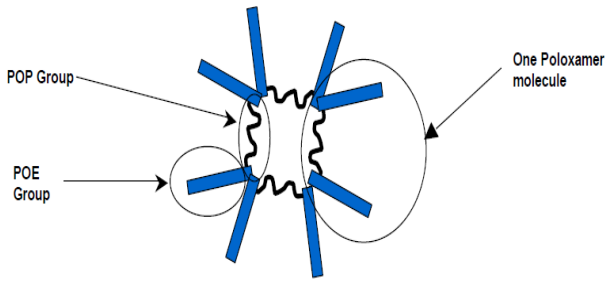

Figure 1.10: Diagrammatic representation of the solubilizing unit of Lutrol F-68 that incorporate the API, taken from (Quadir, 2005).

Poloxamers are widely used as solubilizer for the enhancement of solubility and dissolution of poor soluble drugs by the way of solid dispersion (Shin and Cho, 1997, Passerini et al., 2002).

1.10.3.2 Soluplus®

Soluplus is a relatively new solubilizer especially designed for preparing the solid solutions of poor water soluble drugs. Chemically, it is a graft co-polymer of polyvinyl caprolactam - polyvinyl acetate - polyethylene glycol. The structural formula (Figure 1.11) contains PEG-6000 (n)/ caprolactam (I)/ vinyl acetate (m) in the ratios of (13/57/30). Its molecular weight is ~ 118000 dalton (Hardung et al., 2010).

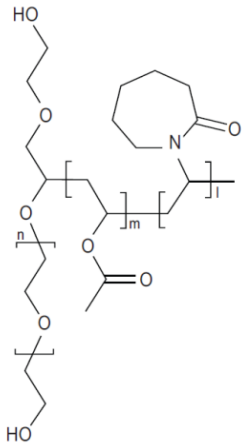

Figure 1.11: Molecular Structure of Soluplus®, taken from (Hardung et al., 2010).

Soluplus occurs as free flowing white or slightly yellowish granules, hygroscopic in nature. It is freely soluble in water and organic solvents. Its melting point is > 58 °C, HLB value is 8 - 14 and glass transition temperature ~ 70 °C. It forms micelles with the critical micellization concentration (CMC) value in water at 23 °C equal to 7.6 µg ml^{-1}. Its bulk density is 500 - 600 Kg m^{-3} (Ali, 2010).

Solubilization action of Soluplus: The vinyl-acetate and vinyl-caprolactam moieties of soluplus interact with the API incorporating it completely while the polyethylene glycol (PEG) moiety forms the backing of the complex (Ali et al., 2011) (Figure 1.12).

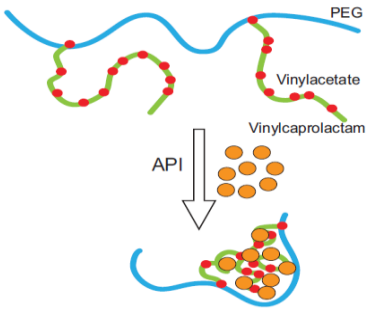

Figure 1.12: Diagrammatic representation of the mechanism of solubilization of API by Soluplus, taken from (Ali et al., 2011).

Because of its high flowability and excellent extrudability, soluplus has become an excellent candidate for solid dispersion especially in hot melt extrusion process (Djuric, 2011) . It has become extremely useful solubilizer since last few years and has been used for the enhancement of solubility of many pharmaceutical actives including itraconazole, fenofibrate, carbamazepine, danzole, clotrimazole, griseofulvin, and ketoconazole in buffer media (Smithey et al., 2010, Djuric et al., 2011). Its solubilizing capacity have shown to be robust toward different pH values and is superior to other commonly used solubilizers (Djuric and Kolter, 2010).

1.10.4 Polymers

1.10.4.1 Polyvinylpyrrolidone (PVP)

PVP also called Polyvidone; is a water-soluble polymer consisting of *N*-vinyl-pyrrolidone monomers (Figure 1.13a).

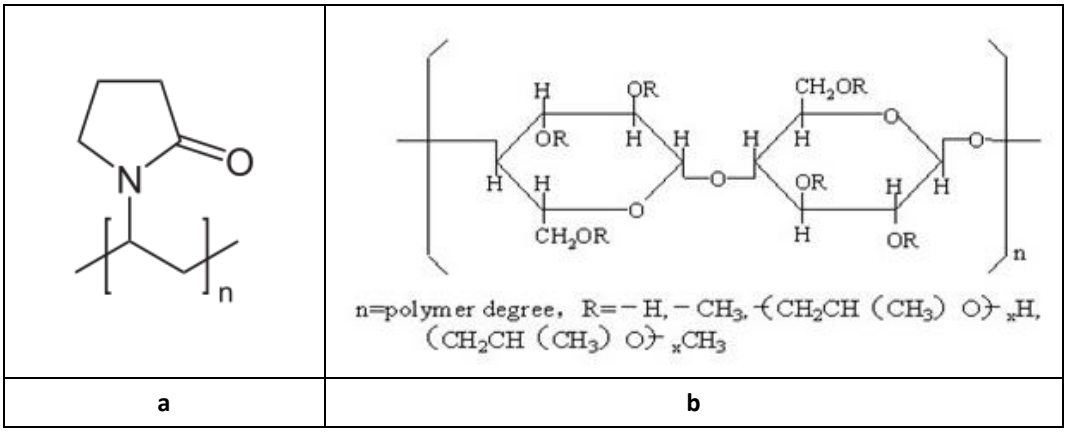

a	b

Figure 1.13: Molecular structure of a) PVP and b) HPMC, taken from google images.

PVP occurs as a light flaky powder that is hygroscopic in nature and readily absorbs atmospheric water up to 40% of its weight. It is soluble in water and other polar solvents. In solution, it has wetting properties and forms readily films, which makes it a good coating or an additive to coatings agents (Folttmann and Quadir, 2008). PVP has been used in many co-milling studies with poorly soluble drugs for the stabilization of amorphous surfaces to enhance the solubility and dissolution rate of these drugs (Balani et al., 2010a, Balani et al., 2010b).

1.10.4.2 Hydroxy Propyl-Methyl Cellulose (HPMC)

HPMC is cellulose 2-hydroxypropyl methyl ether (Figure 1.13b) that is widely used in pharmaceutical formulation as stabilizing agent, suspending agent, tablet binder and rate controlling polymer for sustained release drugs. It occurs as white, odourless and tasteless fibrous or granular powder. It melting point is 190 °C - 200 °C and glass transition temperature 170 °C - 180 °C. It is hygroscopic in nature and is soluble in water forming viscous colloidal solution (Raymond C Rowe, 2003). HPMC has been used in many co-milling studies for the improvement of dissolution of poorly water soluble drugs (Sugimoto et al., 1998).

2 Surface Characterization of Milled Pharmaceuticals (Lactose Monohydrate) using Different Analytical Techniques – The Study of Percolation Phenomenon

2.1 Background/Context

The process of milling produces defects in the crystal lattice, such as the dislocation of crystal planes, which ultimately results in the fracturing of particles when the number of defects exceeds the critical limit (Bates et al., 2006). Milled materials, having high surface to volume ratios, are considered to be porous in the sense that there are likely to have channels (fissures and cracks) which run from the surface to some point towards the core of the particles. In consideration of the new surfaces that are formed on milling, it may be important to recognize 'external' and the 'internal' surface. The external surface is mostly the geometrical envelope of the discrete particles or aggregates and includes all the surfaces of those cracks which have more width than their depth, while the internal surface comprises the walls of all cracks, pores and cavities which are deeper than they are wide and which are accessible to the adsorptive probes (Sing et al., 1982).

External surfaces have a diffusion layer controlling the dissolution rate, the thickness of which is a function of the rate of stirring/agitation within the dissolution medium. In contrast, the internal surfaces may indeed provide opportunities for the dissolution fluid to wick into the particle and allow for dissolution to occur. However, in a non-swelling particle this water will soon become saturated and therefore choke off any further dissolution of the particle. The direct contribution of this internalized dissolution process, to the overall dissolution rate, is likely to be insignificant. Instead, the role of these internal surfaces in promoting dissolution of the particle is more likely to be associated with the impact that the localized internal dissolution process have on the 'bridges' holding the partially fragmented particle together. The dissolution of these bridges and the creation of new external surfaces is most probable mechanism that explains the increased dissolution rate of a particle which is partially damaged.

The requirement to distinguish between external and internal surfaces is a question of "rate limiting steps". If the rate of conversion of the internal surface to an external surface (as a result of the break-up of a partially fractured particle) is faster than the rate of dissolution of

the external surfaces present then it might be considered that any internal surface is in effect contributing to the overall dissolution of the particle, in the same was as if it started out as an external surface. However, conversely, if the rate of particle break-up is much slower than the rate of dissolution of an external surface then there will be a need to differentiate between these two categories of surface, using appropriate measurement techniques, so that the impact of milling on the mechanism of dissolution rate enhancement may be more clearly understood. Given the potential criticality of the rate of break up to the resultant overall dissolution rate, then it may also be important to examine the factors which control the rate of break-up of partially damaged particles. Clearly, whether a particle swells on absorption of water into the internalized surfaces will be a key factor, as that in itself is likely to promote break-up of the particle. In other cases of non-swelling particles it may be a question of the number and strength of the bridges which hold the particle together that will control the rate of break-up of the particle. The mechanisms of dissolution are therefore potentially rather complex and may require multiple analytical technologies in order to establish the dominant processes.

The techniques commonly applied for studying the impact of milling on crystalline particles includes; SEM for changes in particle shape (Rasenack and Müller, 2004), laser diffraction for particle size (Kwan et al., 2004), nitrogen adsorption studies for specific surface (Joshi et al., 2002), PXRD for assessing the changes in crystallinity, DSC for measuring loss of crystallinity, FTIR for any structural change (Patterson et al., 2007, De Gusseme et al., 2008), (Michael Lee, 2011), IGC for measuring surface chemistry/energies (Heng et al., 2006); MT-DSC, micro-calorimetry and dynamic vapour sorption for determination of amorphous content (Mackin et al., 2002b, Guinot and Leveiller, 1999) and TGA for measuring the moisture content (Ward and Schultz, 1995).

The measurement of specific surface area of the milled material is important in explaining the role of cracks and fissures in dissolution and water sorption because an assessment of particle size reduction, alone, is unlikely to be sufficient to explain the complete impact of milling on the dissolution rate. The surface area measuring techniques, such as nitrogen adsorption has the potential for assessing the entire surface contributions from both external and internal surfaces. The technique involves long pre-exposure of the milled sample to the elevated temperature (~60 °C) and reduced pressure before the measurement

is made. The issue with this approach of the surface area measurement for a crystal hydrate is that the process may result in the creation of new surfaces by the evaporation of the water of hydration (Raut et al., 2011). There are few, if any techniques, which can measure the native/inherent moisture content at the surfaces of the crystal and within the new amorphous phase, which exists immediately after milling.

Recent work on porous materials has shown that the features of hydration surface, in term of micro-clusters of water, may be estimated from the dielectric measurements of percolation phenomenon; whereby the surface moisture provides the charge carriers, protons, that percolate over the surface of the solid to provide an assessment of the fractal dimension of the percolation pathways and the porosity of the solid (Feldman et al., 2006).

The focus of the work presented in this Chapter is to investigate the surface changes (including the particle size, surface area, creation of amorphous surface domain and changes in the surface chemistry) after ball milling of a pharmaceutical material (lactose monohydrate, LMH). The measurement of these changes is important as they affect the behaviour of the milled pharmaceuticals during or post milling manipulations and storage. A special focus of study is the percolation phenomena estimated by broadband dielectric spectroscopy (BDS). The study offers the evaluation of a hydrated sugar by some routinely used techniques (SEM, TGA, BET, DVS and IGC) with the aim of highlighting the advantages and limitations of these techniques. Moreover the opportunities of using BDS in characterizing the surface defects of milled materials are explored.

Lactose monohydrate was chosen, as it is one of the most commonly used excipients in the pharmaceutical industry, as a diluent in tablet formulations (Jivraj et al., 2000) and the carrier in dry powder inhalers (DPI) (Kou et al., 2012). Milling of LMH occurs through ductile fracture (high energy dissipation and lower fracture velocities) reduces its particle size, generates the disordered amorphous phase and converts a portion into the metastable β-anomer (Willart et al., 2004). The loss or re-distribution of the water of hydration also occurs on the milling of this hydrated sugar (Thomsen et al., 2005).

2.2 Materials and Methods

Lactose monohydrate (EP/BP) was sieved at room temperature (~ 23 °C) and ~40% relative humidity. The particles that passed through an 80 mesh sieve and retained on a 100 mesh

sieve (corresponding to linear size between 150 and 180 µm), were taken for the analysis. The measured average particle size by SEM was ~172 µm. Laser diffraction technique has shown that 50% of particles (d_{50}) were of the size less than 154 µm.

2.2.1 Ball Milling

The material was milled in the vibratory ball mill (MM 301, Retsch, Germany, Figure 2.1) equipped with two 50 ml stainless steel cylindrical jars each containing one stainless steel ball of 25 mm diameter (Figure 2.1). A weight of 2.5 g of LMH was loaded into each jar, which were then closed tightly and clamped in position of the mill. The mill was operated at frequency of 18 Hz for 15, 30, 45, 60, 90, 180, 270 and 360 min. The sample was collected into a glass vial and used immediately or stored in desiccator until used for further analysis.

Figure 2.1: Vibratory ball mill (MM-301) with the milling jars and balls of different sizes.

Note: The mill frequency of 18 Hz was selected after an initial screening of three speeds *i.e.* 15, 18 and 25 Hz as previously used by (Kwan et al., 2004) based on the fact that this frequency had a significant impact on the crystallinity without a marked increase in the temperature of the mill. The temperature of milled material was ~40 °C, estimated by insertion of a thermocouple probe into the powder immediately after milling.

2.2.2 Laser Diffraction Technique/Particle Size Determination

The particle size distribution (PSD) of un-milled and milled lactose monohydrate was determined by dry dispersion laser diffraction technique according to the method described by (Krause et al., 2011). The powder was dispersed in compressed air at pressure of 3 ± 0.05 bar using a dispersion unit, RODOS (Sympatec, Germany), dispensed at the feed rate of 60 mm sec^{-1} using a micro-dosing unit, ASPIRO (Sympatec, Germany) and measured under the pressure of ~0.5 bar with a laser diffractometer (HELOS H1360, Sympatec, GmbH, Germany)

fitted with R5 lens (Sympatec) that measures the size between the range of 4.5 to 875 µm. The data analysis was performed with WINDOX 5 software and the parameters d_{50}, and d_{90} were calculated, that represent 50%, and 90% of the particles are lower than the given size, respectively.

2.2.3 Scanning Electron Microscopy (SEM)

The un-milled and milled samples of LMH were photographed by ZEISS EVO HD 15 scanning electron microscope (Carl Zeiss, NTS Ltd. Cambridge, UK) according to the method used by (Qiao et al., 2013). The samples were mounted on the carbon adhesive tape fixed on aluminium stubs (Agar Scientific Ltd., Stansted, UK), flushed with air and imaged at the voltage of 10 KV by using secondary electron and backscatter detectors.

2.2.4 Thermogravimetric Analysis (TGA)

TGA of un-milled and milled LMH was carried out in a TGA instrument with auto-sampler system (Perkin Elmer, US) according to the method already described by (Hurtta et al., 2004). The empty aluminium pan was loaded into the TGA instrument and tarred. Then the sample was placed in the pan and the pan returned to the instrument. The weight of sample was recorded in the temperature range from 25 °C to 250 °C at the rate of 20 °C min^{-1}.

2.2.5 Brunaer Emmet Teller (BET) Surface Area Measurement

The BET surface area of the milled samples of LMH were determined by nitrogen adsorption technique using ASAP 2420 (Micromeritics Instrument Corporation, USA). The samples were degassed at 60 °C under reduced pressure for 24 hours (this removes moisture and other dissolved gases). Helium was used to measure the free space, space of the sample tube left over from sample. The nitrogen adsorption isotherms were collected from 0.002 to 0.995 p/p_o in liquid nitrogen (-162°C).

2.2.6 Dynamic Vapour Sorption (DVS)

DVS of milled lactose monohydrate were measured with a DVS Advantage automated moisture sorption instrument (Surface Measurement Systems Ltd., London, UK) at 25 °C with sample size of about 10 mg for each analysis. The working concentration range of the instrument was 0-98% p/p_o; and temperature stability of 0.1 °C. Prior to measure, the samples were dried at 25°C under a continuous flow of air to establish the dry mass. Then

exposed to the following typical partial pressure profile: 0, 10, 20, 30, 40, 50, 60, 70, 80, 90, 95, 90, 80, 70, 60, 50, 40, 30, 20, 10 and 0% RH. A fixed time of 180 min was selected for all relative humidity steps.

2.2.7 Inverse Gas Chromatography (IGC)

The surface properties of milled lactose monohydrate were evaluated by measuring the BET surface area, surface energy profiles and the acid/base numbers. The measurements were made in a second generation IGC-SEA Analyser (Surface Measurement Systems Ltd., London, UK) having a flame ionization detector. The data were analysed using both standard and advanced SEA Analysis Software.

The samples (67 to 980 mg) were packed into standard columns (30. 0.3 cm ID) employing a tapping machine. The sample column was pre-conditioned for 1 hour at 30 °C and 0% relative humidity with 10 ml min^{-1} helium as a carrier gas. The experiments were conducted at same temperature and humidity conditions during which the samples were run at a series of surface coverage with alkanes (Decane, Nonane, Octane, Heptane, Hexane, Pentane) and polar (Ethanol, Ethyl acetate, Acetone, Dichloromethane, Acetonitrile, Chloroform) probe molecules to determine the dispersive surface energy (γ_S^D) as well as the acid-base free energy of adsorption (ΔG_{SP}). The specific surface area of each sample was first determined by measuring the Octane or Heptane adsorption isotherms. The BET specific surface areas of the samples were calculated from the corresponding isotherms, within the partial pressure range of 5% to 35% p/p_0.

Note: DVS and IGC studies were conducted by Surface Measurement Systems, London, U.K, BET measurement by Nottingham University and the Laser diffraction studies is the courtesy of AstraZeneca, Macclesfield, UK. All these were included here as supplementary studies.

2.2.8 Broadband Dielectric Spectroscopy (BDS)

Dielectric measurements were performed in BDS Solartron 1296 instrument connected to a Solartron 1255 frequency response analyser (Figure 2.2a) according to the method taken from (Ermolina and Smith, 2011). The powder sample was placed between two electrodes of gold sample cell (Figure 2.2b) to form a uniform thin layer. The diameter and thickness of the sample were measured from the geometry of sample cell using vernier calliper. The sample cell was mounted in sample holder and placed in the Oxford Instruments Cryostat (Figure

2.2c) which provides the temperature control using liquid nitrogen. The sample was measured applying the frequencies between 0.1 Hz and 10 MHz and temperature range of −120 to +100 °C with 5 °C increments.

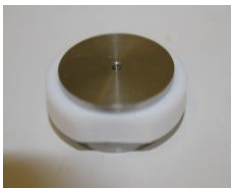

a b c

Figure 2.2: Solartron dielectric spectrometer showing a) frequency response analyser, b) sample cell containing two gold plated electrodes mounted in Teflon assembly and c) sample holder and cryostat assembly for the regulation of temperature during the measurements.

Note: In order to maintain the uniformity that the same milled sample will used in all analytical techniques, each measurement was done once only.

2.3 Results and Discussion

2.3.1 Particle Size Distribution

In un-milled lactose monohydrate, the cumulative particle size distribution plot has shown that majority of the particle (~90%) have the size greater than 80 μm (as indicated by the dotted lines 'A' & 'B' in Figure 2.3a while the the rest of particles are smaller than this value. The density distribution plot (Figure 2.3b) show a Guassian distribution that ranges between 100 - 400 μm with the peak at ~160 μm.

On the other hand, in case of **milled samples of lactose monohydrate** (15 min to 90 min), the cumulative plots show that the PSD shift towards smaller size with ~75% particles are of the size less than 80 μm in all milled samples (dotted line 'A' Figure 2.3a). The density distribution plots of these milled samples show that the size of particles spreads over the range of few micron to 400 μm with the density of ~0.5 (dotted line 'D' Figure 2.3b). These profiles presents three modalities of size distribution *i.e* ~7 μm, 50 μm and 200 μm

(indicated by arrow arrows in Figure 2.3b) which largely remain unchanged in lactose monohydrate milled for 15 min to 90 min.

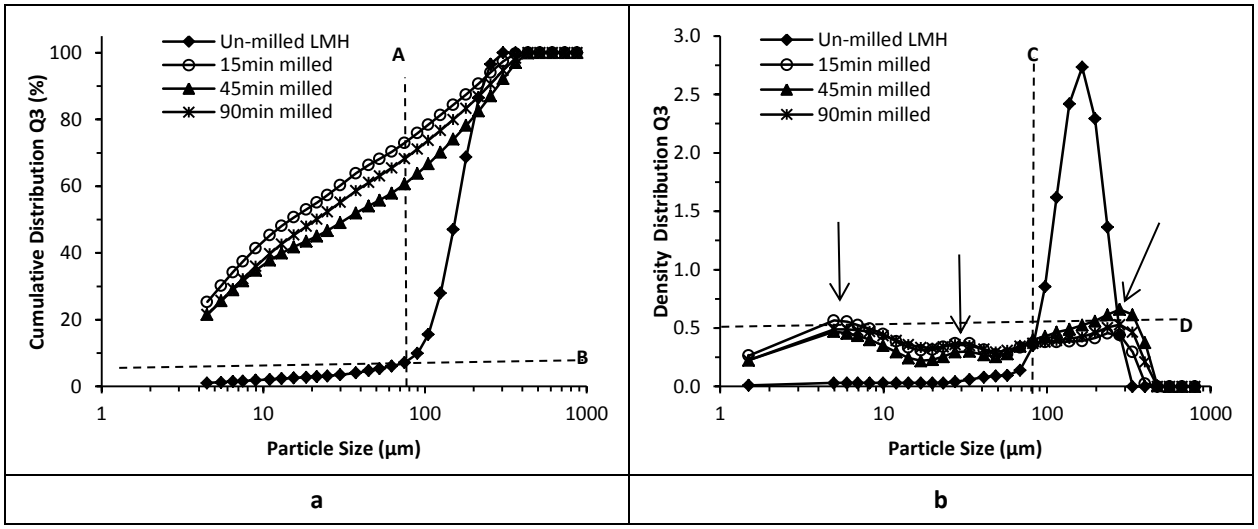

Figure 2.3: Particle size distribution plots of un-milled and milled lactose monohydrate showing a) cumulative distribution and b) density distribution plots. The dotted lines represent cut off size (A & C) or frequency (B & D) for different samples.

The parameters of PSD including d_{50} and d_{90} have been summarized in Table 2.1. The value of d_{50} that was ~155 µm for un-milled LMH, reduced to ~15 µm after 15 min of milling. It does not reduce further, rather it goes up slightly in 45 min milled sample (~30 µm) and ~20 µm in 90 min milled sample. The values of d_{90} that decrease slightly in short milled sample (*i.e.*15 min milled), but increase again in 45 min and 90 min milled sample.

Table 2.1: Particle size distribution of un-milled and milled lactose monohydrate showing the values of d_{50} and d_{90} that represent the 50 and 90% particle less than the given size respectively.

Milling time	d_{50} (µm)	d_{90} (µm)
0	153.9	228.9
15	14.8	206.9
45	32.4	283.1
90	21.4	247.2

These results have indicated that the particle size is reduced on ball milling, with the greatest reduction occurring in the early few min of milling time (≤ 15 min) where there is more than 10 times reduction in particle size. After this significant reduction in particle size distribution there appears a little change in size on long milling times *i.e.* at 45 min and 90 min. Rather there is some regain in particle size (as the d_{90} values of long milled samples are greater than that of un-milled samples). This probably represents the formation of clusters of particles which is investigated in SEM of these milled samples. It is also possible that

during the initial phase of milling most of the energy input is used in particle size reduction while on longer milling the energy input is dissipated in the generation of the amorphous phase with no further reduction in size. Given that the milling of lactose monohydrate releases the water of hydration there is still another possibility of re-crystallization of the amorphous phase generated in long milled samples. Thus, there is interplay between the size reduction, clustering/aggregation of particles and re-crystallization, which results in hardly any significant change in particle size between 15 min to 90 min of milling. These changes are further investigated by SEM, BET, TGA and DVS.

2.3.2 Scanning Electron Microscopy Results

The SEM micrographs of **un-milled lactose monohydrate** (Figure 2.4) showed that the particles are crystalline with well-defined cuboidal shapes and appear to be having the 'hard' surfaces which are not completely smooth. The sizes of these particles lie in the range of 50–220 μm, which is consistent with the laser diffraction results (Section 2.3.1).

In **milled samples of lactose monohydrate**, the large and small fragments of crystalline particles are visible. The shapes of these particles are irregular with rough and fragmented surfaces (Figure 2.4) which is consistent with the observations of (Price and Young, 2005). The 15 min and 30 min milled sample showed the particle that range in size from few microns to 70 μm and they have irregular and damaged surface. On milling, beyond 30 min, the size of particles is further reduced (it is 2 -15 μm in 45 min and 90 min sample) and they appear to have 'soft'/'fluffy' surfaces (see Figure 2.4) with an underlying 'hard' crystalline particle. At the 180 and 270 min milling time points, the clusters of uniform nano-sized particles are observed which aggregate together forming clusters of ~500- 1000 nm as speculated in particle size results. In these samples there are hardly (if any) large particle.

Note: Appendix I show some more micrographs of milled samples of lactose monohydrate at different magnifications.

The SEM results have indicated the size reduction on ball milling (initial rapid reduction followed by relative slower decrease), which is almost consistent with the particle size results by laser diffraction. However the presence of larger particle (equal to or larger than the size of un-milled particles) in milled samples as speculated in particle size results (Section 2.3.1) are not observed in SEM. Instead the clusters of smaller particles are seen in longer

milled samples. At this point, there is need for a technique that can measure the exact contribution of milling to the size reduction or increase in surface area.

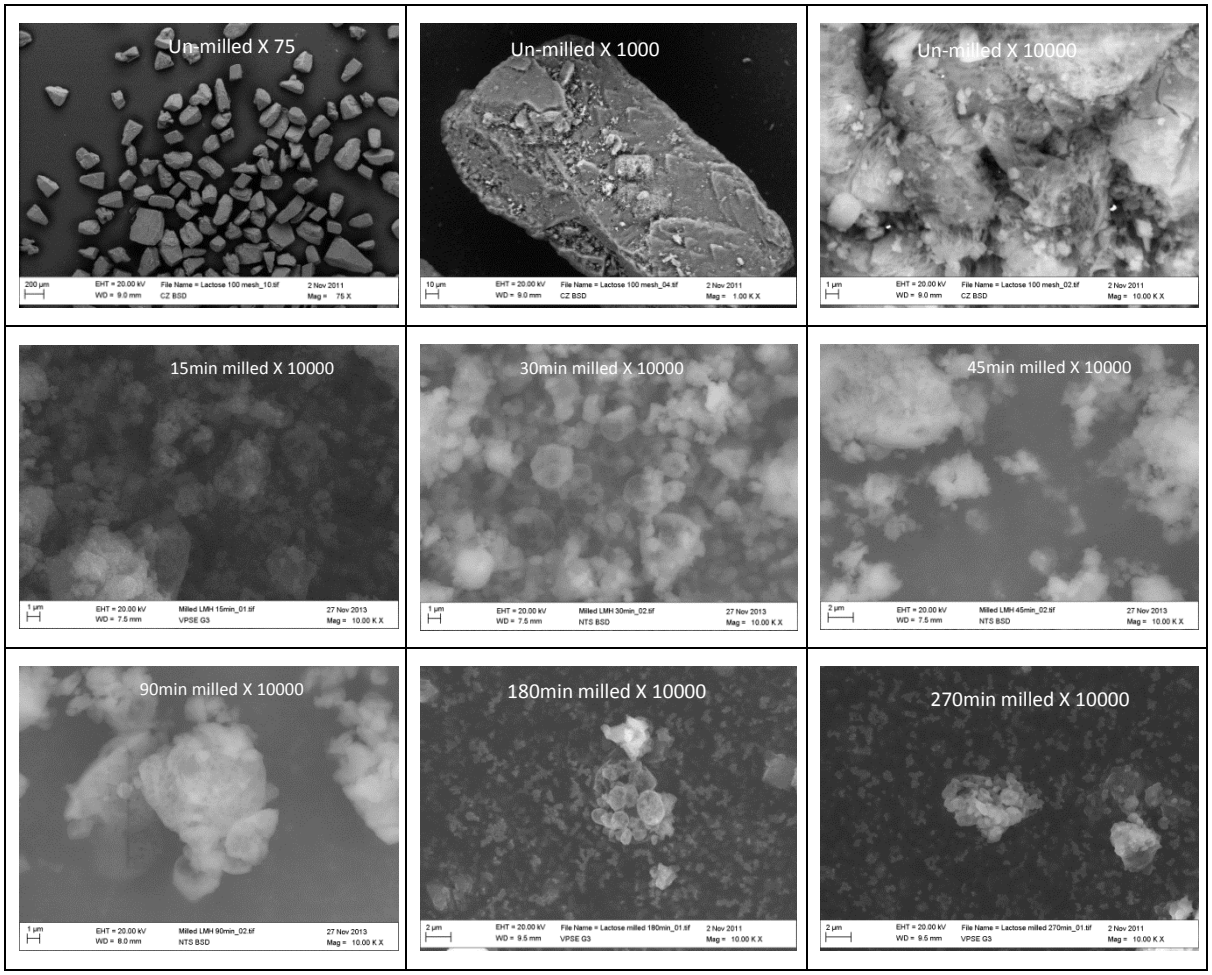

Figure 2.4: SEM images of un-milled and milled lactose monohydrate for different time intervals. Milling times and magnification have been indicated in boxes on each micrograph.

2.3.3 BET Surface Area Results

The surface area measurement by the nitrogen adsorption technique involves the partial pressure of adsorptive gas which is gradually increased to form a monolayer on the surface of adsorbent. The plot of partial pressure of gas against quantity adsorbed gives the adsorption isotherm. If this relationship is linear (which usually occur for p/p^0 range of 0.05 - 0.30) the adsorbed amount can be calculated by applying Brunauer-Emmett-Teller (BET) gas adsorption relation (Equation 2.1).

$$\frac{\mathbf{p}}{\mathbf{n^a.(p^0-p)}} = \frac{\mathbf{1}}{\mathbf{n_m.C}} + \frac{\mathbf{(C-1)}}{\mathbf{n_m.C}} \cdot \frac{\mathbf{p}}{\mathbf{p^0}} \qquad \textbf{Equation 2.1}$$

Where 'n^a' is the amount adsorbed at the relative pressure p/p^0, n_m is the monolayer capacity and 'C' is BET constant related exponentially to enthalpy of adsorption to first layer. The value of 'C' < 10 indicates that the sample is non-porous and all surface area is external.

The plots of quantity adsorbed against relative pressure of gas for un-milled and milled LMH are linear, indicating the uniform surface adsorption in all the samples. In milled samples of LMH, these plots not only shift upwards indicating the increase in the quantity adsorbed but also the gradient of these plots increases indicating the increase in the surfaces available for adsorption of the gas (Figure 2.5). This trend continues with milling time till 45 min and reverts again in long milled sample (*i.e.* 90 min).

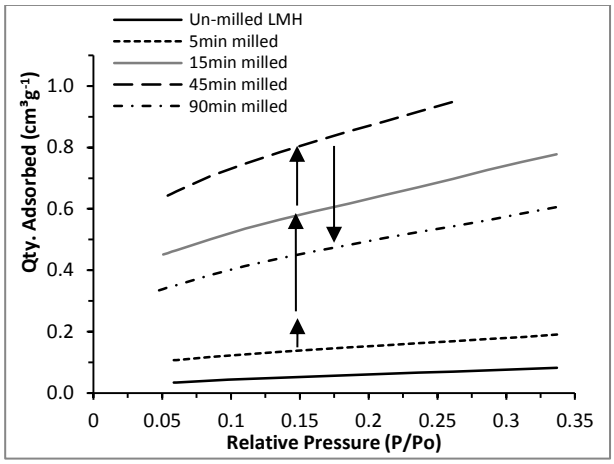

Figure 2.5: Nitrogen adsorption isotherm of un-milled and milled sample of lactose monohydrate. The arrow heads are showing increase or decrease in quantity adsorbed with increasing the milling time.

BET surface area is calculated from the quantity adsorbed at monolayer coverage by applying the BET relation (Equation 2.2).

$$\mathbf{A_s(BET) = n_m^a \cdot L \cdot a_m} \qquad \textbf{Equation 2.2}$$

Specific surface area of un-milled lactose, as determined from BET is 0.26 m^2g^{-1} (Table 2.2), which is not consistent with the particle size results (as from the average size of ~160 µm the specific surface area is lower than this value). Also this value of surface area is higher than that of the anhydrous sugar (sucrose, 0.035 m^2g^{-1}) but lower than the dihydrate sugar, trehalose (*i.e.* 1.43 m^2g^{-1}) with almost the same particle size. The main reason for high surface area of hydrated sugars is likely to be that, during pre-treatment (exposure to 60 °C overnight) water of hydration is desorbed from the crystals, leaving some pores that

contribute to the total surface area. Another reason is the presence of pits/fissure on the surface of these particles in comparison with the smooth surfaces of the anhydrous one. This is evidenced from the SEM micrographs of sucrose (Appendix II) and trehalose dihydrate (Appendix III).

The value of BET constant 'C' for un-milled LMH is greater than 10, indicating the porous surfaces that probably have been created by the evaporation of water during the pre-treatment.

Table 2.2: BET surface area parameters of un-milled and milled lactose monohydrate determined from the nitrogen adsorption isotherms.

	Un-milled LMH	5min milled	15min milled	45min milled	90min milled
BET Surface Area (m^2g^{-1})	0.26 ± 0.0028	0.57 ± 0.0019	2.32 ± 0.0062	3.15 ± 0.0062	1.82 ± 0.0065
Slope (g cm^{-3})	15.5 ± 0.1737	7.4 ± 0.0241	1.8 ± 0.0048	1.4 ± 0.0026	2.4 ± 0.0084
Y-Intercept (g cm^{-3})	1.01 ± 0.0364	0.16 ± 0.0050	0.02 ± 0.0009	0.015 ± 0.0004	0.038 ± 0.0016
C	16.32	48.78	71.24	91.51	62.25
Qm (cm^3g^{-1})	0.06	0.13	0.53	0.72	0.42
Correlation Coeff.	0.999	0.999	0.999	0.999	0.999
Molecular cross-Sectional area (nm^2)	0.162	0.162	0.162	0.162	0.162

Specific surface area of milled lactose monohydrate increases gradually with milling time till 45 min, and then it decreases in the 90 min milled sample (Table 2.2). These results (apparently in agreement with SEM and particle size results) show that there is a notable increase in the specific surface area particularly during early minutes of milling (*i.e.* 0.26 m^2 g^{-1} of un-milled to 2.32 m^2 g^{-1} of 15 min milled sample; ~10 times increase). This is followed by a small increase where the value of specific surface area is 3.15 m^2g^{-1} in case of 45 min milled sample and then decrease (1.82 m^2 g^{-1}) in 90 min milled sample. However these findings are not consistent with the particle size results (section 2.3.2) as the 10 times reduction in particle (that occurs in first 15 min of milling) would be expected to increase the surface area by the square of the size reduction factor (*i.e.* ~100 times). This observation is probably a result of the high contribution from internal surfaces that have been created through the loss of water in the pre-treatment process of elevated temperature and high vacuum.

Also between 15 min to 45 min milling, where the particle size increases slightly (Table 2.1) due the formation of aggregates as visible in SEM images (Figure 2.4), the surface area

continues to increase (Table 2.2), which indicates the area of surfaces which are in effect internal to the agglomerates are accessible to the nitrogen gas probe.

On milling beyond 45 min, where particle clusters are more frequent, and amorphous content of the sample also high (as discussed in Chapter 3, Section 3.3.3.9) the specific surface area appears to decrease (although the magnitude of this decrease is not consistent with particle size results). The reasons for this decrease might include; i) the amorphous content entering the interior of cluster that re-crystallizes owing to the high water content and high temperature of the mill, making the clusters non-accessible to the nitrogen probe (Figure 2.6), ii) the decrease in surface free energy in long milled samples after an initial increase in short milled one (see IGC results, Section 2.3.6.1).

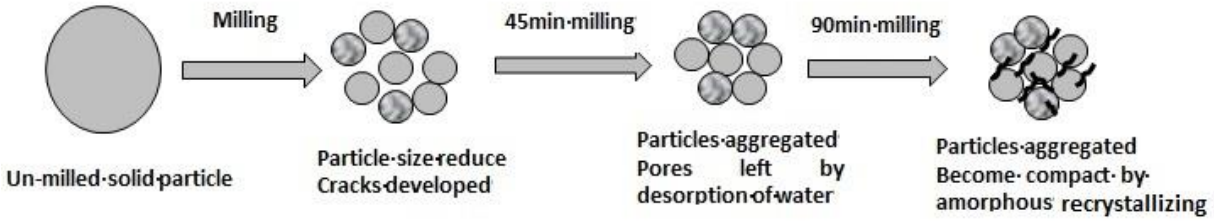

Figure 2.6: An illustration of the changes in surface area on milling and desorption of water of hydration (that is facilitated by milling). The clusters of particles are lose till 45min milling but are compact when amorphous content increase on long milling.

It can be concluded that the surface to volume ratio increases on milling, however on long milling particles get aggregated decreasing the specific surface area (Figure 2.6). The present techniques measure the different scale lengths; where laser diffraction measures the scale length of particles, SEM visualizes the surfaces and the BET measures the surfaces accessible to nitrogen probe. Provided that the milled hydrated material like lactose monohydrate is a complex system containing a range of crystallites and different levels of amorphous (Chapter 3) and moisture content (Section 2.3.4). The uncertainties about the contribution of each phase would exist and the complete characterization of such material is not reliable from these techniques. Therefore, we explored the application of dielectric spectroscopy.

2.3.4 Thermogravimetric Analysis Results

The desorption profiles of un-milled and milled lactose monohydrate are considered in terms of the release of both surface (*physi-sorbed*) and bound (*chemi-sorbed*) water and the impact that the defected crystalline structure of milled samples are likely to exert on the

onset temperatures for desorption of water. The TGA curves (Figure 2.7) show that desorption of water from the milled samples of lactose monohydrate is not straightforward, rather it occurs over a number of temperature ranges representing the presence of different assemblies of water.

TGA curve of un-milled lactose monohydrate (top curve in Figure 2.7) has shown that the weight of sample remains almost constant until a small step of weight loss at ~120 °C followed by the desorption of the water of crystallization at ~144 °C. The initial small weight loss (~0.4%) is assumed to be desorption of *physi-sorbed* water. However, it seems improbable that the surface water would be released at such an elevated temperature. It is more likely that this apparent increase in the TGA thermogram (that probably occur because of uptake of moisture from environment as the analysis is carried in open pans) is in fact masking the analysis of the surface water loss, which is otherwise observed from 30 -70 °C.

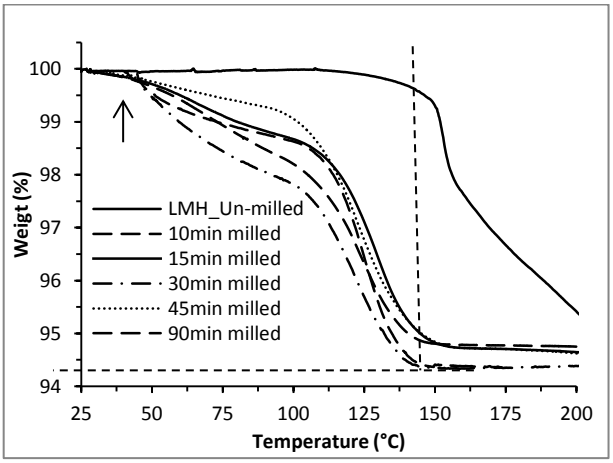

Figure 2.7: TGA thermograms of un-milled and milled lactose monohydrate, the onset temperature for desorption of crystallization water is indicated by vertical dotted line. The horizontal dotted line represents the plateau in weight. The arrow heads are showing the onset temperature for the release of surface water in milled and un-milled samples.

In contrast, the desorption of surface water from the milled samples of LMH has a more realistic, early onset temperature of approximately 30 °C which continues until ~110 °C from where the desorption of the water of crystallization starts. Taking 0.4% as the value for the un-milled sample, it would then appear that the surface water increase almost linearly with milling time, with the 15 and 45 min milled samples containing 1.69% and 1.25% surface water respectively (Table 2.3). This proportion increase further in long milled samples (90 and 180 min milled), where the percentages surface water are 2.20 and 1.60%, respectively. The other principle difference between the TGA curves for the un-milled and milled LMH is

the onset temperature of desorption of water of crystallization. It is ~144 °C in the un-milled LMH (comparable to an endothermic peak of water desorption in the DSC curve, Figure 3.4 in Chapter 3), this temperature is ~110 °C in the milled samples.

The factors that might be responsible for 35 - 40 °C decrease in the onset temperature for desorption of the crystallization water in the milled LMH (from ~144 °C of un-milled sample to ~105 °C in the 90 min milled one) are; the development of new pathways for dehydration in a structurally compromised crystalline phase, (Garnier et al., 2008) and the decrease in particle size (Shariare et al., 2011).

Table 2.3: Values of un-bound and bound water in un-milled and milled lactose monohydrate as calculated from the weight changes in TGA thermograms.

	Un-bound/Surface water			Bound/Crystallization water			
Milling time	**Start wt. (%)**	**End wt. (%)**	**Weight loss (%)**	**Onset temp. (°C)**	**Start wt. (%)**	**End wt. (%)**	**Weight loss (%)**
0	100.1	99.8	0.40	144	99.8	96.6	5.0
10	100	98.24	1.76	106	98.24	94.4	3.84
15	100	98.31	1.69	112	98.27	94.7	3.57
30	100	97.28	2.72	102	97.8	94.35	3.45
45	100	98.75	1.25	107	98.7	94.75	3.95
90	100	97.8	2.20	106	98	94.8	3.2
180	100	98.4	1.60	106	98.4	94.8	3.6

*from the stoichiometric ratio of water in lactose monohydrate

It is important to note that in case of un-milled LMH, the change in the gradient beyond 160 °C (after the release of ~2.5% water) remains incomplete may be due to the fact that it is increasingly harder to remove the water as the drying front recedes into the crystals. The tail of desorption process then merges with the melting onset at approximately 210 °C, so the experiment is stopped. Given that the heating rate is relatively high *i.e.* 20 °C min^{-1}, there is not sufficient time for the release of all the water of crystallization before the material starts to decompose. It follows that the estimation of percentage concentration of water of crystallization (bound water) is not realized by this technique. Therefore, we assume that the bound water concentration is that calculated from the stoichiometric ratio of lactose to water in lactose monohydrate (*i.e.* ~5% w/w). In milled samples where the weight loss reaches the plateau at ~165 °C with release of 3.5 to 4.5% (w/w) of water in 10 min to 180 min milled samples (Table 2.3).

From these observations of the increase in surface water in the milled materials might be due to, in part, the water of crystallization that is released from the crystals which then becomes adsorbed onto the surface of the new fragments of the original particles. However, the increase in surface water in the milled material cannot be due to the water of crystallization alone, it must also include a proportion of water adsorbed from the environment because +1% of surface water can't be 'found' from a ~0.5% loss in the water of crystallization (in 45 min milled sample). The other 0.5% must have come from the atmosphere as a direct result of the increased surface area of the milled material.

A further consideration is the characteristics of new surfaces generated on milling. As the particle size decreases with increased milling time, there is an increase in the surface area of particles with 'hard crystalline' surfaces, *i.e.* those surfaces which result from the cleavage of the parent particle. However, some particles may not fracture on impact but rather the energy is absorbed by the particle, causing an increase in the local temperature which results in the formation of an amorphous surface domain. This new amorphous phase will also adsorb the moisture.

Note: the un-bound/surface moisture of lactose with particles size (45, 60, 80, 100, 150 and 200 mesh) was also determined and it lies in the range of 0.3 to 0.4%. Therefore it was considered that the starting moisture is almost negligible and is not dependent on the particle size of un-milled material.

2.3.5 Dynamic Vapour Sorption Results

DVS studies are conducted to estimate the surface domain of amorphous phase that is produced on milling which can influence the moisture uptake and dissolution rate of the milled materials. The results of DVS are usually expressed as vapour sorption plots that represent the percent change in mass of a material (based on dry mass) versus time at various humidity levels. The vapour sorption plots of 15 min and 90 min milled LMH are shown in Figures 2.8a and 2.8b, respectively. The continuous line plotted on the left y-axis shows the % change in mass (based on dry mass). The dotted line, plotted on the right y-axis, represents the target % partial pressure of water vapour in the DVS as a function of time. These results have indicated that both the samples began to lose mass around 50% RH and showed a unique pattern of gain and loss of water steps. This is most likely due to the

crystallization of the amorphous phase present in these milled samples. This transition continues with each humidity step until the samples reaches around 90% RH.

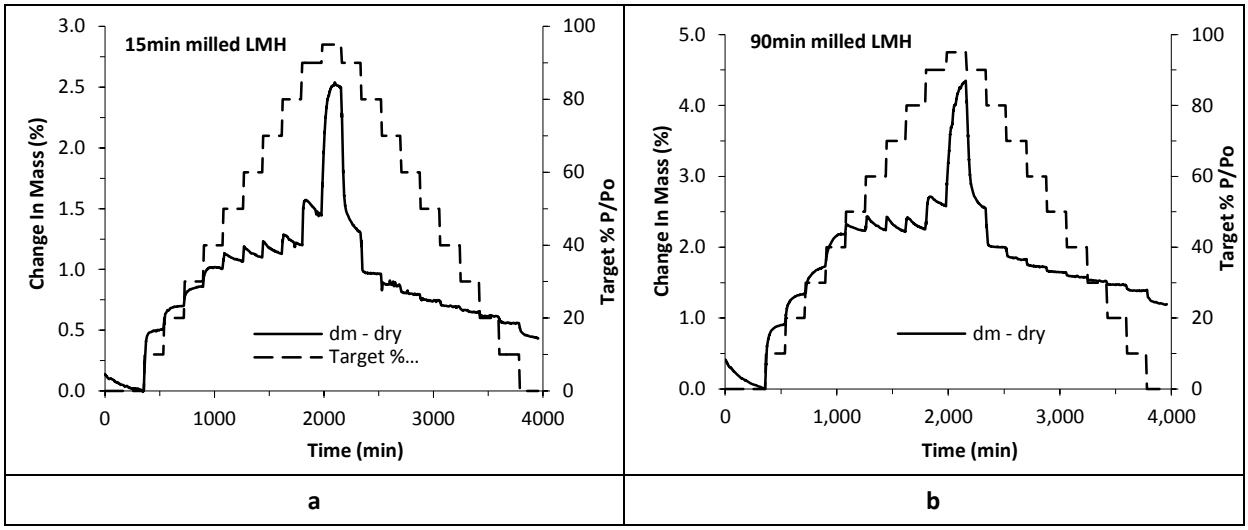

Figure 2.8: DVS mass change response with different humidity steps for a) 15 min milled and b) 90 min milled (b) lactose monohydrate. Note that the Y-axis scale in Figure 'a' is 0-3, while in Figure 'b' is 0-5.

The water vapour sorption isotherms are obtained by plotting mass increment (endpoint at equilibrium) against each humidity level. These plots for cycle 1 and 2 of 15 min and 90 min milled samples have been shown in Figures 2.9a and 2.9b respectively.

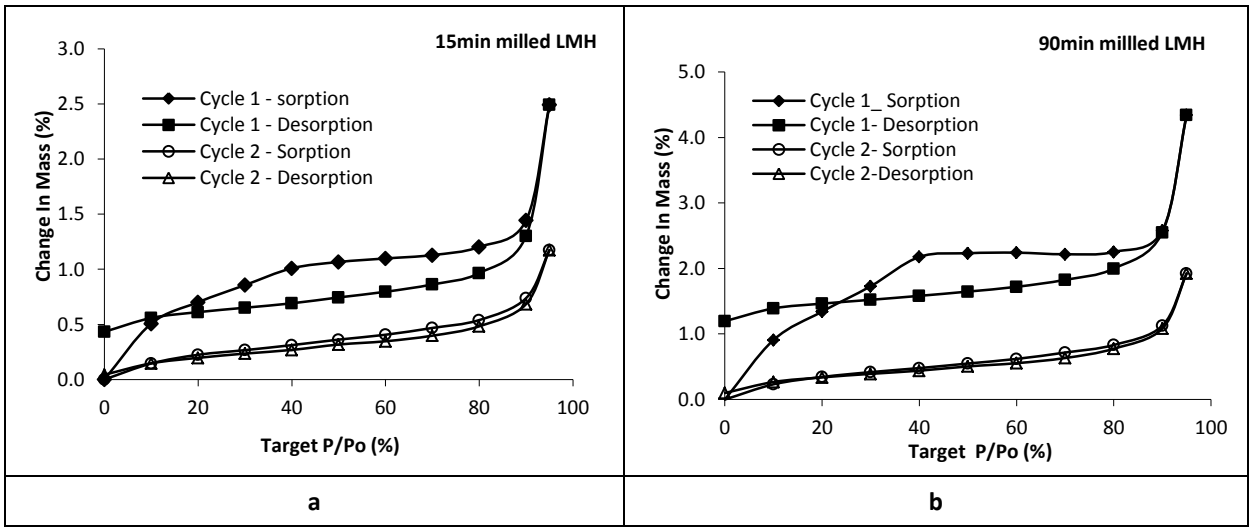

Figure 2.9: DVS isotherm plots for a) 15min milled and b) 90min milled lactose monohydrate for cycle-1 (filled marker) and cycle-2 (open marker).

The cycle 1 shows a clear difference between the total vapours ~~up~~ taken up and desorbed, as indicated by a wide hysteresis gap across the humidity range which narrows down during cycle-2. This indicates that both the milled samples contain amorphous content, most of which recrystallize to hydrated lactose after sorption in cycle 1. Hence, there is hardly any

change in mass during the cycle-2. The early sharp rise in mass followed by a slow increase after 40% humidity indicates that the sorption of water vapours occurs in two steps; probably because of the presence of particles of different size that sorb water at different rates.

It is also worth to note that these samples still hold some water (0.433% in 15 min milled and 1.195% in 90 min milled sample) even after desorption in cycle1 is complete. This might represent the weight used in forming the hydrated crystals during re-crystallization. The weight retained by each sample at the end of desorption cycle can be used to calculate the amorphous content in these milled samples (Burnett et al., 2004). Based on the assumption that the 100% amorphous lactose if re-crystallized completely: would retain 5.26% water (18 g H_2O/342 g of anhydrous lactose to form 1 mole of stoichiometric monohydrate). Therefore, the 15 min and 90 min milled sample contains 8.23% (0.433/5.26) and 22.72% (1.195/5.26) amorphous content, respectively.

Another way to estimate the amorphous content from DVS results is to consider the water uptake by the test sample at a particular level of relative humidity and comparing it to 100 % amorphous of that material. At 55% RH the water uptake by 15 min milled LMH was ~1.08% while it is ~2.24 % for 90 min milled sample. By comparing these values to the DVS isotherm of 100% amorphous lactose *i.e.* ~11% (Burnett et al., 2006), the amorphous content in these milled samples was calculated. The amorphous content in 15 min and 90 min milled sample was 9.84% (1.08/11) and 20.33% (2.24/11), respectively.

2.3.6 Inverse Gas Chromatography Results

2.3.6.1 Dispersive and Specific (Acid-base) Surface Energies

Dispersive (γ_S^D), specific or acid-base (γ_S^{AB}) and total surface energy (γ_S^T) profiles of 15 min and 90 min milled LMH are obtained directly from the IGC SEA (Figures 2.10a-c). These profiles are energetically heterogeneous; as the surface energy changes with surface coverage. In addition, it can be observed that the dispersive component contributes a major part of the surface energy in both milled samples.

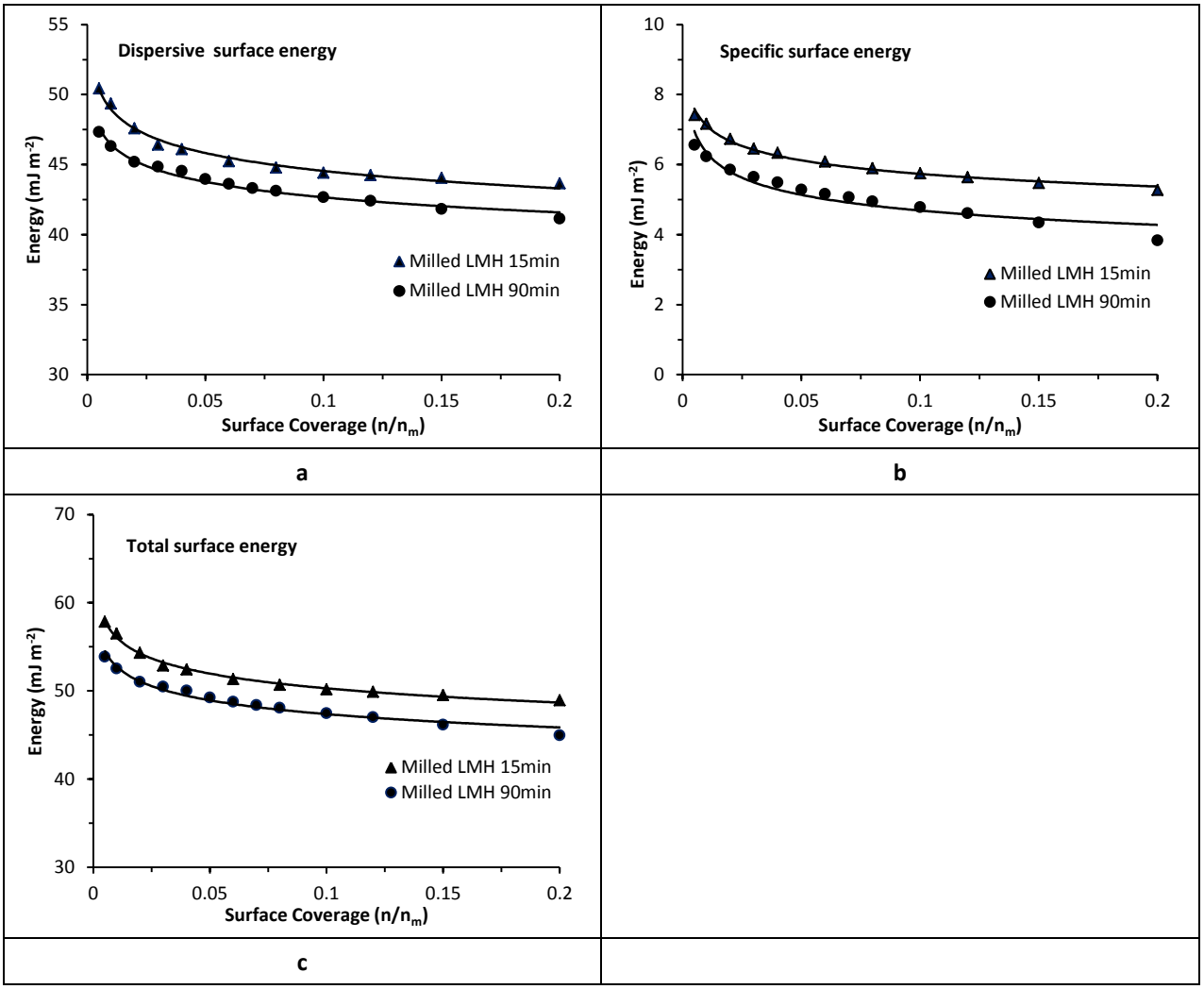

Figure 2.10: The plots of a) dispersive surface energy b), specific energy and c) total surface energy of both 15 min and 90 min milled lactose monohydrate samples.

The value of dispersive energy at zero coverage (corresponding to the infinite dilution) of 15 min and 90 min milled samples were 51 and 47 mJm^{-2} respectively (Table 2.4). These values are in agreement with (Thielmann et al., 2007), and higher than the dispersive energy of un-milled lactose monohydrate *i.e.* 31.2 mJ m^{-2} which is taken from literature (Newell et al., 2001). The increase in surface energies of LMH is expected as the milling increase in surface area and surface domain of amorphous content as shown by BET and DVS analysis, respectively. It is interesting to note that the total surface energy of longer milled (90 min) sample is less than the short milled (15 min) one, indicating that the surfaces which were active with more surface free energy on short milling become less active on long milling. This was in agreement with the results of SEM and BET where the aggregation of particles and decrease in surface area was observed in comparison with the previous milling time point *i.e.* 15 and 45 min.

Table 2.4: Dispersive (γ_S^D), specific (γ_S^{AB}) and total (γ_S^T) surface energy distribution of milled lactose monohydrate.

	Dispersive (γ_S^D) energy (mJ m^{-2})			Specific (γ_S^{AB}) energy (mJ m^{-2})			Total surface energy (γ_S^T) (mJ m^{-2})		
	Min	Average	Max	Min	Average	Max	Min	Average	Max
Un-milled LMH	-	31.2*	-	-	-	-	-	-	-
Milled LMH 15min	44.04	45.38	51.20	5.34	5.73	7.47	49.46	51.18	58.64
Milled LMH 90min	41.15	42.27	47.17	3.58	4.12	6.47	44.85	46.49	53.63

* Values taken from literature (Newel, 2001)

2.3.7 Broadband Dielectric Spectroscopy Results

2.3.7.1 Percolation Phenomenon

The dielectric response of un-milled lactose monohydrate is presented as 3D spectra constructed between imaginary permittivity (ε″) against frequency and temperature (Figure 2.11a) and shows a simple response surface with a single peak at 5 °C. This peak is due to the water, as evidenced by decrease (~50%) in peak height on drying (Figure 2.11b) as the same sample is measured during the back run of the experiment. Therefore this peak is assigned as percolation and occurs because of water (proton) hopping over the hard crystalline surfaces of the un-milled particles of LMH (Smith G., 2007). The shape of percolation peak also appears to have changed in the dried sample; it is now broader, less symmetrical and extends to lower temperatures (*i.e.* the peak starts at -50 °C as compared to -30 °C in case of original sample).

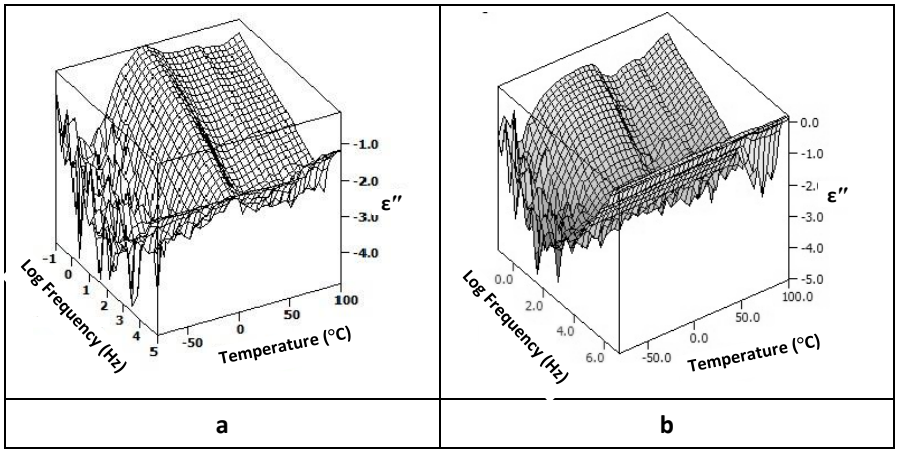

Figure 2.11: 3D dielectric spectra of un-milled lactose monohydrate before and after drying (a & b respectively), showing the plots of imaginary permittivity (ε″) vs temperature and frequency.

2.3.7.2 Effect of Particle Size on Percolation

The 3D dielectric spectra of large particles (45 through to 100 mesh) of lactose monohydrate shows only one percolation peak between 0 °C and 5 °C (shown by arrow heads in Figure 2.12a-d). This peak became broader as the particles size decrease from 45 mesh to 60 and 85 mesh. In samples with further smaller particles (100 mesh), this peak becomes again sharp with the appearance of shoulders on the sides of main peak as highlighted by dotted circle in Figure 2.12d.

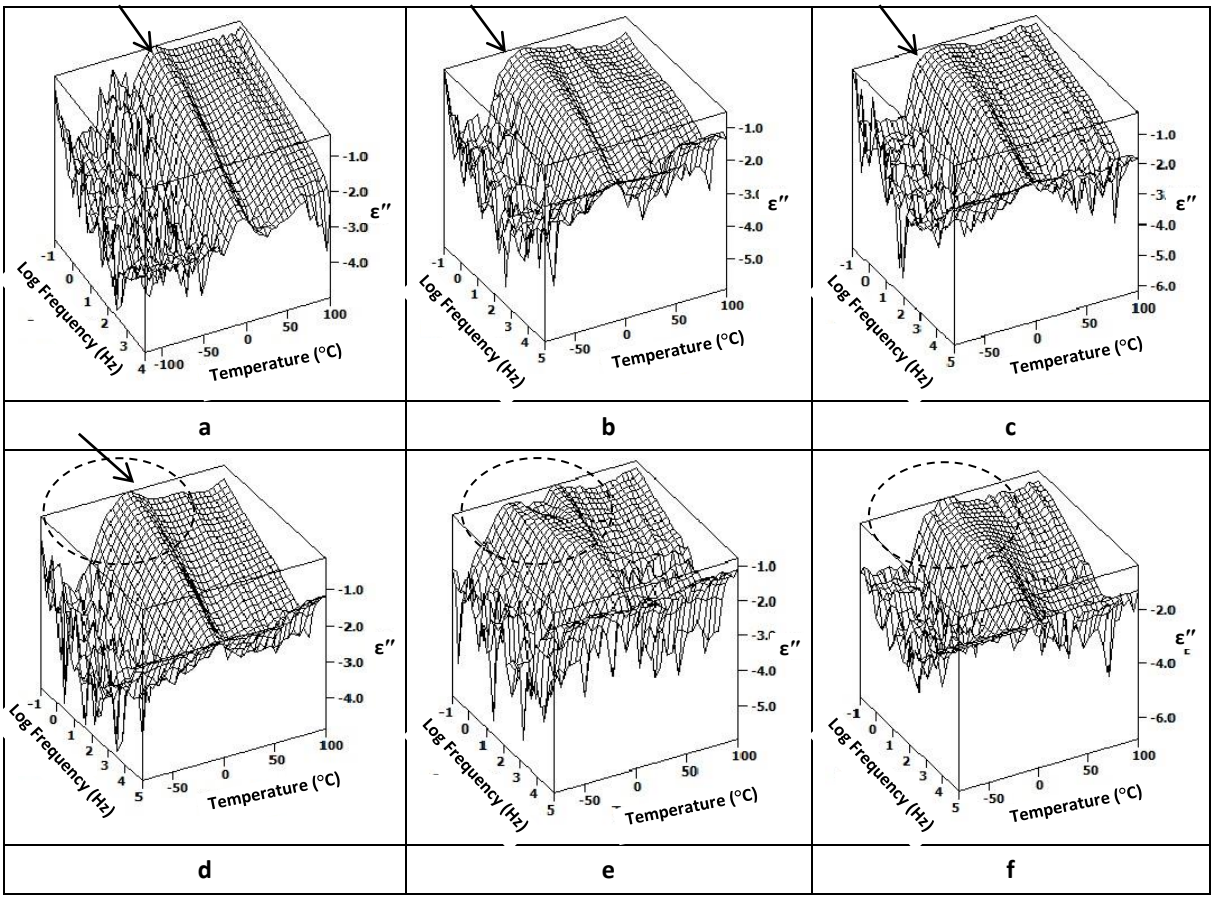

Figure 2.12: 3D dielectric spectra of lactose monohydrate samples having different particle size distribution a) 45mesh, b) 60mesh, c) 80mesh, d) 100mesh, e) 150mesh and f) 200mesh. The arrow heads indicate the position of percolation peak while the dotted circles highlight the change in shape of spectra around the percolation.

In the samples with relatively smaller particles (150 and 200 mesh), the dielectric spectra apparently contain two to three peaks (as shown by dotted circle in Figure 2.12e & f) and these occur at much lower temperatures (between -20 to 10 °C) than the percolation peak in the larger size range particles. It seems more probable that the shoulders around percolation that started in 100 mesh particles become sharper in 150 and 200 mesh particles and the

shape of spectra (particularly of 150 mesh) looks like a horse shoe with the percolation peak present in the middle.

The appearance of percolation peak in different mesh size samples of LMH at almost the same temperature (0 - 5 °C) is contrary to our previous results *i.e.* T_p is proportional to $1/d_2$ (Smith G., 2007). However, the results of 150 and 200 mesh suggest that although the particle size affects the percolation process, it is the path length available for proton hopping that defines the percolation temperature. The path length is influenced by other factors including: i) moisture content, ii) aggregation and iii) surface energies of the particles.

2.3.7.3 Effect of Ball Milling on the Percolation of Lactose Monohydrate

The dielectric spectrum of the short milled lactose monohydrate (*i.e.* 15 min milled) showed that the percolation splits into two peaks, both having a huge magnitude as compared to the un-milled sample (Figure 2.13a). The first percolation peak (indicated as PP1 in Figure 2.13a) is sharp while the second percolation peak (PP2) is relatively broad and occurs towards the higher temperature side.

On the other hand, in long milled samples (≥ 45 min) where the magnitude of process drops again, a change in the dielectric spectra occurs; *i.e.*, the shoulders appear on both sides of the percolation peak (Figure 2.13b). These shoulders gradually grow in height as milling progresses (Figure 2.13c) and the spectrum takes the saddle-shape (this shape resemble horse shoe) in 180 min milled sample (Figure 2.13d), with the percolation present in the centre. On further milling beyond 180 min the shoulders of this process decrease in 270 min milled sample (Figure 2.13e) and the percolation again becomes conspicuous at 360 min milled sample with the disappearance of saddle shape (Figure 2.13f). Appearance of such saddle shape in the dielectric spectrum was previously ascribed to the water confined in the porous glasses or to the complex materials (Ryabov et al., 2001, Feldman et al., 2002). This will be discussed in detail in Section 2.3.7.5, here we return to some more description of percolation phenomenon.

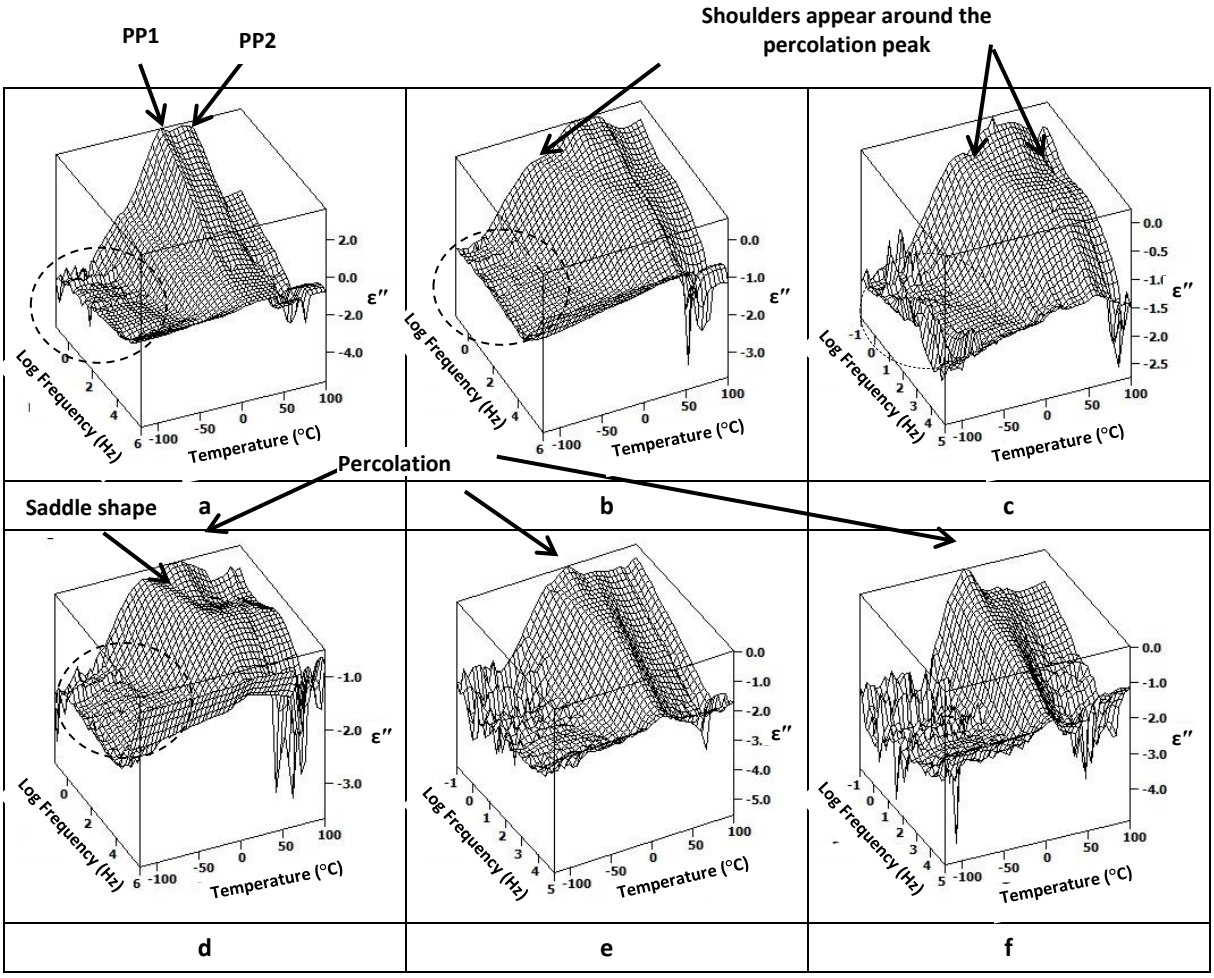

Figure 2.13: 3D dielectric spectra of various samples of lactose monohydrate a) 15min, b) 45min, c) 90min, d) 180min, e) 270min and f) 360min. PP1 & PP2 represent first and second percolation peaks in short milled samples. The saddle-shape develops in long milled samples that disappear on further milling. The dotted circles highlight the low temperature window where the processes linked with amorphous phase (γ and β processes) are not prominent.

The percolation phenomenon in different milled samples of LMH is analysed i) qualitatively (by measuring its temperature change with milling time), ii) quantitatively (by measuring the amplitude of this process) and iii) by expressing this process in time domain to determine the dipole correlation function that may be helpful in defining the fractal dimension of the milled samples.

Percolation Temperature: The temperature slices from the dielectric loss spectra of milled samples of LMH at 0.1 Hz are given in Figure 2.14, while at four different frequencies (Figure 2.15) has shown that the single percolation peak of un-milled sample splits into two peaks in 15min milled sample (Figure 2.15a). The first percolation peak (PP1) occurs at 5 °C, similar to the un-milled sample, while the second peak (PP2) occurs at 30 °C. The temperature of both percolation peaks shifts towards higher side with milling time till 90 min and then decreases

on further milling (Figure 2.15c & f). The 360 min milled sample has the percolation again at 5 °C. These values have been summarised in Table 2.5.

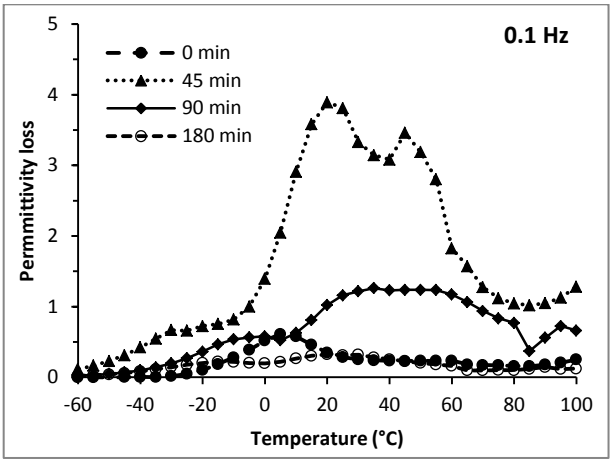

Figure 2.14: Temperature slices at 0.1Hz frequency from the dielectric spectra of a) un-milled and 45min, 90min and 180min milled of lactose monohydrate.

Table 2.5: Values of temperature of first and second percolation peaks (PP1 & PP2) for the milled samples of lactose monohydrate.

Milling time (min)	Percolation temperature (°C)	
	1st	2nd
0	5	-
15	5	30
45	20	45
90	35	55
180	20	30
360	5	-

Amplitude of Percolation: In short milled sample of LMH (15 min milled), the amplitude of both percolation peaks (PP1 & PP2) is enormously higher than that in the un-milled one (Figure 2.15a & b). However, in longer milled samples (45 and 90 min milled), the amplitude of percolation drops but it is still higher than that of the un-milled one (Figure 2.15c & d). In 180 min milled sample the percolation decreases to less than that in un-milled one but increases again in 360 min sample (Figure 2.15e & f).

The milling of LMH results in the release of water along with the size reduction. This water then adsorbs onto the lactose particles or small fragments (which still have a 'hard surface'), hence results in the continued observation of the first percolation peak– though now much bigger) while the appearance of second percolation peak represent the presence of internalized surfaces. May be the exact mechanism depends on surface water coverage (*i.e.*

the concentration per unit area). However, it is a complex phenomenon which seems to be dependent on many factors simultaneously.

At the same time, the size reduction and amorphization promote the packing of powder bed which therefore requires more energy for the percolation of charges through it (this is a different argument to scale length being linked to particle size). Hence the temperature of percolation increases in the milled samples. However, in 360 min milled sample where the small particle aggregate (SEM micrographs, Appendix I) and the amorphous phase re-crystallizes (residual crystallinity start increasing at 90 min milling, thus the powder bed is less compact and results in the occurrence of percolation at lower temperature. The regain of hard crystalline surfaces at this milling point also results in the increase in amplitude of percolation.

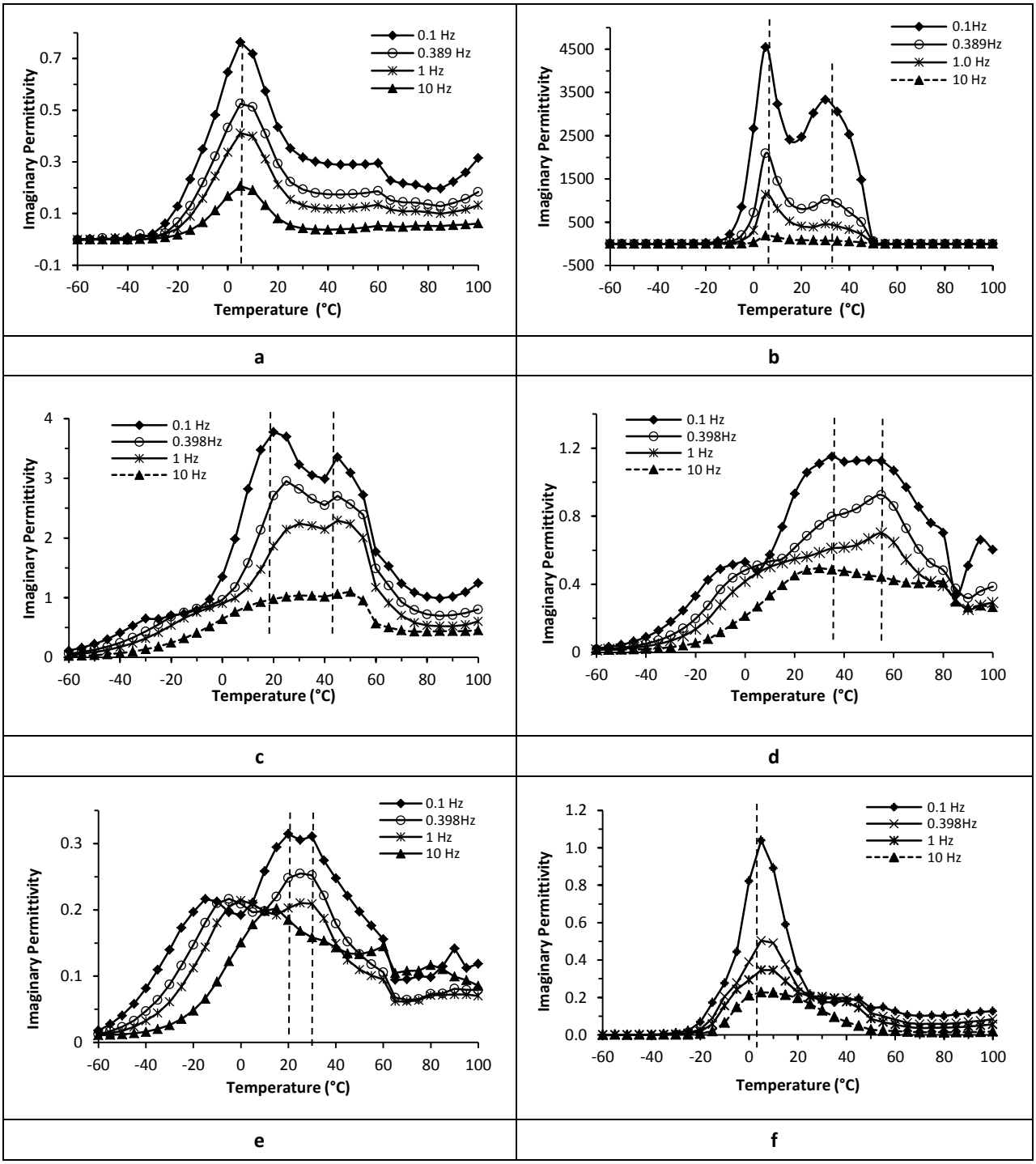

Figure 2.15: Temperature slices (plots of imaginary permittivity (ε") vs temperature) at various frequencies from the dielectric spectra of a) un-milled and b) 15min, c) 45min, d) 90min, e) 180min and f) 360min milled of lactose monohydrate. The vertical dotted lines show the temperature of first and second percolation peaks respectively.

The enormous increase in amplitude of percolation in short milled sample is presumably because of the following reasons

i. At the start of milling the creation of surface cracks and fragmentation of particles results in generation of a large number of new surfaces (as evident from laser

diffraction, SEM and BET results, Section 2.3.1, 2.3.2 and 2.3.3, respectively) that are available for percolation as the surfaces were still crystalline and leads to the reduction of percolation path for proton diffusion.

ii. Increased moisture in milled sample which is released on disrupting the monohydrate crystals adsorbs onto the surfaces of particles (TGA results have shown higher water content in milled samples).

However, on milling beyond 15 min, the amplitude of percolation peak abruptly drops, although the surface area is still high (the particle size of 45 min milled sample is smaller than 15 min one). The one reason might be the less proportion of water which is driven off by the raised temperature of the mill. Another reason to explain the decrease in peak height in long milled samples is the presence of amorphous surfaces. The intimate interaction between water and the multi-hydrogen bonding opportunities provided by the amorphous phase (basically the defects within it) would reduce the frequency of proton exchange/slow the proton flux through the material.

Therefore, the height of the peak is dependent on the water percolating on the hard crystalline surfaces while the shift in percolation temperature would be associated with changes in surface area available for the diffusion of water. Basically, there is a change in the diffusion path length that might be either path 1 or path 2 (Figure 2.16 a-b) or combination of these.

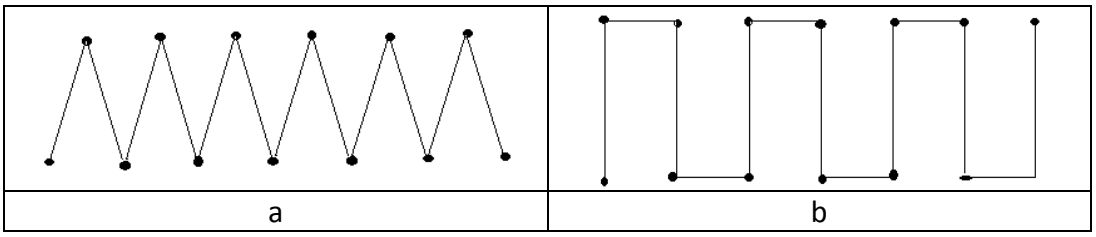

Figure 2.16: Proposed paths 1 and 2 (a & b) for the hopping of protons that are responsible for percolation peaks in the dielectric spectra of milled lactose monohydrate.

The percolation processes so observed for hard crystalline materials has led to the partial development of a method for characterizing the amorphous external surface with hard internal surface of micronized particles. In particular the observation of a second percolation process in milled lactose and the observation of a saddle shaped process appear to suggest that clusters of water appear in the material on extended milling. We speculate in general that the observation of these processes might be indicative of the internalized surfaces, *i.e.*

surfaces inside the particles that are associated with defects in the crystal structure and that these might provide additional routes for water to penetrate the crystal resulting in an increased dissolution rate.

The milling of anhydrous sugar clearly show the evidences of the amorphous phase in dielectric spectra (Chapter 4), while in case the hydrated materials the signatures of amorphous phase are not prominent rather a complex behaviour was observed that is dictated by the presence of water released from the wreaked hydrated crystals. A comparison of dielectric properties around the percolation of this monohydrate sugar with that of anhydrous (sucrose) and dihydrate (trehalose) is given in Appendix IV.

2.3.7.4 Changes in Fractal Dimensions and Porosity on Milling

The dielectric results at percolation have indicated that the milled sugars behave like porous material that provides a network of interconnected channels through which the electric excitation travels across the material. This transfer of excitation can be described by using the dipole correlation function (DCF) (Puzenko et al., 1999). The DCF is obtained by expressing the dielectric relaxation spectrum at the percolation temperature in the time domain (*i.e.* by Fourier transform (FT) of the frequency domain data obtained from the dielectric analyser).

This is accomplished by the plotting the frequency slices at percolation temperature of the dielectric spectra of each milled sample (Figure 2.17 a & b). One can see immediately that the strength of the process increases dramatically after 15 min of milling and appears to shift to higher frequencies. After selecting the appropriate frequency range (0.1-10 Hz) the time domain data are obtained by IFT.

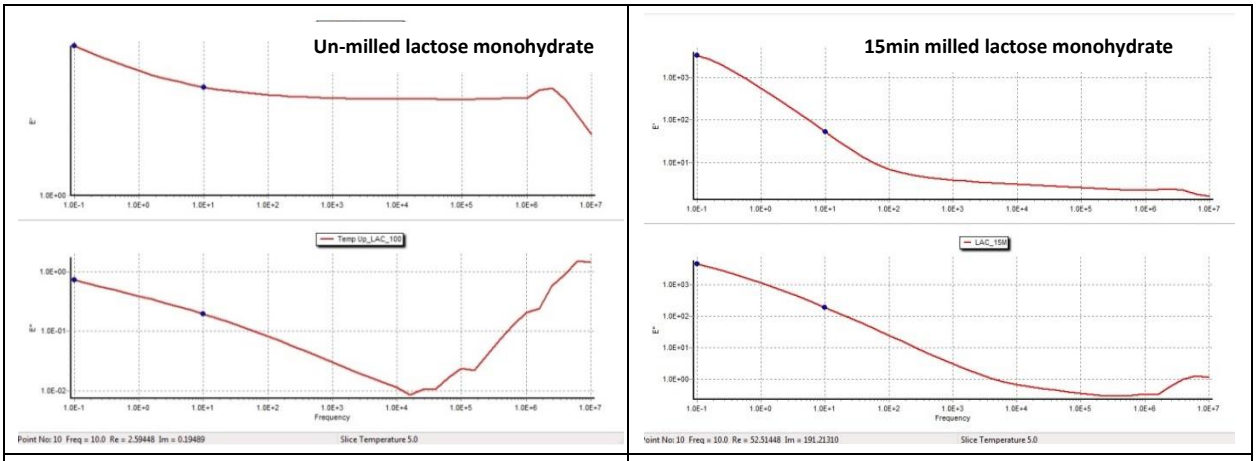

Figure 2.17: Screen shots showing the frequency slices at percolation temperature from the dielectric spectra of a) un-milled b) 15min milled. The frequency range selected for IFT have been shown by dots on these plots.

The frequency slices on the imaginary permittivity plots of un-milled and short milled (i.e. 15 min) sample shows a single relaxation process. Based on these observations, it can be concluded that only the short milled samples show Debye relation and therefore DCF can be used to describe the fractal dimension for this sample. Whereas in long milled samples where the particle start aggregating (as evidenced by BET and SEM results, 2.3.1 and 2.3.2, respectively) and the amorphous content also increase (DVS results, Section 2.3.5), the fractal dimension cannot be estimated from the DCF.

As the DCF displays complex non-exponential time behaviour (non-Debye), a stretched exponent function of Kohlrausch-Williams-Watts (KWW) given in Equation 2.3 is used to fit the data in Datafit-9 software (Oakdale Engineering).

$$\mathbf{Y = a * exp(-(x/\tau)\text{^}\nu) + x * d + e} \qquad \textbf{Equation 2.3}$$

Where 'Y' is diploe correlation function, 'a' and 'd' are the intercept and slope of fit line respectively, 'τ' is relaxation time and 'ν' is stretching exponent while 'e' is a constant. The plot of DCF vs time for un-milled and milled LMH (Figure 2.18) has shown that this 5-parameter function fits well to the data.

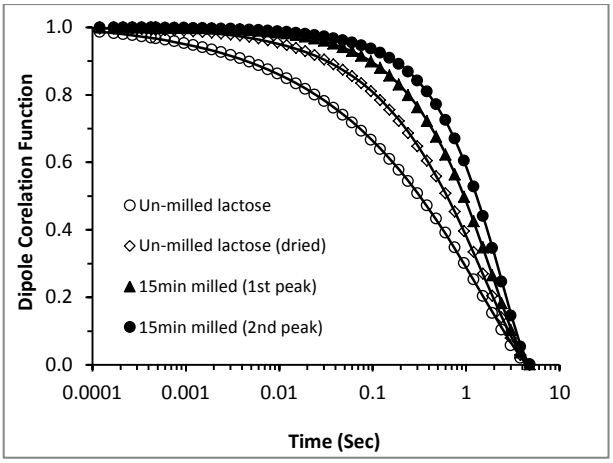

Figure 2.18: Time domain plots of the dielectric spectra of un-milled and milled lactose monohydrate showing plot of dipole correlation function (DCF) against time at percolation temperature. The solid lines represent the fit function.

Now using the values of this stretched exponent (ν), the fractal dimension (D_f) of un-milled and milled LMH are obtained by using the Equation 2.4. These values are summarized in Table 2.6.

$$\mathbf{D_f = 3\nu} \qquad \textbf{Equation 2.4}$$

The value of fractal dimension for un-milled LMH is approximately equal to unity, indicating the propagation of the excitation occurs along a linear path with lot of hydration centres as present with each molecule of un-milled LMH. However, in the dried sample of un-milled LMH the value of fractal dimension is between 1 and 2 may imply that the excitation now occurs through the hydration centre present on the inner pore surface (which is developed by the evaporation of water from the sample). In the short (15 min) milled sample, the value of D_f calculated from both percolation peaks is between 2 and 3, which indicates a more three dimensional path, possibly due to the presence of ultra-small porous structure (cracks/fissures) produced within the milled material. The huge increase in the magnitude of the percolation process at this milling point is likely to be a consequence of the water of hydration being dislocated (released) from the crystal lattice which may now propagate through fault lines (defects) within the lattice to provide for extensive 3-dimensional percolation paths for protons (Gutina et al., 2003). The fractal dimension of this sample is approximately equivalent to that of rough pore surface *i.e.* 2.5 (Agamalian et al., 1997).

Table 2.6: Values of stretched exponent obtained from the fitting of dielectric data at percolation temperature of un-milled and milled samples of lactose monohydrate and the fractal dimension calculated from it.

Material	Stretched exponent (ν)	Fractal dimension (D_f)
Un-milled lactose	0.36	1.06
Un-milled lactose (dried)	0.57	1.70
15min milled (1st peak)	0.79	2.36
15min milled (2nd peak)	0.95	2.84

In summary, the dielectric excitation linked with percolation gives the useful information on the fractal geometry of milled hydrated material. This is important in explaining the presence of internalized surfaces present in the milled materials that contribute to the enhanced surface area available for dissolution or water sorption in such materials.

2.3.7.5 Relaxation Processes in Dielectric Spectra of Milled Lactose Monohydrate

An important observation about the dielctric spectra of milled LMH is that the low temperature (γ and β) process characteristics of the amorphous phase (as discussed in chapter 4) are absent (the region is highlighted by dotted circles in Figure 2.13). Rather a small temperature dependent process with a typical saddle shape is observed in long milled samples of LMH (≥ 45 min milled). The changes in dielectric spectra around this process have been described in section 2.3.7.3, where it is shown that this process is most prominent in 180 min milled sample, probably because of some or all of the following reasons:

i. The particles size is uniform at 180 min milling point and it is close to that of the 150 or 200 mesh samples (where this process was also present- Figure 2.12e & f). In both cases the nano-sized particles form clusters of 500 nm to 1000 nm.
ii. The amorphous content sample is maximum in 180 min milled and there is no further reduction in crystallinity even after 90 min milling (as described in Chapter 3).
iii. This sample also has a reasonably high proportion of surface moisture, including both the moisture adsorbed from environment by the newly created soft surfaces and that which is released from the hydrated crystals on milling (as discussed in Section 2.3.4).

The characteristics of this saddle shaped process are better understood by making frequency slices (f-slices, the plot of imaginary permittivity against frequency at different

temperatures) through the dielectric spectra of the 180 min milled sample. The plot shows that this process starts in the low frequency side of the experimental window at a temperature of -50 °C and shifts toward higher frequencies with increasing the temperature till 40 °C from where it again returns towards low frequencies indicating the temperature dependence nature of this process (Figure 2.19).

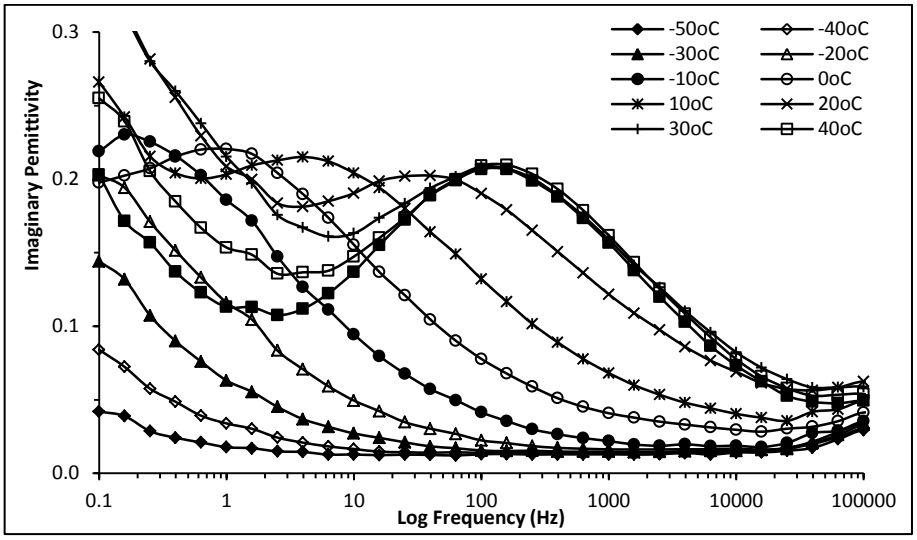

Figure 2.19: Frequency slices (obtained by plotting the imaginary permittivity against log of frequency) from the dielectric spectrum of 180min milled lactose monohydrate.

The plot of relaxation time against the inverse of temperature for this process of 180 min milled sample shows Arrhenius behaviour at low temperatures (-10 to +20 °C) but as the temperature increases above +20 °C, it shows deviation from this behaviour (Figure 2.20).

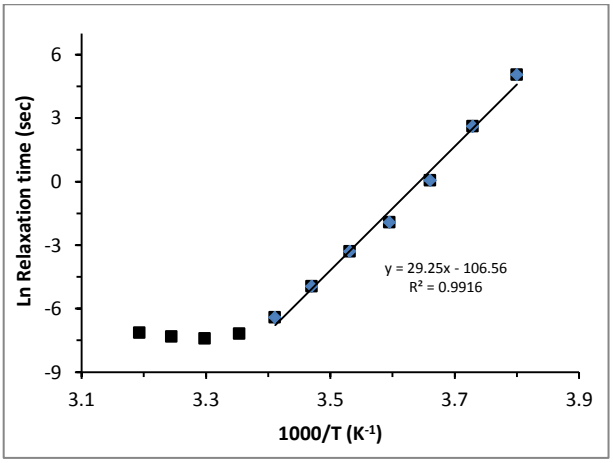

Figure 2.20: Plot of natural log of relaxation time against inverse of temperature for 180min milled lactose monohydrate. The plot shows Arrhenius trend towards lower temperature but deviate from this behaviour towards higher temperatures.

The activation energy calculated from the linear part of this plot is ~240 KJmol^{-1}, which is comparable with the activation energy of α-relaxation of sugars/monosaccharide *i.e.* 205 – 450 KJmol^{-1} (Noel et al., 2000). From this behaviour one might surmise that the saddle shaped process is the structural relaxation of the amorphous phase. Looking for the other possibilities the dynamic glass transition temperature is calculated from the relaxation time (τ = 100sec) for this process. This value is -9 °C for 180 min milled sample, which is lower than one might expect for an amorphous disaccharide. However, the presence of water in such systems has changed the cooperative relaxation of the amorphous phase with the scale length close to the cooperative units and therefore one can expect the confinement dynamics. The confinement of the amorphous phase can decrease the glass transition temperature, which then has implications on the stability of such material (Kremer and Schönhals, 2003, Noel et al., 1996).

Now there are two possibilities;

i. Confinement of water molecules in nano-porous structure of disordered LMH OR
ii. Amorphous phase confined within thin domain on the surface of milled particles.

In order to test the second hypothesis; firstly, it is assumed that the amorphous phase is restricted to a thin uniform layer on the surface of milled spherical particle (Figure 2.21) and from the limiting size (~100 nm from SEM) the volumes of external (total) and internal (without amorphous layer) particles are calculated using the Equation of volume of sphere (Equation 2.5).

$$\mathbf{V = \frac{4}{3}\pi r^3} \qquad \textbf{Equation 2.5}$$

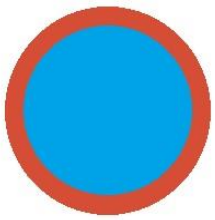

Figure 2.21: A hypothetical spherical particle having a thin surface layer of amorphous phase as indicated by red external circle.

The scale length of amorphous phase is then obtained from the difference of radii of two spheres. The scale length for 180 min milled samples is ~3.9 that indicates the confinement

of the amorphous phase but whether confined or not depends on the scale length of the domain in relation to the scale of the minimum cooperative unit which is un-known for amorphous disaccharides.

Secondly, the glass transition temperature of this phase is obtained from the amorphous content and the moisture present in the milled sample by applying Gordon-Taylor equation (Equation 2.6) as used by (Roos, 1995) and compared with the T_g of bulk amorphous phase *i.e.* from DSC results.

$$\mathbf{T_g} = \frac{\mathbf{w1T_g1 + Kw2T_g2}}{\mathbf{w1 + Kw2}} \qquad \textbf{Equation 2.6}$$

The calculated value of T_g for 180 min milled lactose monohydrate is ~42 °C, that is very close to the measured value from DSC *i.e.* 47 °C. This suggests that the amorphous phase is not confined on the surfaces of particles as presumed; rather it is more likely concentrated within a few domains across the surface. In real state of the particle is probably someway in between the two extremes, A and B (Figure 2.22).

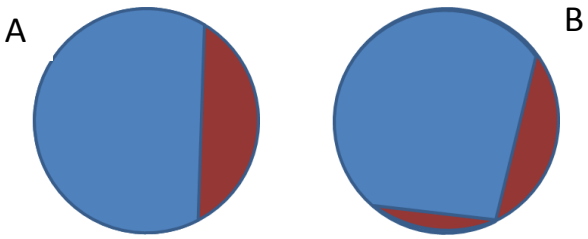

Figure 2.22: Proposed location of amorphous phase (red colour) in supposed spherical particles.

Therefore the saddle shape might be the confined structured water in the vicinity of defects of milled lactose. Given that the activation energy of this process is quite high than the bulk ice (Gutina et al., 2003), again there is difficulty to consider that the water alone is responsible for such response of the milled LMH. Therefore, it is assumed that the complex system with porous geometry developed in the milled LMH that consisted of amorphous, crystallites and water is responsible for the behaviour like the adsorbed water in porous glasses as already reported (Feldman et al., 2003).

In summary, the changes brought about by milling with their mechanism and implication on the solubility and dissolution rate have been summarized in Table 2.7.

Table 2.7: Summary of changes brought about milling as measured by different techniques and their mechanistic effect on the solubility/dissolution rate of solid materials.

Changes brought about by milling	Analytical techniques	Observation	Key implication	Mechanism
Particle size reduction	SEM BDS	Actual change in particle size and surface topography (specific surface area) Shift in percolation peak to higher temperature	Dissolution rate improvement	Increase in surface to volume ratio
Surface and internal cracks on particles	BDS BET	Internal surfaces provide routes for percolation within inside the particles resulting in the appearance of new, high temperature percolation peaks Increase in specific surface area	Dissolution rate improvement	Infiltration of water into the particles
Partially damaged crystal lattice	DSC (results discussed in Chapter 3, Section 3.3.2.1)	For crystal hydrates a shift in desorption peak to lower temperature. Shift in melting peak and reduction in enthalpy of melting.	Solubility enhancement	Increased ease by which water leaves the crystal structure (through a reduction in the crystal hydrates energy) may also support the opposite effect of increased ease by which water penetrates the crystal during the process of dissolution
Amorphous phase generation	TGA DSC BDS DVS	Decrease in bound water loss peak Shift in desorption peak to lower temperature Shift in melting peak and reduction in enthalpy of fusion A process of dielectric relaxation in typical horse shoe shape DVS isotherm show hysteresis gap between sorption and desorption curve	Solubility enhancement	Changes in thermal analysis indicate the change in phase (generation of phase with compromised crystalline structure or with totally disordered structure *i.e.* amorphous phase).
Change in moisture content of powder	TGA	Shift in onset of desorption peak to lower temperature Increase in surface water loss in milled material.	Solubility enhancement	Increased water has plasticizing effect on the powder that might increase its solvation.
Change in surface energy	IGC	Increase in dispersive and specific surface energy	Solubility enhancement	Higher surface energy makes the solution faster

2.4 Conclusion

Ball milling can produce nano-structured systems in the milled hydrated material (lactose monohydrate). These systems consisted of water, damaged crystals along with amorphous phase. The nitrogen adsorption technique has shown an increase in surface area (linked with the smaller particle in milled material). However the dielectric spectroscopy has revealed the presence of cracks and fissures thus expose the more surfaces present in the milled materials. The increase in surface energies on long milling causes the clustering of particles and they develop the fractal geometry of porous structures. These observations may be important in explaining the enhancement of dissolution in materials that are milled for a short period (before any amorphous phase is generated). The presence of surface domain of

amorphous phase although show the bulk characteristics in DSC but the characteristic dielectric behaviour indicated that the amorphous phase, rather exist as a complex system in milled hydrated material and its characteristic might be different.

3 Quantification of Crystallinity/Amorphicity of Ball Milled Pharmaceuticals (lactose and ibuprofen) using Thermo-Analytical Techniques and Terahertz Pulsed Spectroscopy

3.1 Background/Context

The generation of amorphous phase from crystalline is the objective of many studies that intend to enhance the solubility and dissolution rate of poorly soluble drugs, milling is one of such techniques (detailed in Chapter 1). However, unless the residual crystalline material or newly generated amorphous phase is quantified, the contribution of milling (in terms of milling times and ball-oscillation frequencies) towards the solubility and dissolution rate enhancement cannot be explained. This quantification is also important in order to control the milling process as well as explaining the impact of milling on the stability of these materials during storage.

The quantification of the residual crystalline/amorphous content in milled materials is challenging because these materials are complex and contain a range of disordered entities from partially defected crystalline particles to wholly amorphous phases (Caron et al., 2011). These states within a milled material, particularly the presence of crystalline seeds and the extensive surface area of the amorphous phase, make them very sensitive to temperature and moisture. It is therefore necessary to develop an appropriate technique which can quantify the degree of residual crystallinity which can then be used to assess the stability of these materials.

The techniques commonly employed for quantification of the crystalline material include dynamic vapour sorption (DVS), isothermal micro-calorimetry, differential scanning calorimetry (DSC), hyper-DSC, near infra-red (NIR), Raman spectroscopy and powder X-ray diffraction (PXRD). Some of these are based on the analysis of the crystalline phase (PXRD, NIR) whereas others (Hyper-DSC, DVS and Microcalorimetry) are based on the analysis of the amorphous phase, while DSC can determine both the crystalline and amorphous phases.
DVS is based on water vapour sorption and may give misleading results for materials in which the crystals also sorb water, alongside the amorphous phase under scrutiny. Organic vapour sorption is a possible alternative method (Young et al., 2007) but this technique is not universal in its application. Isothermal micro-calorimetry detects the heat associated

with the sorption of water by the amorphous phase but it requires the crystallization of the amorphous to be favoured kinetically (Dilworth et al., 2004).

PXRD might be considered as gold standard for measuring crystallinity but the results are inconsistent as it requires the preferred orientation of crystals in the path of X-ray beam, therefore whole pattern fitting is required for the complete characterization of a powder (Shah et al., 2006). Also it can give wrong results if the sample is not prepared adequately particularly the particle size, distribution and pre-treatment are critical (Buhrke et al., 1998). Measurement of crystallinity by Raman spectroscopy can induce photochemical reaction in the materials. In NIR, amorphization is inferred from a shift in the baseline of the spectral region rather than any changes in the specific absorption peaks (Buckton et al., 1988), therefore the first or second derivative of spectra are taken for quantification of amorphicity (Bai et al., 2004). In addition, the NIR measurements are influenced by moisture (Shah et al., 2006). Although both these vibrational techniques (Raman and NIR) are sensitive and quick, each requires a complex multivariate calibration curve to be constructed from known crystalline and amorphous mixtures (Buckton and Darcy, 1999).

TGA measures the weight change associated with loss of adsorbed water (if any) and the water of crystallization, in the case of a hydrated material. From the weight of the latter, the changes in crystallinity in milled hydrated materials may be estimated (Buckton et al., 1998, Chidavaenzi et al., 1997). In order to use the TGA technique, one has to assume that the water of hydration in the residual crystalline material (within the milled material) provides an opportunity to quantify the proportion of un-damaged crystalline material remaining. However, there is always the possibility that the hydration water of the partially compromised crystalline particles will behave differently than the material in its native state, resulting in some uncertainty in the estimates of crystallinity so derived.

DSC is routinely used for the analysis of crystalline/amorphous materials. The crystallinity may be determined from the analysis of either the crystalline form or the amorphous state. The endothermic event associated with the melting of the crystalline phase that remains post milling may be used to determine the change in crystallinity on milling. However, the presence of an amorphous phase in a milled material may also manifest in the thermogram as a step in the baseline (indicating a glass transition) and/or exothermic peak in the thermogram (indicating a de-vitrification event). This de-vitrified amorphous phase will then

contribute to the enthalpy of melting. Therefore one must subtract this contribution from the enthalpy of crystallization, in order to calculate the crystalline content of the milled material prior to analysing the DSC data.

Terahertz pulsed spectroscopy (TPS) is a relatively new technique that has been used for the characterization (Strachan et al., 2004) and quantification (Strachan et al., 2005) of the crystallinity of APIs. TPS produces pulses in the femtosecond time scale and therefore has the ability to probe crystal lattice and hydrogen bonding vibrations, which occur at frequencies in the low terahertz region (0.1 – 4 THz). The intensity of the specific absorption peaks can be used to quantify the degree of crystallinity in a mixed phase system. This technique has also been employed to differentiate hydrous and anhydrous forms (Liu et al., 2007) and for studying dehydration process in various pharmaceuticals (Zeitler et al., 2007). This technique has been used recently for the measurement of crystallinity in amino acids (Darkwah et al., 2013) and freeze dried sugars (Ermolina et al., 2014).

In this chapter, TPS was used for the determination of residual crystallinity in milled pharmaceuticals; the results were compared to that of the thermal methods (DSC and TGA) in an attempt to highlight the issues with the latter techniques for quantification of residual crystallinity.

Two types of lactose (monohydrate and anhydrous) were used in this study to demonstrate the effect of milling on hydrated and anhydrous crystals in term of changes in crystallinity or anomeric composition. The lactose monohydrate and anhydrous lactose studied in this work were taken from commercial sources and therefore there is inevitably a proportion of the sample which is in other *i.e.* alpha or beta lactose (Raymond C Rowe, 2003). The residual crystallinities quoted throughout this chapter are therefore stated as a relative measure of the change in crystallinity from the original starting material. To that end the term relative residual crystallinity (RRC) has been adopted.

Ibuprofen is also used in this study. Milling of this drug at room temperature has not been studied yet because of its low melting temperature (*i.e.* ~80 °C). However, the short time milling that reduces its particle size and damages the crystals may be useful for imparting a positive effect on the dissolution rate of this drug. The estimation of extent of damage to the crystalline structure of this drug on milling is the focus of this study.

3.2 Materials and Methods

Lactose monohydrate (as described in Section 2.2) was used in this study. Anhydrous lactose was also used in this study for the comparison with its hydrated counterpart. It was purchased from Fluka, UK and used as received from the supplier. It was a fine crystalline powder and contained mainly beta lactose with a small proportion of alpha lactose. It is commercially produced by roller drying a solution of lactose above 93.58°C. The resulting product is then milled and sieved and contains 70–80% β-lactose and 20–30% α-lactose (Raymond C Rowe, 2003).

Note: The lactose monohydrate used in this study is alpha lactose monohydrate and abbreviated as LMH or α-LMH, while the anhydrous lactose is beta lactose and abbreviated as β-LA.

Ibuprofen was purchased from Fagron, UK and used as received from the supplier. It was a white crystalline powder with characteristic odour. The ibuprofen exists as acicular crystals in SEM having the approximate particle size between 10 to 60 µm.

3.2.1 Ball Milling

Milling of both types of lactose was performed as per method described in Section 2.2.1 using milling speed of 18 Hz and time till 60 min. However in case of ibuprofen, the speed of 15 Hz and time interval of 30 min was used to avoid the risk of vitrification of this drug.

3.2.2 Thermogravimetric analysis (TGA)

TGA of un-milled and milled materials was carried out according to the method already described in Section 2.2.4.

3.2.3 Differential Scanning Calorimetry (DSC)

DSC experiments were performed according to the method described in literature (Hurtta et al., 2004) using a Jade DSC (Perkin Elmer, US). The heating rate and heat flow were calibrated at 20 °C min^{-1} using indium and zinc standard. Approximately 7 mg sample was taken in 50 µL aluminium pans, sealed non-hermetically with perforated lids to allow the evaporation of water and then loaded in the analyser by the auto-sampler. All samples were analysed over the temperature range 25 °C to 250 °C (in case of ibuprofen the range was 25 to 110 °C) at the heat flow rate of 20 °C min^{-1}, applying the calibration of 20 °C min^{-1}. The

crystallization temperature was reported as the onset of exothermic peak while melting temperatures was taken as the midpoints of endothermic peaks. The residual crystalline content was calculated from the enthalpy of melting and/or crystallization.

3.2.4 Terahertz Pulsed Spectroscopy (TPS)

3.2.4.1 Sample Preparation

The samples for THz measurement were prepared by manually mixing polyethylene (PE) powder with spatula (at room temperature and humidity conditions, 23 °C and 40%, respectively) with un-milled lactose monohydrate (at concentrations of 4%, 6%, 8%, 10% and 12% w/w) or milled LMH (10% w/w). PE powder was provided by Teraview, UK and used as the THz blank. The geometrically mixed samples were pressed to the disc shaped pellets using Gamlen Tablet Press (CT5, Gamlen Tableting Nottingham, UK- shown in Figure 3.1) with a compaction force of 500 Kg. The weight of each pellet was of ~400 mg and thickness of 3.80 ± 0.08 mm. The same weight pellets containing 100% PE were also prepared to act as a reference.

Figure 3.1: Gamlen tablet press CT5 used for the preparation of pellets for THz measurement, photograph taken from our lab.

3.2.4.2 Terahertz Measurement

The experimental setup and principles of terahertz pulsed spectroscopy (TPS) have been documented well in the literature (Beard et al., 2002, Dorney et al., 2001, Yamamoto et al., 2005, Taday et al., 2003, Strachan et al., 2005).

Terahertz spectra were acquired in transmission mode by TPS spectra 3000 (Teraview Limited, UK – shown in Figure 3.2a). Each terahertz waveform was obtained by averaging

900 scans applying the frequency of 30 scans per second and spectral resolution of 1.2 cm^{-1}. The reference pellet (PE alone) and all samples were individually placed in a 13 mm (diameter) sample holder, which helps to focus the terahertz beam onto the centre of the pellet (Dorney et al., 2001). The sample is placed into a compartment (Figure 3.2b) which is dried by purging with nitrogen gas for 10 min prior to and during each measurement. All samples were prepared in triplicate and the THz spectrum of each pellet was measured at three different points across its diameter and mean was taken of the resultant 9 measurements (n = 9).

a b

Figure 3.2: Photograph of a) THz spectroscopy unit (TeraView 3000) and b) sample holder unit and assembly, taken from google images of Teraview webpage.

3.2.4.3 Principal of operation of THz Pulsed Spectroscopy

A schematic operation of THz spectroscopy has been shown in Figure 3.3. THz spectrometer contains cryogen cooled heat detectors (bolometer) that acts as photoconductive switch. A laser beam of femtosecond pulses (Titanium sapphire NIR laser, 800 nm) splits into two by the splitter placed in its way, one of which after attenuated to 25% is focused on semiconductor material with switch open. This generates the electron hole pairs that are accelerated by the applied field through substrate generating the THz radiations. A parabolic mirror is used to collimate and reflect the beam of radiation into the test material. Another set of mirrors is used to collimate and reflect the transmitted radiations on to the detector. The second laser reflected from the beam splitter (attenuated by 75%) is combined with the transmitted beam from the test material and focussed on the detector. A photo-diode detector is applied to detects and monitor the changes in probe beam. The output signal is

amplified and recorded as change in electrical field as a function of time which is then converted to frequency domain spectra by inverse Fourier transform (Storey and Ymen, 2011).

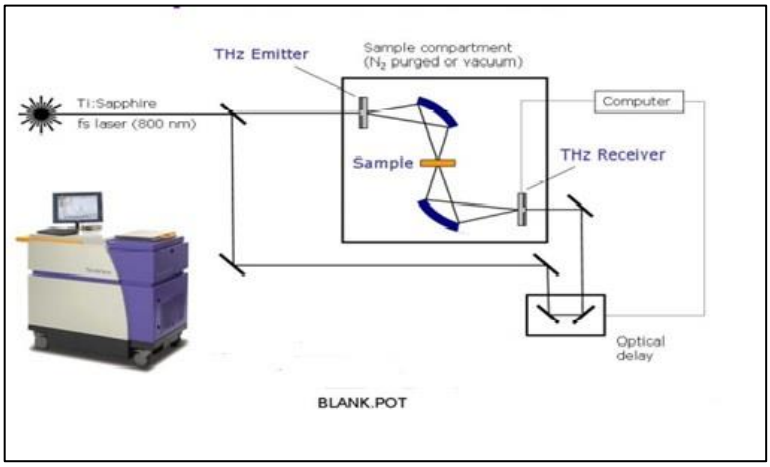

Figure 3.3: Flow diagram showing of Terahertz operation (Taday, 2004).

3.3 Results and Discussion

3.3.1 Thermogravimetric Analysis Results

The TGA results of un-milled and milled lactose monohydrate have been described in Chapter 2, Section 2.3.4. Using those results, the relative residual crystallinity (%RRC) in the milled samples was calculated from the weight loss linked with desorption of the water of crystallization (Table 3.1), having assumed that the starting material of crystalline lactose monohydrate contains 5% water of crystallization (Dilworth et al., 2004).

Table 3.1: **The values of weight changes corresponding to desorption of water of crystallization of un-milled and milled lactose monohydrate and the relative residual crystallinity (%RRC) calculated from these values.**

Milling time	Onset temp of desorption (°C)	Weight loss of crystallization water (%)	Residual Crystallinity (%)
0	144.0	5.0*	100.0
10	106.0	3.8	76.8
15	112.0	3.6	71.4
30	102.0	3.4	69.0
45	107.0	3.9	79.0

*from the stoichiometric ratio of water in lactose monohydrate

The results have shown that the estimates for residual crystallinity decreases erratically with milling time(Table 3.1), with the most significant decrease in crystallinity occurring over the first 10 min where there is ~25% loss in crystallinity. There is an approximate ± 10% variation

in estimates of crystallinity in all milled samples of LMH (between 65% to 75%) thus, it is not clear as to whether there is a progressive decrease in crystallinity as the milling time increases beyond 10 min.

3.3.2 Differential Scanning Calorimetry Results

3.3.2.1 DSC Curves of Un-milled Lactose (Monohydrate and Anhydrous)

The DSC curve of **un-milled lactose monohydrate** (Figure 3.4a) shows one endothermic peak with an onset temperature of 144 °C corresponding to the release of water of crystallization (as evident from TGA results in Figure 3.4a), followed by one melting endotherm at 222 °C associated with the melting of α-lactose. Such DSC results of LMH are in agreement with the data reported by (Gombas et al., 2002, Moolchandani et al., 2014) but contrary to the observations in these studies, whereas they have shown two melting peaks (corresponding to the alpha and beta forms of lactose), we observe only one melting endotherm.

DSC results of **anhydrous lactose** are described in Chapter 4, Section 4.3.1, here only the DSC curve (Figure 3.4b) is given for the purpose of comparison with monohydrate.

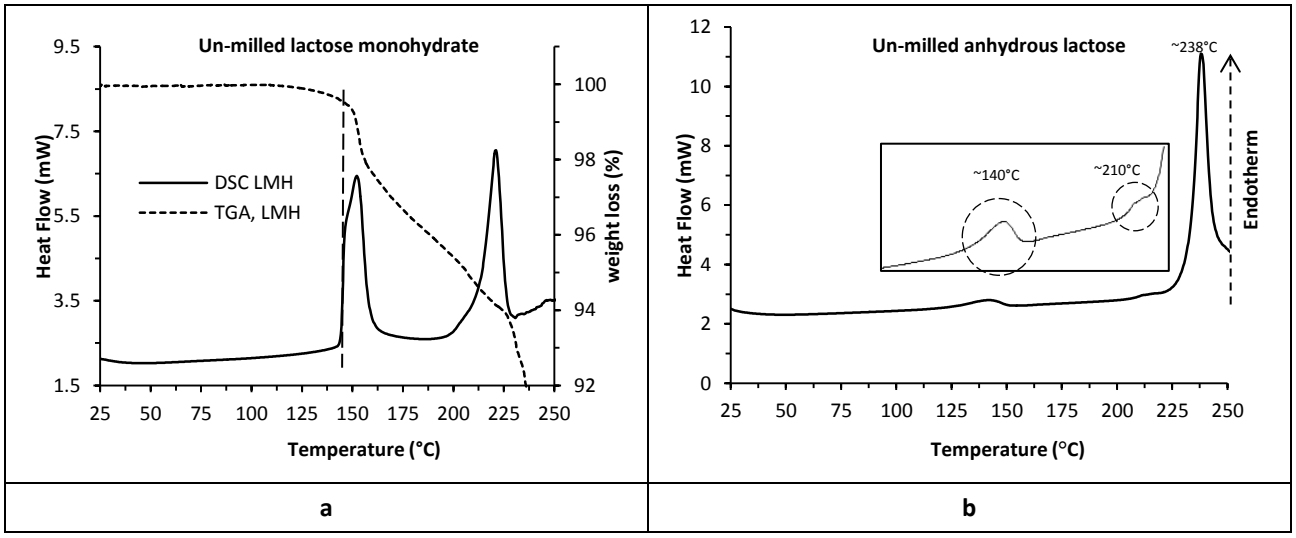

Figure 3.4: a) DSC curve of un-milled lactose monohydrate overlaid by its TGA curve showing the onset temperature for desorption of water of crystallization ~ 144°C as indicated by the dotted line, b) DSC curve of un-milled anhydrous lactose showing melting endotherm at 238°C, the inset highlights the endotherm of desorption at 140°C and melting endotherm of α-lactose at 210°C.

3.3.2.2 DSC Curves of Milled Lactose (Monohydrate and Anhydrous)

The DSC curves of milled LMH (Figure 3.5a) have shown that the desorption event splits into two peaks, first broad peak between 116 °C and 143 °C followed by a relatively sharp peak between 131 °C and 157 °C. The melting peak also splits into two peaks; the first occur from

210 °C to 222 °C while the second occur from 227 °C to 236 °C. These peaks represent the melting of α and β forms of lactose, respectively (Garnier et al., 2008).

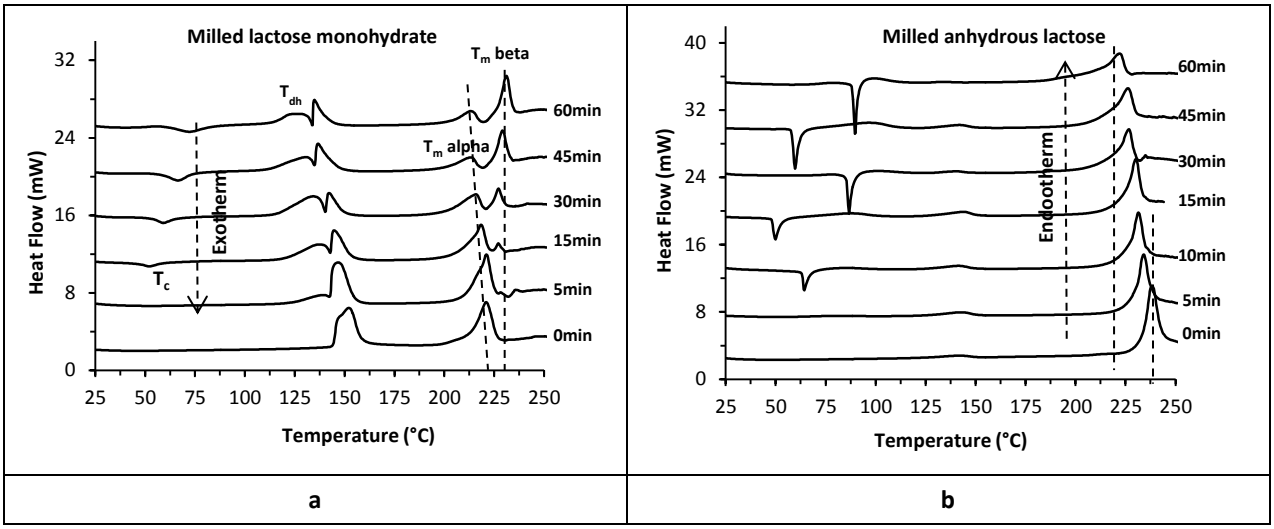

Figure 3.5: a) DSC curves of milled lactose monohydrate (a) and anhydrous lactose (b). The milling time intervals have been indicated against each curve. The dotted lines represent the change alpha form to beta or vice versa. The downward and upward arrows indicated exotherm and endotherm respectively. (T_c = temperature of crystallization; $T_{m\ alpha}$ = melting temperature of alpha lactose; $T_{m\ beta}$ = melting temperature of beta lactose; T_{dh} = temperature of desorption of water of crystallization).

In samples milled for 15 min or higher, an exothermic process is also observed between 52 °C and 73 °C that represents the de-vitrification of amorphous lactose. This event was previously reported at ~170 °C in fully amorphous (spray dried) or in short milled lactose (Gombas et al., 2002, Shariare et al., 2011) but in collapsed amorphous (produced by exposure of high relative humidity) it was reported at 70 °C (Darcy and Buckton, 1997). Therefore it was inferred that the milling reduces the glass transition temperature due to plasticization effect of water (released from hydrated crystals during milling). This inference is supported by the fact that the onset temperature for water desorption decrease and the percentage of un-bound water increase in the milled samples. When this milled material is exposed to heat in DSC it undergoes structural collapse at a reduced T_g and gives a low temperature re-crystallization peak. This structural collapse was complete as we did not observe the high temperature crystallization peak (Darcy and Buckton, 1997).

Mutarotation of lactose monohydrate (i.e. conversion of α-form of lactose to the beta form or vice versa) is observed in the milled samples which is induced by heat and the presence of water during the DSC run (Garnier et al., 2002a, Garnier et al., 2002b). The area of the de-vitrification peak and the ratio of the melting peak for beta lactose (as compared to alpha peak) increases as the milling time increases up to 60 min. This suggests that as the damage

to the crystals increases, there is a greater proportion of amorphous lactose and a greater propensity to produce beta lactose. Therefore, it was inferred that the de-vitrified amorphous lactose forms β-lactose either at the de-vitrification temperature or it first re-crystallizes to the α-form (McIntosh et al., 2013), which subsequently undergoes mutarotation on heating to produce the beta form. Therefore, the greater the amorphous content, the greater is the structural collapse and the greater will be the β-anomer content in the lactose sample (Gombas et al., 2002, Shariare et al., 2011, Buckton, 1997).

DSC results of **milled anhydrous lactose** are described in Chapter 4, Section 4.3.1, here only the DSC curves (Figure 3.5b) are given for the purpose of comparison with monohydrate.

The DSC curve of milled samples of anhydrous lactose have revealed the transfer from beta to alpha form of lactose particularly at 60 min milling point (Figure 3.5b), where the largest de-vitrification peak is observed among all the milled samples. This indicates that the amorphous phase de-vitrified to alpha form that gives the melting endotherm at ~217 °C. The results of TPS do not confirm this transfer as there is no peak related to of alpha lactose in milled samples of β-LA (see THz results, Figure 3.8b). This is contrary to the reports of the early 1990s (Otsuka et al., 1991), that there occur ~20% mutarotation of lactose on milling. Instead we suggest that mutarotation is merely an artefact occurred during DSC experiment and not a real transition due to milling (Willart et al., 2004). However the featureless THz spectrum of 60 min milled sample confirmed the DSC results that this sample has the highest amorphous content. The overlaid DSC curves of lactose monohydrate and anhydrous lactose have been given in Appendix V for a comparison of the changes that occur on milling.

3.3.2.3 DSC Curves of Un-milled and Milled Ibuprofen

The DSC curve of **un-milled Ibuprofen** (Figure 3.6a) showed a single endothermic peak at 79.9 °C representing the melting of ibuprofen with the value of enthalpy of melting as 116.46 Jg^{-1}. The temperature of melting peak is in agreement, while the value of enthalpy is less than that already reported in literature (Madhuri Newa and Bong Kyu Yoo, 2008). The DSC curves of **milled ibuprofen** at the milling times of 2.5 to 30 min heated from the room temperature have shown only a single melting peak with the melting temperature almost similar in all milled samples (indicated by dotted line in Figure 3.6b). However, the milled sample annealed and heated from negative temperature (-60 °C) have shown a de-vitrification peak with onset temperature at ~25 °C similar to that observed in amorphous

(quenched cooled) ibuprofen (event 'B' in Figure 3.6a). However, it does not show T_g step in contrary to quenched sample (event 'A' in Figure 3.6a).

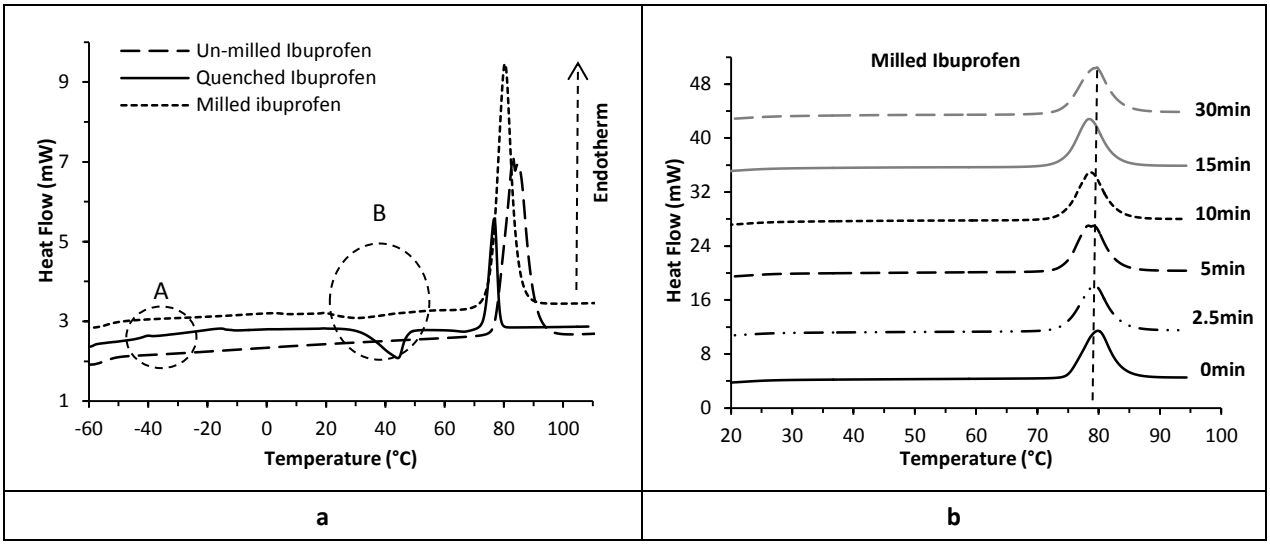

Figure 3.6: a) DSC curves of un-milled; 15min milled and quenched ibuprofen. The dotted circle 'A' shows the T_g step as present only in quenched ibuprofen and the circle 'B' highlights the de-vitrification peak as a mark of amorphous phase present in quenched and milled sample. b) DSC curves of milled ibuprofen for different times, when heated from room temperature single only melting peak is observed.

3.3.2.4 Estimation of Relative Residual Crystallinity from DSC Data

The relative residual crystalline (%RRC) content in milled samples (*i.e.* that proportion of the original starting material which has retained its native state and has not undergone a transformation to either another crystalline state, a partially damaged state, or a wholly amorphous state) was calculated from DSC data by following two methods.

DSC Analysis Method 1 is based on the approach taken from the literature (Phillips, 1997). This method takes the enthalpy of melting peak and divides it by the melting enthalpy of the 100% crystalline material to provide the assessment of the remaining crystalline phase (Equation 3.1).

$$\mathbf{X_c}(\%) = \frac{\mathbf{\Delta H_{m,}}}{\mathbf{\Delta H_{m,}(100\%\ crystalline)}} \times \mathbf{100} \qquad \textbf{Equation 3.1}$$

where X_c is the estimate for residual crystallinity, $\Delta H_{m,}$ is melting endotherm (Jg^{-1}).

This method is used only for lactose monohydrate where the assumptions is that, the second melting endotherm from the anhydrous β-form is merely an artefact of the DSC method, as it is generated from the de-vitrification of the amorphous phase and therefore is not used in the calculation.

For anhydrous lactose and ibuprofen where amorphous phase re-crystallizes, the calculation of residual crystallinity is based on the approach taken from literature (Van den Mooter, 2012). This involves the subtraction of enthalpies of crystallization and melting, which yields the enthalpy due to the initial crystallinity of different milled samples; and then dividing it by the enthalpy of fusion of the pure crystalline sample (Equation 3.2).

$$\mathbf{X_c}(\%) = \frac{\mathbf{\Delta H_m - \Delta H_c}}{\mathbf{\Delta H_m(100\%\ crystalline)}} \times \mathbf{100} \qquad \textbf{Equation 3.2}$$

here ΔH_c is enthalpy of crystallization of the amorphous phase of lactose or ibuprofen.

Given that there is significant variation in the enthalpies of melting of alpha lactose as reported in literature (Table 3.2) it was not possible to select any one value that could satisfy the criteria of a reference value (Drapier-Beche et al., 1999).

Table 3.2: Literature values of enthalpy of melting (ΔH_m) of alpha (both anhydrous and monohydrated) and beta (anhydrous) lactose.

Reference	Material used	ΔH_m(Jg^{-1})
Drapier. et. al, 1999	α-lactose monohydrate (used as received from Sigma, Germany)	134
Ticehurst et. al, 1996	α-lactose monohydrate (Four different batches used as received from Lactochem, Netherland)	125 101 87 92
Dilwarth et al, 2004	α-lactose monohydrate (used as received from Borculo Whey Product U.K.)	169
Caron et. al.2011	Anhydrous α-lactose (Dehydration of lactose monohydrate from Sigma)	151
Drapier. et. Al, 1999	Anhydrous α-lactose (Dehydration of lactose monohydrate from Sigma)	122
Drapier. et. Al, 1999	Anhydrous β-lactose (treatment of lactose monohydrate from Sigma)	198
Dilwarth et al, 2004	Anhydrous β-lactose (treatment of lactose monohydrate from Borculo Whey Product U.K.)	197

Therefore in our study, the molar heat of fusion for the un-milled lactose monohydrate and anhydrous lactose of ΔH_m as 115.2 Jg^{-1} and 173 Jg^{-1}, respectively were taken as reference values, and the residual crystallinity in milled samples represented as the percent relative residual crystallinity (%RRC) of the starting material. Similarly for ibuprofen 116.5 Jg^{-1} was taken as reference value.

DSC Analysis Method 2 is used for both types of lactose (monohydrate and anhydrous). This method is based on the approach taken from (Lehto et al., 2006), whereby the amorphous content 'X_a' is first estimated from the enthalpy of de-vitrification of the milled material divided by the enthalpy of de-vitrification of a 100% amorphous material using Equation 3.3.

$$\mathbf{X_a}(\%) = \frac{\mathbf{\Delta H_c}}{\mathbf{\Delta H_c(100\%\ Amorphous)}} \times \mathbf{100} \qquad \textbf{Equation 3.3}$$

The 'ΔH_c' value (105 Jg^{-1}) of 100% amorphous (spray dried) lactose was taken for calculations (Lehto et al., 2006). The crystalline content was then determined by applying Equation 3.4.

$$\mathbf{X_c}(\%) = \mathbf{100} - \mathbf{X_a}(\%) \qquad \textbf{Equation 3.4}$$

3.3.2.5 Results of Residual Crystallinity from DSC Data

Milled lactose monohydrate: The results of residual crystallinity of milled LMH by DSC method 1, are in contrast to methods 2; in that there is monotonous decrease in %RRC with milling time up to 60 min where it reaches ~25% (Table 3.3). The DSC analysis method 2, shows the monotonic trend in %RRC with milling time similar to method 1, but it produces higher estimates for %RRC compared to the method 1 (*i.e.* ~75% at 60 min milling which is ~25% in method 1).

Table 3.3: Values of enthalpies of de-vitrification (ΔH_c) and melting (alpha form) (ΔH_m) of milled lactose monohydrate sample and the estimates of relative residual crystallinity based on these enthalpies.

Milling time (min)	ΔH_c (Jg^{-1})	ΔH_m (α) (Jg^{-1})	Residual Crystallinity (%) (DSC Method 1)	Residual Crystallinity (%) (DSC Method 2)
0	-	115.2	100.0	100
5	-	100.2	86.9	100
15	13.6	67.2	58.3	87.0
30	16.6	49.9	43.4	84.1
45	26.6	35.3	30.6	74.7
60	26.6	29.8	25.9	74.6

Milled anhydrous lactose: DSC method 1 has indicated that there is a monotonic decrease in crystallinity, where there is a 50% loss of %RRC in first 15 min of milling. Afterward the loss is gradual after 30 min of milling (Table 3.4). The 60 min milled sample has shown a ~70% loss of residual crystallinity.

DSC method 2, shows a similar monotonic trend in the loss of crystallinity with milling time but it over estimates the amount of residual crystallinity compared to method 1, probably because this method is based on the de-vitrification process. At the scan rate of 20 °C min^{-1} there may be insufficient time for complete de-vitrification to occur. Moreover, there is loss of sensitivity at early time points where the amorphous content is too low to observe the de-vitrification peak.

Table 3.4: Values of enthalpies of de-vitrification (ΔH_c) and melting (alpha forms) (ΔH_m) of milled anhydrous lactose and the estimates of residual crystallinity based on these enthalpies.

Milling time (min)	ΔH_c (Jg^{-1})	ΔH_m (Jg^{-1})	Residual Crystallinity (%) (DSC method 1)	Residual Crystallinity (%) (DSC method 2)
0	Nil	173.2	100	100
5	Nil	125.9	72.7	100
10	20.8	119.5	57.0	80.2
15	26.1	113.9	50.7	75.1
30	37.6	97.8	34.8	64.2
45	42.9	105.3	36.0	59.1
60	41.8	96.9	31.9	60.2

Milled ibuprofen: The estimates of residual crystallinity from the only method applied to DSC data of milled ibuprofen (method 1) decreases gradually with the milling time. However this reduction is very small as compared to the both types of lactose there is only ~15% loss in 30 min of milling (Table 3.5).

Table 3.5: The values of enthalpies of de-vitrification (ΔH_c) and melting (ΔH_m) for milled ibuprofen and percentage crystallinity calculated from these values.

Milling time	ΔH_c (Jg^{-1})	ΔH_m (Jg^{-1})	Residual Crystallinity (%)
0	-	116.5	100.0
2.5	-	115.2	98.9
5	-	111.5	95.8
10	5.6	110.9	90.4
15	7.9	108.9	86.7
30	8.7	107.1	84.6

3.3.3 Terahertz Pulsed Spectroscopy Results

3.3.3.1 THz Spectrum of Un-milled Lactose Monohydrate

THz time domain signals are attenuated by the presence of lactose in the path of beam indicating the absorbance of THz waves, while the other small deflections are due to the complex permittivity of this molecule. The solid state THz spectrum of un-milled lactose monohydrate in transmission mode has shown four absorption peaks at 0.52, 1.18, 1.37 and 1.80 THz corresponding to 17.3, 39.2, 45.2 and 60.1 cm^{-1} (as indicated by letters A-D on Figure 3.7a). Also there is another peak near 82 cm^{-1}, and the spectra become noisy in this region particularly in the samples with higher concentrations of LMH in the pellet (Figure 3.7b).

The first and third peaks (Peak 'A' and 'B' at 0.52 and 1.37 THz, respectively in Figure 3.7a) are considered as the signatures of LMH (Brown et al., 2007) and these peaks are assigned to

the intermolecular vibrations of hydrogen bonded crystalline structure (Euna Jung and Kiwon Moon, 2008) or more specifically the peak at ~0.52 THz to a hindered rotational mode of a particular axis of its crystals (Allis et al., 2007). The peaks at 1.18 and 1.80 THz (Peak 'C' and 'D', respectively in Figure 3.7a) are because of the beta lactose present in the samples of lactose monohydrate. This is supported by the comparison of THz spectrum of α-lactose monohydrate to that of the beta lactose (commercial source) by highlighting the peaks by dotted lines in Figure 3.7a and 3.7c.

The THz spectrum of anhydrous lactose (Figure 3.7c) has shown three peaks at 39, 45 and 61 cm^{-1} indicated as peak B, C and D, respectively. The peak at 45cm^{-1} (peak B) represents the presence of a small amount of the alpha lactose in the sample of anhydrous beta lactose (its signature is also present in the THz spectrum of the alpha lactose monohydrate – Figure 3.7a and DSC results- Figure 3.4b). The other two peaks (C and D in Figure 3.7a) are typical to the anhydrous beta lactose (Strachan et al., 2005).

Another feature of the THz spectra of un-milled lactose was the manifestation of Mie scattering. This is the phenomenon, of increased absorbance towards higher frequencies as a consequence of the mean particle size of sample reaches the wavelength of the incidence radiation (Shen et al., 2008). Mie scattering was especially prominent in the lactose monohydrate due to the presence of large particles of approximately 150 μm in diameter (as described in Chapter 2, Section 2.3.1) and it increases as the concentration of material increases in the pellet (Figure 3.6b). While in β-LA, where the particles are relatively smaller (100 μm) this scattering is lower (Figure 3.7). In the milled samples of both types of lactose this effect is diminished (Figure 3.7 a & b) indicating the particle size reduction.

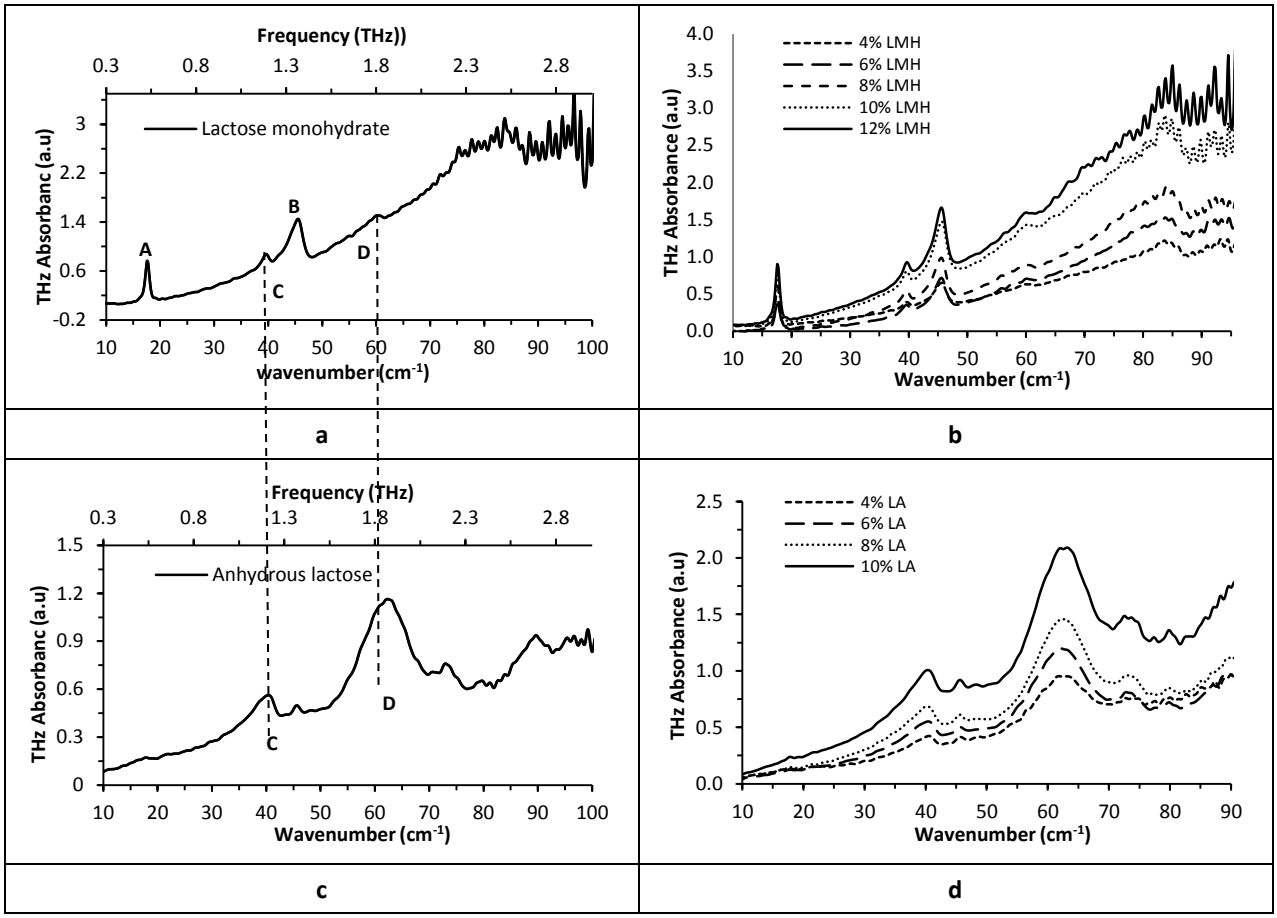

Figure 3.7: THz absorption spectra of a) un-milled lactose monohydrate and b) its different concentartions, c), un-milled anhydrous lactose and d) its different concentration. THz peaks in both types of lactose are marked as A, B, C and D. Peaks A & B represents the characteristic peaks of lactose monohydrate while peaks (C & D) represents anhydrous lactose as shown by the dashed lines dropping on the spectra of anhydrous lactose.

Note: The plots showing the time domain signals and sample spectra each of lactose monohydrate, anhydrous lactose and ibuprofen are given in Appendix VI.

3.3.3.2 THz Spectrum of Milled Lactose Monohydrate

The THz spectra of milled lactose monohydrate (Figure 3.8a) are similar to that of the un-milled LMH in terms of the position of characteristic absorption peaks. However, the intensities of the major peaks (A and B in Figure 3.7a) decrease with milling time, indicating a progressive damage to the crystalline structure. The 2nd peak (near 45 cm^{-1}) is more prominent in the short milled samples (< 10 min) but diminishes on further milling (> 10 min). The spectra of the long milled (45 min and 60 min) samples show only two peaks with a diminished shoulder of the 2nd peak and an almost flat and featureless spectrum toward longer wavenumbers, which is rather typical of an amorphous material (Strachan et al., 2005).

It is important to note that the spectral peaks of β-lactose (*i.e.* at ~39 and ~60 cm^{-1}) diminishes with milling time as shown by dotted lines in Figure 3.8a, so that the milled samples (> 30 min) contain only the traces of the beta lactose. Therefore, THz results indicate that the milling does not cause any promising mutarotation as previously reported by (Willart et al., 2004) but it is contrary to the reports of (Otsuka et al., 1991) that milling caused ~20% mutarotation.

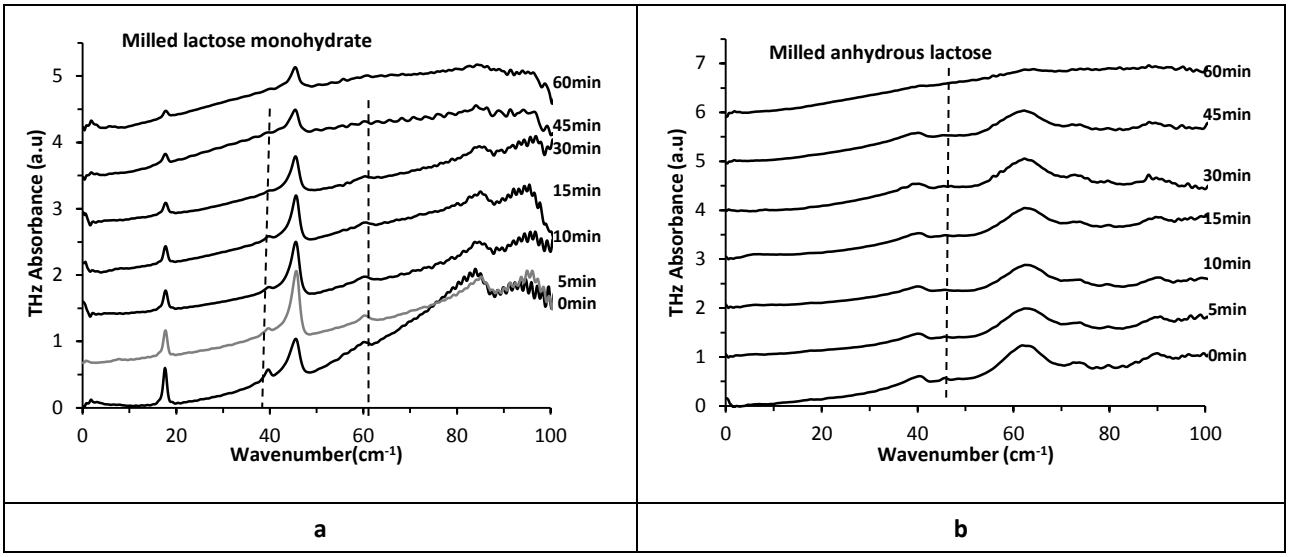

Figure 3.8: THz spectra of a) milled lactose monohydrate and b) milled anhydrous lactose for various time intervals as indicated against each curve. The dotted lines show the changes in peak heights of contaminant anomer of lactose with the milling time.

3.3.3.3 THz Spectrum of Milled Anhydrous Lactose

The spectra of the milled anhydrous lactose (Figure 3.8b) are almost similar to the un-milled one in shape but the area of major peaks (C and D in Figure 3.7c) decrease with the milling time. The small peak at 45 cm^{-1} representative of the α-LMH, which was present in un-milled samples, was also observed in short milled samples (5 and 10 min). However it disappeared in sample milled for 15 min or beyond as highlighted by dotted line in Figure 3.8b. The spectrum of 60 min milled sample is almost flat, with very small peaks at position as with the un-milled sample.

Note: The overlaid THz spectra of different milled samples of both types lactose have been given in Appendix VII to show the actual scattering and other changes in the THz absorption peaks.

3.3.3.4 THz Spectrum of Un-milled Ibuprofen

The THz spectrum of ibuprofen (Figure 3.9a) has shown only a single absorption peak at 1.035 THz corresponding to ~34.5 cm^{-1} and a noisy spectral region near 60 cm^{-1}. The phenomenon of Mie scattering (as described in case of lactose) is also observed in case of ibuprofen.

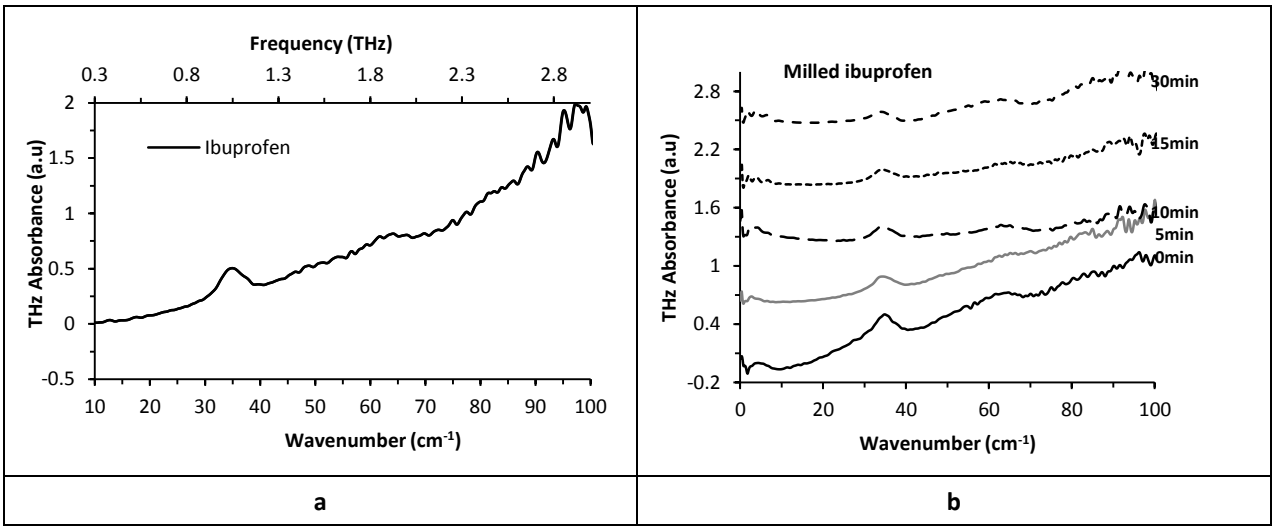

Figure 3.9: a) THz spectrum of un-milled ibuprofen showing the single prominent peak as highlighted by arrow head and increase in absorption towards higher wavenumbers (Mie scattering), b) THz spectra of milled ibuprofen for various time intervals showing the decrease in area of absorption peak as the milling time increases and the diminishing of Mie scattering in milled samples >5min.

3.3.3.5 THz Spectra of Milled Ibuprofen

The THz spectra of the milled ibuprofen for different times have indicated that the overall shape of spectra was almost the same as the un-milled one (Figure 3.9b). The notable changes are i) the intensity (measured as area) of the only absorption peak decreases as the milling time increases, ii) The raised spectra of un-milled and 5 min milled ibuprofen towards higher wavelength that represents the Mie scattering of larger particle, now trodden in milled samples.

3.3.3.6 Estimation of Residual Crystallinity from THz Data

The **THz spectral region** for quantitative analysis of each material was selected based on the largest spectral difference between its spectrum and that of the polyethylene. This region contains one representative peak in case of ibuprofen (at ~35 cm^{-1}), while two peaks for each of lactose monohydrate (first at ~17 cm^{-1} and the second ~45 cm^{-1}) and anhydrous

lactose (first at ~39 cm^{-1} and the second ~61 cm^{-1}). The other peaks are either not true representative or least prominent, therefore were ignored for quantitative analysis.

3.3.3.7 Peak Selection of Lactose for Quantitative Analysis

Among the two THz peaks of alpha lactose monohydrate (as described in Section 3.3.3.1), the first peak is sharp, has well defined start and end points and has an approximately linear baseline in both un-milled and milled samples (Figure 3.10a & b).

The second peak shows more scattering (shift of baseline in term of its gradient or offset) and presents difficulties in clearly defining the baseline, particularly in the milled samples (Figure 3.10c-f) which could lead to an under or overestimate of the residual crystallinity in milled samples. Therefore peak 1 was selected for the quantitative analysis of lactose monohydrate. The same region of THz spectrum was used previously for studying the crystallization process in amophous lactose monohydrate (McIntosh et al., 2013). Similarly, in case of anhydrous lactose peak 1 was selected for the quantitative analysis.

3.3.3.8 Methods of Quantitative Analysis

The THz spectra of un-milled and milled materials were analysed by a conventional method, based on estimation of area under absorption peak, as well as by multivariate method. It was recognized that accuracy of the former method, which does not account for the equipment noise and other external variables, is therefore dependent on the estimation of baseline of the peak. The multivariate analysis applied was based on partial least square (PLS) regression. Unlike the univariate peak area analysis approach, this method identifies a number of prediction variables, and scores each as a different principal component. The component with the highest score is the factor that contributes most to the observations. Multivariate chemo-metric analysis has been used previously for calculation of crystallinity of from NIR data (Nørgaard et al., 2005) and THz data (Darkwah et al., 2013).

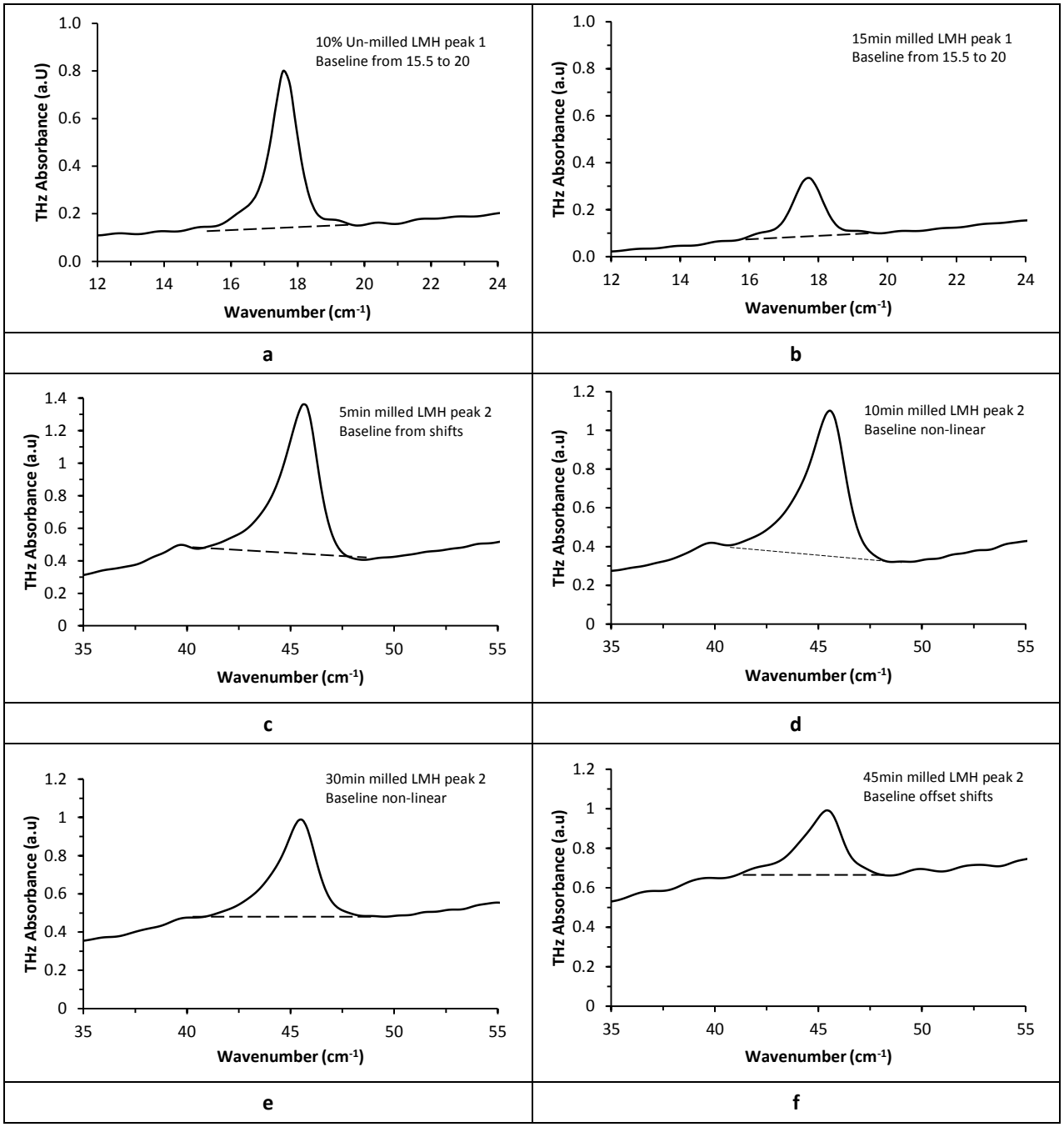

Figure 3.10: Baseline characteristics from THz absorption data of lactose monohydrate. Peak 1 shows linear baseline in un-milled and milled samples (a, b) while peak 2 shows a non-linear baseline in milled samples (c-f) in terms of shifts in gradient and offset with milling time.

A) Area Under the Peak Method

The THz absorption spectra of different concentrations (i.e. 4 to 12% w/w) in case of lactose or 6 to 20 %w/w ibuprofen were measured in the frequency range of 0 to 100 cm^{-1}.The area under the absorption peak was then calculated by a trapezoidal method, following subtraction of the linear baseline between the start and end points of the peak (Figure 3.11a, c & e) and used to construct a calibration curves. This gives straight lines with a R^2

close to unity as described on each graph (Figure 3.11b, d & f). The linear function parameters of these calibration curves were then used to calculate the concentration of crystalline material remaining in each milled material.

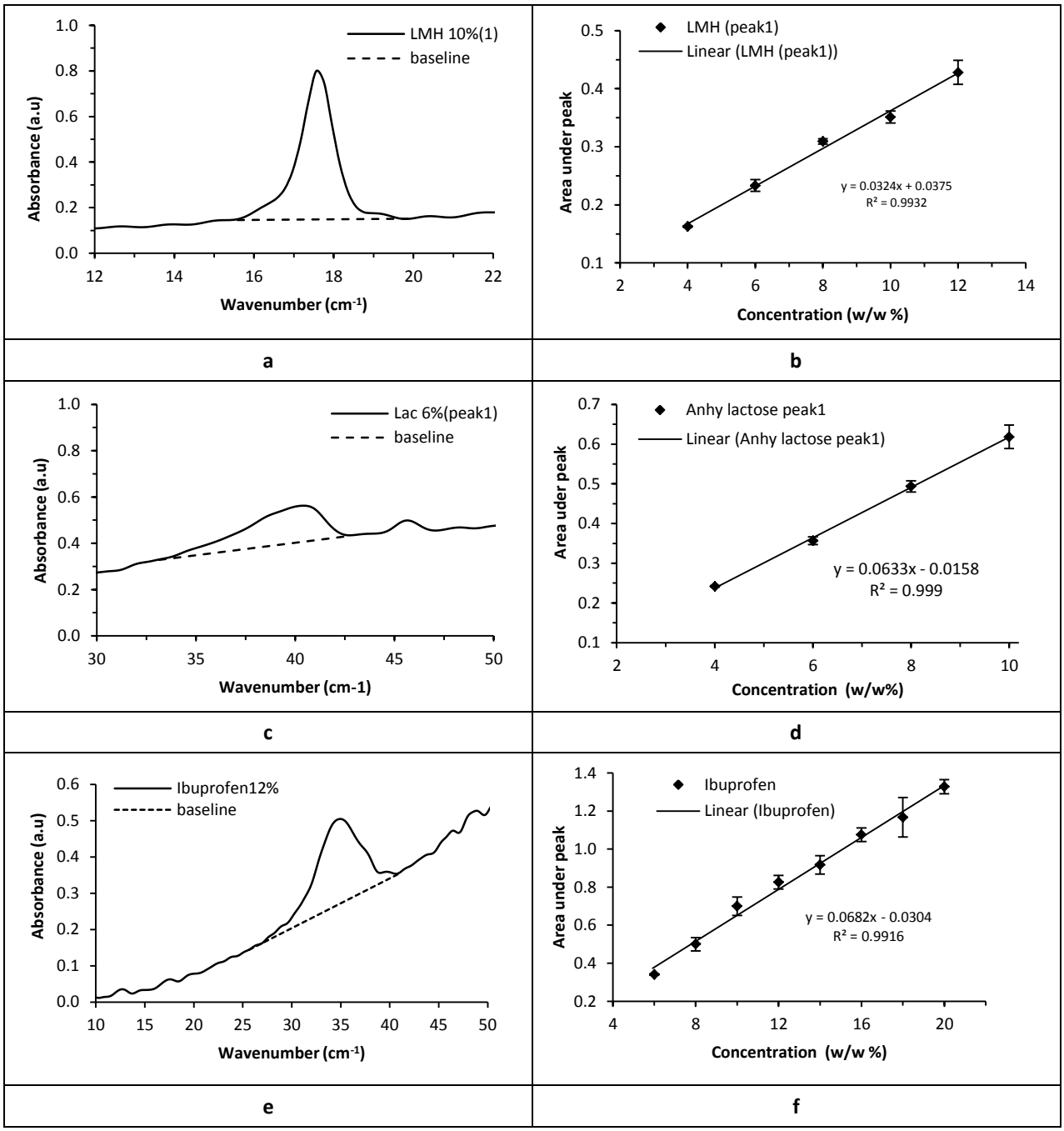

Figure 3.11: Baseline subtraction from THz absorption peaks (a, c, e) for lactose monohydrate, anhydrous lactose and ibuprofen, respectively and their calibration curves (b, d, f) from area under peak method in the same order. The error bars represent the standard deviation of 9 measurements (n=9).

B) Partial Least Square Method

The multivariate calibration model was constructed using the un-processed THz absorption data of the selected region at different concentrations (4%, 6%, 8%, 10% and 12% w/w) of the un-milled lactose or 6 to 20 w/w % ibuprofen. A PLS algorithm was applied on the response (THz absorbance) and input (*i.e.* concentrations) using the *Matlab* software (R2010a) and a model with 4 latent variables was selected. The applied model demonstrated good agreement (constant of proportionality ~1) between the predicted and the actual concentrations for each of lactose monohydrate, anhydrous lactose and ibuprofen (Figure 3.12a, b & c, respectively). The PLS regression coefficients ('Beta' coefficients) were then calculate and used to estimate the % (w/w) relative crystallinity remaining in the milled samples from the measured THz spectra.

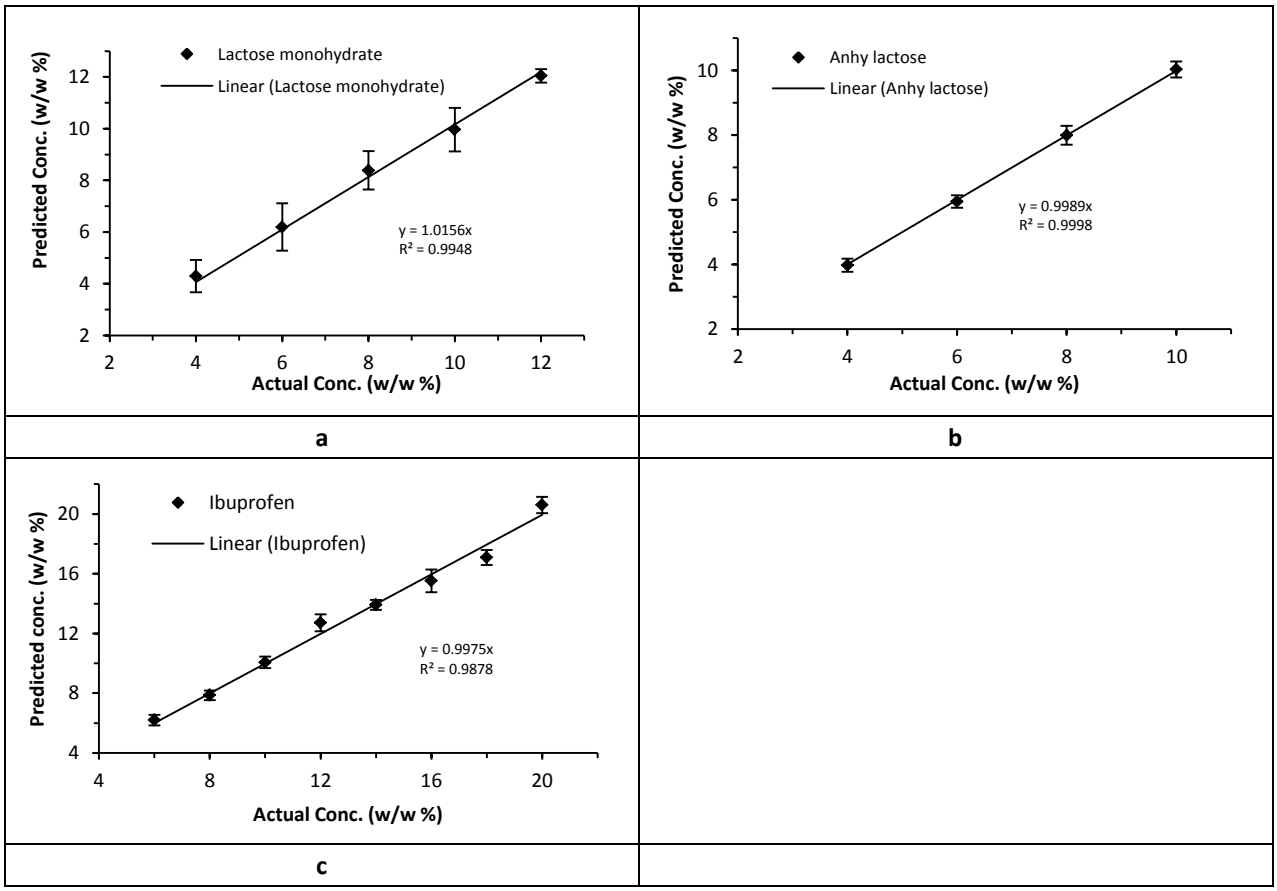

Figure 3.12: Calibration models based on partial least square (PLS) applied to THz data of un-milled a) lactose monohydrate b) anhydrous lactose and c) ibuprofen. All these showing a good agreement between the predicted concentrations against calculated from this model. The error bars represent the standard deviation (SD) of the measurements (n=9).

The limit of detection (LOD) and the limit of quantification (LOQ) for each material are calculated using Equations 3.5 to 3.6, and the output values (Table 3.6) are used to compare the quality of each model.

$$\mathbf{LOD} = \mathbf{3.3} * \mathbf{RMSE} \qquad \textbf{Equation 3.5}$$

$$\mathbf{LOQ} = \mathbf{10} * \mathbf{RMSE} \qquad \textbf{Equation 3.6}$$

RMSE is root mean square error calculated from AUC data or PLS regression.

Table 3.6: The LOD and LOQ values of lactose monohydrate, anhydrous lactose and ibuprofen as calculated from the both THz methods (AUC and PLS).

	Area of peak method			Partial least square		
	RMSE	LOD (w/w %)	LOQ (w/w %)	RMSE	LOD (w/w%)	LOQ (w/w %)
Lactose monohydrate (Peak 1)	0.23	0.77	2.35	0.24	0.78	2.37
Anhydrous Lactose (Peak 1)	0.14	0.48	1.45	0.23	0.74	2.26
Ibuprofen	0.42	1.39	4.22	0.50	1.65	5.0

3.3.3.9 Results of Residual Crystallinity of Milled Lactose Monohydrate from THz Data

In the milled samples of lactose monohydrate, both area under the peak data and the PLS data show a monotonic decrease in crystallinity with the milling time (Figure 3.13). The most intensive/sharp reduction of crystallinity occurs at the beginning of milling where the %RRC reaches ~25% after 30 min of milling. Beyond this time point there is relatively slow loss of further 5% to 15% crystallinity during next 30 min and %RRC is ~15% in the 60 min milled sample.

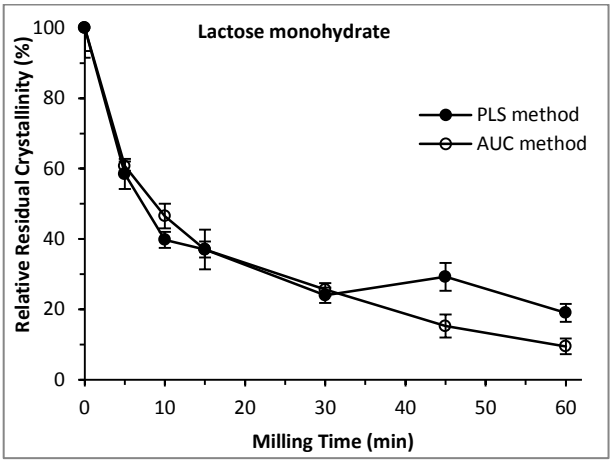

Figure 3.13: Comparison of relative residual crystallinity (%RRC) on milling of lactose monohydrate as calculated by area under peak method and PLS methods applied to THz data. The error bars represent the standard deviation (SD) of the measurements (n=9).

3.3.3.10 Results of Residual Crystallinity of Milled Anhydrous Lactose from THz Data

For the milled anhydrous lactose, both the area under the peak data and the PLS data show a rapid reduction in crystallinity at the beginning of milling where the %RRC reaches ~70% after 10 min of milling (Figure 3.14). Beyond this time point there is a net increase of 15% crystallinity with the next 45 min followed by a sharp reduction in crystallinity until it reaches ~35% in the 60 min milled sample.

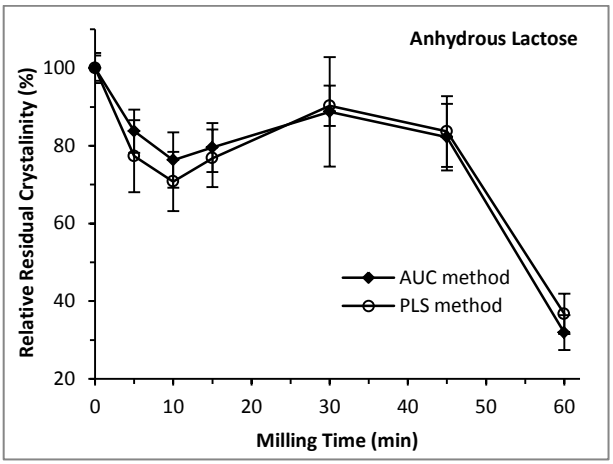

Figure 3.14: Comparison of relative residual crystallinity (%RRC) on milling of anhydrous lactose as calculated by area under peak method and PLS methods applied to THz data. The error bars represent the standard deviation (SD) of the measurements (n=9).

3.3.3.11 Results of Residual Crystallinity of Milled Ibuprofen from THz Data

The method based on area under the peak, shows an intensive reduction of crystallinity of ibuprofen at the beginning of milling where the %RRC reaches ~50% after 10 min of milling. Beyond this time point there is relatively slow loss of further 15% crystallinity in next 20 min of milling (Figure 3.15). While the PLS method show that the residual crystallinity decreases erratically with milling time, with the most remarkable decrease in the crystallinity occurring over the first 5 min. There is an approximate ± 10% variation in the estimates of crystallinity in all milled samples of ibuprofen (between 42% to 52%) meaning that it is not clear as to whether there is a progressive decrease in crystallinity as the milling time increases beyond 10 min.

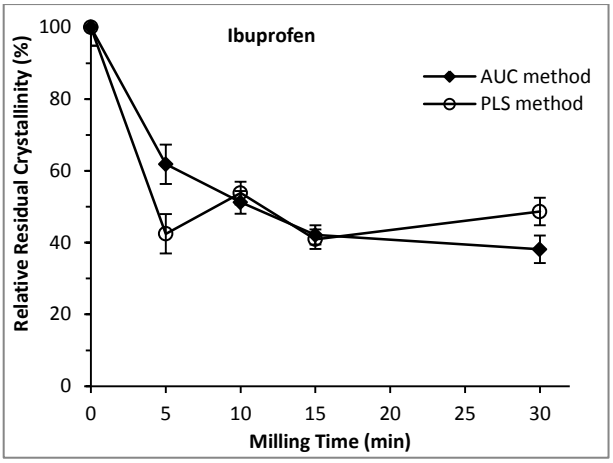

Figure 3.15: Comparison of relative residual crystallinity (%RRC) on milling of ibuprofen as calculated by area under peak method and PLS methods applied to THz data. The error bars represent the standard deviation (SD) of the measurements (n=9).

3.4 Discussion

It is expected that ball milled materials will contain a number of phases from the partially damaged (*i.e.* compromised) crystalline material to the fully amorphous phases, as a consequence of the high energy collisions of the particles. Results from the various techniques and methods of data analysis provide a range of estimates for the residual crystallinity, with all techniques generally showing similar behavior, *i.e.* a generalised decrease in the proprtion of the crystalline part with the milling time. This outcome may be considered somewhat inevitable given that each approach is based on the analysis of a different facet of the collection of milled particles. The discussion will focuss on the exploration of these differences between approaches used in this study (*i.e.* TGA, DSC and THz) for the determination of residual crystallinity.

3.4.1 Comparison of DSC and TGA of Lactose Monohydrate

One feature of the estimates for %RRC, as determined by TGA, is that they are generally much higher than the estimates obtained from the DSC method 1 (Figure 3.16).

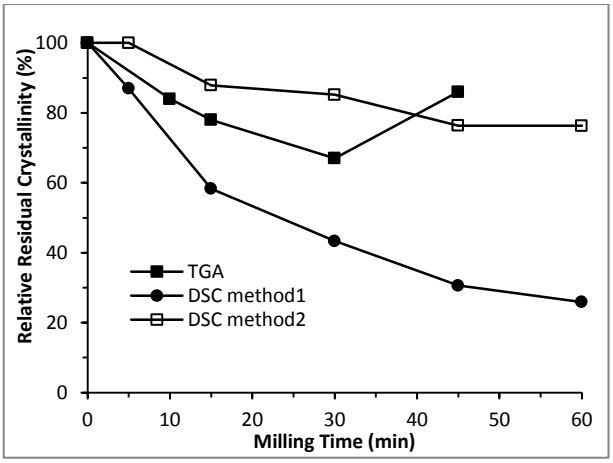

Figure 3.16: Comparison of relative residual crystallinity (%RRC) of lactose monohydrate as calculated by TGA and DSC (method 1 & 2).

The disparity between TGA and DSC was probably due to the fact that; in case of TGA, the assessment was based on the weight loss linked to the release of water of crystallization. Therefore, while the estimate of crystallinity may actually represent that part of the (crystalline) material which is largely un-changed during milling process, it may also include that part which is partially damaged during milling but still retains some form of the entrapped water (which may in fact be considered as some form of water of crystallization). This would lead to a higher estimate of crystallinity in the milled material than a method which is based on the assessment of the melting enthorm of lactose monohydrate (*i.e.* DSC method 1). Another fact is that the percentage loss of crystallinity as determined by TGA is based on the assumption that the starting material comprises only alpha lactose monohydrate, with a water content of 5%. Inevitably this is added to the over estimate of the residual crystalline content.

Another feature of the estimates for %RRC from TGA is the undulation of data over time, which could result from the variation in the characteristics of the material taken as a sample from the ball mill. It is possible that a material in which crystals are weakened on milling, may allow water to leach out before analysis, and this would reflect less %RRC than the sample in which water of crystallization is relatively stable. Such effects would be exacerbated from a lack of uniformity across the milled material.

DSC method 2 also gives a higher estimate of crystallinity than DSC method 1. The descrepancy in DSC method 2 is because of its reliance on the process of de-vitrification and the presumption that this process is completed within the time frame of the DSC analysis.

However, at the scan rate of 20 °C min^{-1} there may be insufficient time to allow for complete de-vitrification. Moreover, this process would be impacted by the amount of water in each sample, therefore introducing a further degree of variability in the assessment of crystallinity. Also there is loss of sensitivity at early time points where the amorphous content is too low to observe the de-vitrification peak. The minimum sensitivity is ~ 13% of amorphous in order to detect and make a reliable estimate of %RRC by this method; so it follows that the estimates for %RRC are likely to be higher than one could expect.

Based on the discussion above we might pre-suppose that the broad agreement between TGA, and DSC method 2 implies that these estimates for the %RRC provide a more realistic assessment of the damage induced by milling. However, it is recognised that the TGA is likely to include, in its estimates the proportions of material that have been structurally compromised in some way. In the case of DSC method 1, the assessment of %RRC is based on the melting endotherm of α-lactose monohydrate and is more realistic. Any amorphous form which de-vitrifies on heating within the DSC experiment is presumed to crystallise out exclusively as the beta form (and not the alpha form as discussed in Section 3.3.2.2) and therefore does not contribute to the metling endotherm of α -lactose monohydrate.

3.4.2 Comparison of DSC (method 1) and THz Results

For lactose monohydrate: The assumption that the de-vitrification of a proportion of the amorphous form to the beta form, on heating within the DSC experiment, is borne out by the THz data which demonstrates the absence of any increase in the beta form, post milling. Therefore the calculation (method 1) of residual crystalline content in milled samples may be based entirely on the melting enthalpy of α-anomer.

For the THz analysis, the estimates for %RRC from both methods of analysis (area under peak and PLS) seemed similar, therefore the average of their estimates were taken and compared with DSC method 1. It represents that both estimates were the closest to one another, in that the rate of decrease of crystallinity followed a similar trend (Figure 3.17). However, the DSC estimates were generally higher than that from the THz analysis. This might suggest that the aforementioned exclusive de-vitrification of the amorphous form into the beta form, may not be strictly true and that de-vitrification may also re-introduce a proportion of the α-form.

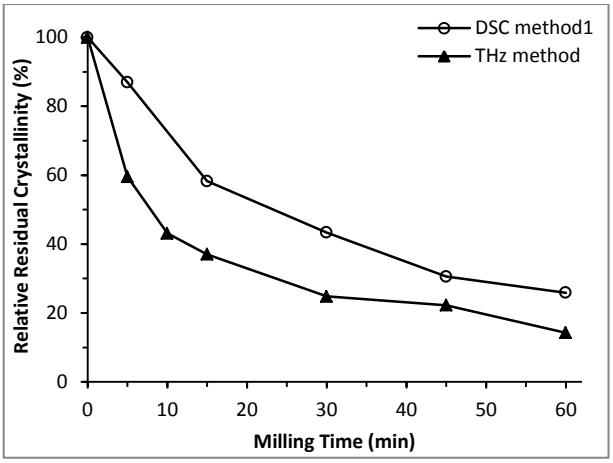

Figure 3.17: Comparison of residual crystallinity (%RRC) for the milled lactose monohydrate as calculated by DSC method 1 and THz methods (average of two THz methods).

In Summary, the THz estimates of residual crystallinity are more promising and consistent. It is futher emphasized that this technique is non-invasive and directly measures the crystallinity by probing the lattice of solid material. In contrast, the thermo-analytical methods are all indirect methods based on the assessment of transitions between different physical states of material, which are dependent on the temperature rate and values that can be applied for the specific enthalpy of melting of each crystalline state.

For anhydrous lactose: The averages of both THz estimates (determined from AUC and PLS methods) provide higher estimates of residual crystallinity, compared to both DSC methods, for all milling time points up to 45min (Figure 3.18). While at the 60 min point, the estimates from both DSC method 1 and THz were almost the same as one another.

The difference in the estimates of residual crystallinity as determined from THz spectroscopy and DSC are probably because the opportunity for de-vitrification of the amorphous phase during sample preparation for the THz measurement at room conditions, given that there are inevitably lot of seeds for de-vitrification in milled samples (Caron et al., 2011). Moreover, the process of de-vitrification may in fact be triggered by the hydrophobic surfaces of PE coupled to the compression force applied during pellet preparation. This may explain why estimates for the residual crystallinity were higher for THz analysis up to the 45 min time point. During this early phase of milling, the amorphous content was small and therefore sufficient seeds remained for the de-vitrification of this amorphous phase. However, at extended milling times (60 min), where the amorphous content is large and there are insufficient seeds to promote the re-crystallization of the amorphous phase, then

the material is more stable and the estimates for %RRC are almost the same as that determined by DSC.

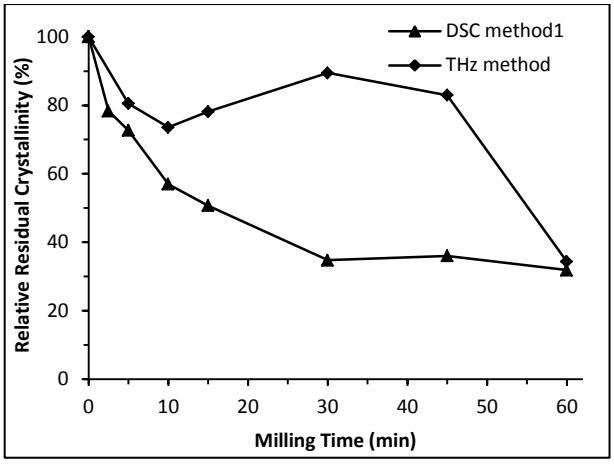

Figure 3.18: Comparison of residual crystallinity (%RRC) for the milled anhydrous lactose as calculated by DSC method 1 and THz methods (average of two THz methods).

In summary, DSC method 1 (based on the melting and de-vitrification enthalpies) is relatively reliable method for the estimation of residual crystallinity in milled anhydrous lactose among the all DSC methods and THz. In contrast to our observations for the lactose monohydrate; where it is established that the THz measurements are relatively more reliable for the estimation of relative residual crystallinity on milling. Therefore, the best methods for each were taken for comparison of residual crystallinity of lactose monohydrate and anhydrous lactose after ball milling (Section 3.4.3).

For milled ibuprofen: The appearance of melting peaks of all milled samples of ibuprofen at almost same temperature as the un-milled one (Figure 3.6b), has indicated that either the crystalline structure of ibuprofen was not damaged, particularly in short milled samples or there was some regain in crystallinity in samples milled for longer than 15 min. However, the signature of amorphous phase (the de-vitrification peak) in long milled sample >15 min (Figure 3.6a) indicates the crystalline damage.

The quantitative analysis (by both DSC and THz) of residual crystallinity in milled samples of ibuprofen as compared to the initial crystalline material has revealed that there is a monotonic loss of crystallinity with milling times (Figure 3.19). However, the estimates of %RRC from DSC results are higher than that from the THz results. This is probably due to the thermal induced de-vitrification of amorphous phase generated on milling (Figure 3.6a),

which has been started even inside the jar of mill (as the temperature is close or higher that the de-vitrification temperature of ibuprofen *i.e.* ~35 °C).

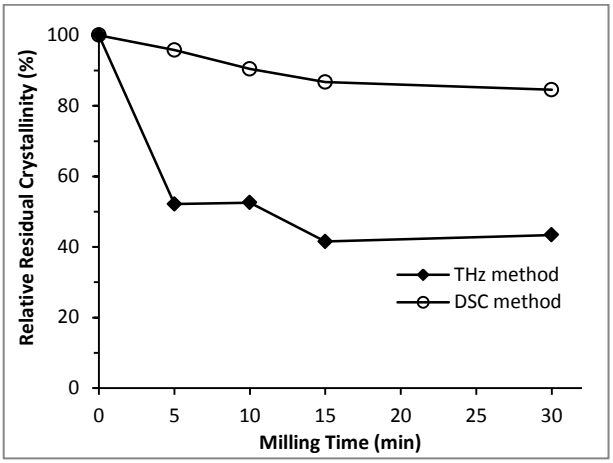

Figure 3.19: Comparison of residual crystallinity for the milled anhydrous lactose as calculated by DSC method 1 and THz methods (average of two THz methods).

Therefore DSC results could not represent true change in crystallinity in ibuprofen on milling. On the other hand, the THz results look promising and reveal a rapid loss of residual crystallinity in first 15 min followed by a plateau afterwards.

3.4.3 Comparison of residual crystallinity of milled lactose monohydrate and anhydrous

A comparison of the residual crystallinity of ball milled lactose monohydrate (from THz data) and anhydrous lactose (from DSC data) shows that there is an initial, steep decline in the residual crystallinity in the first 15 min, followed by a more gradual reduction in crystallinity over the subsequent 45 min (Figure 3.20). After 5 min milling the two profiles reveal a systematic difference ~10% at each milling time point.

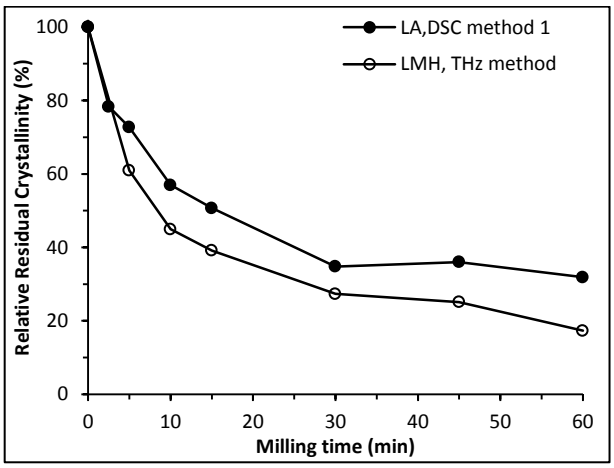

Figure 3.20: Changes in relative residual crystallinity of lactose monohydrate and anhydrous lactose as calculated from THz (for LMH) and DSC (for LA).

The higher estimate of the residual crystallinity in case of anhydrous lactose (DSC method 1) as compared to the lactose monohydrate (THz method) is probably due to the fact that α-LMH is more brittle than β-LA. The mechanical parameters such as tensile strength and Young's modulus of α-LMH promotes its cleavage while the likelihood of cleavage is less in the case of anhydrous β-lactose (Busignies et al., 2004). The brittleness of LMH is also related to particle size. Previously it was shown that particles with the size > 45 μm are more brittle than fine powder particles (Peters, 2009). The size of particles for both materials under investigation is different. The α-LMH which was used in this study consisted of coarse particles of 150-180 μm; as compared to the particles of β-LA which were relatively fine (< 100 μm). Another explanation might be due to the fact that the coarse particles (of α-LMH) have good flow behaviour and are therefore more mobile within the milling jar. As a consequence, they may experience a greater number of collisions with the moving ball and more shearing events against the side walls (Shariare et al., 2011) *i.e.* leading to greater attrition of the powder. On the other hand the fine powder of β-LA having poor flow, probably sticks to the walls of the milling jars and therefore only experiences the compaction force of ball against the wall of mill jar.

3.5 Conclusion

The results of residual crystallinity estimates for the milled lactose monohydrate has shown that both DSC method 1 and the THz methods yield almost similar results indicating that there is a limit of ~ 80% loss of starting crystalline content which occurs after 60 min milling. While TGA appears to show higher estimates of crystallinity because the estimation is based on the weight of crystallization water without any consideration of the structural damage to the crystal or the presence of an amorphous phase. Therefore it can be concluded that; TGA is un-reliable for the estimation of crystallinity, DSC works but requires more steps in the calculation (to account for the induced de-vitrification and mutarotation of LMH during analysis by DSC) and therefore more assumptions and expected sources of error may associate with the method, while THz measures the material in its native state and is based on simple absorption spectra, requiring fewer assumptions and therefore standard computational techniques are satisfactory. In addition, a principle advantage of THz over

DSC might be that the technique could be adapted for on-line measurements and process control.

On the other hand, for anhydrous lactose; DSC is more reliable method than THz, for measuring the crystallinity of materials after milling because of the de-vitrification of amorphous phase during sample preparation is more probable than for milled α-lactose monohydrate.

In case of ibuprofen, where thermal analysis can induce partial de-vitrification of the amorphous phase, again THz spectroscopy is more reliable technique for the determination of loss of crystallinity in respect of the staring material.

4 Study of Molecular Dynamics of Amorphous Phase in Milled Sugars (Lactose and Sucrose) by Dielectric Relaxation Spectroscopy

4.1 Background/Context

The amorphous phase has the advantage of increasing the solubility and dissolution rate of poor soluble drug substances (Dudognon et al., 2006). At the same time, this phase is metastable (owing to the high surface free energy) and may ultimately revert back (*i.e.* de-vitrify) to its original form, or even a different crystalline form, thus compromising the stability of the product during its shelf life. This instability is often associated with the sorption of moisture, which has the effect of reducing the glass transition and increasing the mobility of the constituent molecules (Zhang et al., 2006).

The methods commonly used for the generation of amorphous phase include quench cooling of melts (Angell, 1995), freeze drying (Yu, 2001), spray drying (Gharsallaoui et al., 2007), precipitation from solution (Li et al., 2000), vapour condensation (Kearns et al., 2007) and milling (Willart et al., 2004). Among these, milling is often considered to be the simplest and versatile method used in pharmaceutical industry. The applications and other benefits of milling have been detailed in Chapter 1. The amorphous phase obtained by milling is probably the most unstable because of the presence of residual crystallites, that act as nuclei for de-vitrification (Crowley and Zografi, 2002). Therefore the benefits of milling could only be achieved if the post-milling de-vitrification is prevented, for example by co-milling with an agent that stabilizes the amorphous phase. At the first stage, it is necessary to study the molecular dynamics of this phase then it may be possible to determine the extent to which a system containing an amorphous phase could be stabilized.

There are a range of techniques available for studying the molecular dynamics and thus stability of the amorphous phase. Parameters such as the structural relaxation time, enthalpy relaxation and/or fragility index (obtained from DSC or isothermal micro-calorimetry techniques) have been used to provide certain measures of molecular mobility (Pokharkar et al., 2006, Graeser et al., 2009, Liu et al., 2002). More recently, studies by dielectric spectroscopy have shown that the structural relaxation (in terms of the characteristics of the α-relaxation) reflects a level of molecular mobility that appears to

underpin the de-vitrification (and hence instability) of system containing amorphous phase (Kolodziejczyk et al., 2013, Rodrigues et al., 2013)

However, it is worth noting that the amorphous phase studied in majority of these studies was usually produced by quench cooling of the melt; a procedure which is not commonly applied in pharmaceutical industry as it may degrade the material. Moreover, it produces a compact, non-porous material that dissolves slowly, a feature of a pharmaceutical product which is invariably undesirable. It is also relevant to recognize that the moisture is excluded from these systems during the quenching, which is not the real situation when amorphous phase is prepared in industry.

Cryo-milling is an alternate method of producing amorphous state without thermal degradation of the material (Wojnarowska et al., 2010), however, it is important to remember that the method by which the amorphous phase is generated has itself an influence on the molecular dynamics characterizing the product (Kaminski et al., 2012). Thus, there is a need to study the specific molecular dynamics of amorphous phases, as they are generated by the more routinely used industrial processes (*i.e.* milling) in order to predict the stability of such materials after milling.

Another important aspect of milling studies is to consider the fact that; the amorphous phase inevitably contains some quantity of the moisture (either generated from within the material in case of hydrated ones or adsorbed from the environment). A recent study on the ball milled indapamide (Wojnarowska et al., 2013) has suggested the presence of water relaxation peak rather than the typical relaxation processes of amorphous phase. The distribution and the impact of this water on the dynamics of the amorphous phase are important in defining the stability of this phase. Therefore the cooperative molecular dynamics of this amorphous phase, as modulated by the 'plasticization' effect of water may be of greater relevance to the stability of amorphous form than experiments taken on quench cooled systems.

The objective of this study is the analysis of the dielectric relaxation processes in milled disaccharides (sucrose and lactose) at different milling times in order to understand the impact of milling on the dynamic behaviour of these widely used pharmaceutical excipients. This is an important aspect to investigate the dielectric properties of milled materials and

may help to establish the approaches for the prediction of the stability of milled pharmaceuticals.

4.2 Materials and Methods

Anhydrous lactose (as described in Chapter 3, Section 3.2) and sucrose used in this study were purchased from Fluka, U.K. and used as received from the supplier. Lactose occurs as a white crystalline powder with finely divided particles while the sucrose was a coarse crystalline material.

4.2.1 Ball Milling

Milling of both lactose and sucrose was performed as per method described in Section 2.2.1 using the milling speed of 18 Hz for 60 min.

4.2.2 Thermogravimetric analysis (TGA)

TGA of un-milled and milled materials was carried out according to the method described in Section 2.2.4.

4.2.3 Differential Scanning Calorimetry (DSC)

DSC experiments of un-milled and milled materials were carried out according to the method described in Section 3.2.3.

4.2.4 Broadband Dielectric Spectroscopy (Novocontrol)

The dielectric measurements were performed at ambient pressure according to the method used by (Kaminski et al., 2008b) in BDS Novocontrol Alpha Analyser (Novocontrol, GMBH Germany- shown in Figure 4.1a). The powder sample was placed in the form of a thin film between two gold plated electrodes of a sample cell (Figure 4.1b). The diameter of the sample was taken from the cell *i.e.* 20 mm and the thickness of sample layer was ~1.0 mm. The cell was then mounted in the sample holder (Figure 4.1c) where it was supplied with liquid nitrogen. The measurements were carried out applying the frequencies between 0.1 Hz and 10 MHz and temperature from −120 to +100 °C with 5 °C increments. The temperature was controlled (with stability of ± 0.1 °C) by Novocontrol Quattro system attached with the cryostat containing liquid nitrogen. The data were analysed by *Data-View* and *Z-view* software.

a	b	c

Figure 4.1: Novocontrol dielectric spectrometer showing a) frequency response NVC alpha analyser unit connected with cryostat Dewar for temperature control during the measurements, b) sample cell containing an outer gold plated sample holder and two small gold plated electrodes mounted in Teflon assembly and c) sample holder assembly.

4.3 Results and Discussion

4.3.1 DSC Results of Anhydrous Lactose

The DSC curve of un-milled lactose has shown a small endotherm at ~140 °C (peak 'A' in Figure 4.2a) followed by a shoulder at ~210 °C (indicated as 'B' in Figure 4.2a), and a large endotherm at ~238 °C (peak 'C' in Figure 4.2a). The first endotherm is desorption of the water of crystallization (as observed in case of lactose monohydrate (LMH) in Section 3.3.2.1), indicating the presence of small quantity LMH in the sample of anhydrous beta lactose (β-LA). The second endotherm (i.e. peak 'B') represents the melting of anhydrous α-lactose (α-LA) while the major endotherm (peak 'C') represents the melting of anhydrous beta lactose (Listiohadi et al., 2009).

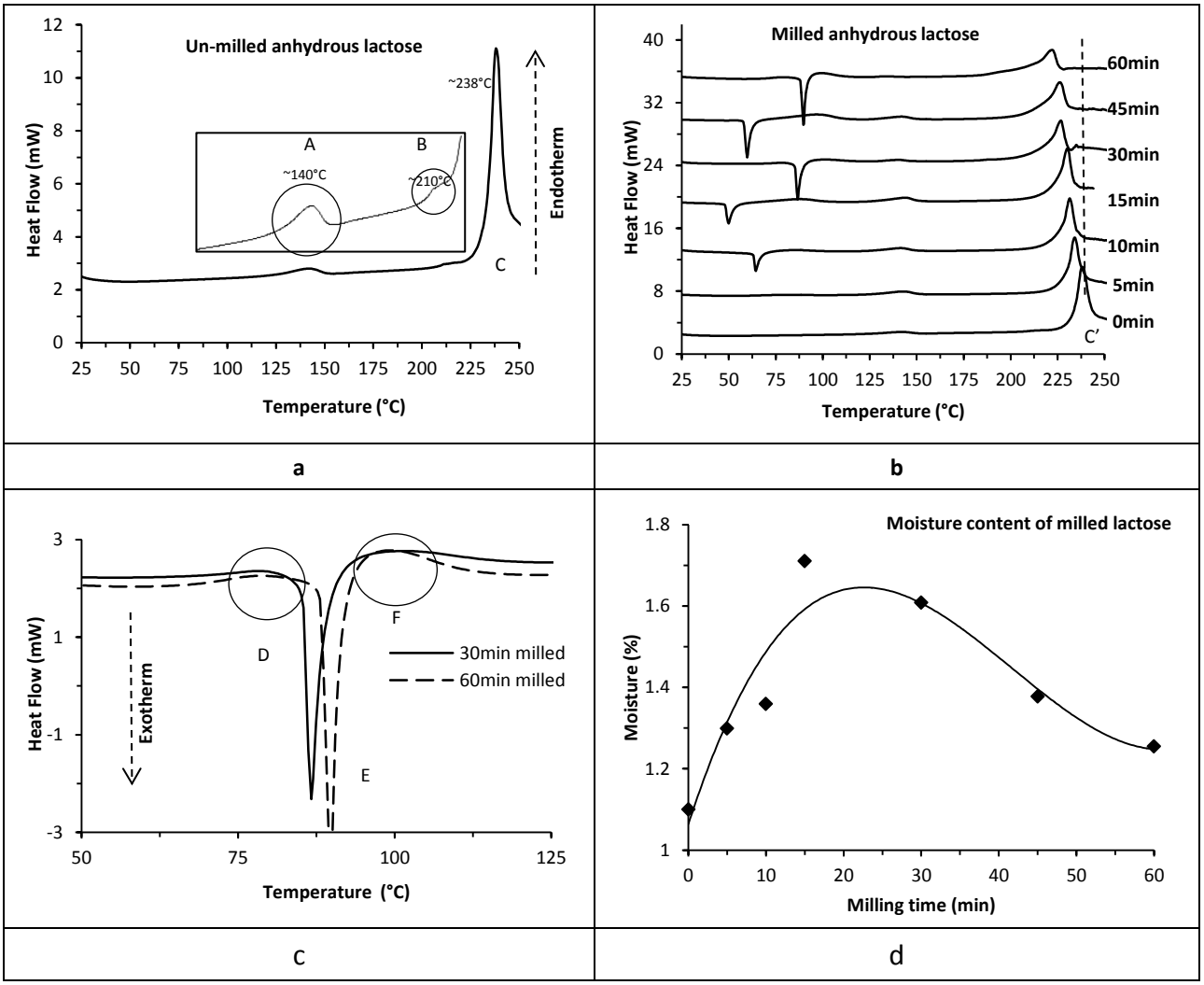

Figure 4.2: DSC curves of a) un-milled anhydrous lactose (showing the two small endotherms 'A' and 'B' shown in the inset and a melting endotherm 'C'), b) milled lactose for various time intervals c) segment from DSC curves of 30 & 60 milled lactose (showing T_g indicated as event 'D', de-vitrification (peak 'E') and water loss peak 'F') d) change in moisture content of anhydrous lactose from TGA (trend line shows the biphasic response.

DSC curves of **milled (for different times) anhydrous lactose** (Figure 4.2b) have shown that the desorption endotherms of the water of crystallization is present in majority of the milled samples (although its enthalpy changes, see Table 4.1), while the melting endotherm of α-LA is not observed in any of the milled samples. The major melting peak (indicated as C' in Figure 4.2b) shifts towards lower temperatures with milling time; from ~238 °C for the un-milled lactose to ~222 °C for the 60 min milled sample.

The signs of an amorphous phase, including a glass transition step (peak 'D' in Figure 4.2c) a de-vitrification (peak 'E' in Figure 4.2c) is also observed in the milled lactose. The onset temperature for de-vitrification (T_{cr}) does not have any regular pattern (Figure 4.2b) and

occurred between 45 and 90 °C. Another event in the DSC curves of milled samples at ~ 95 °C (event 'F' in Figure 4.2c) probably represents the loss of surface water.

The change in enthalpies of devitrification and melting on milling (Table 4.1), indicates the loss in crystallinity of anhydrous lactose (described in Chapter 3, Section 3.3.3.10), while the changes in melting temperature represent the thermally induced mutarotation, which may be considered as an artefact of the DSC analysis (Shariare et al., 2011) and the beta lactose is not sufficiently present in the native milled samples (prior to DSC measurement) as evidenced by the non-thermal technique *i.e.* THz (Chapter 3, Section 3.3.3.4). The observation of a glass transition indicates the presence of a real glassy state within the samples of lactose that had been milled for extended time period (45 – 60 min), as opposed to what has been described previously as a non-crystalline state by (Willart et al., 2004), *i.e.* one which is intermediate between a purely 'intact' crystalline state and the wholly amorphous state.

Table 4.1: Values of crystallization temperature (T_c), enthalpy of crystallization (ΔH_c), enthalpy of dehydration (ΔH_{dh}), melting temperature (T_m) and enthalpy of melting (ΔH_m) for milled anhydrous lactose.

Milling time (min)	T_c (°C)	ΔH_c (Jg^{-1})	ΔH_{dh} (Jg^{-1})	T_m (°C)	ΔH_m (Jg^{-1})
0	-	-	10.1	238.1	173.2
5	-	-	14.8	234.0	125.9
10	63.1	20.8	15.9	231.6	119.5
15	48.0	26.1	20.1	230.1	113.9
30	85.3	37.6	5.7	226.5	97.8
45	57.9	42.9	14.0	226.2	105.3
60	88.2	41.8	2.1	222.1	96.9

4.3.2 Change in Moisture Content of Milled Lactose from TGA

The moisture content of milled samples of anhydrous lactose (Figure 4.2d) show a biphasic response, with an initial increase at short milling times (from ~ 1.1% in un-milled lactose to 1.7% in the 15 min milled), probably because of the water of hydration released form the material, followed by a reduction in moisture (1.25% in the 60 min milled sample) presumably as a consequence of drying as the temperature of the mill increases to ~ 40 °C in 60 min milled sample as compared to ~30 °C in 15 min milled sample.

4.3.3 DSC Results of Sucrose

The DSC curve of un-milled sucrose (Figure 4.3a) has shown a single endotherm at ~192 °C, corresponding to melting of this sugar (Beckett et al., 2006). In milled samples (5 to 60 min

milling times) the melting temperature remains almost constant (within 192 ± 4 °C, Figure 4.3b) and, the de-vitrification peak appears in the samples milled for 10 min or greater. The onset temperature for the de-vitrification decreases initially in the 15 min milled sample and afterwards increases gradually with milling time. For the samples exceeding 30 min milling time the glass transition step (event 'A' in Figure 4.3c) occur preceding the de-vitrification (peak 'B' in Figure 4.3c), which is followed by surface water loss (peak 'C' in Figure 4.3c) similar to those observed for lactose (Figure 4.2c).

Again, the milled samples show a decrease in the enthalpy of the melting (from ~125 to ~110 Jg^{-1}) and increase in the enthalpy of de-vitrification (from ~20 to ~40 Jg^{-1}) as the milling time increases from 5 min to 60 min (Table 4.2), indicating the amorphization of sucrose.

Table 4.2: Values of Crystallization temperature (T_c), enthalpy of crystallization (ΔH_c), melting temperature (T_m) and enthalpy of melting (ΔH_m) for milled sucrose.

	T_c (°C)	ΔH_c (J g^{-1})	T_m (°C)	ΔH_m (J g^{-1})
0	-	-	193.4	125.7
5	-	-	194.4	113.3
10	48.7	18.4	193.7	115.3
15	42.0	18.5	195.0	120.2
30	44.4	28.6	195.7	116.0
45	49.0	33.2	195.0	119.3
60	56.6	40.4	191.5	110.7

4.3.4 Change in Moisture Content of Milled Sucrose from TGA

TGA results for the un-milled sucrose shows no change in weight with temperature, indicating the absence of any moisture in the sample. While the milled sucrose samples showed an increase in surface moisture with milling time. It was 0.8% in 15 min milled sample and 1.6% in 45 min milled sucrose and afterward decreased slightly; *i.e.* 1.4% in 60 min milled sucrose (Figure 4.3d).

The change in enthalpy of de-vitrification and melting of both sugars in DSC data indicates that the amorphous content increases with milling time (Font et al., 1997).and then de-vitrifies with temperature. The amorphous phase of anhydrous lactose initially (when water released from hydrated crystals is high) de-vitrifies to α-monohydrate as evidenced from the increase in enthalpy of desorption peak (Table 4.1). Beyond 15 min of milling the de-vitrified form also contains β- lactose as the water is driven off by the raised temperature of the mill.

The onset temperature for the de-vitrification was variable in milled lactose, in spite of the increase in the amorphous content with milling time. This was probably because of the

change in moisture content that goes up and down with milling time (Figure 4.2d). Therefore the moisture plays a key role in the dynamics of amorphous phase in the milled lactose.

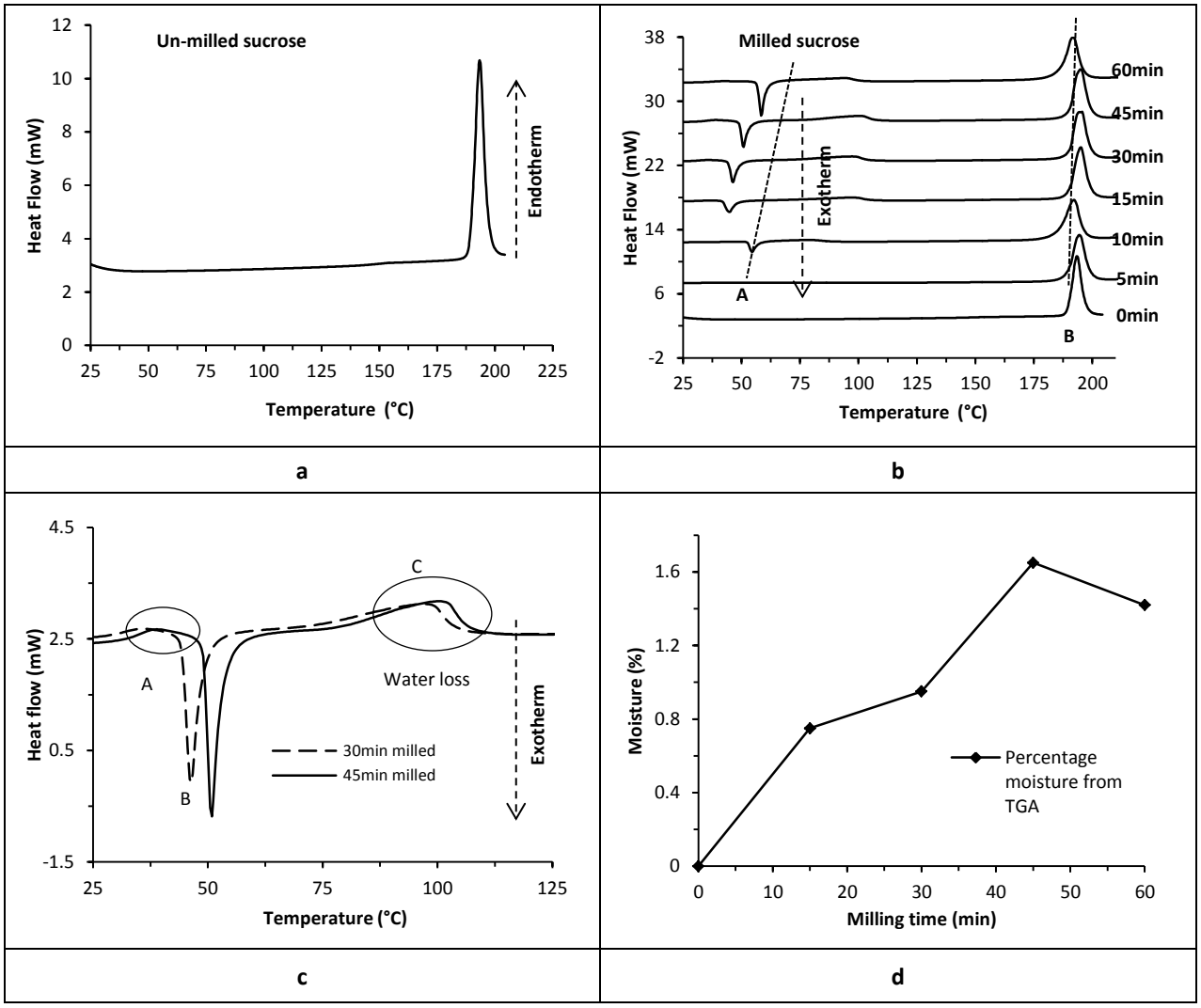

Figure 4.3: DSC curve of a) un-milled sucrose b) milled sucrose for different milling times (dotted lines 'A' and 'B' indicate the shifts of de-vitrification and melting endotherms respectively), c) Segments of DSC curves of 30 & 45min milled sucrose (showing T_g indicated as event 'A', de-vitrification (peak 'B') and water loss peak 'C'), d) change in moisture content of sucrose with milling time as determined by TGA.

In milled sucrose, the shift of onset temperature for de-vitrification towards higher temperature with milling time indicates that the crystallization seeds were probably reduced with the increase in amorphous content and the onset for de-vitrification was delayed with each milling time and the adsorbed moisture has played a little role in de-vitrification onset.

4.3.5 Dielectric Relaxation Processes in Un-milled Sugars

The 3D dielectric loss spectra of un-milled samples of both lactose and sucrose are almost flat in the low temperature window (Figure 4.4a & b) indicating the absence of any low temperature process, however, in lactose there is a small process in this region as shown by

the dotted circle in Figure 4.4a. In the higher temperature window there is a large process in both sugars (shown by the arrow heads in Figure 4.4a & b), probably representing the percolation of protonic charges through the water present on the hard crystalline surface of these un-milled sugars. This is followed by dc conductivity in both sugars as the temperature is increased further again indicated by the arrow heads in Figure 4.4a & b.

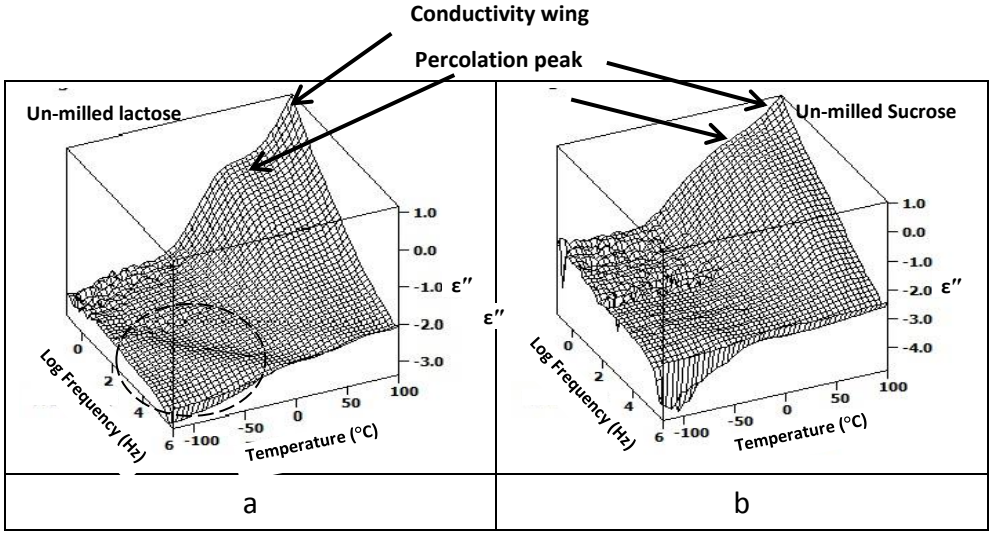

Figure 4.4: 3D dielectric loss spectra of a) un-milled anhydrous lactose and b) sucrose, showing the plot of imaginary permittivity against temperature and frequency. The spectrum of lactose shows a low temperature process highlighted by dotted circle.

The dielectric spectra of each lactose and sucrose are expressed in term of temperature and frequency slices (t-slices and f-slices, respectively) for their detailed analysis.

The t-slices (plot of imaginary permittivity against temperature at specific frequencies) through the dielectric spectra of un-milled lactose (Figure 4.5a & b) show that the percolation process starts near -20 °C at low frequency (indicated by line 'A' in Figure 4.5a) and move gradually towards the higher temperatures, as the frequency increases.

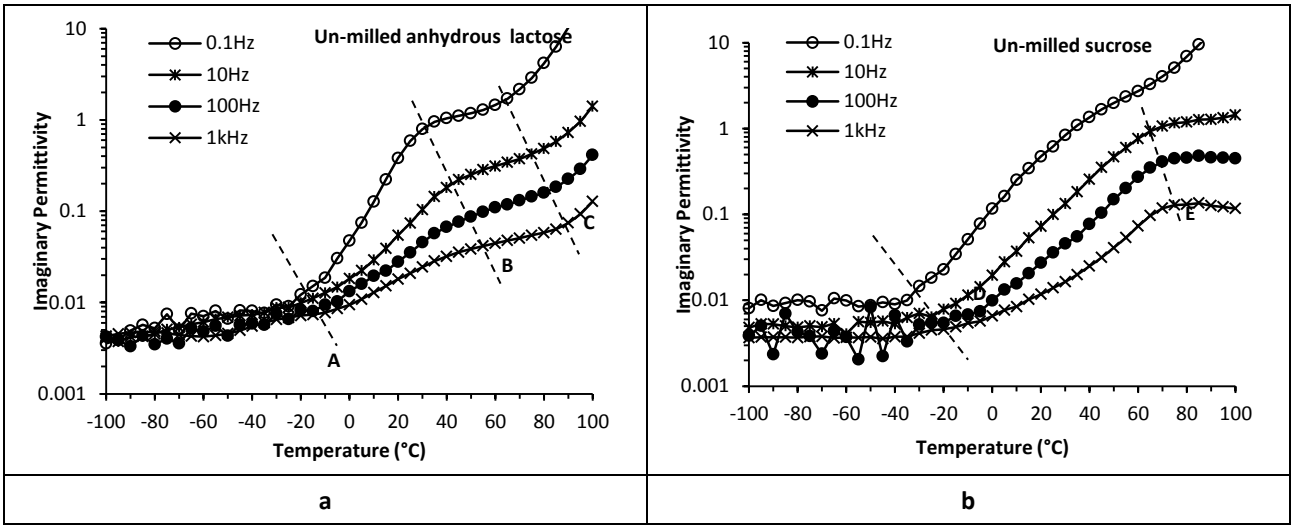

Figure 4.5: t-slices from the dielectric spectra of a) anhydrous lactose and b) sucrose, showing the plot of imaginary permittivity against temperature. The dotted line 'A' & 'D' indicates the start, 'B' & 'E' plateau of percolation and 'C' the start of conductivity.

The magnitude of the process (as indicated by the plateau region- line 'B' in Figure 4.5a) also decreases with increasing frequency. The temperature at which the conductivity wing (line 'C' in Figure 4.5a) appears also increases with frequency from 60 °C at low frequency and 85 °C at high frequency (Figure 4.5a).

The comparison of dielectric behaviour of both un-milled sugars show that, the onset of the percolation process of sucrose is similar to that of lactose (*i.e.* -20 °C, line 'D' in Figure 4.5b) however the plateau is shifted to higher temperatures (line 'E' in Figure 4.5b), suggesting a broader process. One of the noticeable differences is that the onset of the conductivity wing is only evident for the low frequency spectrum of sucrose and cannot be seen in the higher frequency spectra. Both observations suggest that the percolation pathways between the lactose particles are more connected than in sucrose, a likely consequence of the differences in particle size and the associated moisture content (TGA results Figure 4.2d & 4.3d) at the surface of the particles. In sucrose the particle size is 425 - 500 µm, whereas the particle size of lactose is < 100 µm.

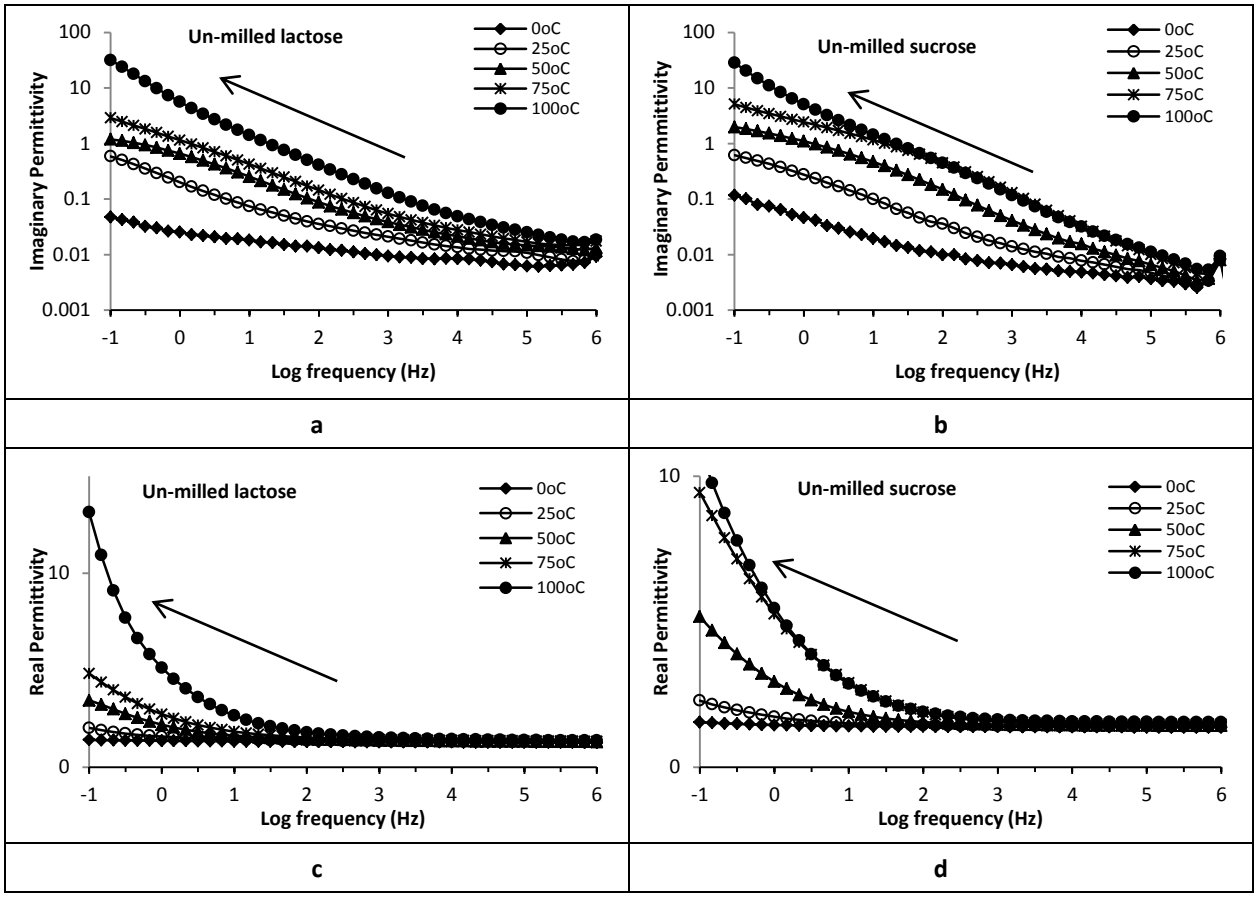

Figure 4.6: f-slices from the dielectric spectra of, a & c) un-milled anhydrous lactose and b & d) sucrose, showing the plot of imaginary permittivity (a & b) or real permittivity (c & d) against frequency. The arrow heads show the increase in both components toward low frequencies.

The f-slices of both sugars (Figure 4.6), show that both the imaginary and real components of dielectric permittivity continues to increase towards lower frequencies, indicating that the low frequency process (observed at high temperatures) is not simply a dc conductivity phenomenon but is instead associated with yet another process in the material, which were presume to be due to the percolation of charge within the particles of the solid, through possible electronic charge transfer. The fact that both lactose and sucrose are the small organic molecules having covalent bonds, the conduction through these involves the mobility of delocalized electrons linked with the conjugated covalent bonds on applying the electric field. The conduction through these molecules occurs by tunnelling (as illustrated in Figure 4.7) rather than by propagation due to the formation of conductive pathway and this conduction is therefore sensitive to the relative orientation of the rings and the bonding between them (Samanta et al., 1996).

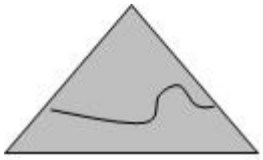

Figure 4.7: An illustration showing the (supposed) conduction through the solid particles.

4.3.6 Dielectric Relaxation Processes in Milled Sugars

In contrast to the un-milled sugars, the dielectric spectra for the milled samples (60 min milled) of these sugars display two secondary relaxation processes in the low temperature window (< 0 °C) represented as relaxation process 1 (RP1) and relaxation process 2 (RP2) by arrows on Figure 4.8 a & b respectively. In the high temperature window (> 0 °C), there are two processes in case of sucrose, RP3 which appears as a shoulder in the narrow temperature range followed by huge and sharp spike (RP4), while in case of lactose these a single process represented as RP3/4.

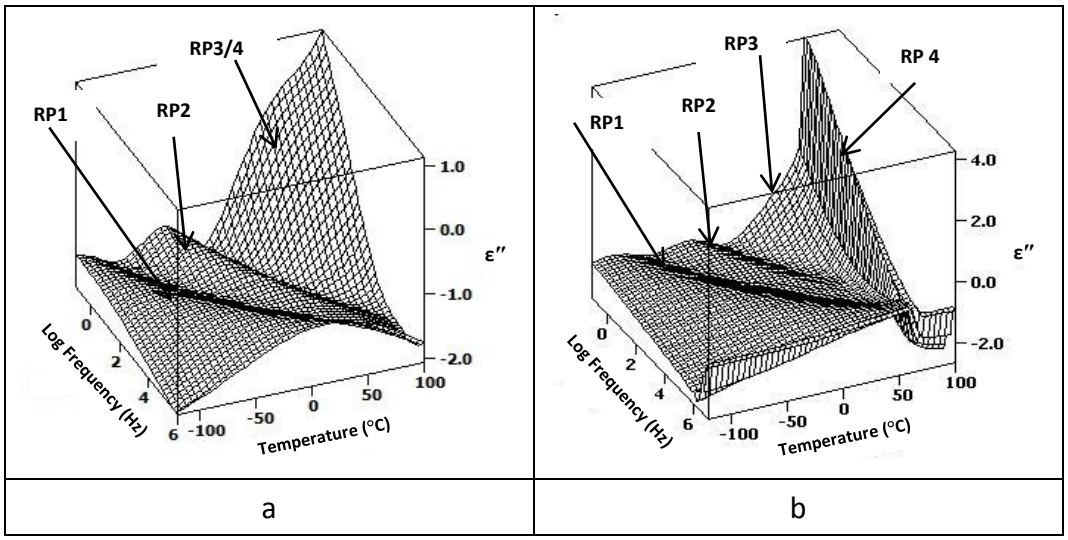

Figure 4.8: 3D dielectric spectra showing the plot of imaginary permittivity against temperature and frequency of a) 60min milled anhydrous lactose and b) 60 min milled sucrose. Both plots show four relaxation processes (RP) as highlighted by arrow heads. RP1 and RP2 are well separated in both milled sugars, RP3 and RP4 are also well separated in case of milled sucrose but appear as a merged single huge wing in case of milled lactose.

The low temperature processes (RP1 and RP2) of both milled sugars are secondary relaxations; γ and β processes, respectively, which are typical of the amorphous phase (Kaminski et al., 2011). These are discussed in more detail in the later section of this chapter (Section 4.3.7).

Note: The 3D dielectric loss spectra of different samples (un-milled to 60min milled) of anhydrous lactose and sucrose have been given in Appendix VIII and Appendix IX respectively.

4.3.6.1 High Temperature Processes in Dielectric Spectra of Milled Sugars

The high temperature processes (RP3 and RP4) represent the structural relaxation (visible as a shoulder in a narrow temperature range) and the dielectric loss/conductivity (occur as sharp spikes in dielectric loss), respectively in the milled sucrose (Figure 4.9). The likely explanation for the spike is that, the material has passed through the glass transition (*i.e.* the structural relaxation phase) and now with enhanced mobility in the system, there is an opportunity for de-vitrification and/or collapse (liquefaction) in sucrose. Given that we observed the material at the end of the measurement cycle and that it appears, to all intents and purposes, as a structurally 'intact' matrix then we presume this conductivity spike is more than likely to be associated with de-vitrification (rather than collapse; a process which is observed in case of hydrated sugar, Section 3.3.2.2). In contrast, the single high temperature process of lactose, which appears as a large wing towards low frequency, as opposed to the two separate processes for sucrose, probably represents a merged structural relaxation and conductivity as already reported in case of freeze dried lactose (Ermolina and Smith, 2011).

The characteristics of high temperature wing in dielectric spectra of milled sugars are more easily recognized and possibly understood by analysing the temperature slices at specific frequencies (Figure 4.9).

The t-slices of **milled lactose**, at low frequency (0.1Hz) show that the structural relaxation (not distinguishable from conductivity and appear as a merged process- Figure 4.9a) starts at almost the same temperature as the percolation in case of un-milled lactose *i.e.* at -20 °C (indicated as line 'A' in Figure 4.9a) and shift towards higher temperature in high frequency windows (Figure 4.9c & e). The height of structural relaxation (as indicated by plateau) also decreases with increasing the frequency followed by the appearance of conductivity towards high temperatures (line 'B' in Figure 4.9a).

Provided that the relative strength of this high temperature wing in milled lactose is almost 100 times the strength of secondary relaxation processes (Figure 4.9a) which is contrary to

the observations of Kaminski, that the fully amorphous sugar has similar strength of structural and secondary relaxation processes (Kaminski et al., 2008a).

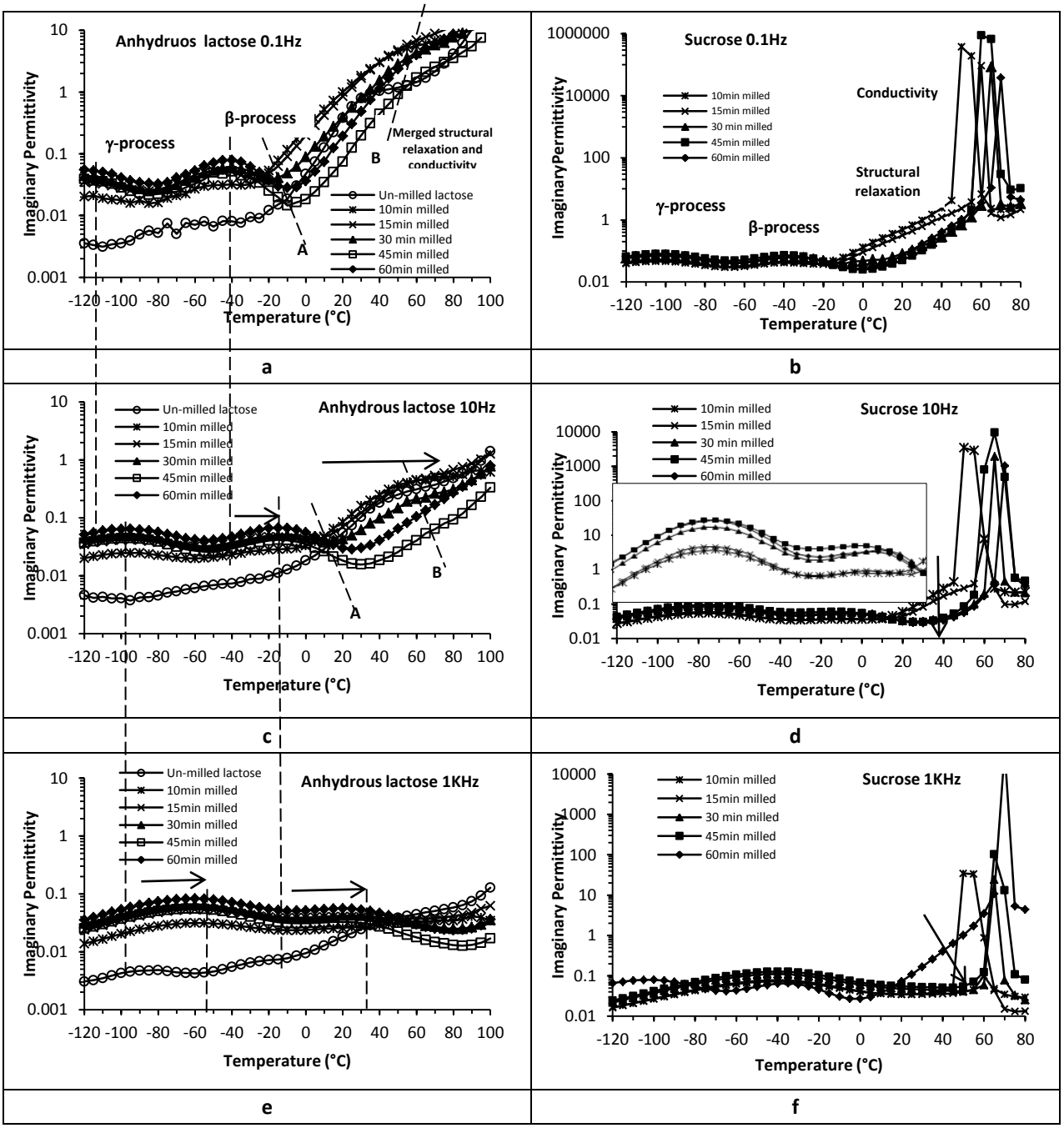

Figure 4.9: Temperature slices (plots of imaginary permittivity against temperature) at 0.1 Hz, 10 Hz and 1K Hz frequencies from dielectric spectra of milled anhydrous lactose (left column) and milled sucrose (right column). The four processes have been labelled as γ, β, structural relaxation and conductivity. The vertical dotted lines indicated the peaks of both γ & β processes of all milled samples processes lie on the same position but shift towards higher temperature by increasing frequency as indicated by the horizontal arrow heads. The inset in Figure 'd' indicates the change in height of γ and β processes with milling time in sucrose. The downward arrow heads indicate the disappearance of structural relaxation signals in sucrose.

This implies that the higher temperature wing in milled lactose cannot be the only structural relaxation of amorphous phase but also it has certain contribution from the percolation

since the milled samples contain particles with hard crystalline surface. The decrease in the strength of this process after an initial increase represents the decrease in percolation component as the hard crystalline surfaces recede with milling time.

The height of this process is higher in short milled sample (10 min milled), then decreases gradually till 45 min and increase again in 60 min milled sample (Figure 4.9a). The probable reasons for this change include; in early few minutes of milling as the particle size gets smaller the size of dipole decreases, percolation path length decreases and dipole strength increases. On further milling, as the amorphous content increases the hard crystalline surfaces decrease so the height of this process. Although the amorphous content does not increase after 30 min (as indicated by DSC and THz results in Chapter 3, Section 3.4.2), the 60 min milled sample is more conductive because of the aggregation of particles in such long milled samples (evidenced by SEM and BET results in Chapter 2, Section 2.3.2 and 2.3.3, respectively).

The point where the high temperature wing takes the plateau of dielectric signals in low frequency window (*i.e.* 0.1 Hz) occurs at high temperature in the short milled samples and at the lower temperature in long milled samples (as indicated by dotted line 'A' in Figure 4.9a); probably represents de-vitrification. In short in milled lactose, as the amorphous content is low, de-vitrification is small and it occurs at higher temperature while in long milled samples where there is a high proportion of amorphous content the plateau in dielectric signals occurs even at relatively lower temperature. It is also worth to note that, this event occurs between 30 °C to 80 °C which is close to the de-vitrification peak temperature in DSC (50 to 90 °C, Figure 4.2b). The small differences in de-vitrification temperature from both techniques might be due to i) the variation in the rate of heating and ii) different geometry of samples in both techniques (Megarry et al., 2014).

Unlike lactose where it is masked under conductivity, the structural relaxation in **milled sucrose (0.1 Hz frequency window)** is observed as a shoulder in all milled samples in the temperature range of -10 °C to 45 °C (Figure 4.9b). In the intermediate frequency window (10 Hz), the range of structural relaxation signals narrows down and its strength drops in longer milled samples (*i.e.* ≥ 30 min milled) (Figure 4.9d). While at higher frequency window (1 KHz) the structural relaxation disappears in all milled samples ≤ 45 min (Figure 4.9f), and appears again in 60 min milled sample (these changes have been indicated by downward

arrows in Figure 4.9 d & f). This is followed by the appearance of huge and sharp peaks that start at ~50 °C and shift towards higher temperature with milling time.(Figure 4.9b) These spikes occur between 50 °C to 70 °C and represent the onset for de-vitrification with temperature very much similar to that observed in DSC results (see Figure 4.3b).

4.3.6.2 Low Temperature Processes in Dielectric Spectra of Milled Sugars

The gamma and beta processes are now discussed in term of temperature and frequency slices of dielectric spectra in order to provide in depth commentary on the dynamics of the amorphous phases produced by milling.

The t-slices from low temperature window (< 0 °C) of **milled lactose** for various time intervals at three different frequencies 0.1 Hz, 10 Hz and 1 KHz (Figure 4.9 a, c & e respectively) show that the γ and β relaxation processes shift toward higher temperatures as the frequency increases (indicated by arrow heads in Figure 4.9e).

The **t-slices of milled sucrose** at same frequency windows again show two (γ and β) relaxation processes (Figure 4.9 b, d & f) in low and intermediate frequency windows. These processes move toward higher temperature in high frequency windows (Figure 4.9 b & d) similar to the anhydrous lactose. However, in high frequency window (1 KHz) there is only one broad process instead of two typical low temperature processes in samples milled for 10 min to 45 min milled; thereafter again two processes are observed in 60 min milled sample (Figure 4.9f) which are again shifted towards lower temperature.

Across the experimental frequency range highlighted in the temperature slices of Figure 4.9 (*i.e.* 0.1 to 1 KHz) the temperature range for the peak of the γ-process, for milled lactose, lies in the range -110 °C to -60 °C while the β process extends from -50 °C to +20 °C. For the sucrose the peak of the γ-process lies in the range -110 °C to -40 °C while the β process extends from -35 °C to -10 °C. The higher the temperature of each process the less mobile one might consider the matrix, it follows that the molecular dynamics in the amorphous phase of lactose are less restricted than in sucrose. This observation is explored further when the frequency slices are analysed using Arrhenius plots (Figure 4.14).

The f-slices from the dielectric spectra 60 min milled samples of both lactose and sucrose at from -100 °C to +100 °C (with increment of 20 °C) are shown in lower (< 0 °C) and higher (> 0 °C) temperature windows in (as shown by arrow heads in Figure 4.10a-d). There is only a

single broad process (gamma) towards lower temperature (in the experimental window), the height of this process increases and it narrows down along with shifting towards the higher frequencies as going towards higher temperature (Figure 4.10a & b). The second process (beta) appears at ~-75 °C as a small process and is more prominent near -20 °C, therefore the f-slices are taken at -20 °C to show both gamma and beta processes in different time milled samples of the both sugars.

In higher temperature window, the beta process which is only present in temperature range ≤ 50 °C continues shifting towards higher frequencies where it is followed by the huge conductivity wings that shifts towards lower frequencies as the temperature increases (as shown by the arrow heads in Figure 4.10c & d).

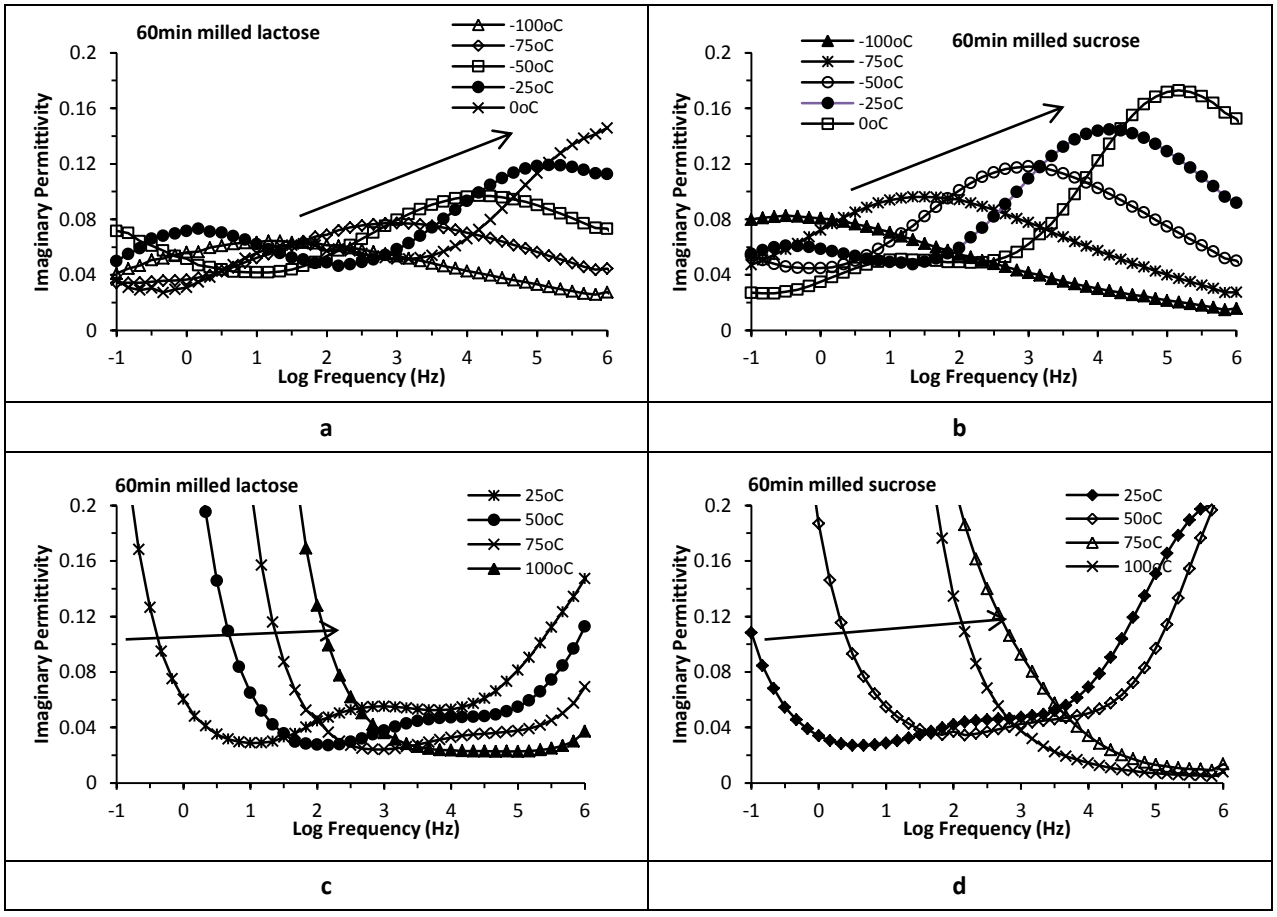

Figure 4.10: The frequency slices (plots of imaginary permittivity against frequency) at low (a & b) and high (c & d) temperatures from dielectric spectra of 60 min milled anhydrous lactose (left column) and 60 min milled sucrose (right column). The shift of relaxation processes with frequency is shown by arrow heads.

The f-slices of the both milled sugars at different milling times at -20 °C have indicated that the position of both secondary relaxations does not move with milling time and these occur at same frequency in all milled samples (as indicated by lines 'A' and 'B' in Figure 4.11 a and

line 'C' and 'D in Figure 4.11b). The γ-relaxation process of milled lactose shows a peak at relatively higher frequency *i.e.* ~10e^5 Hz than milled sucrose that occurs between 10e^2 and 10e^3 Hz. On the other hand the β-relaxation process occurs at relatively lower frequency *i.e.* between 10^0 and 10^1 Hz for milled lactose and at ~10e^0 Hz for milled sucrose. The height of these processes is assessed for both sugars at different milling times.

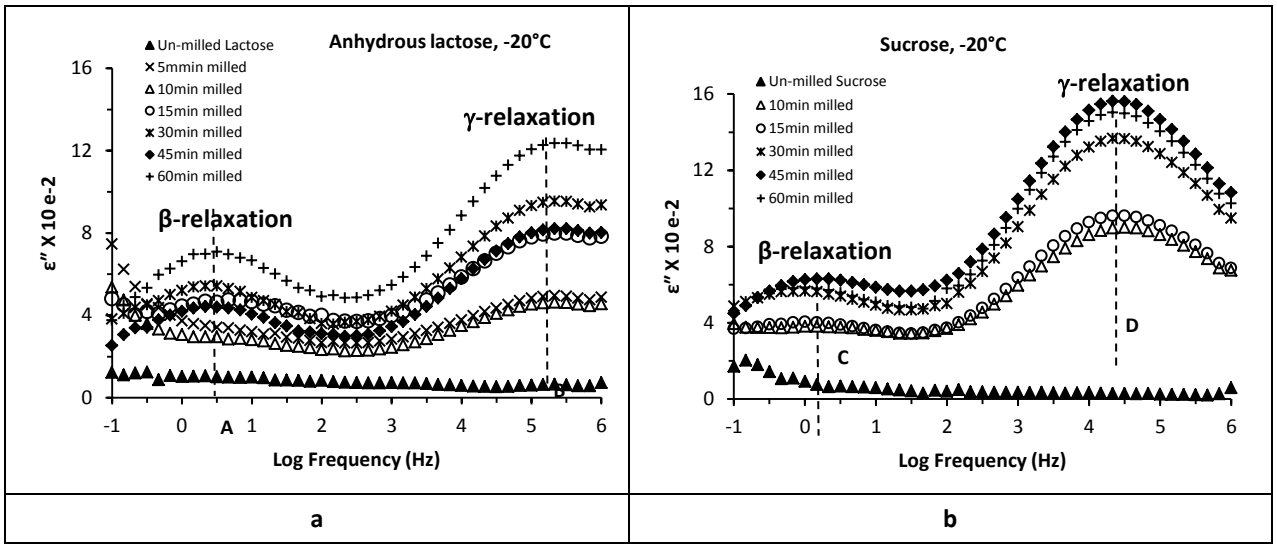

Figure 4.11: Frequency slices of different milled samples of a) lactose and b) sucrose showing β and γ processes from lower to higher frequencies respectively. The vertical dotted lines indicate the peak point for each process. The arrow head in Figure b show the shift of process towards higher frequencies.

The amplitude of secondary relaxation processes for each of lactose and sucrose were estimated in term of imaginary permittivity (ε″) and plotted against the milling time (Figure 4.12). The results for lactose show that the amplitude of both gamma and beta processes increases with milling time until 15 min afterward there is a only a slow increase/plateau in 30 and 45 min and increase again in 60 min milled sample (Figure 4.12a). In case of sucrose the peak heights increase with milling time until 30 min, thereafter almost plateau is achieved in 45 and 60 min milled sample (Figure 4.12b).

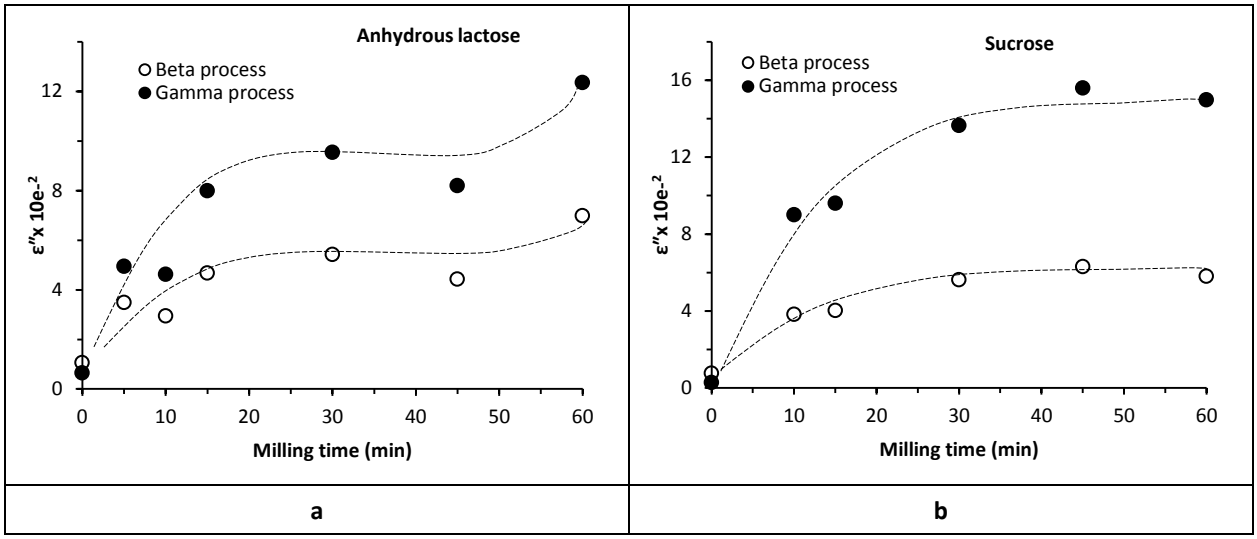

Figure 4.12: The plot of imaginary permittivity of secondary relaxation (gamma and beta processes) against milling time for a) milled anhydrous lactose b) milled sucrose.

The magnitude of gamma process of milled lactose is slightly higher than the milled sucrose contrary to beta process, which is higher in case of sucrose.

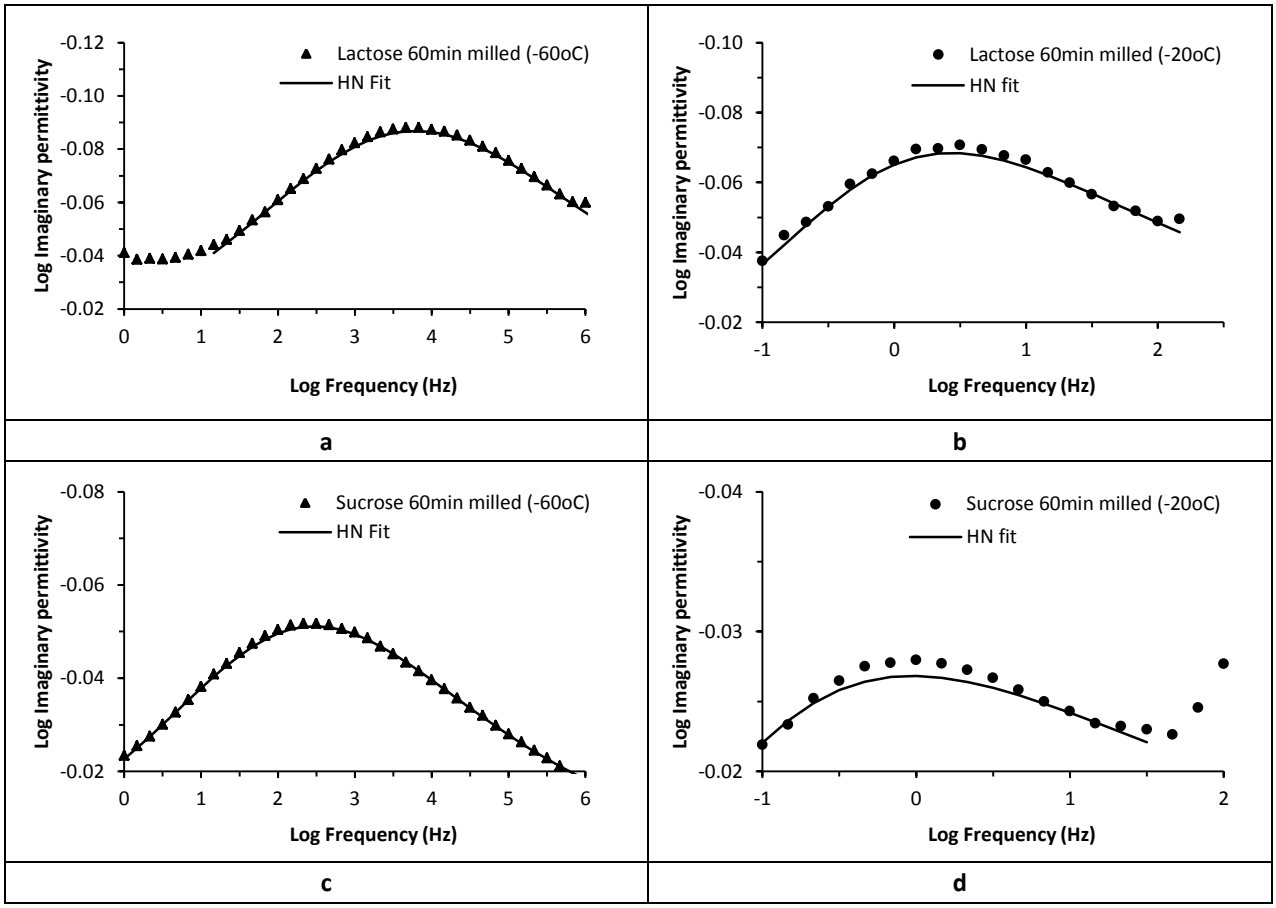

Figure 4.13: Plots of permittivity loss against log frequency showing fit results for 60min milled lactose (a-b) and 60min sucrose (c-d). The figures in left column show γ-process and while the β-process in right column.

In order to determine the specific parameters representing the dynamics of amorphous phase of these milled sugars, both γ and β-processes were fitted applying the Haviliak-Negami function (Equation 4.1). Some examples of the fitting have been shown in Figure 4.13 a-d.

$$\varepsilon^*(\omega) = \varepsilon_\infty + \frac{\varepsilon_s - \varepsilon_\infty}{[1+ (i\omega\tau_m)\alpha]\beta} \qquad \text{Equation 4.1}$$

The plot of relaxation time against the reciprocal of temperature for both γ and β-processes of milled lactose and sucrose has indicated that the temperature dependence in term of linear Arrhenius behaviour (Figure 4.14). The gradients of these plots for γ-process do not change on milling (Figure 4.14a & b), however these change for β-process (Figure 4.14c & d). This indicated that the β-process is more influenced by the milling of these sugars than the γ-process. In order to investigate it further two parameters; activation energy (E_a) and relaxation time (tau/τ) are obtained for these processes.

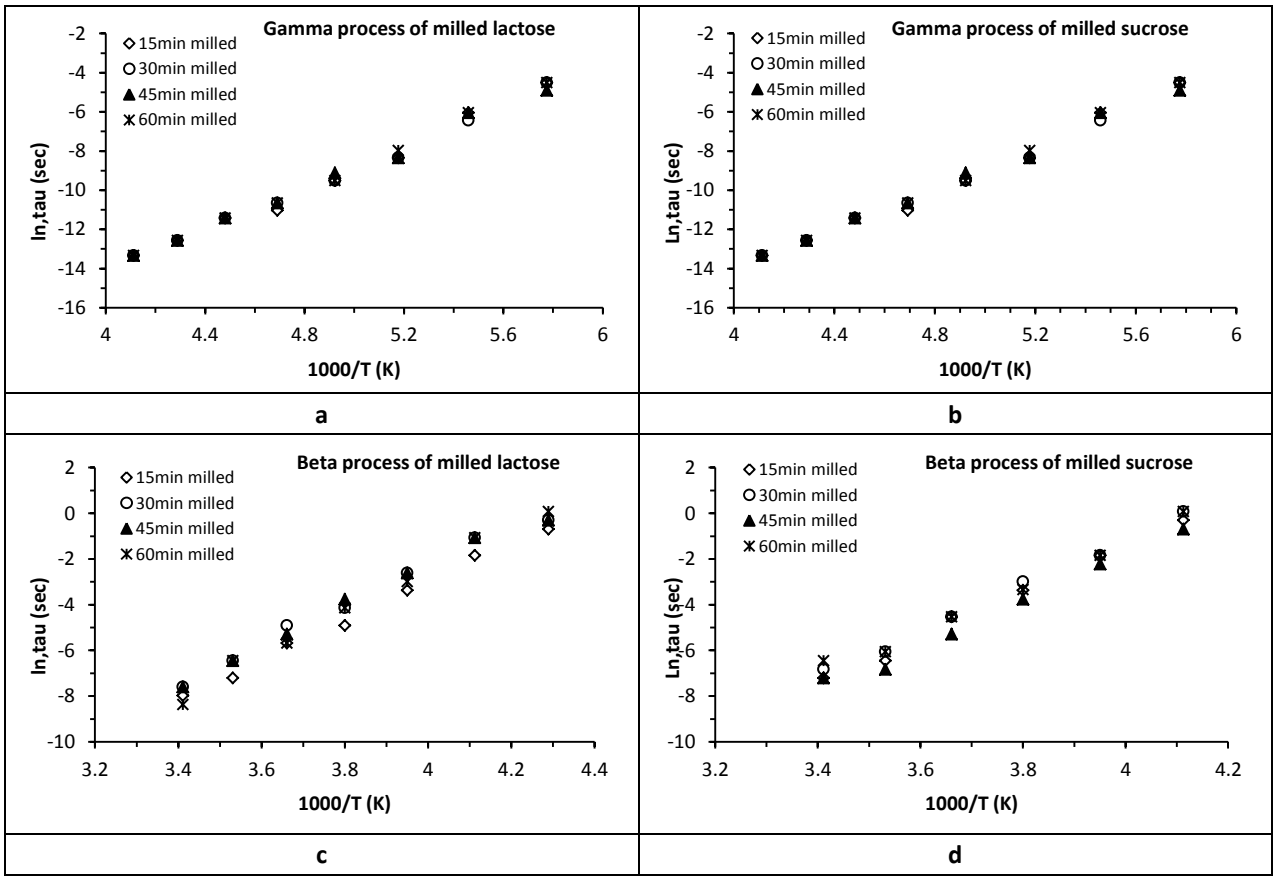

Figure 4.14: The plots of relaxation time against inverse of temperature (Arrhenius plots) for different milled samples of lactose and sucrose. Figure a & b) show the plots of gamma process while c & d show the beta process of both milled sugars respectively.

The activation energies of both γ and β-processes are calculated from the gradient of these plots, by applying Arrhenius relation (Equation 4.2), while the 'τ' is obtained from the fit results/peak frequency at -60 °C and -20 °C for the γ and β-processes, respectively. The results for both are summarized in Table 4.3.

$$\mathbf{K = Ae^{-Ea/RT}} \qquad \textbf{Equation 4.2}$$

where 'E_a' represents the activation energy, 'T' is temperature in kelvin and 'R' is universal gas constant. The values of activation energy of γ-process of all milled lactose samples are ~44 KJ mol^{-1}, which is very close to the values reported for this process in freeze dried lactose (Ermolina and Smith, 2011). For milled samples of sucrose the activation energy is ~50 KJ mol^{-1} which is in agreement with that in amorphous sucrose (Kaminski et al., 2008a). The activation energies of β-relaxation process of milled lactose samples *i.e.* ~ 72 KJ mol^{-1} are in agreement with that is freeze dried lactose and that of milled sucrose sample ~ 82 KJ mol^{-1} in agreement with that of amorphous sucrose, therefore the β-process is true Johari Goldstein process. Also, it is of worth to note that the activation energies for both secondary relaxations in milled sucrose are higher than that in the milled lactose (Table 4.3) which potentially indicates the higher stability or rigidity of sucrose as compared to lactose.

Table 4.3: The values of activation energies as calculated for the milled lactose and sucrose. (E_a= energy of activation in KJ mol^{-1}).

milling time(min)	Anhydrous lactose		Sucrose	
	Gamma process E_a (KJmol^{-1})	**Beta process** E_a (KJmol^{-1})	**Gamma process** E_a (KJmol^{-1})	**Beta process** E_a (KJmol^{-1})
15	44 ± 1.6	71 ± 3.8	51 ± 0.5	84 ± 8.4
30	43 ± 1.1	71 ± 5.9	50 ± 0.5	83 ± 4.8
45	43 ± 1.2	72 ± 5.7	50 ± 0.5	82 ± 7.0
60	44 ± 1.0	79 ± 5.9	52 ± 0.7	79 ± 7.6

4.4 Discussion

The molecular dynamics of the amorphous phase in both milled lactose and sucrose were described in term of secondary relaxation processes. Among the two secondary relaxation processes; **γ-process** in sugars originates from the movement of pendant groups on the surface of the molecule (Ermolina and Smith, 2011). In the milled anhydrous lactose this process occurs at a relatively higher frequency and its amplitude is larger than that in the milled sucrose, which may indicate that the pendant groups of lactose are more hindered as compared to those of sucrose.

The amplitudes of this process increase with milling time up to 30 min in both sugars and till 60 min milling in lactose only. This increase is greater in milled lactose than that in the milled sucrose. This indicates relatively higher mobility in milled lactose as compared to the milled sucrose. Although the γ-relaxation represents a local scale movement but its change with milling time indicates an increase in the fluidity of the molecules due to the crystal damage that facilitates the movement of pendant groups. However on longer milling (45 and 60 min), the amplitude does not increase further that probably because of the lower moisture in long milled samples (TGA results, Figure 4.2d & 4.3d) that decreases the overall fluidity.

The β-process shows somewhat more facilitative intramolecular movements with the scale length larger than that of the γ-relaxation. In the small molecules of disaccharides it involves the bending/twisting of the two constituent mono-saccharides around the glycosidic linkage (Ermolina and Smith, 2011). It is shows somewhat cooperativity therefore can be considered as the precursor of structural relaxation (Ngai and Capaccioli, 2004) . The β-process for both milled sugars occur at almost the same frequency, however the amplitude for sucrose is larger in short milled samples than for lactose which is affected more by milling (in the framework of experimental error), whereas both have almost the same amplitude at 60 min milling. This represents relatively more freedom/flexibility in lactose molecule and the higher rigidity of the sucrose as already stated (Kaminski et al., 2008a). The larger amplitude of lactose or its variation with milling is probably due to the fact that it absorbs more moisture than milled sucrose.

The conformation of activation energies of both milled sugars with that from freeze dried and super cooled sugars represents that amorphous phase is almost the same regardless of processing methods. As the activation energy of sucrose is decreasing with milling time, it is counterintuitive to the results from DSC that the crystallization is delayed with milling time as the amorphous content increases particular. Therefore, E_a alone cannot be primitive factor in defining the stability of milled sucrose.

4.5 Conclusion

In this study we have presented the dynamics of amorphous phase produced by ball milling the two common sugars; lactose and sucrose. The molecular dynamics in terms of 'γ' and Johari-Goldstein β process at various milling time and de-vitrification kinetics indicate that

the lactose is more mobile and it has more propensities for de-vitrification than sucrose after milling. The study also indicates that both the gamma and beta processes are not affected by milling time, although the height increases with amount of amorphous phase but within each phase, the dynamics of amorphous phase remains unaffected by milling time. Also the moisture is found to play a key role in the onset for de-vitrification in milled lactose.

5 Study of Milling and Co-milling: Techniques for the Improvement of Solubility and Dissolution Rate of Poorly Soluble Drug – Ibuprofen

5.1 Background/Context

Milling and co-milling are well known techniques that have a positive influence on solubility and dissolution rate of sparingly soluble drugs (Jagadish et al., 2010, Bahl and Bogner, 2008). Co-milling is defined as milling in the presence of an excipient. It has been shown to be a simple, efficient and economical process that does not require any sophisticated instruments. It is also environment friendly as it does not involve the use of any organic solvent (Friedrich et al., 2005). A further detail of this phenomenon is given in Chapter 1, Section 1.6.

Ibuprofen is one of the propionic acid derivatives that provide analgesia through the inhibition of the enzyme cyclooxygenase (COX). It is widely used in the treatment of rheumatoid arthritis, osteoarthritis, ankylosing spondylitis and acute gouty arthritis (Brunton et al., 2006). Ibuprofen is practically insoluble in water or acidic medium (Saleh et al., 2008), resulting in poor bioavailability when administered as a conventional dosage form.

The issue of poor solubility of ibuprofen has been addressed in the literature by applying different approaches e.g. milling (Plakkot et al., 2011), preparation of solid dispersions with PEG (Hasnain and Nayak, 2012) or poloxamer (Newa et al., 2008, Passerini et al., 2002), complexion with β-cyclodextrin (Chowdary and Susmitha, 2012, Salústio et al., 2011) and co-milling (Mallick et al., 2008b, Mallick et al., 2008a, Han et al., 2011).

In the majority of these studies, size reduction or dispersion of the drug in an amorphous matrix were the underlying mechanisms for the improvement of solubility and dissolution rate. It was noted that there was only a little improvement in dissolution rate with particle size reduction from milling ibuprofen alone. However, milling in the presence of inorganic salts (Kaolin, aluminium hydroxide) or hydrophilic substance (PVP) resulted in the amorphization, chemical interaction, de-aggregation and improved wettability of the drug, which in turn resulted in higher dissolution rates.

Among the excipients used in co-milling with ibuprofen, neither would be expected to solubilise the drug. To that end, the recent work with soluplus (Thakral et al., 2012), on the

solubility enhancement by the way of hot melt extrusion, solid dispersion, electro-spinning, solvent evaporation, spray drying and freeze drying (Shamma and Basha, 2013, Nagy et al., 2012) has suggested that this excipient may be used to advantage when co-milled with drugs. In addition, there are many other potential candidate excipients which have not been investigated to date for their potential in enhancing the solubility and dissolution rate of ibuprofen. Nevertheless, these including HPMC, PVP, MCC and lactose are the widely used excipients for their hydrophilic and wettability enhancing properties (Garg et al., 2009, Vogt et al., 2008c, Vogt et al., 2008b).

The objectives of this study are the potential enhancement of the solubility and dissolution rate of a poorly soluble drug, ibuprofen by co-milling (this will include the development of a UV-spectroscopic method for the determination of ibuprofen in unknown samples in the presence of interfering excipient) and to characterise the co-milled mixtures for changes in particle size, morphology, physicochemical interactions and the changes in crystallinity/amorphicity.

The initial part of the work involving the solubility study was carried out in two phases; in the **first phase;** the excipient type and processing conditions (including the speed and time of milling) were selected on the basis of best outcomes in term of processing properties (like flowability) and solubility of the drug in water. In the **second phase** the selected parameters were applied to prepare co-milled mixtures and to determine their effect on solubility and dissolution rate (in phosphate buffer pH 7.4). In the last part of this study, the co-milled mixtures based on these selected excipients were characterized by various analytical techniques to establish the mechanism of solubility and dissolution rate enhancement.

5.2 Materials and Methods

Ibuprofen (Zafa Chemie, Lahore Pakistan), was obtained from Unexo lab, Lahore Pakistan. Soluplus® (a graft co-polymer of PEG) and Lutrol® F-68 (or Poloxamer is a block co-polymer non-ionic surfactant consisting of Poly-oxyethylene-(POE-) and Polyoxypropylene-(POP-) units) were obtained from BASF, UK. Polyvinyl pyrrolidone (PVP K30) (Jiaozou Fine Chemical, China), hydroxy-propylmethyl cellulose (HPMC-E5) (Ashland, US), micro-crystalline cellulose (MCC, avicel Ph-101) (Accent Microcell Pvt. Ltd. India), and PEG-6000 were obtained from

CCL Pharmaceuticals Pvt Ltd, Lahore Pakistan. All excipients were of pharmaceutical grade and were used as received from the suppliers.

5.2.1 Co-milling of Ibuprofen with Different Excipients

Ibuprofen was co-milled with different excipients: (Soluplus, HPMC, Lutrol, PVP, MCC, lactose and PEG-600 in screening phase while the first two in extended phase) in the vibratory ball mill according to the method described in Section 2.2.1. The mill was operated at frequency of 15 Hz for 15 min (this low speed was selected for ibuprofen and its mixtures to avoid the melting of this drug). The sample was collected into a glass vial and immediately used for solubility determination or stored in desiccator until used for the further analysis.

Note: Based on the highest solubility of ibuprofen in their co-milled mixtures (see results in Figure 5.7); soluplus and HMPC were selected for the next phase of this study. In this phase, different drug to excipient ratios (*i.e.* 1:0.25, 1:0.5, 1:0.75 and 1:1) of selected excipients were used in order to determine the effect of excipient concentration. The physical and milled physical mixtures (abbreviated as PM and mPM, respectively) of Ibuprofen with these excipients were also prepared for the purpose of comparison with co-milled mixtures. The PM was prepared by simple mixing the both components with spatula in a weighing boat (Barzegar-Jalali et al., 2010) and the milled physical mixtures were prepared by milling the ibuprofen and excipients separately in ball mill then mixing these in 1:1 ratio.

5.2.2 Solubility Studies

Shake flask method (Nandi et al., 2003) was used to determine the solubility of ibuprofen in distilled water and phosphate buffer pH 7.4. Excess quantity of ibuprofen or its co-milled mixtures (equivalent to 200 mg ibuprofen) with each of the excipients was added to a 100 ml conical flask containing 50 ml of the solvent. The flasks were capped and shaken at 100 rpm on a multi-flask shaker (Heidolph Unimax 2010, Germany) at room temperature (~25 °C). The samples were collected after 6, 12, 24 and 48 hours, filtered through 0.45 µm syringe filters (Millipore, US) and diluted adequately. The concentration of ibuprofen was determined by the UV spectrophotometry.

Note: The standard solutions of known concentrations of ibuprofen in distilled water and phosphate buffer pH 7.4 were prepared and the calibration curves were constructed. These curves in adherence to Beer-Lambert law (*i.e.* $A < 1$) were linear in the range of 0.005 to 0.08

mg ml^{-1} in distilled water (Figure 5.1a) and 0.05 to 0.45 mg ml^{-1} in phosphate buffer (Figure 5.1b) with value of correlation coefficient near unity and value of intercept on the ordinate, near to zero.

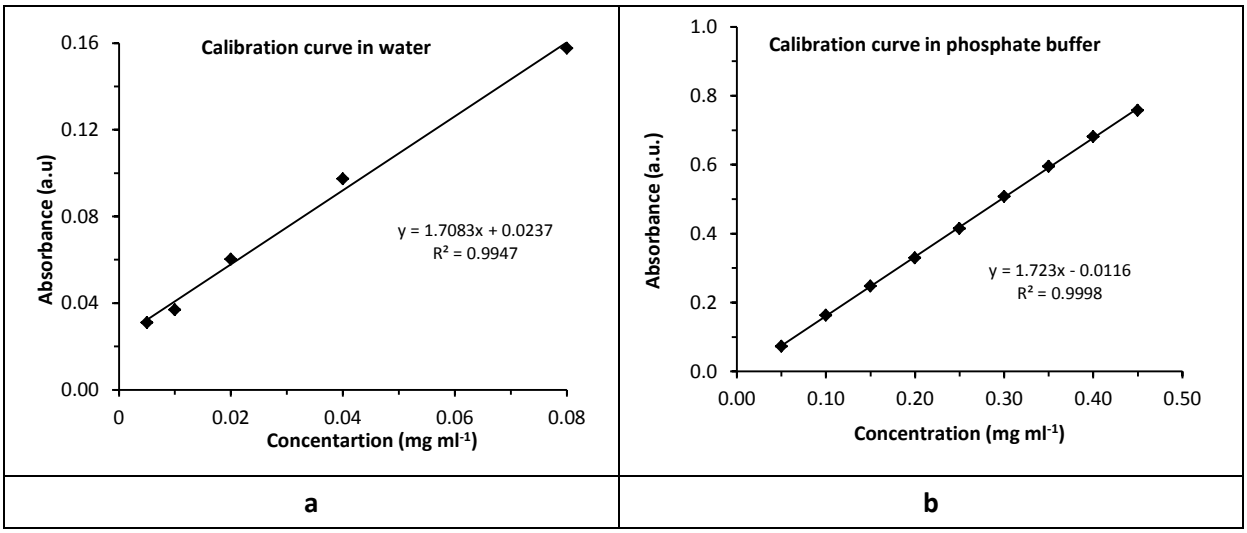

Figure 5.1: Calibration of ibuprofen as prepared in distilled water (a) and phosphate buffer pH 7.4.

5.2.3 Dissolution Studies

Ibuprofen and its co-milled mixture with different excipients, equivalent to 200 mg ibuprofen, were filled in colourless hard gelatine capsule shells and subjected to dissolution studies in USP type-I (paddle) apparatus (DT-700, Erweka Germany). The phosphate buffer pH 7.4 was selected as the dissolution medium. The temperature of the medium was maintained at 37 $\pm$ 0.4 °C with a paddle rotating speed of 50 rpm. Aliquots of 5 ml were withdrawn at intervals of 5, 10, 20, 30, 45, 60 and 90 min and replaced with the equal volume of the fresh dissolution medium. Each sample was filtered through a syringe filter (0.45 µm) and then diluted adequately (*i.e.* $A_{max} < 1$) for assay by the UV spectrophotometry.

The release of ibuprofen from physical and co-milled mixtures was also expressed in term of dissolution parameters (calculated from the dissolution profile) including Q30 min (mean percentage of drug dissolved in the first 30 min), dissolution efficiency (area under the dissolution-time curve up to time 't') and the mean dissolution time (average time for the drug dissolution).

5.2.4 Determination of the Intrinsic Dissolution Rate (IDR)

Sample preparation: The weighed quantity of ibuprofen or its co-milled mixtures were pressed into 13 mm circular compacts by hydraulic press (Perkin Elmer, US), at the pressure

of ~10 kPa. These compacts were weighed and placed in the centre of a cylindrical plastic die placed on glass sheet. The molten hard paraffin wax (temperature near 40 °C) was poured in the plastic die to cover the sample compacts completely (Figure 5.2a). These dies were cooled to avoid the overheating of ibuprofen and allowed to solidify. After solidification, the waxed compacts were removed from dies and cut to size of dissolution basket by sharply edged metal pipe. The compacts now have one surface available for exposure to the dissolution medium (Figure 5.2b). These plugs were inserted in baskets of dissolution apparatus facing downward.

a b

Figure 5.2: a) Formation of wax plugs around the compacts in the plastic moulds b) tablet embedded in wax plug.

Dissolution study was carried out in phosphate buffer (pH 7.4) using a USP type II (basket) apparatus, applying the method as described in Section 5.2.3.

5.2.5 Laser Diffraction for Particle Size Determination

Particle size distribution (PSD) of un-milled Ibuprofen and its co-milled mixtures was determined with dry dispersion laser diffraction technique according to the method already described in Section 2.2.2.

5.2.6 Scanning Electron Microscopy (SEM)

The un-milled, milled and co-milled Ibuprofen samples were photographed according to the method described in Section 2.2.3.

5.2.7 Differential Scanning Calorimetry (DSC)

DSC experiments of un-milled ibuprofen and its co-milled mixtures with different excipients were performed according to method described in Section 3.2.3. The sample was analysed over the temperature range of 25 to 150 °C at a heat flow rate of 20 °C min^{-1}.

In order to compare results of milled ibuprofen with that of a 100% amorphous sample, the ibuprofen contained in non-hermetically sealed DSC pan was vitrified by heating in an oven

at 90 °C for 10 min then quenched by dipping it in the liquid nitrogen. This pan was loaded in a pre-cooled DSC furnace and heated from -60 °C to 110 °C at the rate of 10 °C min^{-1}.

5.2.8 Attenuated Total Reflectance (ATR) Spectroscopy

The IR spectra of un-milled, milled and co-milled ibuprofen were recorded in Bruker Alpha – FTIR Spectrophotometer (Bruker, Japan) fitted with a Smart Performer, platinum ATR accessory, according to the method described in (Singh et al., 2009). The data were analyzed by Alpha Opus Software. The instrument was configured with ATR sample cell containing a diamond crystal with scanning depth of 2 µm. Sample powder was placed on the surface of crystal and secured in place with clutch type lever. Each sample was scanned for 20 times against air between 4000 - 400 cm^{-1} at the resolution of 2 cm^{-1}.

5.2.9 Powder- X-ray Diffraction (PXRD)

The samples for PXRD were mounted on the zero background silicon wafers and the measurements performed on a Bruker D4 diffractometer according to the method as described by (Dong et al., 2008) using Cu Kα radiation, and λ = 1.5418 A° . The samples were spun to improve the counting statistics. Each sample was exposed to X-rays for 0.12 seconds per 0.02° of 2θ increment (continuous scan mode) over the range 2° to 40° in theta-theta mode.

5.2.10 Terahertz Pulsed Spectroscopy (TPS)

THz measurements of un-milled and co-milled materials were carried out according to the method already described in Section 3.2.4. The pellets of polyethylene powder contained the co-milled mixture equivalent to 10% w/w of the ibuprofen.

5.3 Results and Discussion

5.3.1 Solubility of Un-milled and Milled Ibuprofen

The solubility of un-milled ibuprofen in distilled water at room temperature (~25 °C) was ~0.09 mg ml^{-1} (n=3). Unsurprisingly, milled Ibuprofen was found to have almost the same solubility. These values were comparable or slightly higher than the reported solubility values of Ibuprofen from the literature (viz. 0.056 $\pm$ 0.004 (Kocbek et al., 2006), 0.09 mg ml^{-1} (Milhem et al., 2000) and 0.081 mg ml^{-1} (Wikarsa et al., 2008).

5.3.2 UV Spectra of Ibuprofen and Excipients

A 0.05% w/v solutions of the un-milled and milled ibuprofen in pH 7.4 phosphate buffer showed a well-defined, large peak at 221 nm (can be seen in the diluted samples) and two other peaks; one at 264 nm and second at 273 nm and a shoulder at 258 nm (Figure 5.3a). The overlaid spectra of solutions (0.05% w/v) of ibuprofen and four major excipients used in this study (Figure 5.3b) have shown that, 0.05% w/v Lutrol and 0.05% w/v HPMC in phosphate buffer have negligible absorbance over the entire UV range. In contrast, 0.05% w/v PVP and 0.05% w/v soluplus in phosphate buffer exhibit a high absorbance, with the former only at wavelengths below 230 nm while the later over the entire range of wavelengths (210 – 330 nm) (see Figure 5.3b).

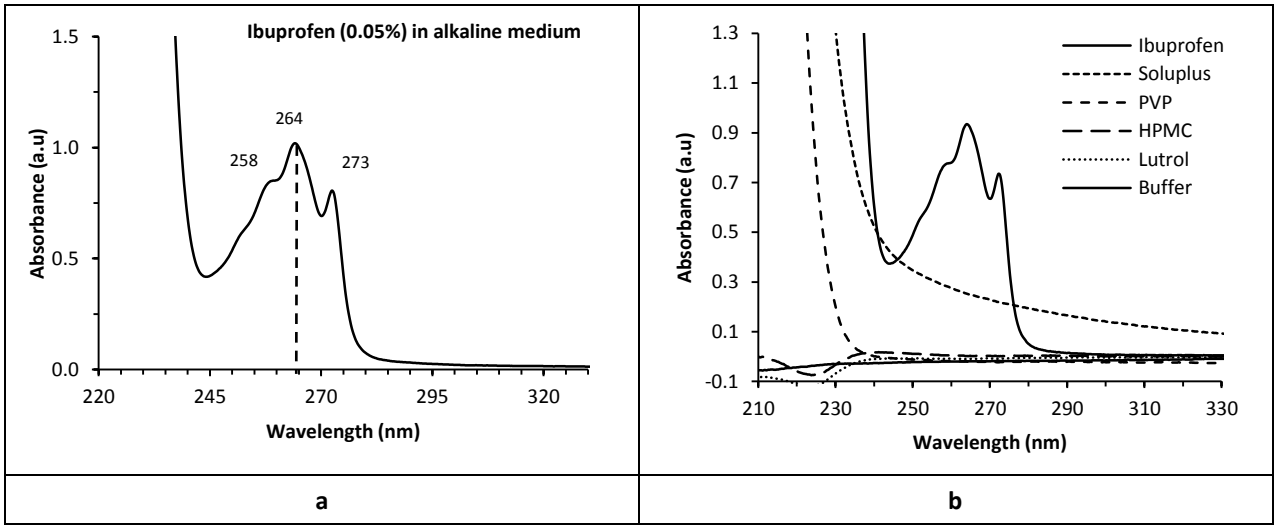

Figure 5.3: UV spectra of a) un-milled ibuprofen in alkaline medium showing two peaks and a shoulder b) Overlaid UV spectra of 0.05% w/v solutions of ibuprofen and the excipients, Soluplus , PVP, HPMC, and Lutrol in phosphate buffer (pH 7.4).

5.3.3 Selection of UV Absorbance Peak for the Ibuprofen Assay

The fact that solutions of soluplus and PVP, in pH 7.4 phosphate buffer, exhibit large absorbance below 230 nm, precluded the use of the absorbance peak of ibuprofen at 221 nm in the development of the UV-assay for these two excipients. For consistency this was also not used for the other excipients. In order to select the analytical wavelength, the absorbance of ibuprofen was determined at 258, 264 and 272.4 nm (Table 5.1a). The results indicated that Lutrol, HPMC and PVP have only 1-2% of the absorbance at the three potential analytical wavelengths for ibuprofen. Therefore, the wavelength of maximum absorbance (λ_{max}) *i.e.* 264 nm, was selected for the assay of ibuprofen in the presence these

excipients. On the other hand, the UV spectrum soluplus solution has shown a significant absorbance over the entire wavelength range, which increases towards lower wavelengths (Figure 5.3b). This spectrum, when overlaid on the spectrum of same concentration of Ibuprofen it shows higher absorbance than ibuprofen solution towards higher wavelength (~285 nm), the point where the absorbance of ibuprofen start increasing which now obviously higher than the soluplus solution absorbance towards lower wavelengths. Therefore, two wavelengths were selected for the estimation of ibuprofen in the presence of soluplus; first 264 nm which is the λ_{max} of ibuprofen and has the highest ratio of absorbance with soluplus among the three potential wavelengths (Table 5.1b), second, 287 nm which is the λ_{max} for soluplus as the absorbance of soluplus to ibuprofen is maximum.

Table 5.1: a) Relative absorbance of the excipients as compared to the absorbance of Ibuprofen at three potential wavelengths of ibuprofen b) ratio of absorbance of ibuprofen and soluplus at three potential wavelengths of ibuprofen.

a)

	Relative absorbance (%) of excipients at three wavelengths of ibuprofen		
	258 nm	264 nm	272.4 nm
HPMC	1.4	1.1	1.2
Lutrol	0.4	0.3	0.4
PVP	2.1	1.5	1.5

b)

Ratio of absorbance of ibuprofen and soluplus		
258nm	264nm	272.4nm
2.8	3.9	3.6

5.3.4 Correction of the Interference (UV Absorbance) of Soluplus in the Quantitative Determination of Ibuprofen in the Mixture

5.3.4.1 Two Wavelength Assay

The two wavelength assay approach which is described as absorbance ratio method (Erk, 2000) or simultaneous equation method (Patil et al., 2009, Nallasivan et al., 2010) in literature with slight modifications but generally involves the measurement of the absorbance of both drug and the interfering excipient (*i.e.* ibuprofen and soluplus in our case) at two different wavelengths; $\lambda 1$ and $\lambda 2$ (as described in Section 5.3.3). The calibration curves are constructed by plotting these absorbance values against concentrations of both

single component solutions of ibuprofen x(d) and soluplus x(e) respectively. From this calibration curve, the absorption of both drug and excipient at two wavelengths can be described by the following relation (Equations 5.1 to 5.4).

$$\mathbf{A(d,\lambda 1) = m(d,\lambda 1)\,.\,x\,(d)} \qquad \textbf{Equation 5.1}$$

$$\mathbf{A(e,\lambda 1) = m(e,\lambda 1)\,.\,x\,(e)} \qquad \textbf{Equation 5.2}$$

Similarly at λ2

$$\boldsymbol{A(d,\lambda 2) = m(d,\lambda 2)\,.\,x\,(d)} \qquad \textbf{Equation 5.3}$$

$$\boldsymbol{A(e,\lambda 2) = m(e,\lambda 2)\,.\,x\,(e)} \qquad \textbf{Equation 5.4}$$

Where m(d, λ1), m(b, λ1) are the slope of curve drawn for the drug at λ1 and λ2; while, m(e, λ1), m(e, λ2) are the slope of excipient at λ1 and λ2 respectively. The total absorbance of the mixture of drug and excipient at both wavelengths is measured as A(T,λ1) and A(T,λ2) respectively. The individual contributions to the total absorbance at λ1 and can be described by Equations 5.5 – 5.6.

$$\mathbf{A(T,\lambda 1) = A(d,\lambda 1) + A(e,\lambda 1)} \qquad \textbf{Equation 5.5}$$

$$\mathbf{A(T,\lambda 2) = A(d,\lambda 2) + A(e,\lambda 2)} \qquad \textbf{Equation 5.6}$$

Now by substitution of the expressions for the individual absorbance of both components from equations 5.1 to 5.4 in Equations 5.5 and 5.6, gives the following expression for total absorption (Equation 5.7 and 5.8).

$$\mathbf{A(T,\lambda 1) = m(e,\lambda 1).x(e) + m(d,\lambda 1).x(d)} \qquad \textbf{Equation 5.7}$$

$$\mathbf{A(T,\lambda 2) = m(e,\lambda 2).x(e) + m(e,\lambda 2).x(d)} \qquad \textbf{Equation 5.8}$$

The unknown concentration of drug x(d) in the mixture is determined by applying the following expression (Equation 5.9) obtained from re-arranging and substituting the above equations.

$$\mathbf{x(d) = \left[\frac{A(T,\lambda 2).\ m(e,\lambda 1) - A(T,\lambda 1.m(e,\lambda 2)}{m(d,\lambda 2).m(e,\lambda 1) - m(e,\lambda 2).m(d,\lambda 1)}\right]} \qquad \textbf{Equation 5.9}$$

5.3.4.2 Multivariate Method

While assaying the ibuprofen in the presence of soluplus by two wavelength method, it is realized that the UV spectrum of 1 to 1 mixture of solution of both ibuprofen and soluplus is expected to overlay exactly with the theoretical mixture (obtained by taking the sum of

individual spectra of both after division by two). However, the measured spectrum was higher than the theoretical one (Figure 5.4). This might be due to the light scattering effect of soluplus that has formed micelles in the solution. Therefore, the interference by the soluplus could not be corrected simply by two wavelength method.

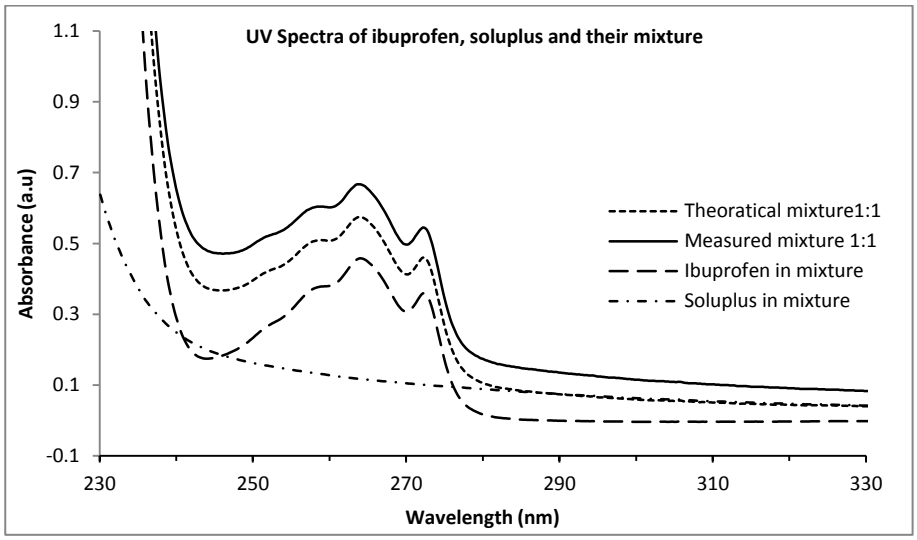

Figure 5.4: Overlaid UV spectra of 0.05% solution (in phosphate buffer pH 7.4) of both ibuprofen and soluplus and their 1 to 1 mixture. The theoretical spectrum is the mathematical sum of individual spectra of these components.

The least-squares solution to calculate the concentrations from the mixture spectrum, using reference spectra of individual components may be given by the Equation 5.10.

$$C = (S'S)^{-1}S'y \qquad \text{Equation 5.10}$$

Where 'C' is the concentration factor, which represents the exact contribution of the individual components in the mixture of ibuprofen and soluplus and 'y' is the measured spectrum of the mixture of both components. For the application of this method, the reference spectra of both ibuprofen and soluplus after division by 2 (denoted by 's1' and 's2') were collated into a single, two column matrix, called 'S' (Figure 5.5).

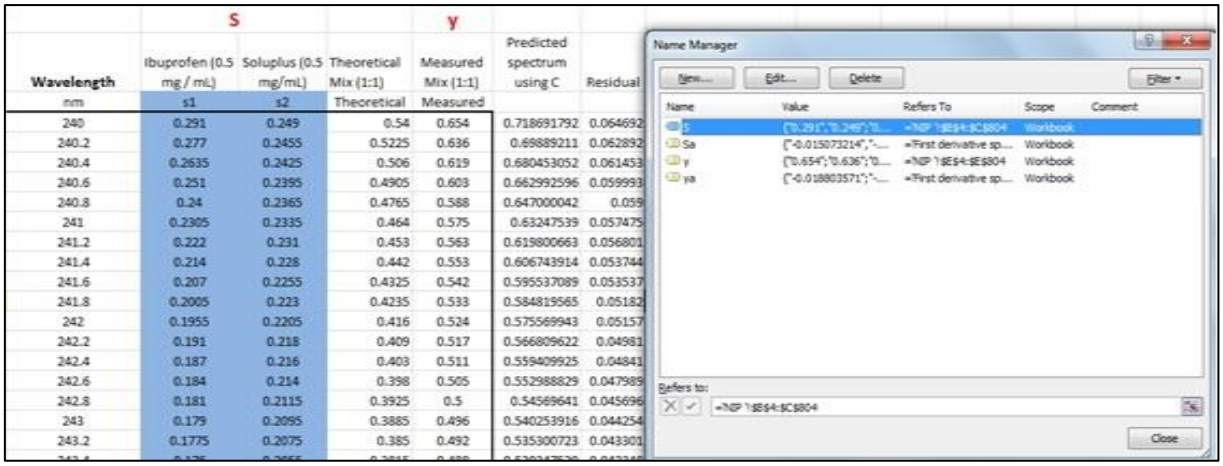

Figure 5.5: Screen shot from the excel spreadsheet showing the collation of individual spectra of ibuprofen and soluplus into single matrix 'S' as highlighted in blue columns. The inset shows the labelling of columns.

The concentration factor is then calculated by applying the matrix multiplication function to the collated matrix 'S' (of individual spectra of ibuprofen and soluplus) and the spectrum of known mixture of both components as shown in Figure 5.6.

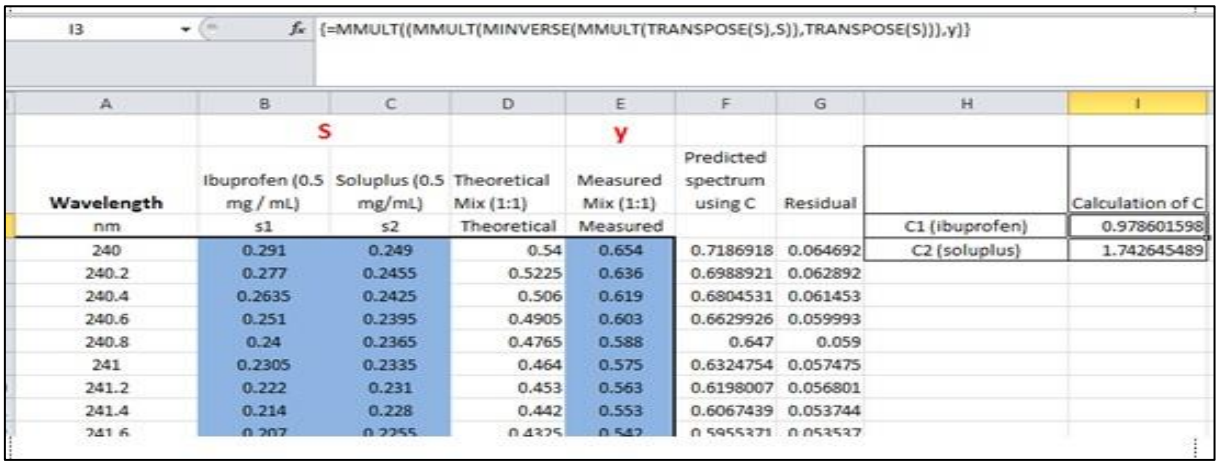

Figure 5.6: The screen shot from the excel spreadsheet showing the calculation of concentration factor from the individual spectra of ibuprofen and soluplus and the spectrum of their mixture.

The new spectrum is predicted from the matrix based on this concentration factor and overlaid on the measured spectrum (Figure 5.7a). It is noted that the spectrum predicted from this method did not exactly overlay the measured spectrum, however the same approach when applied to the derivatives of individual and measured spectra, both exactly overlaying (Figure 5.7b). Therefore the concentration factor 'C' from this predicted relation is used to calculate the concentration of drug in the unknown solution.

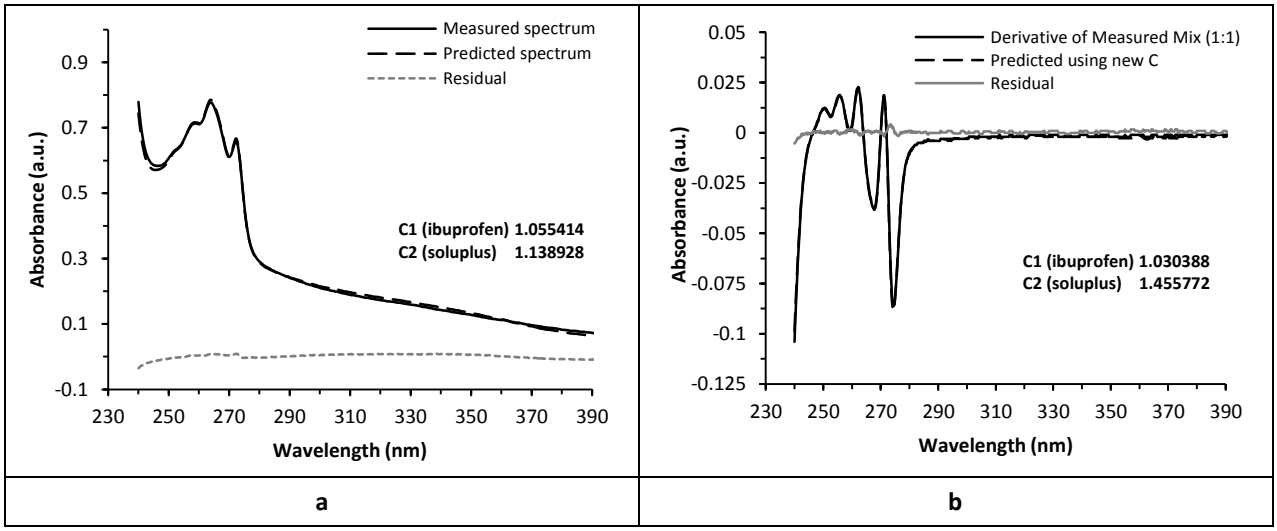

Figure 5.7: a) UV spectra of 1 to 1 mixture of 0.05% ibuprofen and soluplus in phosphate buffer (pH 7.4). The measured spectrum is directly obtained from the machine while the predicted spectrum is calculated by using concentration factors for both components. b) first derivatives approach to the same spectra.

Having developed this assay for ibuprofen-soluplus mixtures (based on the use of derivative spectra) it was then possible to determine the solubility of ibuprofen in co-milled mixtures of the ibuprofen and soluplus. The solubilities of ibuprofen in all other excipient-drug combinations were determined by simply taking the absorbance at the analytical wavelength of 264 nm and equating that to ibuprofen via the calibration curve for pure ibuprofen in distilled water or phosphate buffer.

5.3.5 Results of Screening Phase

5.3.5.1 Effect of Excipient Type on the Solubility of Ibuprofen after Co-milling

Figure 5.8 shows the comparison of solubilities of ibuprofen and its co-milled mixtures with different excipients. The results indicate that the solubility of ibuprofen in co-milled mixtures is higher than the un-milled drug alone. The highest effect is observed in co-milled mixtures with HPMC-E5, Lutrol and soluplus whereby the solubilities of ibuprofen in 1:1 CM mixtures with these excipients are 0.56 mg ml^{-1}, 0.62 mg ml^{-1} and 1.96 mg ml^{-1}, respectively. In contrast, the milling with lactose, PEG-6000, PVP-K10 and MCC-101 hardly increase the solubility of ibuprofen; the values are 0.14 mg ml^{-1}, 0.19 mg ml^{-1}, 0.22 mg ml^{-1}, and 34 mg ml^{-1}, respectively. The statistical comparison of these values with that of un-milled ibuprofen have indicated that the co-milled mixtures with HPMC, Lutrol and soluplus have significant difference with the value of confidence interval <0.05, while all other mixtures have this value >0.05 so statistically non-significant.

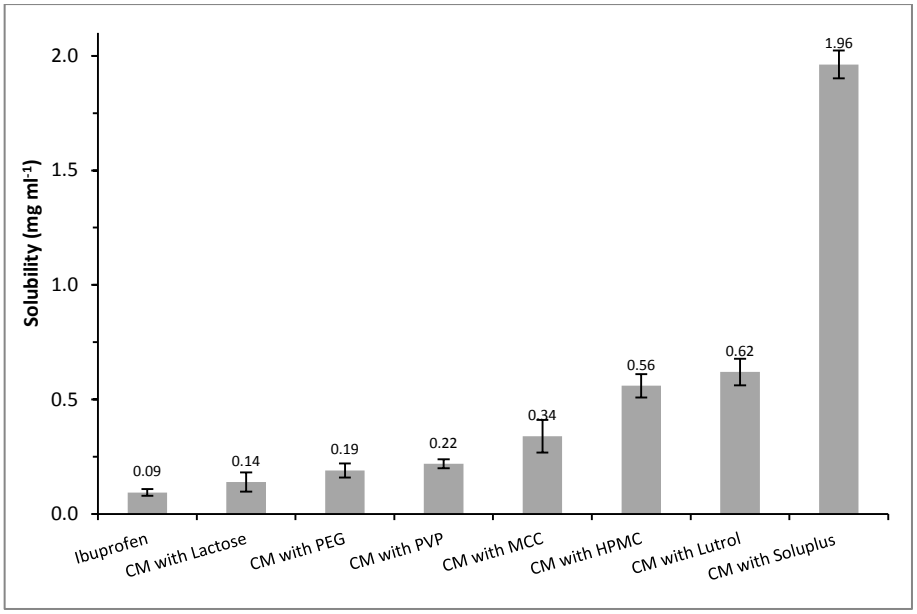

Figure 5.8: Solubility values of Ibuprofen and its co-milled mixtures with 1:1 ratio of different excipient. (CM is co-milled). The error bars represents the standard deviation from repeats of the milling processes (n=3).

Based on the highest solubility of ibuprofen of its co-milled mixture, soluplus is selected for the optimization of processing conditions (mill speed and time).

5.3.5.2 Selection of Milling Speed

The ibuprofen and soluplus were milled at three different speeds, *i.e.* 15, 18 and 25 Hz, for the time period of 15 min. The solubility of ibuprofen increased with the milling speed, however at the higher speed (> 20 Hz), the co-milled mixture became clammy and difficult to recover from the jar of the mill. Therefore, the speed of 18 Hz was used for the milling experiments.

5.3.5.3 Selection of Milling Time

Now at the constant mill speed (*i.e.* 18Hz), the ibuprofen was co-milled with soluplus for 5, 10, 15 and 30 min at in two different ratios (1:0.25 and 1:0.5) and the solubility of drug in these co-milled mixtures was determined in distilled water. The solubilities with 1 to 0.25 mixtures are 0.19, 0.19, 0.71 and 0.63 mg ml^{-1} with 5, 10, 15 and 30 min milling times respectively. While with drug to excipient ratio of 1:0.5 the solubility values are 0.31, 0.54, 1.26 and 1.30 mg ml^{-1}, respectively. This indicate that the solubility increase with increasing the milling time from 5 min to 30 min. However, the milling for long time (> 15 min) results in the clammy mixtures due to increased temperature in the milling jar. This mixture has

poor flowability and is difficult to extract from the mill, therefore 15 min milling time is selected for the next phase of this study.

5.3.6 Results of Extended phase

5.3.6.1 Effect of Concentration of Excipients on the Solubility of Ibuprofen

Solubility in distilled water: The co-milled mixtures of ibuprofen and HPMC with 1:0.25, 1:0.5, 1:0.75 and 1:1 ratios, have the solubility values 0.41, 0.53, 0.57 and 0.56 mg ml^{-1}, respectively (Figure 5.9a), while the physical mixture even with highest ratio *i.e.* 1:1 has the solubility 0.25 mg ml^{-1}. On the other hand, the co-milled mixtures with same ratios of soluplus have the solubility values 0.71, 1.26, 1.42 and 1.96 mg ml^{-1} respectively and the physical mixture (1:1 ratio) has the solubility value of 0.93 mg ml^{-1} (Figure 5.9a). Thus the solubility of ibuprofen in co-milled mixtures with HPMC is 4 to 5 times higher as compared with the un-milled or milled drug and 10 to 20 times higher in the co-milled mixtures with soluplus.

Solubility in phosphate buffer (pH 7.4): The solubility values of un-milled ibuprofen *i.e.* ~2.40 mg ml^{-1} remains almost the same in the co-milled mixtures with HPMC; However the mixtures with soluplus results in slightly increase in the values of solubility of *i.e.* ~3.0 mg ml^{-1} (Figure 5.9b).

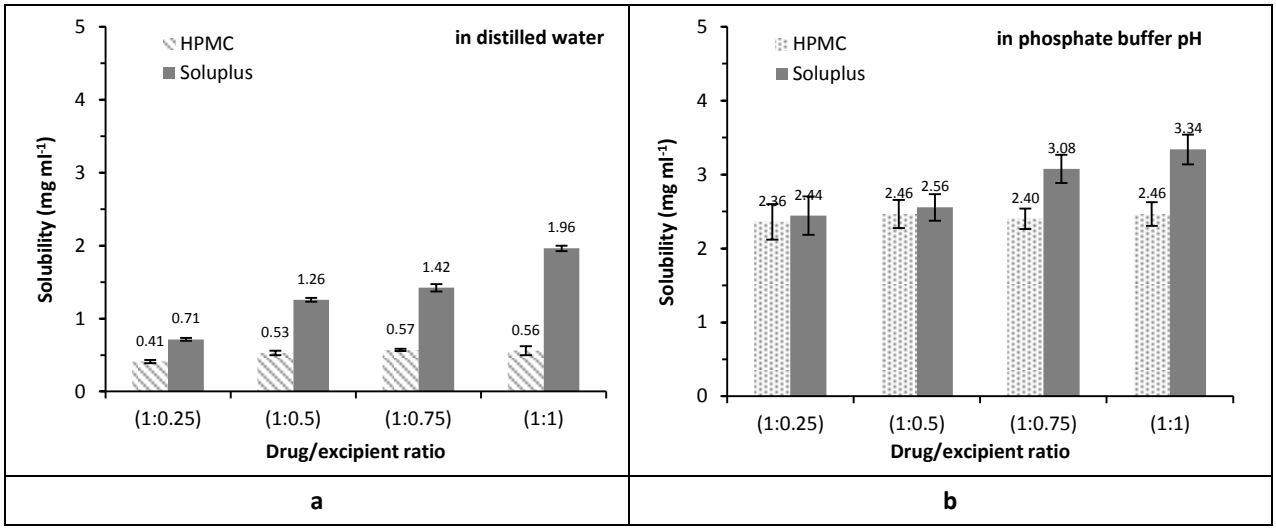

Figure 5.9: Solubility values of ibuprofen and its co-milled mixture in different ratios with HPMC and soluplus as measured in a) in distilled water b) in phosphate buffer pH 7.4. (PM is physical mixture, CM is co-milled mixture). The error bars represents the standard deviation of three values (n = 3).

5.3.6.2 Dissolution of Ibuprofen and its co-milled mixtures

The *in-vitro* release profile of un-milled, milled and co-milled ibuprofen with soluplus in phosphate buffer (pH 7.4) has been illustrated in Figure 5.10a. The percentage of un-milled ibuprofen dissolved in first 15 min is ~40% and ~75% at 90 min, whereas the milled (15 min) ibuprofen exhibited a slightly higher profile with ~45% drug dissolving in first 15 min and ~80% in 90 min. The co-milled mixtures with soluplus exhibited the greatest release of drug *i.e.* 60 to 85% in first 15 min and ~95% to ~100% after 90 min (Figure 5.10a) which increased with the proportion of soluplus in the mixture. The physical and milled physical mixtures of soluplus also have higher dissolution rate than the ibuprofen alone (both un-milled and milled).

The co-milled mixtures with HPMC, in contrast, show a relatively slow release of drug that gradually increases as the amount of HPMC increases in the co-milled mixtures (Figure 5.10b). The percentage release from 1:1 physical mixture was almost similar as from the un-milled ibuprofen *i.e.* ~40% in 15 min time. The cumulative release increases by ~5% in milled physical mixture and further 10% in each co-milled mixture with increasing the HPMC ratio from 1:0.5 to 1:1. At the end of 90 min there is ~90% release from the co-milled mixture as compared to ~70% of physical mixture.

The co-milled mixtures of ibuprofen with both HPMC and soluplus have shown better wettability and better release as compared to the drug alone.

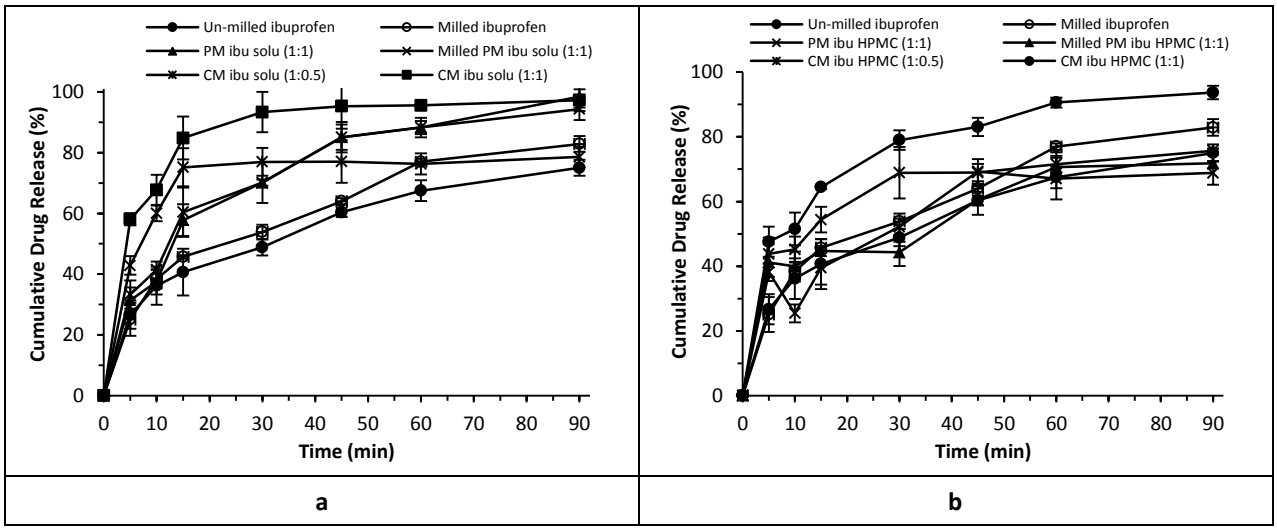

Figure 5.10: Dissolution profiles (in phosphate buffer pH 7.4) of un-milled, 15min milled ibuprofen and its physical and co-milled mixtures with a) soluplus, b) HPMC. The error bars represent standard deviation with n = 3.

The dissolution parameters (shown in Table 5.2) indicate that the values of Q30 min increases in the order of physical mixture < milled physical mixture < co-milled with HPMC < co-milled with soluplus. The DE of ibuprofen which is hardly affected by milling or in physical mixtures with HPMC; increases by ~40% in co-milled mixtures of both HPMC and soluplus and physical mixture with soluplus. The MDT is ~23 min in un-milled ibuprofen that increases slightly in milled sample representing the agglomeration on milling with overall decrease in effective surface area. While in the co-milled mixture it decreases by 2-3 folds indicating the increase in effective surface area for dissolution.

Table 5.2: Dissolution parameters of ibuprofen and its physical and co-milled mixtures with Soluplus and HPMC. (Q30min = the percentage of drug released in 30min, DE = dissolution efficiency and MDT = median dissolution time).

	Q30min (%)	DE	MDT (min)
Un-milled Ibuprofen	48.9	0.56	23.3
Milled Ibuprofen 15min	53.9	0.61	23.4
PM with HPMC (1:1)	52.2	0.56	16.2
Milled PM with HPMC (1:1)	44.3	0.57	19.1
CM with HPMC (1:0.5)	68.9	0.64	13.4
CM with HPMC(1:1)	79.0	0.78	15.1
PM with Soluplus (1:1)	70.2	0.75	21.8
Milled PM with Soluplus	70.2	0.75	18.9
CM with Soluplus (1:0.5)	76.9	0.72	7.65
CM with Soluplus (1:1)	93.4	0.88	8.64

5.3.6.3 Intrinsic Dissolution Rate of Ibuprofen and its Co-milled Mixtures

The interference of the wax plugs in the IDR results of ibuprofen was first determined by incorporating a plug of same size (without ibuprofen compact) as used for embedding the ibuprofen compacts; in the dissolution medium (phosphate buffer, pH 7.4) and subjected to the conditions of IDR. The aliquots of the medium were drawn at different intervals till 90 min and its absorbance was measured in UV spectrophotometer. The absorbance of all the samples was almost equal to the absorbance of blank indicated that the interference by wax was negligible.

The changes in the surface of exposed part of the compacts were observed by stereo zoom microscope at 15 min, 30 min and 60 min during IDR (Figure 5.11). These indicated that the surfaces erode gradually and pits were developed on the entire surface. The compacts containing co-milled mixture with HPMC showed the highest degree of erosion while the co-milled mixture with soluplus showed the least erosion and milled ibuprofen is in between.

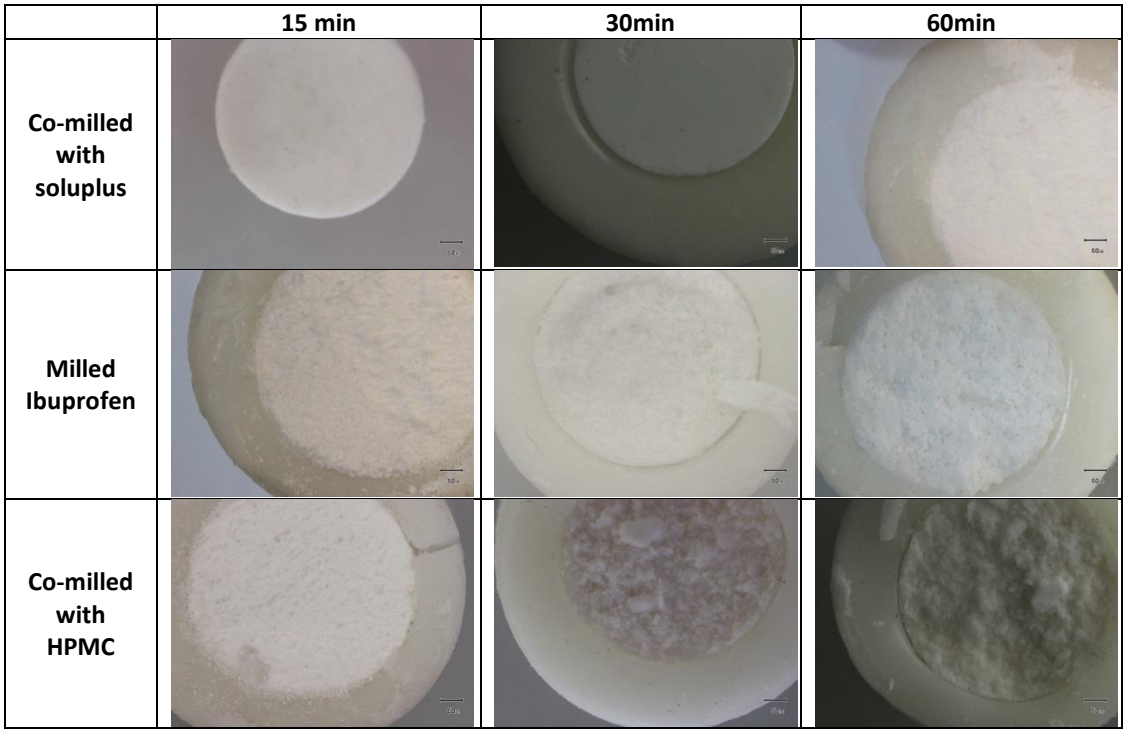

Figure 5.11: Photographs of wax plugged compacts of 15min milled ibuprofen and the co-milled mixtures with soluplus and HPMC taken during different stages of dissolution test (stereo zoom microscope camera)

IDR was calculated from the cumulative drug released over the period of 90 min and the area of exposed surface of the compact. The results indicated that the IDR of un-milled ibuprofen was 0.3 mg $cm^{-2}min^{-1}$ which is in agreement with (Viegas et al., 2001). The 15 min milled Ibuprofen has IDR of ~0.6 mg $cm^{-2}min^{-1}$ *i.e.* approximately twice higher than that of un-milled drug.

The process of milling results in the increase of effective surface area exposed to the dissolution medium which is evident from the nitrogen adsorption results. The BET surface area of 15 min milled ibuprofen is 0.58 m^2 g^{-1} that is almost thrice than that of un-milled one (0.20 m^2 g^{-1}). The co-milled mixtures of ibuprofen with HPMC seems to have higher IDR values (~0.7 mg $cm^{-2}min^{-1}$) than the milled drug (Figure 5.12a), while the co-milled mixture with soluplus has the IDR only slightly higher than un-milled drug (Figure 5.12b). There is the possibility of two opposing mechanisms in co-milled mixtures with HPMC, where the high concentration of HPMC forms gel after absorbing the water and hinders the drug release; the erosion and disruption on the other hand might increase the drug release. The higher values of IDR in co-milled mixtures with HPMC than with soluplus are probably due to the swelling property of HPMC that resulted in higher wettability and erosion of compacts and hence prevailing of second mechanism. This was evidenced from the observation of the

surfaces at different times during IDR experiments, the compacts of HPMC co-milled mixtures erode rapidly and pits are developed that leads to movement of dissolution medium inside the compact (Figure 5.11). On the other hand the compacts containing soluplus remained intact even at the end of 90 min; therefore the release occurs from the exposed surface only.

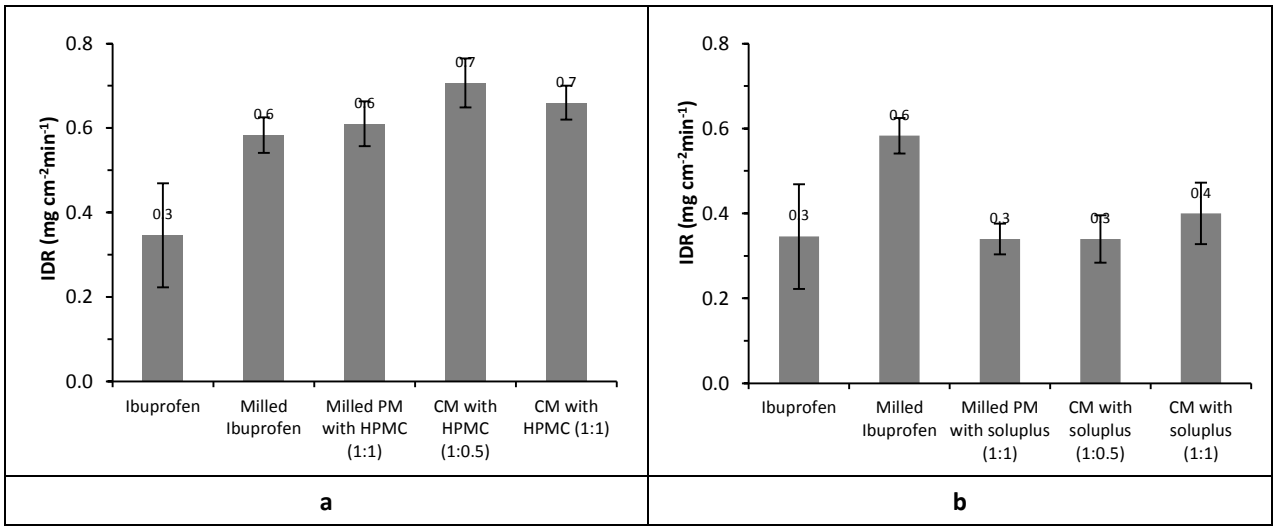

Figure 5.12: IDR of ibuprofen and its co-milled mixtures with different ratios of a) HPMC and b) soluplus. (PM= physical mixture, CM=co-milled mixture). The error bars represent the standard deviation of three readings (n=3).

5.3.7 Characterization of Co-milled Mixtures

5.3.7.1 Changes in Particle Size Distribution on Co-Milling (Laser Diffraction Results)

The cumulative particle size distribution plot of **un-milled ibuprofen** indicates that majority of the particle (~70%) have the size greater than 70 μm (as shown by the dotted lines in Figure 5.13a. The density distribution plot shows Gaussian distribution (size distribution range between 70 – 400 μm) with the peak at ~160 μm and a shoulder of peak towards smaller particle size (10 – 70 μm).

The co-milled mixture with 10% soluplus has a bimodal size distribution (Figure 5.13b) with a broad peak (~8 μm) and a small peak at ~100 μm. This plot indicates that ~80% are less than 50 μm and there is still a small percentage (~20%) of particle that remains unchanged with respect to their size. Similarly the co-milled mixture with 10% HPMC has almost the same PSD curve as that of 10% CM with soluplus except the presence of an extra small peak with the particle size even greater than the original ones (Figure 5.13c). In the co-milled mixture

with 1:1 ratio with HPMC, there is only one peak towards smaller particle size (~10 µm) and a small shoulder toward large particle size(Figure 5.13d).

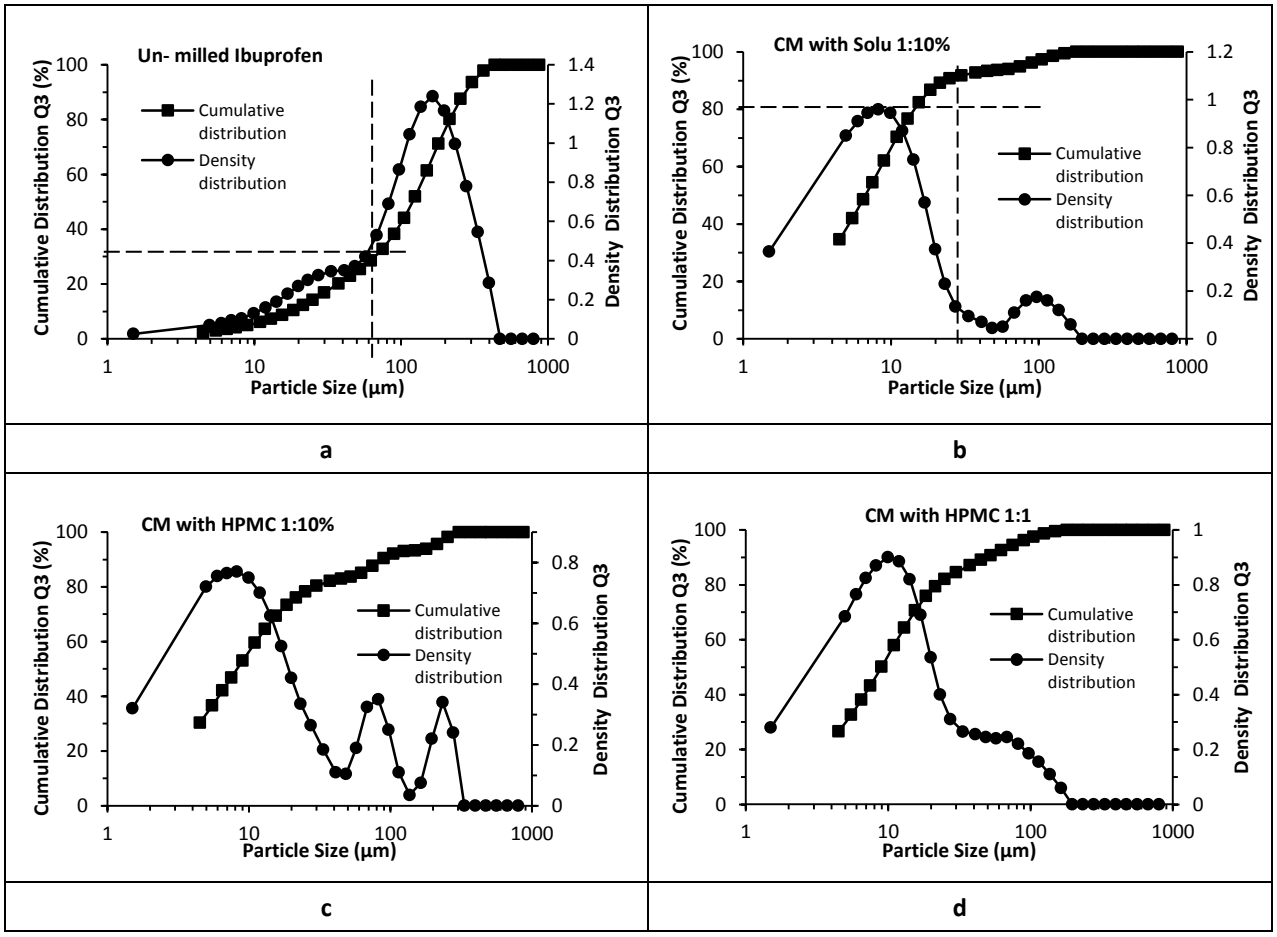

Figure 5.13: Particle size distribution plots (density distribution and cumulative distribution) of a) un-milled Ibuprofen and its co-milled mixture with b) Soluplus and c-d) HPMC.

The PSD parameters have indicated that the value of d_{50} (~120 µm for un-milled ibuprofen) was greatly reduced in all co-milled mixtures; it was 8.4 µm and 8.9 µm for co-milled mixture with 10% and 50% (*i.e.* 1:1) HPMC while 6.7 µm for co-milled mixture with 10% Soluplus, respectively (Table 5.3).

Table 5.3: Values of d_{50} and d_{90} for un-milled ibuprofen and its co-milled mixtures with HPMC and Soluplus

Sample	d(v,0.5),µm	d(v,0.9),µm
Un-milled Ibuprofen	119.7	274.9
CM with HPMC 1:10%	8.4	131.1
CM with HPMC 1:1	8.9	49.2
CM with Soluplus 1:10%	6.7	23.2

The results of PSD have revealed that the co-milling with both soluplus and HPMC shifts the size distribution of ibuprofen towards lower values and increase in the density of the fines. It

is of worth to note that the density of fines was higher in co-milled mixture with 10% soluplus in comparison with the co-milled mixture of HPMC with all ratios. This reduction in the particle size has resulted in a greater increase in the surface area in co-milled mixtures of soluplus than that of HPMC resulting in higher dissolution rate of ibuprofen co-milled with the former. However the presence of large size particles (equivalent or greater than the original un-milled particle) in the co-milled mixtures indicates that either there is some proportion of particle that survive milling (milling time was small *i.e.* only 15min) or some particle are aggregated or may be some large excipient particles. There is another possibility *i.e.* the re-crystallization of the ibuprofen on milling (as discussed in Section 5.3.7.3).

5.3.7.2 Changes in Size, Shape and Dispersibility of Ibuprofen on Co-milling/SEM Results

The SEM images of ibuprofen have shown that the un-milled ibuprofen (Figure 5.14, upper panel) occurs as acicular shape crystals (80 to 160 µm in size) that are longer than width and have smooth surfaces (Han et al., 2011). On milling, the particles are fragmented and show lots of eruptions and cracking on the surface of particles (Figure 5.13, middle panel), which might have provided the enlarged surface for wicking of the solvent during dissolution experiment.

The co-milled mixtures of ibuprofen with HPMC and soluplus (Figure 5.14, lower panels) show that the drug particles lose their geometric shape and adhere to the surface of excipients. This phenomenon prevents the aggregation of particles and therefore, enhances the dispersibility, leading to an increase in surface area exposed to the dissolution medium. This might be one of the reasons for enhanced dissolution of drug in these co-milled mixtures. The aggregation of drug particle in co-milled mixtures (as speculated in particle size results) is not confirmed from the SEM images.

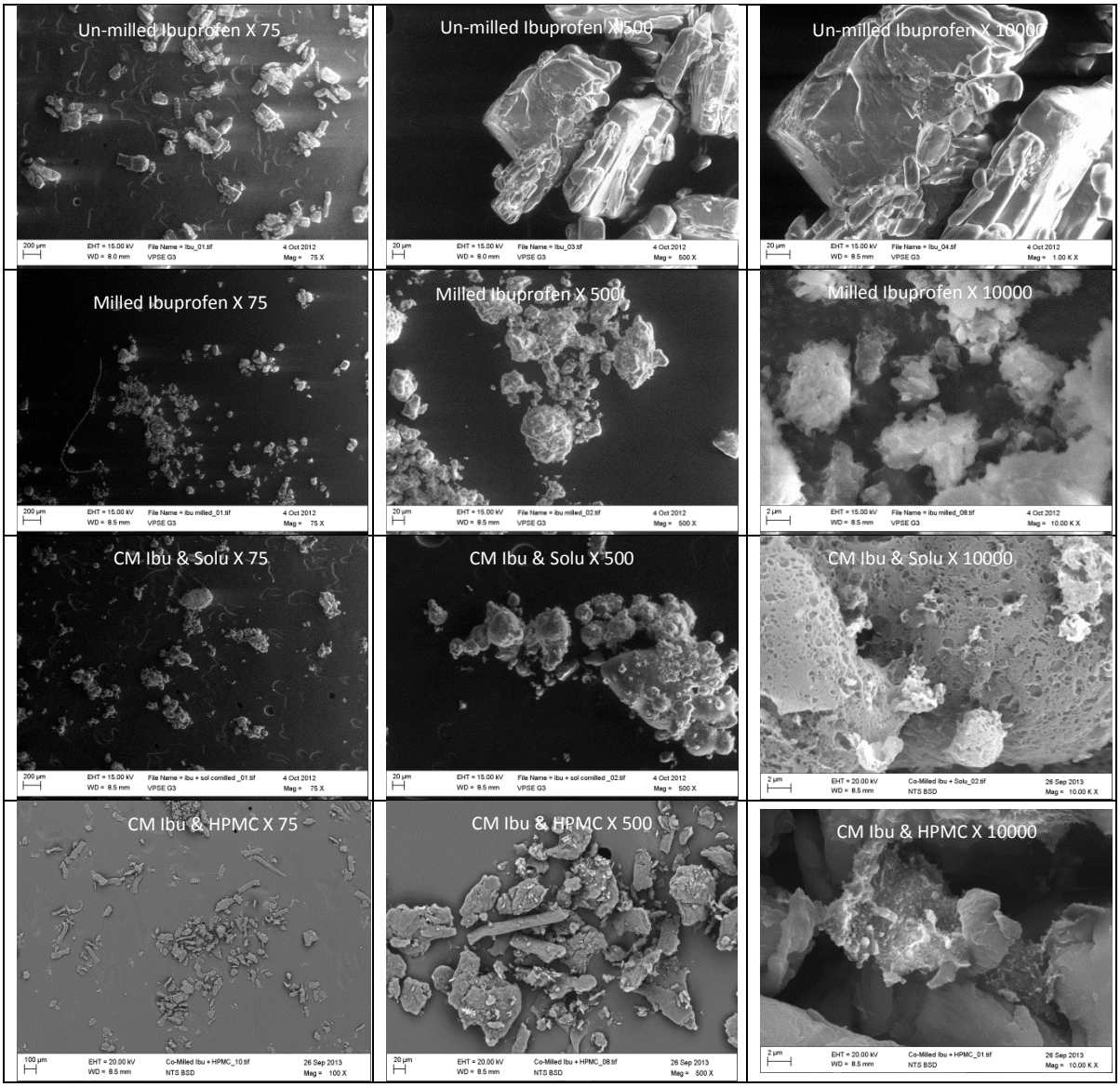

Figure 5.14: SEM images of un-milled, 15min milled ibuprofen and its co-milled mixtures with Soluplus and HPMC at different magnifications.

5.3.7.3 Changes in Crystallinity of Ibuprofen on Milling and Co-Milling/ DSC Results

The DSC curve of **un-milled Ibuprofen** (Figure 5.15a) shows a single endothermic peak at ~ 79.9 °C corresponding to the melting of ibuprofen (Madhuri Newa and Bong Kyu Yoo, 2008). In the **milled ibuprofen,** the melting temperature is almost the same but the enthalpy of melting slightly decreases from ~116 Jg^{-1} to ~107 Jg^{-1} after 15 min of milling. The glass transition step, the first signature of amorphous phase, is not observed in milled ibuprofen, however the de-vitrification peak is present at almost the same temperature as observed in case of fully amorphous (quenched) ibuprofen (Figure 5.15a).

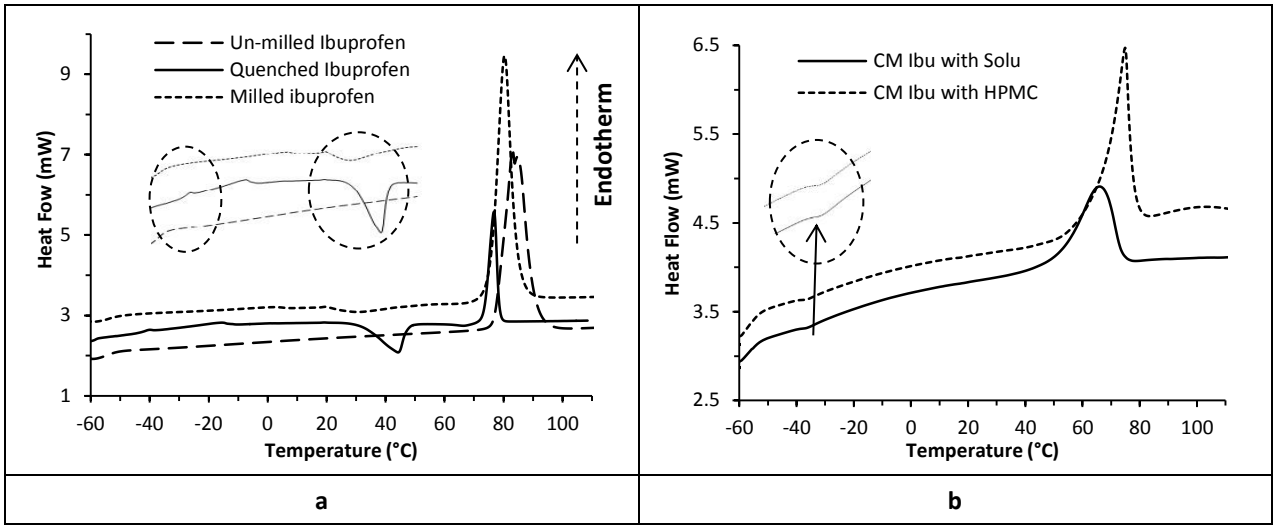

Figure 5.15: a) DSC curves of un-milled, 15min milled and amorphous (quenched) ibuprofen, the inset shows the T_g step near -40°C in quenched ibuprofen and de-vitrification peaks in quenched and milled ibuprofen near 25°C which were otherwise absent in un-milled ibuprofen.

The DSC curves of co-milled mixtures of ibuprofen with HPMC and soluplus (Figure 5.15b) have shown that the melting peak of ibuprofen shifts toward lower temperature (Table 5.4) and the T_g appears near -35 °C indicating the presence of amorphous phase. However, the de-vitrification peak that is present in the milled ibuprofen near 30 °C is not observed in any of the co-milled sample. This indicated the stabilization of amorphous phase by the co-milled excipients (Pokharkar et al., 2006).

Table 5.4: The values of melting temperature and enthalpy of melting for un-milled, 15min milled ibuprofen and its co-milled mixtures and the percentage crystallinity as calculated from the enthalpies of melting.

Sample	Melting peak (°C)	Enthalpy of melting (Jg^{-1})	Residual Crystallinity (%)
Un-milled Ibuprofen	79.7	116.5	100
15 min milled	79.7	108.9	86.7
CM with HPMC 1:10%	78.4	102.2	87.8
CM with HPMC 1:20%	78.0	93.1	80.0
CM with HPMC 1:1	74.9	51.4	44.1
CM with Soluplus 1:10%	77.5	93.8	80.6
CM with Soluplus 1:20%	76.1	85.6	73.5
CM with Soluplus 1:1	65.8	39.6	34.0

The melting enthalpies also decrease gradually as the proportion of soluplus or HPMC increases in the co-milled mixtures (Table 5.4). The percentage residual crystallinity of ibuprofen in the co-milled mixtures is calculated from the changes in enthalpies by using the method already described in Chapter 3, Section 3.2.3. The un-milled ibuprofen was considered as 100% crystalline with ΔH_m as 116.2 Jg^{-1} (which is lower than the value given in

literature 129 Jg^{-1} (Madhuri Newa and Bong Kyu Yoo, 2008). The results of residual crystallinity have been summarized in Table 5.4.

The loss of crystallinity/presence of amorphous phase of ibuprofen (in stabilized form) in co-milled mixtures might be responsible for the increased solubilities and hence dissolution rates of as compared to drug alone.

5.3.7.4 Change in Crystallinity of Ibuprofen on Milling and Co-milling/PXRD Results

The PXRD pattern of un-milled ibuprofen (Figure 5.16a) show the characteristic peaks of ibuprofen at angles 2θ of 6.16°, 12.27°, 16.76°, 17.75°, 22.42° and 24.86°. The residual crystallinity of ibuprofen in the co-milled mixtures was estimated by peak intensity ratio method (Fix and Steffens, 2004). The results (Figure 5.16b) indicate that there is ~75% loss of crystallinity on 15 min milling. The PXRD pattern of co-milled mixture of ibuprofen with HPMC and soluplus also produce the characteristics peaks of ibuprofen but their intensities are reduced with the halo pattern observed in co-milled mixture with HPMC due to the amorphous nature of HPMC. This indicated that the crystalline nature of drug is not fully disappeared in these co-milled mixtures, however the loss in crystallinity occurs which is calculated to be ~75% in co-milled mixture with HPMC and 65% in co-milled mixture with soluplus. However, this high percentage of crystallinity loss may not be true and it require whole pattern fitting of PXRD data.

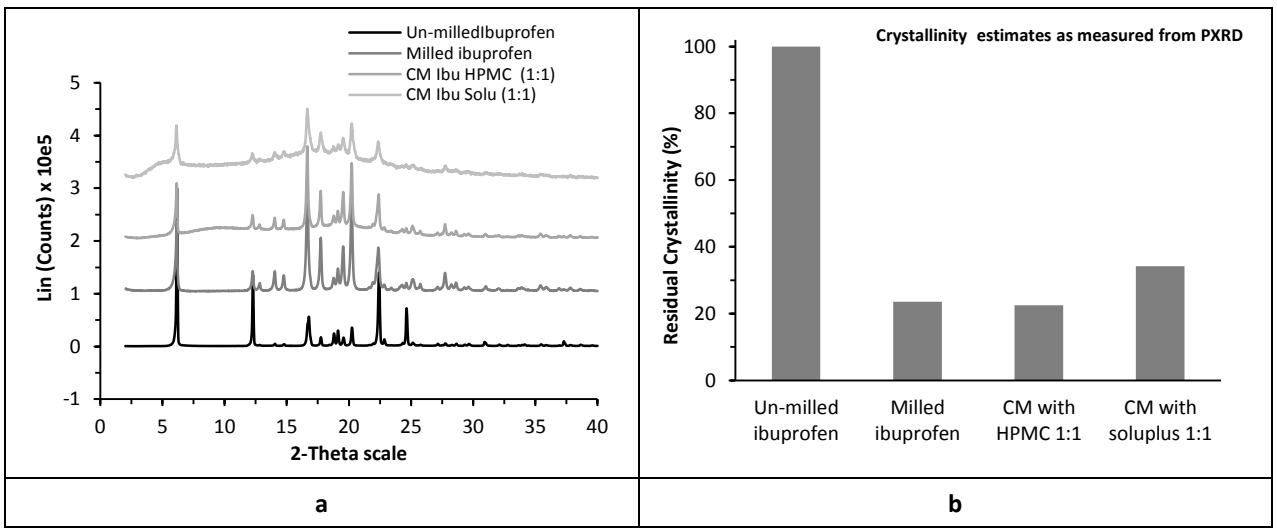

Figure 5.16: a) Powder X-ray diffraction patterns of un-milled, 15min milled ibuprofen and its co-milled mixtures with HPMC and Soluplus b) percentage residual crystallinity as calculated from peak intensity ratios of these samples.

5.3.7.5 Change in Crystallinity of Ibuprofen on Milling and Co-Milling/THz results

The THz spectrum of un-milled ibuprofen has the absorption peak at ~35 cm^{-1} while, the overall shape of the spectra of co-milled mixtures with HPMC and soluplus is almost the same (5.17a). The major changes in the spectra of co-milled mixtures are i) the decrease in area of the only absorption peak and ii) the increase in the intensity of absorption as the proportion of excipients is increased in the co-milled mixture (Figure 5.17a). The first effect is because of the milling while the second is the combined effect due to Mie scattering and effect of amorphous nature of HPMC and soluplus (Strachan et al., 2004).

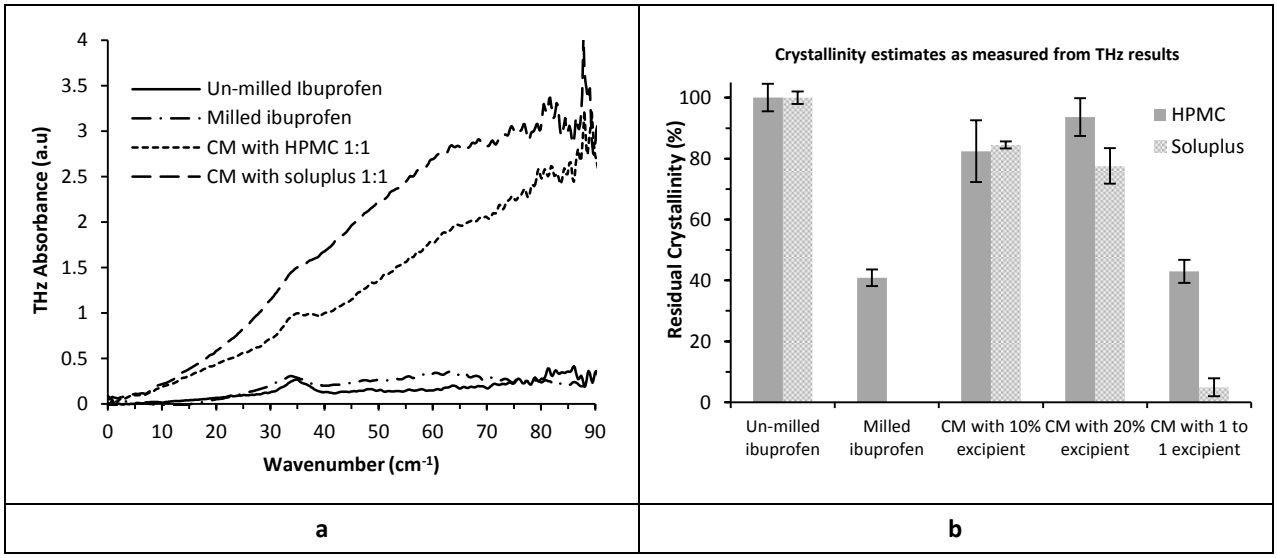

Figure 5.17: a) THz spectra of un-milled, 15min milled and co-milled ibuprofen with HPMC and soluplus b) Crystallinity of these samples as calculated from area under peak method. The error bars represent the standard deviation of 9 measurements (n=9).

The residual crystallinity in co-milled mixtures is calculated from area under the absorption peak of THz data (as described in Chapter 3, Section 3.3.3.8) show that, there is ~60% loss in crystallinity when the drug is milled alone and co-milling with small proportion (10 or 20%) of excipients (HPMC or soluplus), reduces only 15-20% of crystallinity of the ibuprofen (Figure 5.17b). However, in the mixtures with equal proportion of excipients (*i.e.* 1:1 with drug), the loss of crystallinity is almost the same (as in case of HPMC) or greater (in case of soluplus) as compared to the milling the ibuprofen alone. This indicates that the co-milling with HPMC stabilize the amorphous phase while the soluplus facilitates the amorphization in co-milled mixture. The above mentioned changes have explained well the solubility enhancement of ibuprofen in co-milled mixtures.

5.3.7.6 Molecular Interaction of Ibuprofen with Co-milled Excipients/ATR Results

The IR spectrum of un-milled ibuprofen (Figure 5.18a) has shown an intense and well-defined peak at ~1704 cm^{-1} corresponding to the carbonyl-stretching of propionic acid group, a characteristic band from 800 to 1500 cm^{-1} due to hydrogen bonding as ibuprofen forms dimer and a spectral band between 2800 and 3000 cm^{-1} due to the stretching of -OH bond (Newa et al., 2008).

The IR spectra of co-milled mixtures of ibuprofen with HPMC and soluplus (Figure 5.18a) are almost similar to that of un-milled ibuprofen, except that the spectral band near 3000 cm^{-1} becomes less intense and the stretching vibration of carbonyl peak near 1700 cm^{-1} was still present indicating that the drug's crystalline form was not completely lost during co-milling. The carbonyl stretching peak that is relatively broad in the un-milled ibuprofen becomes sharper and shifts towards higher wavenumbers on milling the drug alone and co-milling it particularly with soluplus (Figure 5.18b). This shift suggests that there is a change in the dimer structure and hydrogen bonding (Nokhodchi et al., 2010). This is probably due to the solubilization action of soluplus, where the vinyl-acetate and vinyl-caprolactam moieties of this surfactant surround the drug while the PEG backbone forms the backing as shown in Chapter 1, Section 1.10.3.2.

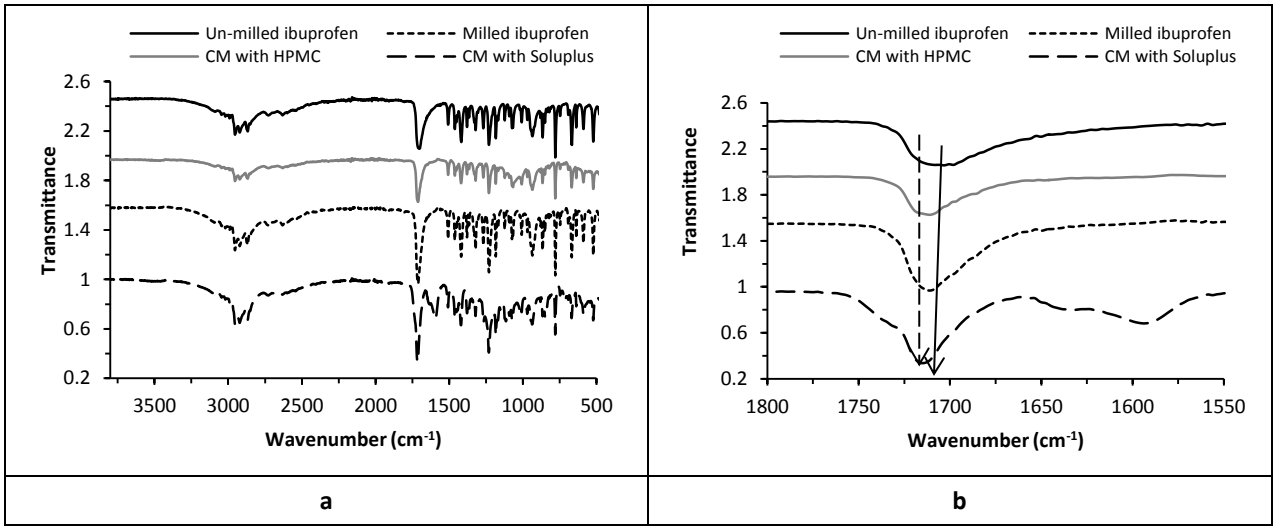

Figure 5.18: a) IR spectra of un-milled, 15min milled ibuprofen and its co-milled mixtures with HPMC and Soluplus in 1:1 ratio b) a segment from IR spectra of these samples showing the shift in position of carbonyl peak is indicated by arrow heads.

5.4 Conclusion

This study indicates that the co-milling with an excipient (polymer or surfactant) effectively enhances the solubility and dissolution rate of ibuprofen. This effect is a result of crystal damage as shown by the decrease in enthalpy of melting in DSC results and change of dimer structure as depicted by FTIR spectra of milled and co-milled samples of ibuprofen. Furthermore, the increased surface area, surface damage and decreased aggregation (from improved dispersibility) as observed in SEM images, along with the generation and of stabilization amorphous phase as observed in DSC results are responsible for the enhanced dissolution rate of the candidate drug. Additionally the improved of wettability as provided by milling with HPMC and solubilization action by soluplus further enhance the solubility and dissolution rate of ibuprofen. Although the size reduction and amorphization are generally accepted changes of milling, however the presence of HPMC and soluplus during milling of ibuprofen facilitates these changes.

The study also presents a comparative analysis of various techniques e.g. DSC, PXRD and THz for measuring the crystalline/amorphous changes in co-milled mixtures of the candidate drug. The study shows THz pulsed spectroscopy can be a complementary technique for such measurements.

6 Conclusions from this Study

It is well known that milling induces a complex series of events which compromise the structure of a crystalline material (from the creation of minor defects and fissures to the fragmentation of the particle and the partial conversation to a disordered crystalline state). Understanding of these events, in terms of the extent and distribution of the morphological changes that result and the achievement of the desired state (of increased solubility and dissolution rate) is inevitably a complex task; one which is made more difficult because of the short comings of a number of the techniques used to study such materials. The short comings of the techniques have been stressed throughout this work, while seeking out additional analytical technologies to study this important, industrial relevant process.

It was pointed out that nitrogen adsorption studies cannot measure the internalized cracks of milled material due to an inability of the probe (*i.e.* nitrogen gas) to penetrate the micro scale pores; Nor can this method be used for crystal hydrates given the fact that the evacuation of the sample chamber results in the desorption of the water of crystallization and the creation of new surfaces that are then explored by the BET gas probe. In addition, SEM and laser diffraction techniques may over or under-estimate the particle size influence on the surface area of milled materials. This is because of the formation of particle clusters and the amorphous phase, and the subsequent re-crystallization of this phase, can impact the apparent size distribution.

While these challenges remain, it was demonstrated in this thesis that dielectric relaxation spectroscopy may provide further insight into the generation of internalized surfaces in short milled samples, which may assist in our understanding of the contribution of these surfaces to the dissolution rate of milled materials (as described in Chapter 2).

In the case of samples being milled for extended periods of time, where the amorphous content is high, the de-vitrification of this phase may be induced by the moisture (inherent as in hydrated materials or taken from the environment) or thermal by treatment during the analysis by DSC and TGA. Here, it was demonstrated that THz spectroscopy can measure the material in its native form, while being encased in a hydrophobic material (PFTE) that in effect stabilises the material to the ingress of further moisture. Therefore it is helpful for the quantification of residual crystallinity in milled material.

Another aspect that is often over-looked in studies of milled materials with significant amorphous content is the dynamics of the phase and the impact of moisture and crystallite seeds within in the phase on stability of the amorphous component. Once again, dielectric relaxation spectroscopy was shown to be a useful technique for studying the molecular dynamics of milled materials which might provide the understanding of relative stabilities of such materials.

Finally, an analytical method for the estimation of a drug in the presence of an excipient that interferes with UV absorbance was developed. This part of thesis, demonstrated that the co-milling with excipients can enhance the solubility and dissolution rate of poor soluble drug, ibuprofen. Moreover, it was shown that the methodologies developed for the analysis of milled material were also applicable for the characterization of co-milled mixture in explaining the mechanism of solubility and dissolution improvement.

7 Future Perspectives

The dielectric spectroscopy of milled hydrated sugars, in this study, has shown a unique behaviour (saddle shaped process in permittivity loss spectrum) in milled lactose monohydrate which is characteristics of complex, micro-porous systems. If such behaviour is a feature of milled material, in the sense that it defines/under pins any beneficial effects on drug solubility and dissolution rate, then such studies are inevitably of interest to the assessment of the stability of nano-structured systems for drug delivery.

In the approach to quantify the residual crystallinity in the milled pharmaceuticals, various concentrations of crystalline material in a matrix of PE were used to construct calibration graphs. As a possible improvement to this method, one might consider using combinations of amorphous and crystalline materials (prepared under controlled humidity conditions) to draw the calibration graphs. While this system may be more realistic of the structural properties of a mixed crystalline/amorphous phase, inevitably, the issues of amorphous phase stability may preclude the use of such mixtures.

Another aspect of the methods that could be improved, relates to the assessment of changes in the crystallinity of lactose in respect of each anomeric form (alpha and beta). Some effort should have been devoted in transforming the minor component to the major component, e.g. the beta content to 100% alpha. Another enhancement would have been to have cryo-measurements to sharpen up the peaks of THz in an attempt to quantify the each component.

From the study of dynamics of amorphous phase, it has been indicated that the instability of milled materials depends on many factors, particularly the presence of moisture (both inherent *i.e.* released from the hydrated crystals and sorbed from the atmosphere), temperature and length of milling process (this may leave the seeds for re-crystallization). The time domain THz measurements (THz-TDS) of the milled material at different temperatures and moisture conditions would demonstrate the effect the above experimental conditions, *viz* moisture, temperature and milling time on the post-milling storage of the milled and co-milled materials. These studies will also help to predict the stability of the milled materials during storage.

Dry milling of an API (ibuprofen) produced micro-particles along with some amorphization of the drug, when co-milled with soluplus and HPMC. It is envisioned that the application of wet milling using appropriate surfactants may produce the nano-size particles of drugs with different degrees of amorphization. Wet milling may also be suggested for the further enhancing the benefits of the co-milling and help to improve the solubility and dissolution of poorly soluble drugs, while producing materials of a desired size which can then be employed for absorption and the delivery of a drug to target sites.

8 References

AGAMALIAN, M., DRAKE, J., SINHA, S. & AXE, J. 1997. Neutron diffraction study of the pore surface layer of Vycor glass. *Physical Review E,* 55**,** 3021.

AL-HAMIDI, H., EDWARDS, A. A., DOUROUMIS, D., ASARE-ADDO, K., NAYEBI, A. M., REYHANI-RAD, S., MAHMOUDI, J. & NOKHODCHI, A. 2012. Effect of glucosamine HCl on dissolution and solid state behaviours of piroxicam upon milling. *Colloids and Surfaces B: Biointerfaces,* 103**,** 189-199.

AL-HAMIDI, H., EDWARDS, A. A., MOHAMMAD, M. A. & NOKHODCHI, A. 2010. Glucosamine HCl as a new carrier for improved dissolution behaviour: Effect of grinding. *Colloids and Surfaces B: Biointerfaces,* 81**,** 96-109.

ALI, S. 2010. Soluplus - The solid solution; opening new doors in solubilization. BASF The chemical company, Ludwigshafin Germany.

ALI, S., LANGLEY, N., DJURIC, D. & KOLTER, K. 2011. Eye on excipients. BASF The chemical company, Ludwigshafin Germany.

ALLIS, D., FEDOR, A., KORTER, T., BJARNASON, J. & BROWN, E. 2007. Assignment of the lowest-lying THz absorption signatures in biotin and lactose monohydrate by solid-state density functional theory. *Chemical Physics Letters,* 440**,** 203-209.

ALY NADA, S. M. A. S., BERND W. MUELLER 2005. Improving the physical and chemical properties of ibuprofen. *Pharmaceutical Technology,* 29**,** 90-101.

AMIDON, G. L., LENNERNÄS, H., SHAH, V. P. & CRISON, J. R. 1995. A theoretical basis for a biopharmaceutic drug classification: The correlation of in-vitro drug product dissolution and in-vivo bioavailability. *Pharmaceutical Research,* 12**,** 413-420.

ANGELL, C. A. 1995. Formation of glasses from liquids and biopolymers. *Science,* 267**,** 1924-1935.

ARNUM, P. V. 2010. Solubilizing the Insoluble "an analysis of the approaches and tools used to tackle the problem of poorly soluble drugs". *Pharmaeutical Technology,* 34**,** 50-56

AVDEEF, A., VOLOBOY, D. & FOREMAN, A. 2007. Dissolution and solubility. *In:* JOHN, B. T. & DAVID, J. T. (eds.) *Comprehensive Medicinal Chemistry II.* Oxford: Elsevier.

BABOOTA, S., DHALIWAL, M. & KOHLI, K. 2005. Physicochemical characterization, in vitro dissolution behavior, and pharmacodynamic studies of rofecoxib-cyclodextrin inclusion compounds. preparation and properties of rofecoxib hydroxypropyl β-cyclodextrin inclusion complex: a technical note. *AAPS PharmSciTech,* 6**,** E83-E90.

BAHL, D. & BOGNER, R. 2008. Amorphization alone does not account for the enhancement of solubility of drug co-ground with silicate: The case of indomethacin. *AAPS PharmSciTech,* 9**,** 146-153.

BAI, S. J., RANI, M., SURYANARAYANAN, R., CARPENTER, J. F., NAYAR, R. & MANNING, M. C. 2004. Quantification of glycine crystallinity by near-infrared (NIR) spectroscopy. *Journal of Pharmaceutical Sciences,* 93**,** 2439-2447.

BALANI, P. N., NG, W. K., TAN, R. B. H. & CHAN, S. Y. 2010a. Influence of excipients in co-milling on mitigating milling-induced amorphization or structural disorder of crystalline pharmaceutical actives. *Journal of Pharmaceutical Sciences,* 99**,** 2462-2474.

BALANI, P. N., WONG, S. Y., NG, W. K., WIDJAJA, E., TAN, R. B. H. & CHAN, S. Y. 2010b. Influence of polymer content on stabilizing milled amorphous salbutamol sulphate. *International Journal of Pharmaceutics,* 391**,** 125-136.

BARZEGAR-JALALI, M., VALIZADEH, H., SHADBAD, M.-R. S., ADIBKIA, K., MOHAMMADI, G., FARAHANI, A., ARASH, Z. & NOKHODCHI, A. 2010. Co-grinding as an approach to enhance dissolution rate of a poorly water-soluble drug (gliclazide). *Powder Technology,* 197**,** 150-158.

BATES, S., ZOGRAFI, G., ENGERS, D., MORRIS, K., CROWLEY, K. & NEWMAN, A. 2006. Analysis of amorphous and nanocrystalline solids from their X-ray diffraction patterns. *Pharmaceutical Research,* 23**,** 2333-2349.

BEARD, M. C., TURNER, G. M. & SCHMUTTENMAER, C. A. 2002. Terahertz spectroscopy. *Journal of Physical Chemistry B,* 106**,** 7146-7159.

BECKETT, S. T., FRANCESCONI, M. G., GEARY, P. M., MACKENZIE, G. & MAULNY, A. P. 2006. DSC study of sucrose melting. *Carbohydrate Research,* 341**,** 2591-2599.

BISWAL, S., SAHOO, J., MURTHY, P., GIRADKAR, R. & AVARI, J. 2008. Enhancement of dissolution rate of gliclazide using solid dispersions with polyethylene glycol 6000. *AAPS PharmSciTech,* 9**,** 563-570.

BLAGDEN, N., DE MATAS, M., GAVAN, P. & YORK, P. 2007. Crystal engineering of active pharmaceutical ingredients to improve solubility and dissolution rates. *Advanced Drug Delivery Reviews,* 59**,** 617-630.

BRANHAM, M. L., MOYO, T. & GOVENDER, T. 2012. Preparation and solid-state characterization of ball milled saquinavir mesylate for solubility enhancement. *European Journal of Pharmaceutics and Biopharmaceutics,* 80**,** 194-202.

BROWN, E., BJARNASON, J., FEDOR, A. & KORTER, T. 2007. On the strong and narrow absorption signature in lactose at 0.53 THz. *Applied physics letters,* 90**,** 061908-3.

BRUNTON, L. L., LAZO, J. S. & PARKER, K. L. 2006. *Goodman & Gilman's the Pharmacological Basis of Therapeutics*, McGraw-Hill New York.

BUCKTON, G. 1997. Characterisation of small changes in the physical properties of powders of significance for dry powder inhaler formulations. *Advanced Drug Delivery Reviews,* 26**,** 17-27.

BUCKTON, G., CHOULARTON, A., BEEZER, A. E. & CHATHAM, S. M. 1988. The effect of the comminution technique on the surface energy of a powder. *International Journal of Pharmaceutics,* 47**,** 121-128.

BUCKTON, G. & DARCY, P. 1999. Assessment of disorder in crystalline powders—A review of analytical techniques and their application. *International Journal of Pharmaceutics,* 179**,** 141-158.

BUCKTON, G., YONEMOCHI, E., HAMMOND, J. & MOFFAT, A. 1998. The use of near infra-red spectroscopy to detect changes in the form of amorphous and crystalline lactose. *International Journal of Pharmaceutics,* 168**,** 231-241.

BUHRKE, V. E., JENKINS, R. & SMITH, D. K. 1998. Practical guide for the preparation of specimens for x-ray fluorescence and x-ray diffraction analysis.

BURNETT, D., THIELMANN, F. & BOOTH, J. 2004. Determining the critical relative humidity for moisture-induced phase transitions. *International Journal of Pharmaceutics,* 287**,** 123-133.

BURNETT, D., THIELMANN, F., SOKOLOSKI, T. & BRUM, J. 2006. Investigating the moisture-induced crystallization kinetics of spray-dried lactose. *International Journal of Pharmaceutics,* 313**,** 23-28.

BUSIGNIES, V., TCHORELOFF, P., LECLERC, B., HERSEN, C., KELLER, G. & COUARRAZE, G. 2004. Compaction of crystallographic forms of pharmaceutical granular lactoses. II. Compacts mechanical properties. *European Journal of Pharmaceutics and Biopharmaceutics,* 58**,** 577-586.

CARON, V., WILLART, J. F., LEFORT, R., DEROLLEZ, P., DANÈDE, F. & DESCAMPS, M. 2011. Solid state amorphization kinetic of alpha lactose upon mechanical milling. *Carbohydrate Research,* 346**,** 2622–2628.

CHATTORAJ, S., SHI, L. & SUN, C. C. 2011. Profoundly improving flow properties of a cohesive cellulose powder by surface coating with nano-silica through co-milling. *Journal of Pharmaceutical Sciences,* 100**,** 4943-4952.

CHEN, Y., DING, Y., PAPADOPOULOS, D. & GHADIRI, M. 2004. Energy-based analysis of milling α-lactose monohydrate. *Journal of Pharmaceutical Sciences,* 93**,** 886-895.

CHIDAVAENZI, O. C., BUCKTON, G., KOOSHA, F. & PATHAK, R. 1997. The use of thermal techniques to assess the impact of feed concentration on the amorphous content and polymorphic forms present in spray dried lactose. *International Journal of Pharmaceutics,* 159**,** 67-74.

CHIENG, N., ZUJOVIC, Z., BOWMAKER, G., RADES, T. & SAVILLE, D. 2006. Effect of milling conditions on the solid-state conversion of ranitidine hydrochloride form-I. *International Journal of Pharmaceutics,* 327**,** 36-44.

CHIKHALIA, V., FORBES, R., STOREY, R. & TICEHURST, M. 2006. The effect of crystal morphology and mill type on milling induced crystal disorder. *European Journal of Pharmaceutical Sciences,* 27**,** 19-26.

CHOWDARY, K. & SUSMITHA, K. 2012. A factorial study on enhancement of solubility and dissolution rate of ibuprofen by β-cyclodextrin and solutol HS-15. *International Journal of Research In Pharmacy and Chemistry,* 2**,** 1043-1048.

COLOMBO, I., GRASSI, G. & GRASSI, M. 2009. Drug mechanochemical activation. *Journal of Pharmaceutical Sciences,* 98**,** 3961-3986.

CROWE, L. M., REID, D. S. & CROWE, J. H. 1996. Is Trehalose special for preserving dry biomaterials? *Biophysical Journal,* 71**,** 2087-2093.

CROWLEY, K. J. & ZOGRAFI, G. 2002. Cryogenic grinding of indomethacin polymorphs and solvates: Assessment of amorphous phase formation and amorphous phase physical stability. *Journal of Pharmaceutical Sciences,* 91**,** 492-507.

DARCY, P. & BUCKTON, G. 1997. The influence of heating/drying on the crystallisation of amorphous lactose after structural collapse. *International Journal of Pharmaceutics,* 158**,** 157-164.

DARKWAH, J., SMITH, G., ERMOLINA, I. & MUELLER-HOLTZ, M. 2013. A THz spectroscopy method for quantifying the degree of crystallinity in freeze-dried gelatin/amino acid mixtures: an application for the development of rapidly disintegrating tablets. *International Journal of Pharmaceutics,* 455**,** 357-364.

DE GUSSEME, A., NEVES, C., WILLART, J. F., RAMEAU, A. & DESCAMPS, M. 2008. Ordering and disordering of molecular solids upon mechanical milling: the case of fananserine. *Journal of Pharmaceutical Sciences,* 97**,** 5000-5012.

DILWORTH, S. E., BUCKTON, G., GAISFORD, S. & RAMOS, R. 2004. Approaches to determine the enthalpy of crystallisation, and amorphous content of lactose from isothermal calorimetric data. *International Journal of Pharmaceutics,* 284**,** 83-94.

DJURIC, D. 2011. Soluplus. *In:* REINTJES, T. (ed.) *Solubility enhancement with BASF pharma polymers: Solubilizer compendium.* BASF SE Pharma Ingredients & Services, Germany.

DJURIC, D., BOYKO, V., KARL, M. & KOLTER, K. 2011. Characterization of polymeric micelles from solid solutions with a polyvinyl caprolactam-polyvinyl acetate-polyethylene glycol graft copolymer and itraconazole. *CRS, 38th Annual Meeting & Exposition of the Gontrolled Release Society.* National Harbor, Maryland USA.

DJURIC, D. & KOLTER, K. Bioavailability enhancement of fenofibrate and itraconazole by forming solid solutions with an innovative amphiphilic co-polymer. PBP World Meeting, Malta, Valletta, 2010.

DONG, W., GILMORE, C., BARR, G., DALLMAN, C., FEEDER, N. & TERRY, S. 2008. A quick method for the quantitative analysis of mixtures. 1. powder X-ray diffraction. *Journal of Pharmaceutical Sciences,* 97**,** 2260-2276.

DORNEY, T. D., BARANIUK, R. G. & MITTLEMAN, D. M. 2001. Material parameter estimation with terahertz time-domain spectroscopy. *Journal of the Optical Society of America a-Optics Image Science and Vision,* 18**,** 1562-1571.

DRAPIER-BECHE, N., FANNI, J. & PARMENTIER, M. 1999. Physical and chemical properties of molecular compounds of lactose. *Journal of Dairy Science,* 82**,** 2558-2563.

DUDOGNON, E., WILLART, J. F., CARON, V., CAPET, F., LARSSON, T. & DESCAMPS, M. 2006. Formation of budesonide/α-lactose glass solutions by ball-milling. *Solid State Communications,* 138**,** 68-71.

ELAMIN, A. A., AHLNECK, C., ALDERBORN, G. & NYSTRÖM, C. 1994. Increased metastable solubility of milled griseofulvin, depending on the formation of a disordered surface structure. *International Journal of Pharmaceutics,* 111**,** 159-170.

ERK, N. 2000. Quantitative analysis of chlorpheniramine maleate and phenylephrine hydrochloride in nasal drops by differential-derivative spectrophotometric, zero-crossing first derivative UV spectrophotometric and absorbance ratio methods. *Journal of Pharmaceutical and Biomedical Analysis,* 23**,** 1023-1031.

ERMOLINA, I., DARKWAH, J. & SMITH, G. 2014. Characterisation of crystalline-amorphous blends of sucrose with terahertz-pulsed spectroscopy: the development of a prediction technique for estimating the degree of crystallinity with partial least squares regression. *AAPS PharmSciTech,* 15**,** 253-260.

ERMOLINA, I. & SMITH, G. 2011. Dielectric spectroscopy of low-losses sugar lyophiles: III: The influence of moisture on the dielectric response of freeze-dried lactose. *Journal of Non-Crystalline Solids,* 357**,** 671-676.

EUNA JUNG, J. K., YOUNHO HAN, & KIWON MOON, M. L. H. H. 2008. Terahertz time domain spectroscopy of crystalline α-lactose monohydrate. *Biochip Journal,* 2**,** 296-299.

FELDMAN, Y., ERMOLINA, I. & HAYASHI, Y. 2003. Time domain dielectric spectroscopy study of biological systems. *Dielectrics and Electrical Insulation, IEEE Transactions on,* 10**,** 728-753.

FELDMAN, Y., PUZENKO, A. & RYABOV, Y. 2002. Non-Debye dielectric relaxation in complex materials. *Chemical Physics,* 284**,** 139-168.

FELDMAN, Y., PUZENKO, A. & RYABOV, Y. 2006. Dielectric relaxation phenomena in complex materials. *In:* RICE, S. A. (ed.) *Fractals, Diffusion, and Relaxation in Disordered Complex Systems.* John Wiley & Sons, Inc., Maryland USA.

FISHER, E. S. 2007. Milling of active pharmaceutical ingredients. *In:* SWARBRICK, J. (ed.) *Encyclopedia of Pharmaceutical Technology.* 3rd ed.: Informa Healthcare, New York, USA.

FIX, I. & STEFFENS, K. J. 2004. Quantifying low amorphous or crystalline amounts of alpha-lactose monohydrate using X-ray powder diffraction, near-infrared spectroscopy, and differential scanning calorimetry. *Drug Development and Industrial Pharmacy,* 30**,** 513-23.

FOLTTMANN, H. & QUADIR, A. 2008. Polyvinylpyrrolidone (PVP)—one of the most widely used excipients in pharmaceuticals: an overview. *Drug Delivery Technology,* 8**,** 22-27.

FONT, J., MUNTASELL, J. & CESARI, E. 1997. Amorphization of organic compounds by ball milling. *Materials Research Bulletin,* 32**,** 1691-1696.

FRIEDRICH, H., NADA, A. & BODMEIER, R. 2005. Solid state and dissolution rate characterization of co-ground mixtures of nifedipine and hydrophilic carriers. *Drug Development and Industrial Pharmacy,* 31**,** 719-728.

GANONG, W. F. & BARRETT, K. E. 2005. *Review of medical physiology*, McGraw-Hill Medical New York, USA.

GARG, A., SINGH, S., RAO, V., BINDU, K. & BALASUBRAMANIAM, J. 2009. Solid state interaction of raloxifene HCl with different hydrophilic carriers during co-grinding and its effect on dissolution rate. *Drug Development and Industrial Pharmacy,* 35**,** 455-470.

GARNIER, S., PETIT, S. & COQUEREL, G. 2002a. Dehydration mechanism and crystallisation behaviour of lactose. *Journal of Thermal Analysis and Calorimetry,* 68**,** 489-502.

GARNIER, S., PETIT, S. & COQUEREL, G. 2002b. Influence of supersaturation and structurally related additives on the crystal growth of α-lactose monohydrate. *Journal of crystal growth,* 234**,** 207-219.

GARNIER, S., PETIT, S., MALLET, F., PETIT, M. N., LEMARCHAND, D., COSTE, S., LEFEBVRE, J. & COQUEREL, G. 2008. Influence of ageing, grinding and preheating on the thermal behaviour of α-lactose monohydrate. *International Journal of Pharmaceutics,* 361**,** 131-140.

GHADIRI, M. & ZHANG, Z. 2002. Impact attrition of particulate solids. Part 1: A theoretical model of chipping. *Chemical Engineering Science,* 57**,** 3659-3669.

GHARSALLAOUI, A., ROUDAUT, G., CHAMBIN, O., VOILLEY, A. & SAUREL, R. 2007. Applications of spray-drying in microencapsulation of food ingredients: An overview. *Food Research International,* 40**,** 1107-1121.

GOMBAS, Á., SZABÓ-RÉVÉSZ, P., KATA, M., REGDON, G. & ERŐS, I. 2002. Quantitative determination of crystallinity of α-lactose monohydrate by DSC. *Journal of Thermal Analysis and Calorimetry,* 68**,** 503-510.

GRAESER, K. A., PATTERSON, J. E., ZEITLER, J. A., GORDON, K. C. & RADES, T. 2009. Correlating thermodynamic and kinetic parameters with amorphous stability. *European Journal of Pharmaceutical Sciences,* 37**,** 492-498.

GUINOT, S. & LEVEILLER, F. 1999. The use of MTDSC to assess the amorphous phase content of a micronised drug substance. *International Journal of Pharmaceutics,* 192**,** 63-75.

GUTINA, A., ANTROPOVA, T., RYSIAKIEWICZ-PASEK, E., VIRNIK, K. & FELDMAN, Y. 2003. Dielectric relaxation in porous glasses. *Microporous and Mesoporous Materials,* 58**,** 237-254.

HAN, X., GHOROI, C., TO, D., CHEN, Y. & DAVÉ, R. 2011. Simultaneous micronization and surface modification for improvement of flow and dissolution of drug particles. *International Journal of Pharmaceutics,* 415**,** 185-195.

HARDUNG, H., DJURIC, D. & ALI, S. 2010. Excipient update; combining HME & solubilization: soluplus®—the solid solution. *Drug Delivery Technology,* 10**,** 20-27.

HASNAIN, M. S. & NAYAK, A. K. 2012. Solubility and dissolution enhancement of Ibuprofen by solid dispersion technique using PEG 6000-PVP K 30 combination carrier. *Bulgarian Journal of Science and Education,* 21**,** 118-132.

HENG, J. Y. Y., THIELMANN, F. & WILLIAMS, D. R. 2006. The effects of milling on the surface properties of form-I paracetamol crystals. *Pharmaceutical Research,* 23**,** 1918-1927.

HU, Y., ZHI, Z., WANG, T., JIANG, T. & WANG, S. 2011. Incorporation of indomethacin nanoparticles into 3-D ordered macroporous silica for enhanced dissolution and reduced gastric irritancy. *European Journal of Pharmaceutics and Biopharmaceutics,* 79**,** 544-551.

HUMBERSTONE, A. J. & CHARMAN, W. N. 1997. Lipid-based vehicles for the oral delivery of poorly water soluble drugs. *Advanced Drug Delivery Reviews,* 25**,** 103-128.

HURTTA, M., PITKÄNEN, I. & KNUUTINEN, J. 2004. Melting behaviour of D-sucrose, D-glucose and D-fructose. *Carbohydrate Research,* 339**,** 2267-2273.

JAGADISH, B., YELCHURI, R., BINDU, K., TANGI, H., MAROJU, S. & RAO, V. U. 2010. Enhanced dissolution and bioavailability of raloxifene hydrochloride by co-grinding with different superdisintegrants. *Chemical & Pharmaceutical Bulletin,* 58**,** 293-300.

JAVADZADEH, Y., SIAHI, M. R., ASNAASHARI, S. & NOKHODCHI, A. 2007. Liquisolid technique as a tool for enhancement of poorly water-soluble drugs and evaluation of their physicochemical properties. *Acta Pharmaceutica (Zagreb),* 57**,** 99-109.

JIVRAJ, M., MARTINI, L. G. & THOMSON, C. M. 2000. An overview of the different excipients useful for the direct compression of tablets. *Pharmaceutical Science & Technology Today,* 3**,** 58-63.

JOSHI, V., DWIVEDI, S. & WARD, G. H. 2002. Increase in the specific surface area of budesonide during storage postmicronization. *Pharmaceutical Research,* 19**,** 7-12.

KAMINSKI, K., ADRJANOWICZ, K., KAMINSKA, E. & PALUCH, M. 2011. Probing of structural relaxation times in the glassy state of sucrose and trehalose based on dynamical properties of two secondary relaxation processes. *Physical Review E,* 83**,** 061502.

KAMINSKI, K., ADRJANOWICZ, K., ZAKOWIECKI, D., KAMINSKA, E., WLODARCZYK, P., PALUCH, M., PILCH, J. & TARNACKA, M. 2012. Dielectric studies on molecular dynamics of two important disaccharides: sucrose and trehalose. *Molecular Pharmaceutics,* 9**,** 1559-1569.

KAMINSKI, K., KAMINSKA, E., HENSEL-BIELOWKA, S., CHELMECKA, E., PALUCH, M., ZIOLO, J., WLODARCZYK, P. & NGAI, K. 2008a. Identification of the molecular motions responsible for the slower secondary (β) relaxation in sucrose. *The Journal of Physical Chemistry B,* 112**,** 7662-7668.

KAMINSKI, K., KAMINSKA, E., WLODARCZYK, P., PAWLUS, S., KIMLA, D., KASPRZYCKA, A., PALUCH, M., ZIOLO, J., SZEJA, W. & NGAI, K. L. 2008b. Dielectric studies on mobility of the glycosidic linkage in seven disaccharides. *The Journal of Physical Chemistry B,* 112**,** 12816-12823.

KAWABATA, Y., WADA, K., NAKATANI, M., YAMADA, S. & ONOUE, S. 2011. Formulation design for poorly water-soluble drugs based on biopharmaceutics classification system: basic approaches and practical applications. *International Journal of Pharmaceutics,* 420**,** 1-10.

KEARNS, K. L., SWALLEN, S. F., EDIGER, M., WU, T. & YU, L. 2007. Influence of substrate temperature on the stability of glasses prepared by vapor deposition. *Journal of Chemical Physics,* 127**,** 154702-154702.

KIM, S., SHI, Y., KIM, J. Y., PARK, K. & CHENG, J.-X. 2010. Overcoming the barriers in micellar drug delivery: loading efficiency, in vivo stability, and micelle-cell interaction. *Expert Opinion on Drug Delivery,* 7**,** 49-62.

KOCBEK, P., BAUMGARTNER, S. & KRISTL, J. 2006. Preparation and evaluation of nanosuspensions for enhancing the dissolution of poorly soluble drugs. *International Journal of Pharmaceutics,* 312**,** 179-186.

KOLODZIEJCZYK, K., PALUCH, M., GRZYBOWSKA, K., GRZYBOWSKI, A., WOJNAROWSKA, Z., HAWELEK, L. & ZIOLO, J. D. 2013. Relaxation dynamics and crystallization study of sildenafil in the liquid and glassy states. *Molecular Pharmaceutics,* 10**,** 2270-2282.

KOLTZENBURG, S. 2011. Introduction. *In:* REINTJES, T. (ed.) *Solubility enhancement with BASF pharma polymers: Solubilizer compendium.* BASF SE Pharma Ingredients & Services, Germany.

KOTHARI, K., RAGOONANAN, V. & SURYANARAYANAN, R. 2014. Influence of molecular mobility on the physical stability of amorphous pharmaceuticals in the supercooled and glassy states. *Molecular Pharmaceutics,* 11**,** 3048-3055.

KOU, X., CHAN, L. W., STECKEL, H. & HENG, P. W. S. 2012. Physico-chemical aspects of lactose for inhalation. *Advanced Drug Delivery Reviews,* 64**,** 220-232.

KRAUSE, B., VILLMOW, T., BOLDT, R., MENDE, M., PETZOLD, G. & PÖTSCHKE, P. 2011. Influence of dry grinding in a ball mill on the length of multiwalled carbon nanotubes and their dispersion and percolation behaviour in melt mixed polycarbonate composites. *Composites Science and Technology,* 71**,** 1145-1153.

KREMER, F. & SCHÖNHALS, A. 2003. *Broadband dielectric spectroscopy*, Springer Verlag.

KRISHNAIAH, Y. S. R. 2010. Pharmaceutical technologies for enhancing oral bioavailability of poorly soluble drugs. *Journal of Bioequivalence & Bioavailability,* 2**,** 28-36.

KÜRTI, L., KUKOVECZ, Á., KOZMA, G., AMBRUS, R., DELI, M. A. & SZABÓ-RÉVÉSZ, P. 2011. Study of the parameters influencing the co-grinding process for the production of meloxicam nanoparticles. *Powder Technology,* 212**,** 210-217.

KWAN, C. C., CHEN, Y. Q., DING, Y. L., PAPADOPOULOS, D. G., BENTHAM, A. C. & GHADIRI, M. 2004. Development of a novel approach towards predicting the milling behaviour of pharmaceutical powders. *European Journal of Pharmaceutical Sciences,* 23**,** 327-336.

LEHTO, V.-P., TENHO, M., VÄHÄ-HEIKKILÄ, K., HARJUNEN, P., PÄÄLLYSAHO, M., VÄLISAARI, J., NIEMELÄ, P. & JÄRVINEN, K. 2006. The comparison of seven different methods to quantify the amorphous content of spray dried lactose. *Powder Technology,* 167**,** 85-93.

LI, Y., HAN, J., ZHANG, G. G. Z., GRANT, D. J. W. & SURYANARAYANAN, R. 2000. In-situ dehydration of carbamazepine dihydrate: a novel technique to prepare amorphous anhydrous carbamazepine. *Pharmaceutical Development and Technology,* 5**,** 257-266.

LIN, S.-Y., HSU, C.-H. & KE, W.-T. 2010. Solid-state transformation of different gabapentin polymorphs upon milling and co-milling. *International Journal of Pharmaceutics,* 396**,** 83-90.

LIPINSKI, C. A., LOMBARDO, F., DOMINY, B. W. & FEENEY, P. J. 2001. Experimental and computational approaches to estimate solubility and permeability in drug discovery and development settings1. *Advanced Drug Delivery Reviews,* 46**,** 3-26.

LISTIOHADI, Y., HOURIGAN, J. A., SLEIGH, R. W. & STEELE, R. J. 2009. Thermal analysis of amorphous lactose and alpha-lactose monohydrate. *Dairy Science and Technology,* 89**,** 43-67.

LIU, H. B., CHEN, Y. & ZHANG, X. C. 2007. Characterization of anhydrous and hydrated pharmaceutical materials with THz time-domain spectroscopy. *Journal of Pharmaceutical Sciences,* 96**,** 927-934.

LIU, J., RIGSBEE, D. R., STOTZ, C. & PIKAL, M. J. 2002. Dynamics of pharmaceutical amorphous solids: The study of enthalpy relaxation by isothermal microcalorimetry. *Journal of Pharmaceutical Sciences,* 91**,** 1853-1862.

MACKIN, L., SARTNURAK, S., THOMAS, I. & MOORE, S. 2002a. The impact of low levels of amorphous material (<5%) on the blending characteristics of a direct compression formulation. *International Journal of Pharmaceutics,* 231**,** 213-226.

MACKIN, L., ZANON, R., PARK, J. M., FOSTER, K., OPALENIK, H. & DEMONTE, M. 2002b. Quantification of low levels (< 10%) of amorphous content in micronised active batches using dynamic vapour sorption and isothermal microcalorimetry. *International Journal of Pharmaceutics,* 231**,** 227-236.

MADHURI NEWA, K. H. B., JONG OH KIM, JONG SEOB IM, JUNG AE KIM, & BONG KYU YOO, J. S. W., HAN GON CHOI,* AND CHUL SOON YONG 2008. Enhancement of solubility, dissolution

and bioavailability of ibuprofen in solid dispersion systems. *Chemical and Pharmaceutical Bulletin,* 56**,** 569—574.

MAESTRELLI, F., CIRRI, M., MENNINI, N., ZERROUK, N. & MURA, P. 2011. Improvement of oxaprozin solubility and permeability by the combined use of cyclodextrin, chitosan, and bile components. *European Journal of Pharmaceutics and Biopharmaceutics,* 78**,** 385-393.

MALLICK, S., PATTNAIK, S., SWAIN, K., DE, P. K., SAHA, A., GHOSHAL, G. & MONDAL, A. 2008a. Formation of physically stable amorphous phase of ibuprofen by solid state milling with kaolin. *European Journal of Pharmaceutics and Biopharmaceutics,* 68**,** 346-351.

MALLICK, S., PATTNAIK, S., SWAIN, K., DE, P. K., SAHA, A., MAZUMDAR, P. & GHOSHAL, G. 2008b. Physicochemical characterization of interaction of ibuprofen by solid-state milling with aluminum hydroxide. *Drug Development and Industrial Pharmacy,* 34**,** 726-734.

MAURYA, D., BELGAMWAR, V. & TEKADE, A. 2010. Microwave induced solubility enhancement of poorly water soluble atorvastatin calcium. *Journal of Pharmacy and Pharmacology,* 62**,** 1599-1606.

MCINTOSH, A. I., YANG, B., GOLDUP, S. M., WATKINSON, M. & DONNAN, R. S. 2013. Crystallization of amorphous lactose at high humidity studied by terahertz time domain spectroscopy. *Chemical Physics Letters,* 558**,** 104-108.

MEGARRY, A. J., BOOTH, J. & BURLEY, J. 2014. Sucrose/glucose molecular alloys by cryo-milling. *Journal of Pharmaceutical Sciences,* 103**,** 2098-2106.

MEHANNA, M. M., MOTAWAA, A. M. & SAMAHA, M. W. 2011. Tadalafil inclusion in microporous silica as effective dissolution enhancer: optimization of loading procedure and molecular state characterization. *Journal of Pharmaceutical Sciences,* 100**,** 1805-1818.

MILHEM, O. M., MYLES, C., MCKEOWN, N. B., ATTWOOD, D. & D'EMANUELE, A. 2000. Polyamidoamine starburst® dendrimers as solubility enhancers. *International Journal of Pharmaceutics,* 197**,** 239-241.

MOHAMMED, A., WESTON, N., COOMBES, A., FITZGERALD, M. & PERRIE, Y. 2004. Liposome formulation of poorly water soluble drugs: optimisation of drug loading and ESEM analysis of stability. *International Journal of Pharmaceutics,* 285**,** 23-34.

MOOLCHANDANI, V., AUGSBURGER, L. L., GUPTA, A., KHAN, M., LANGRIDGE, J. & HOAG, S. W. 2014. Characterization and selection of suitable grades of lactose as functional fillers for capsule filling: part 1. *Drug Development and Industrial Pharmacy***,** 1-12.

MOSHARRAF, M. & NYSTRÖM, C. 1995. The effect of particle size and shape on the surface specific dissolution rate of microsized practically insoluble drugs. *International Journal of Pharmaceutics,* 122**,** 35-47.

MOSHARRAF, M., SEBHATU, T. & NYSTRÖM, C. 1999. The effects of disordered structure on the solubility and dissolution rates of some hydrophilic, sparingly soluble drugs. *International Journal of Pharmaceutics,* 177**,** 29-51.

MURALI MOHAN BABU, G., KUMAR, N., SANKAR, K., RAM, B., KUMAR, N. & MURTHY, K. 2002. In-vivo evaluation of modified gum karaya as a carrier for improving the oral bioavailability of a poorly water-soluble drug, nimodipine. *AAPS PharmSciTech,* 3**,** 55-63.

MURDANDE, S. B., PIKAL, M. J., SHANKER, R. M. & BOGNER, R. H. 2011. Solubility advantage of amorphous pharmaceuticals, part 3: is maximum solubility advantage experimentally attainable and sustainable? *Journal of Pharmaceutical Sciences,* 100**,** 4349-4356.

NAGY, Z. K., BALOGH, A., VAJNA, B., FARKAS, A., PATYI, G., KRAMARICS, Á. & MAROSI, G. 2012. Comparison of electrospun and extruded soluplus®-based solid dosage forms of improved dissolution. *Journal of Pharmaceutical Sciences,* 101**,** 322-332.

NALLASIVAN, P. K., SARANYA, K., KUMAR, R. S., JEEVANANTHAM, S. & VENKATNARAYANAN, R. 2010. Simultaneous determination of ibuprofen and tizanidine in bulk drug and its combined dosage form by spectrophotometry. *Scholar Research Library,* 2**,** 289-295.

NANDI, I., BATESON, M., BARI, M. & JOSHI, H. 2003. Synergistic effect of PEG-400 and cyclodextrin to enhance solubility of progesterone. *AAPS PharmSciTech,* 4**,** 1-5.

NEWA, M., BHANDARI, K., OH, D., KIM, Y., SUNG, J., KIM, J., WOO, J., CHOI, H. & YONG, C. 2008. Enhanced dissolution of ibuprofen using solid dispersion with poloxamer-407. *Archives of Pharmacal Research,* 31**,** 1497-1507.

NEWELL, H. E., BUCKTON, G., BUTLER, D. A., THIELMANN, F. & WILLIAMS, D. R. 2001. The use of inverse phase gas chromatography to measure the surface energy of crystalline, amorphous and recently milled lactose. *Pharmaceutical Research,* 18**,** 662-666.

NGAI, K. & CAPACCIOLI, S. 2004. Relation between the activation energy of the Johari-Goldstein β relaxation and T g of glass formers. *Physical Review E,* 69**,** 031501.

NOEL, T. R., PARKER, R. & RING, S. G. 1996. A comparative study of the dielectric relaxation behaviour of glucose, maltose, and their mixtures with water in the liquid and glassy states. *Carbohydrate Research,* 282**,** 193-206.

NOEL, T. R., PARKER, R. & RING, S. G. 2000. Effect of molecular structure and water content on the dielectric relaxation behaviour of amorphous low molecular weight carbohydrates above and below their glass transition. *Carbohydrate Research,* 329**,** 839-845.

NOKHODCHI, A., AMIRE, O. & JELVEHGARI, M. 2010. Physico-mechanical and dissolution behaviours of ibuprofen crystals crystallized in the presence of various additives. *Daru: Journal of Faculty of Pharmacy, Tehran University of Medical Sciences,* 18**,** 74.

NOKHODCHI, A., TALARI, R., VALIZADEH, H. & BARZEGAR-JALALI, M. 2007. An investigation on the solid dispersions of chlordiazepoxide. *International Journal of Biomedical Science.***,** 211-217.

NORDIN, M. & FRANKEL, V. H. 2001. *Basic biomechanics of the musculoskeletal system,* Philadelphia, PS, USA, Lippincott Williams & Wilkins.

NØRGAARD, L., HAHN, M. T., KNUDSEN, L. B., FARHAT, I. A. & ENGELSEN, S. B. 2005. Multivariate near-infrared and Raman spectroscopic quantifications of the crystallinity of lactose in whey permeate powder. *International Dairy Journal,* 15**,** 1261-1270.

OTSUKA, M., OFUSA, T. & MATSUDA, Y. 1998. Dissolution improvement of water-insoluble glybuzole by co-grinding and co-melting with surfactants and their physicochemical properties. *Colloids and Surfaces B: Biointerfaces,* 10**,** 217-226.

OTSUKA, M., OHTANI, H., KANENIWA, N. & HIGUCHI, S. 1991. Isomerization of lactose in solid-state by mechanical stress during grinding. *Journal of Pharmacy and Pharmacology,* 43**,** 148-153.

PARROTT, E. L. 1987. Milling. *In:* LACHMAN, L. (ed.) *The theory and practice of industrial pharmacy.* 3rd ed. Hind Rajasthan Building Dadar Bombay: Varghese Publishing House.

PASSERINI, N., ALBERTINI, B., GONZÁLEZ-RODRíGUEZ, M. L., CAVALLARI, C. & RODRIGUEZ, L. 2002. Preparation and characterisation of ibuprofen–poloxamer 188 granules obtained by melt granulation. *European Journal of Pharmaceutical Sciences,* 15**,** 71-78.

PATIL, P. R., RAKESH, S. U., DHABALE, P. N. & BURADE, K. B. 2009. Simultaneous estimation of ramipril and amlodipine by uv spectrophotometric method. *Research Journal of Pharmacy and Technology,* 2**,** 304-307.

PATIST, A. & ZOERB, H. 2005. Preservation mechanisms of trehalose in food and biosystems. *Colloids and Surfaces B: Biointerfaces,* 40**,** 107-113.

PATTERSON, J. E., JAMES, M. B., FORSTER, A. H., LANCASTER, R. W., BUTLER, J. M. & RADES, T. 2007. Preparation of glass solutions of three poorly water soluble drugs by spray drying, melt extrusion and ball milling. *International Journal of Pharmaceutics,* 336**,** 22-34.

PELTONEN, L. & HIRVONEN, J. 2010. Pharmaceutical nano-crystals by nano-milling: critical process parameters, particle fracturing and stabilization methods. *Journal of Pharmacy and Pharmacology,* 62**,** 1569-1579.

PERRUT, M., JUNG, J. & LEBOEUF, F. 2005. Enhancement of dissolution rate of poorly-soluble active ingredients by supercritical fluid processes: Part I: micronization of neat particles. *International Journal of Pharmaceutics,* 288**,** 3-10.

PETERS, H. 2009. Lactose for direct compression; *Special Report*. *Chemical Weekly.* Friesland Foods Domo, Netherland.

PHILLIPS, E. M. 1997. An approach to estimate the amorphous content of pharmaceutical powders using calorimetry with no calibration standards. *International Journal of Pharmaceutics,* 149**,** 267-271.

PILCER, G. & AMIGHI, K. 2010. Formulation strategy and use of excipients in pulmonary drug delivery. *International Journal of Pharmaceutics,* 392**,** 1-19.

PLAKKOT, S., DE MATAS, M., YORK, P., SAUNDERS, M. & SULAIMAN, B. 2011. Comminution of ibuprofen to produce nano-particles for rapid dissolution. *International Journal of Pharmaceutics,* 415**,** 307-314.

POKHARKAR, V. B., MANDPE, L. P., PADAMWAR, M. N., AMBIKE, A. A., MAHADIK, K. R. & PARADKAR, A. 2006. Development, characterization and stabilization of amorphous form of a low Tg drug. *Powder Technology,* 167**,** 20-25.

PRICE, R. & YOUNG, P. M. 2005. On the physical transformations of processed pharmaceutical solids. *Micron,* 36**,** 519-524.

PUZENKO, A., KOZLOVICH, N., GUTINA, A. & FELDMAN, Y. 1999. Determination of pore fractal dimensions and porosity of silica glasses from the dielectric response at percolation. *Physical Review B,* 60**,** 14348.

QIAO, N., WANG, K., SCHLINDWEIN, W., DAVIES, A. & LI, M. 2013. In-situ monitoring of carbamazepine–nicotinamide co-crystal intrinsic dissolution behaviour. *European Journal of Pharmaceutics and Biopharmaceutics,* 83**,** 415-426.

QIU, Y., LIU, L., CHEN, Y. & ZHANG, G. G. Z. 2009. *Developing solid oral dosage forms: pharmaceutical theory and practice*, Elsevier Science.

QUADIR, A. 2005. Characterization of newly developed micronized poloxamers for poorly soluble drugs. *Controlled Release Society Meeting.* BASF The Chemical Company Miami, Florida.

RASENACK, N. & MÜLLER, B. W. 2004. Micron-size drug particles: common and novel micronization techniques. *Pharmaceutical Development and Technology,* 9**,** 1-13.

RAUT, D. M., ALLADA, R., PAVAN, K., DESHPANDE, G., PATIL, D., PATIL, A., DESHMUKH, A., SAKHARKAR, D. & BODKE, P. 2011. Dehydration of lactose monohydrate: analytical and physical characterization. *Der Pharmacia Lettre,* 3**,** 202-212.

RAWAT, S. & JAIN, S. K. 2004. Solubility enhancement of celecoxib using β-cyclodextrin inclusion complexes. *European Journal of Pharmaceutics and Biopharmaceutics,* 57**,** 263-267.

RAYMOND C ROWE, P. J. S., PAUL J WELLER (ed.) 2003. *Handbook of pharmaceutical excipients,* Pharmaceutical Press, London

RODRIGUES, A. C., VICIOSA, M. T., DANÈDE, F., AFFOUARD, F. & CORREIA, N. T. 2013. Molecular mobility of amorphous S-flurbiprofen: A dielectric relaxation spectroscopy approach. *Molecular Pharmaceutics,* 11**,** 112-130.

ROOS, Y. H. 1995. *Phase transitions in foods*, Academic Press, London, UK.

RYABOV, Y., GUTINA, A., ARKHIPOV, V. & FELDMAN, Y. 2001. Dielectric relaxation of water absorbed in porous glass. *The Journal of Physical Chemistry B,* 105**,** 1845-1850.

SAHOO, N. G., KAKRAN, M., LI, L., JUDEH, Z. & MÜLLER, R. H. 2011. Dissolution enhancement of a poorly water-soluble antimalarial drug by means of a modified multi-fluid nozzle pilot spray drier. *Materials Science and Engineering: C,* 31**,** 391-399.

SAILAJA, U., SHAHIN THAYYIL, M., KRISHNA KUMAR, N. S. & GOVINDARAJ, G. 2013. Molecular dynamics in liquid and glassy states of non-steroidal anti-inflammatory drug: Ketoprofen. *European Journal of Pharmaceutical Sciences,* 49**,** 333-340.

SALEEM, I. & SMYTH, H. 2010. Micronization of a soft material: air-jet and micro-ball milling. *AAPS PharmSciTech,* 11**,** 1642-1649.

SALEH, W., DENIS, D., JEAN-LOUIS, D., GILLES, B. & BERNARD, B. 2008. The Improvement of ibuprofen dissolution rate through microparticles spray drying processed in an aqueous system. *Drug Development and Industrial Pharmacy,* 34**,** 485-491.

SALÚSTIO, P. J., CABRAL-MARQUES, H. M., COSTA, P. C. & PINTO, J. F. 2011. Comparison of Ibuprofen release from minitablets and capsules containing ibuprofen: β-cyclodextrin complex. *European Journal of Pharmaceutics and Biopharmaceutics,* 78**,** 58-66.

SAMANTA, M., TIAN, W., DATTA, S., HENDERSON, J. & KUBIAK, C. 1996. Electronic conduction through organic molecules. *Physical Review B,* 53**,** R7626.

SERAJUDDIN†, A. T. M. 1999. Solid dispersion of poorly water-soluble drugs: early promises, subsequent problems and recent breakthroughs. *Journal of Pharmaceutical Sciences,* Vol. 88**,,** 1059-1066.

SHAH, B., KAKUMANU, V. K. & BANSAL, A. K. 2006. Analytical techniques for quantification of amorphous/crystalline phases in pharmaceutical solids. *Journal of Pharmaceutical Sciences,* 95**,** 1641-1665.

SHAKHTSHNEIDER, T., VASILTCHENKO, M., POLITOV, A. & BOLDYREV, V. 1996. The mechanochemical preparation of solid disperse systems of ibuprofen-polyethylene glycol. *International Journal of Pharmaceutics,* 130**,** 25-32.

SHAMMA, R. N. & BASHA, M. 2013. Soluplus®: A novel polymeric solubilizer for optimization of carvedilol solid dispersions: formulation design and effect of method of preparation. *Powder Technology,* 237**,** 406-414.

SHARIARE, M. H., DE MATAS, M., YORK, P. & SHAO, Q. 2011. The impact of material attributes and process parameters on the micronisation of lactose monohydrate. *International Journal of Pharmaceutics,* 408**,** 58-66.

SHEN, Y., TADAY, P. & PEPPER, M. 2008. Elimination of scattering effects in spectral measurement of granulated materials using terahertz pulsed spectroscopy. *Applied physics letters,* 92**,** 051103.

SHIN, S.-C. & CHO, C.-W. 1997. Physicochemical characterizations of piroxicam-poloxamer solid dispersion. *Pharmaceutical development and technology,* 2**,** 403-407.

SHIRAKI, K., TAKATA, N., TAKANO, R., HAYASHI, Y. & TERADA, K. 2008. Dissolution improvement and the mechanism of the improvement from cocrystallization of poorly water-soluble compounds. *Pharmaceutical Research,* 25**,** 2581-2592.

SIBIK, J., SARGENT, M. J., FRANKLIN, M. & ZEITLER, J. A. 2014. Crystallization and phase changes in paracetamol from the amorphous solid to the liquid phase. *Molecular Pharmaceutics,* 11**,** 1326-1334.

SING, K., EVERETT, D., HAUL, R., MOSCOU, L., PIEROTTI, R., ROUQUEROL, J. & SIEMIENIEWSKA, T. 1982. Reporting physisorption data for gas/solid systems. *Pure and Applied Chemistry,* 54**,** 2201.

SINGH, J., DUTTA, P., DUTTA, J., HUNT, A., MACQUARRIE, D. & CLARK, J. 2009. Preparation and properties of highly soluble chitosan–L-glutamic acid aerogel derivative. *Carbohydrate Polymers,* 76**,** 188-195.

SINGH, R. & LILLARD JR, J. W. 2009. Nanoparticle-based targeted drug delivery. *Experimental and molecular pathology,* 86**,** 215-223.

SMITH G., E. I. Dielectric properties of lactose monohydrate: mechanisms of relaxation and the influence of particle size and hydration water APS PharmSci, 2007 Manchester, U.K.

SMITHEY, D., FENNEWALD, J., GAUTSCHI, J., CREW, M., ALI, S., LAN, Y. & LANGLEY, N. Evaluation of the polymer soluplus® for spray-dried dispersions of poorly soluble compounds. AAPS Annual Meeting and Exposition, 2010.

STEGEMANN, S., LEVEILLER, F., FRANCHI, D., DE JONG, H. & LINDÉN, H. 2007. When poor solubility becomes an issue: From early stage to proof of concept. *European Journal of Pharmaceutical Sciences,* 31**,** 249-261.

STOREY, R. A. & YMEN, I. 2011. *Solid state characterization of pharmaceuticals*, Wiley Online Library.

STRACHAN, C. J., RADES, T., NEWNHAM, D. A., GORDON, K. C., PEPPER, M. & TADAY, P. F. 2004. Using terahertz pulsed spectroscopy to study crystallinity of pharmaceutical materials. *Chemical Physics Letters,* 390**,** 20-24.

STRACHAN, C. J., TADAY, P. F., NEWNHAM, D. A., GORDON, K. C., ZEITLER, J. A., PEPPER, M. & RADES, T. 2005. Using terahertz pulsed spectroscopy to quantify pharmaceutical polymorphism and crystallinity. *Journal of Pharmaceutical Sciences,* 94**,** 837-846.

SUGIMOTO, M., OKAGAKI, T., NARISAWA, S., KOIDA, Y. & NAKAJIMA, K. 1998. Improvement of dissolution characteristics and bioavailability of poorly water-soluble drugs by novel cogrinding method using water-soluble polymer. *International Journal of Pharmaceutics,* 160**,** 11-19.

TADAY, P. F. 2004. Applications of terahertz spectroscopy to pharmaceutical sciences. *Philosophical Transactions of the Royal Society of London. Series A: Mathematical, Physical and Engineering Sciences,* 362**,** 351-364.

TADAY, P. F., BRADLEY, I. V., ARNONE, D. D. & PEPPER, M. 2003. Using terahertz pulse spectroscopy to study the crystalline structure of a drug: A case study of the polymorphs of ranitidine hydrochloride. *Journal of Pharmaceutical Sciences,* 92**,** 831-838.

TAO, T., ZHAO, Y., WU, J. & ZHOU, B. 2009. Preparation and evaluation of itraconazole dihydrochloride for the solubility and dissolution rate enhancement. *International Journal of Pharmaceutics,* 367**,** 109-114.

THAKRAL, N. K., RAY, A. R., BAR-SHALOM, D., ERIKSSON, A. H. & MAJUMDAR, D. K. 2012. Soluplus-solubilized citrated camptothecin—A potential drug delivery strategy in colon cancer. *AAPS PharmSciTech,* 13**,** 59-66.

THIELMANN, F., BURNETT, D. J. & HENG, J. Y. Y. 2007. Determination of the surface energy distributions of different processed lactose. *Drug Development and Industrial Pharmacy,* 33**,** 1240-1253.

THOMSEN, M. K., JESPERSEN, L., SJOSTROM, K., RISBO, J. & SKIBSTED, L. H. 2005. Water activity−temperature state diagram of amorphous lactose. *Journal of Agricultural and Food Chemistry,* 53**,** 9182-9185.

VADHER, A., PARIKH, J., PARIKH, R. & SOLANKI, A. 2009. Preparation and characterization of co-grinded mixtures of aceclofenac and neusilin US_2 for dissolution enhancement of aceclofenac. *AAPS PharmSciTech,* 10**,** 606-614.

VAN DEN MOOTER, G. 2012. The use of amorphous solid dispersions: A formulation strategy to overcome poor solubility and dissolution rate. *Drug Discovery Today: Technologies,* 9**,** e79-e85.

VEMULA, V. R., LAGISHETTY, V. & LINGALA, S. 2010. Solubility enhancement techniques. *International Journal of Pharmaceutical Sciences Review and Research,* 5**,** 41-51.

VENKATRAMANA M.RAO, R. S. A. H. J. Z. 2009. Solubility of pharmaceutical solids. *In:* YIHONG QIU, Y. C., GEOFF G, Z ZHANG (ed.) *Developing Solid Oral Dosage Form Pharmaceutical Theory and Practice.* Academy Press Elsevier, London UK.

VIEGAS, T. X., CURATELLA, R. U., VAN WINKLE, L. L. & BRINKER, G. 2001. Measurement of intrinsic drug dissolution rates using two types of apparatus. *Pharmaceutical Technology,* 25**,** 44-53.

VISHWESHWAR, P., MCMAHON, J. A., PETERSON, M. L., HICKEY, M. B., SHATTOCK, T. R. & ZAWOROTKO, M. J. 2005. Crystal engineering of pharmaceutical co-crystals from polymorphic active pharmaceutical ingredients. *Chemical communications***,** 4601-4603.

VOGT, M., KUNATH, K. & DRESSMAN, J. B. 2008a. Dissolution enhancement of fenofibrate by micronization, cogrinding and spray-drying: Comparison with commercial preparations. *European Journal of Pharmaceutics and Biopharmaceutics,* 68**,** 283-288.

VOGT, M., KUNATH, K. & DRESSMAN, J. B. 2008b. Dissolution improvement of four poorly water soluble drugs by co-grinding with commonly used excipients. *European Journal of Pharmaceutics and Biopharmaceutics,* 68**,** 330-337.

VOGT, M., VERTZONI, M., KUNATH, K., REPPAS, C. & DRESSMAN, J. B. 2008c. Co-grinding enhances the oral bioavailability of EMD-57033, a poorly water soluble drug in dogs. *European Journal of Pharmaceutics and Biopharmaceutics,* 68**,** 338-345.

WARD, G. H. & SCHULTZ, R. K. 1995. Process-induced crystallinity changes in albuterol sulfate and its effect on powder physical stability. *Pharmaceutical Research,* 12**,** 773-779.

WATANABE, T., HASEGAWA, S., WAKIYAMA, N., KUSAI, A. & SENNA, M. 2003. Comparison between polyvinylpyrrolidone and silica nanoparticles as carriers for indomethacin in a solid state dispersion. *International Journal of Pharmaceutics,* 250**,** 283-286.

WATANABE, T., OHNO, I., WAKIYAMA, N., KUSAI, A. & SENNA, M. 2002. Stabilization of amorphous indomethacin by co-grinding in a ternary mixture. *International Journal of Pharmaceutics,* 241**,** 103-111.

WESTERMARCK, S., JUPPO, A. M., KERVINEN, L. & YLIRUUSI, J. 1998. Pore structure and surface area of mannitol powder, granules and tablets determined with mercury porosimetry and nitrogen adsorption. *European Journal of Pharmaceutics and Biopharmaceutics,* 46**,** 61-68.

WIKARSA, S., DURAND, D., DELARBRE, J. L., BAYLAC, G. & BATAILLE, B. 2008. The improvement of Ibuprofen dissolution rate through microparticles spray drying processed in an aqueous system. *Drug Development and Industrial Pharmacy,* 34**,** 485-491.

WILLART, J. F., CARON, V., LEFORT, R., DANÈDE, F., PRÉVOST, D. & DESCAMPS, M. 2004. Athermal character of the solid state amorphization of lactose induced by ball milling. *Solid State Communications,* 132**,** 693-696.

WILLART, J. F., DE GUSSEME, A., HEMON, S., ODOU, G., DANEDE, F. & DESCAMPS, M. 2001. Direct crystal to glass transformation of trehalose induced by ball milling. *Solid State Communications,* 119**,** 501-505.

WILLART, J. F., DUJARDIN, N., DUDOGNON, E., DANÈDE, F. & DESCAMPS, M. 2010. Amorphization of sugar hydrates upon milling. *Carbohydrate Research,* 345**,** 1613-1616.

WOJNAROWSKA, Z., GRZYBOWSKA, K., ADRJANOWICZ, K., KAMINSKI, K., PALUCH, M., HAWELEK, L., WRZALIK, R., DULSKI, M., SAWICKI, W., MAZGALSKI, J., TUKALSKA, A. & BIEG, T. 2010. Study of the amorphous glibenclamide drug: analysis of the molecular dynamics of quenched and cryo-milled material. *Molecular Pharmaceutics,* 7**,** 1692-1707.

WOJNAROWSKA, Z., GRZYBOWSKA, K., HAWELEK, L., DULSKI, M., WRZALIK, R., GRUSZKA, I., PALUCH, M., PIENKOWSKA, K., SAWICKI, W., BUJAK, P., PALUCH, K. J., TAJBER, L. & MARKOWSKI, J. 2013. Molecular dynamics, physical stability and solubility advantage from amorphous indapamide drug. *Molecular Pharmaceutics,* 10**,** 3612-3627.

WONGMEKIAT, A., TOZUKA, Y., OGUCHI, T. & YAMAMOTO, K. 2003. Formation of fine drug particle by cogrinding with cyclodextrins: Part II. The influence of moisture condition during cogrinding process on fine particle formation. *International Journal of Pharmaceutics,* 265**,** 85-93.

WU, C., WANG, Z., ZHI, Z., JIANG, T., ZHANG, J. & WANG, S. 2011. Development of biodegradable porous starch foam for improving oral delivery of poorly water soluble drugs. *International Journal of Pharmaceutics,* 403**,** 162-169.

YAMAMOTO, K., TOMINAGA, K., SASAKAWA, H., TAMURA, A., MURAKAMI, H., OHTAKE, H. & SARUKURA, N. 2005. Terahertz Time-Domain Spectroscopy of Amino Acids and Polypeptides. *Biophysical Journal,* 89**,** L22-L24.

YANG, W., KWAN, C. C., DING, Y. L., GHADIRI, M. & ROBERTS, K. J. 2007. Milling of sucrose. *Powder Technology,* 174**,** 14-17.

YOUNG, P. M., CHIOU, H., TEE, T., TRAINI, D., CHAN, H.-K., THIELMANN, F. & BURNETT, D. 2007. The use of organic vapor sorption to determine low levels of amorphous content in processed pharmaceutical powders. *Drug Development and Industrial Pharmacy,* 33**,** 91-97.

YU, L. 2001. Amorphous pharmaceutical solids: preparation, characterization and stabilization. *Advanced Drug Delivery Reviews,* 48**,** 27-42.

ZEITLER, J. A., KOGERMANN, K., RANTANEN, J., RADES, T., TADAY, P. F., PEPPER, M., AALTONEN, J. & STRACHAN, C. J. 2007. Drug hydrate systems and dehydration processes studied by terahertz pulsed spectroscopy. *International Journal of Pharmaceutics,* 334**,** 78-84.

ZHANG, H.-X., WANG, J.-X., ZHANG, Z.-B., LE, Y., SHEN, Z.-G. & CHEN, J.-F. 2009. Micronization of atorvastatin calcium by antisolvent precipitation process. *International Journal of Pharmaceutics,* 374**,** 106-113.

ZHANG, J., EBBENS, S., CHEN, X., JIN, Z., LUK, S., MADDEN, C., PATEL, N. & ROBERTS, C. J. 2006. Determination of the surface free energy of crystalline and amorphous lactose by atomic force microscopy adhesion measurement. *Pharmceutical Research,* 23**,** 401-7.

9 Appendices

Appendix I

SEM micrographs of un- milled and various milled samples of lactose monohydrate. Each row shows the micrographs of same sample at different magnifications (the milling time and magnification is indicated on each micrograph).

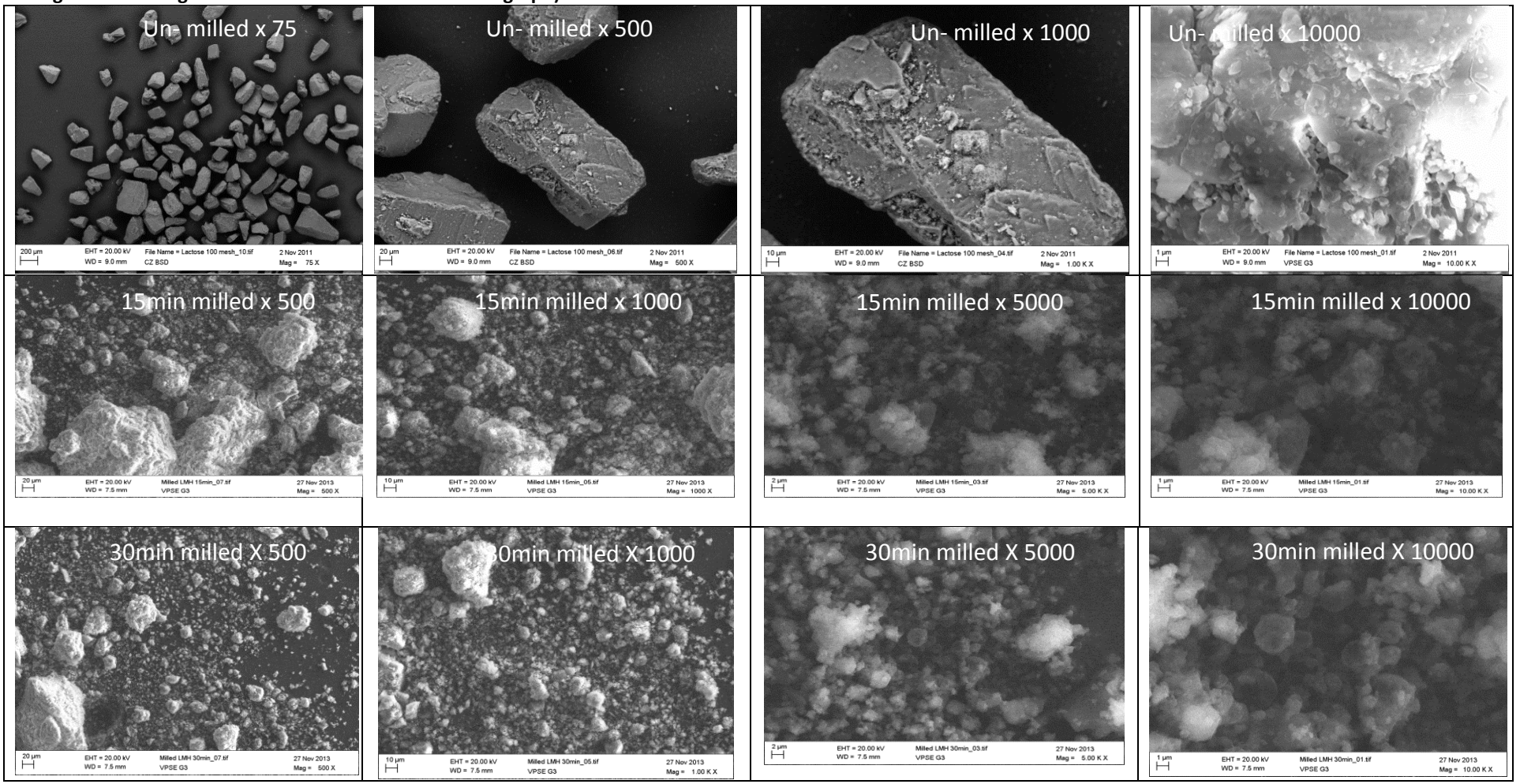

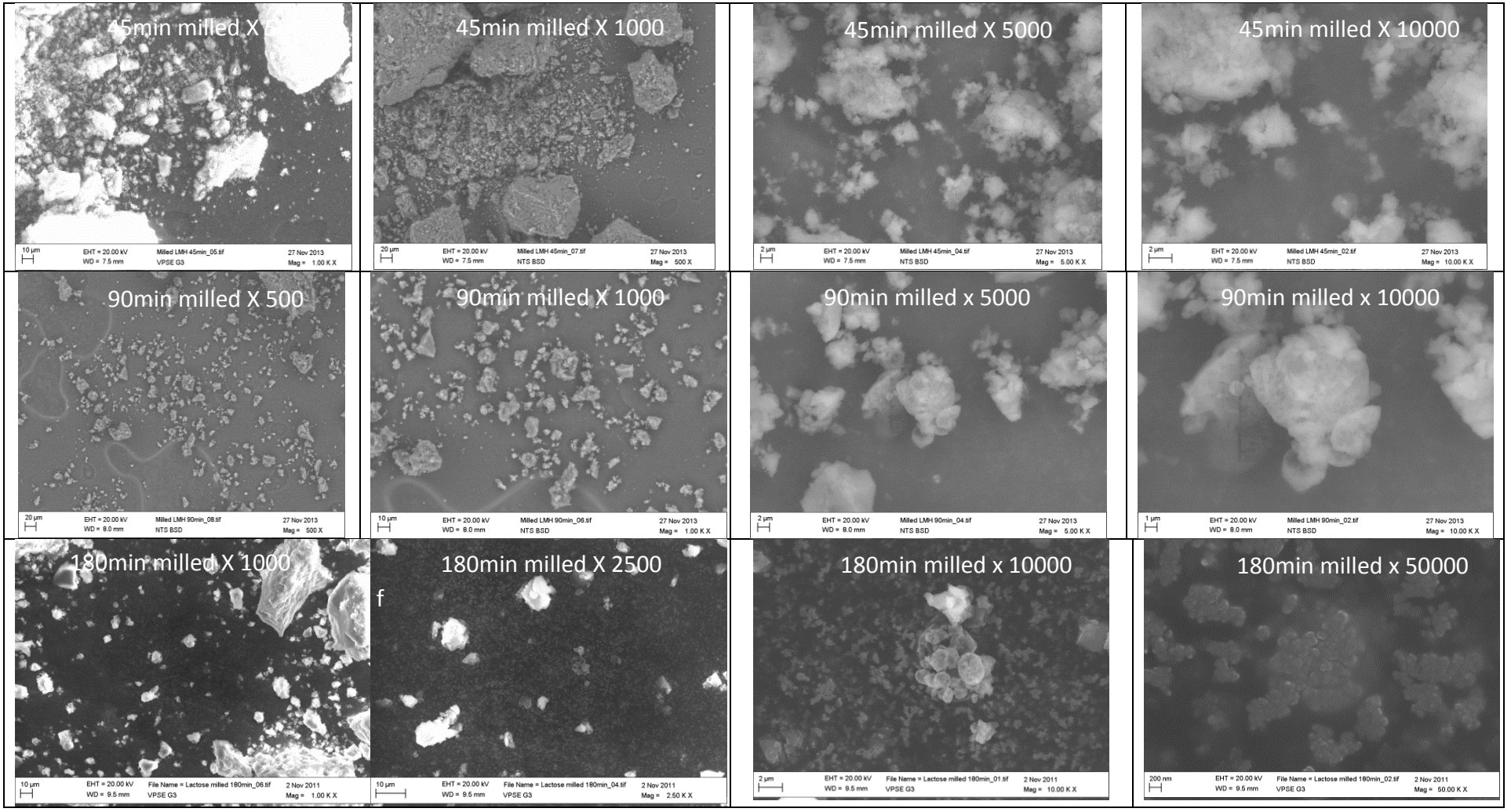
45min milled X
45min milled X 1000
45min milled X 5000
45min milled X 10000
90min milled X 500
90min milled X 1000
90min milled x 5000
90min milled x 10000
180min milled X 1000
180min milled X 2500
f
180min milled x 10000
180min milled x 50000

Appendix II

SEM micrographs of un- milled and various milled samples of Sucrose. Each row shows the micrographs of same sample at different magnifications (the milling time and magnification is indicated on each micrograph).

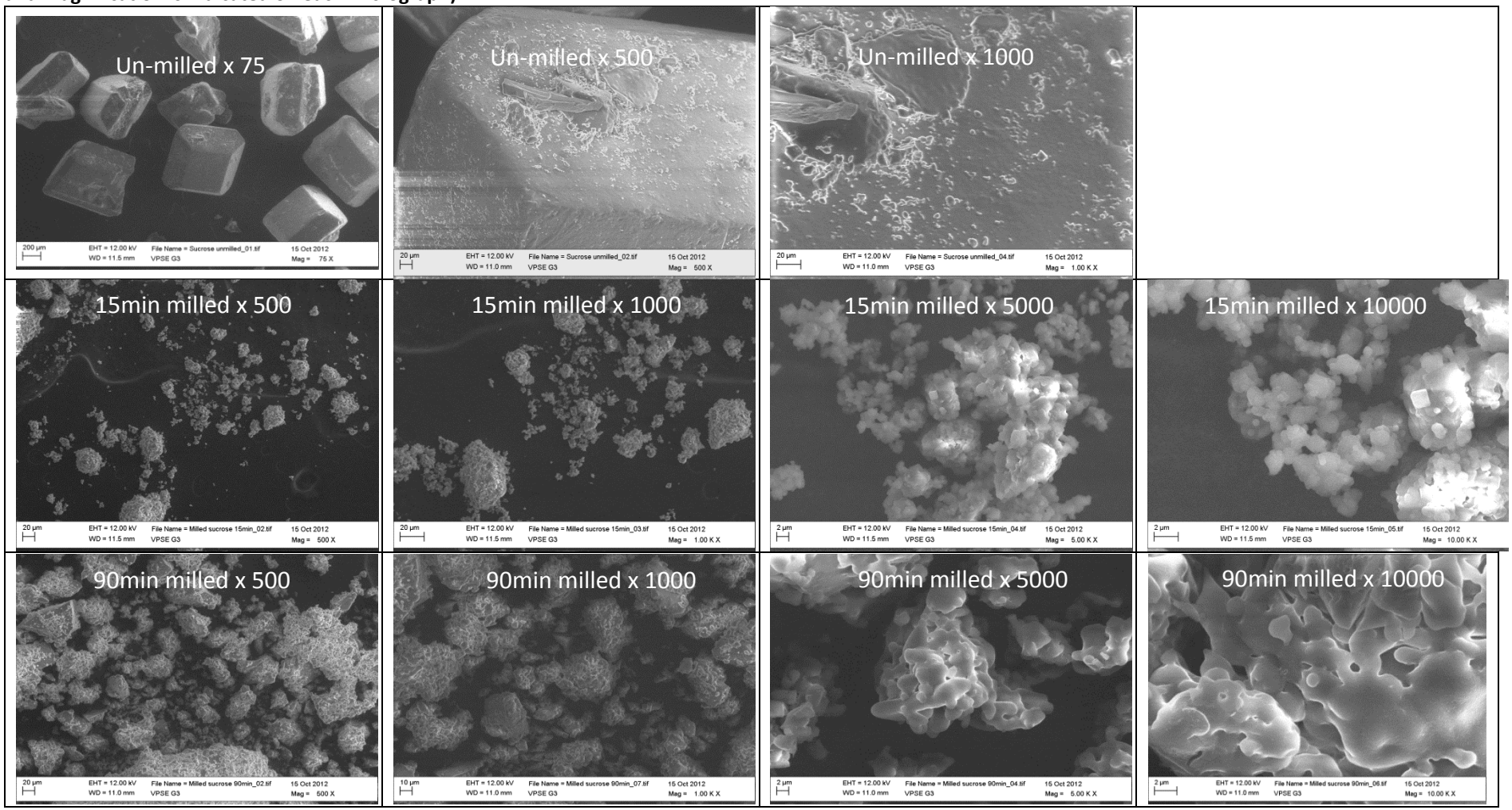

Appendix III

SEM micrographs of un- milled and various milled samples of Trehalose dihydrate. Each row shows the micrographs of same sample at different magnifications (the milling time and magnification is indicated on each micrograph).

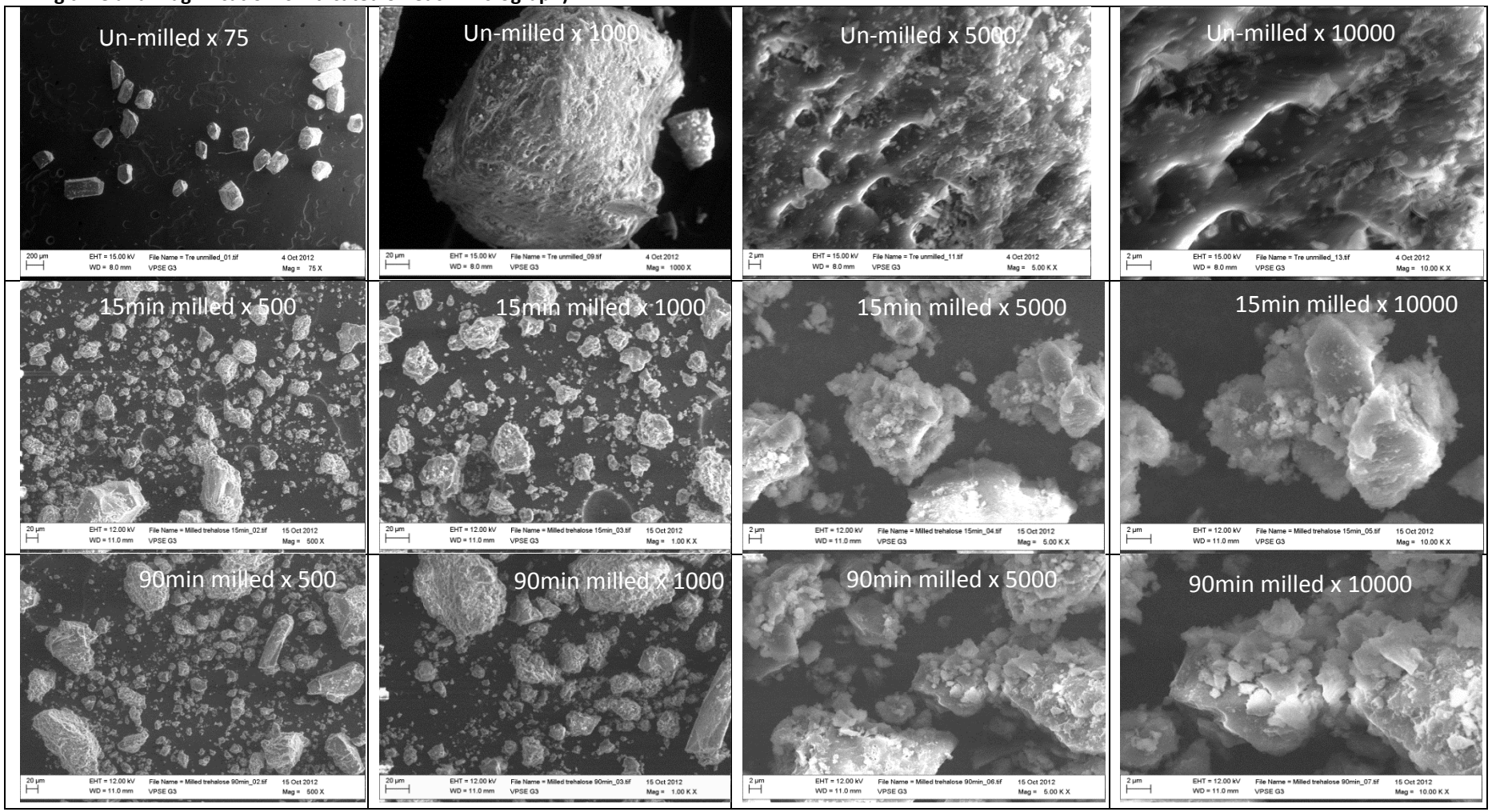

Appendix IV

Comparison of the dielectric properties of un-milled and milled samples of three sugars (sucrose, lactose monohydrate and trehalose dihydrate) around the percolation peak (measured by BDS Solartron instrument). The left Y-axis represents log frequency in Hz, while the unit of temperature is °C.

Milling time	Sucrose	Lactose monohydrate	Trehalose dihydrate
0min	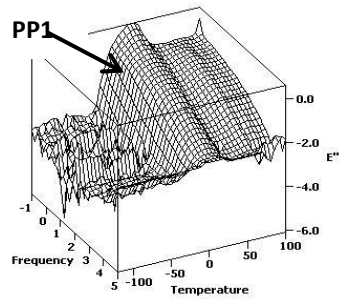	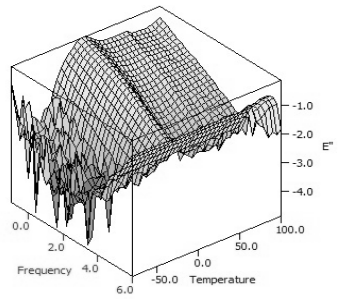	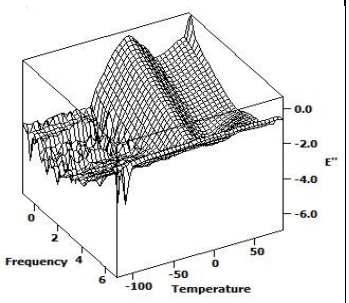
	Single broad PP at 5°C No sub T_g process (crystalline)	Single broad PP at 5°C No sub T_g process (crystalline)	Single broad PP at 10°C No sub T_g process (crystalline)
15min	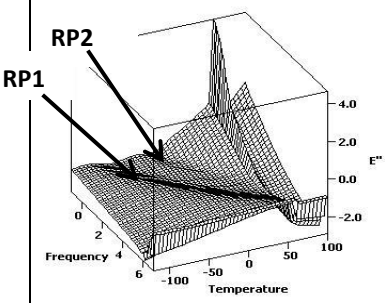	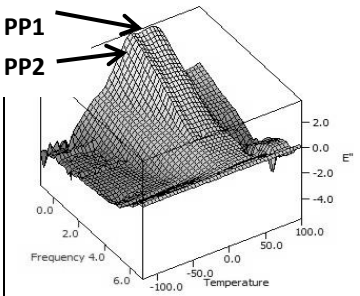	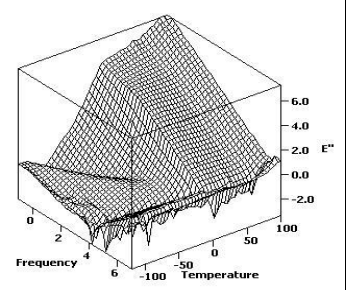
	No percolation Low temp.RP 1 & 2 appear a sharp peak at 60°C	Percolation splits into two peaks (at 5°C & at 30°C) Both have a huge amplitude	Huge PP at 5°C itsmerges with conductivity RP 1 towards low temp.
30min	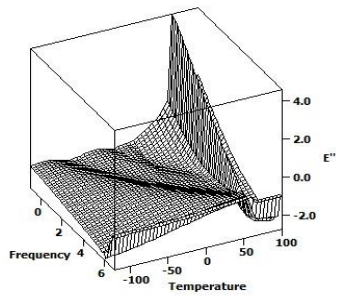	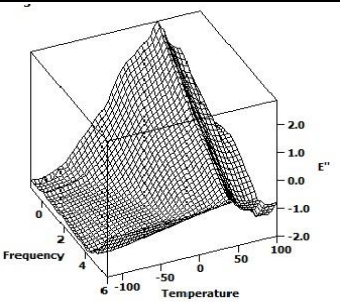	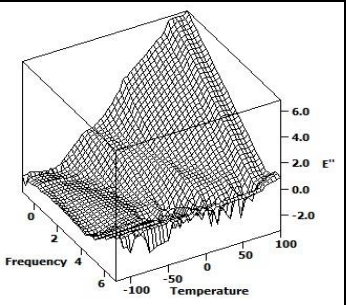
	RP 1 & 2 more prominent sharp peak shifts at 65°C	PP1 with Huge amplitude sharp and its shoulders grow On both sides	PP merge with conducttivity wing Another process in low temperature region

PP – Percolation peak, RP - Relaxation process; RP1 – γ process, RP2 - β process, structural relaxation α process

Milling time	Sucrose	Lactose monohydrate	Trehalose dihydrate
45min	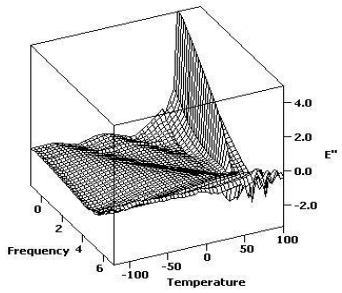	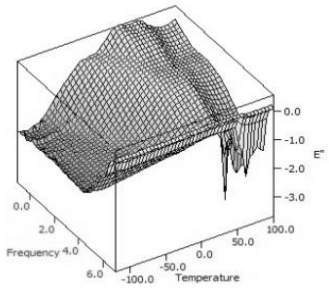	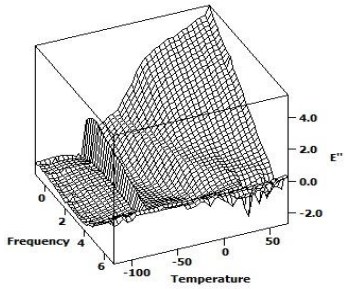
	RP 1 & 2 more prominent sharp peak persists at 65°C	Shoulders around percolation more prominent, with low magnitude	Merged PP & conducttivity wing Low temp. process again present
90min	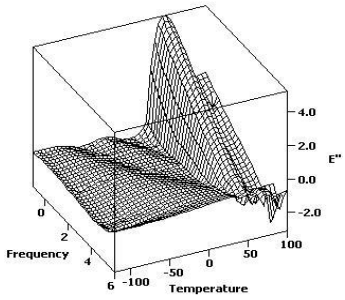	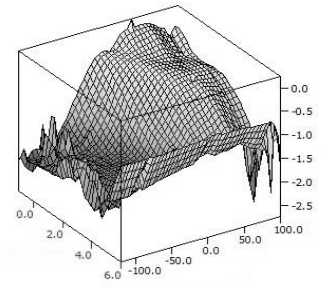	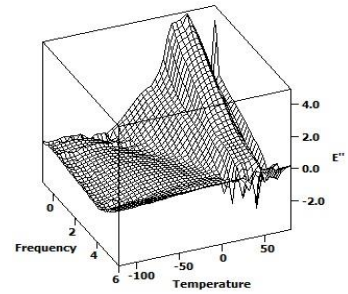
	RP 1 & 2 more prominent Relatively broad peak at 65°C	Percolation becomes broad and shoulders continue to grow	PP at 30-45°C (recrystallization) RP 1 & 2 appaer as merged broad process
180min	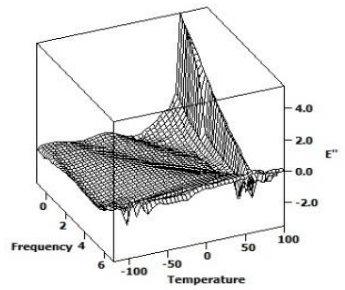	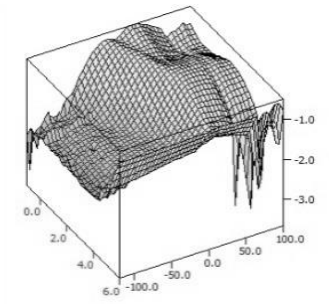	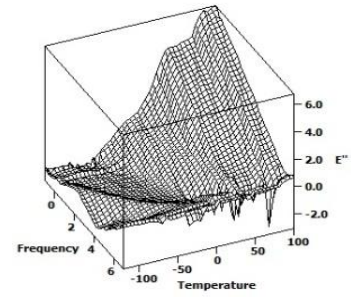
	RP 1 & 2 prominent peak at 70°C again becomes sharp	Spectrum takes the Saddle shape with PP present in the centre	PP & conducttivity wing again start merging

PP – Percolation peak, RP - Relaxation process; RP1 – γ process, RP2 - β process, structural relaxation α process

Appendix V

Overlaid DSC curves of un-milled and milled samples of lactose monohydrate and anhydrous lactose showing the peaks of de-vitrification, desorption of water and melting from left to right of the curves in sequence.

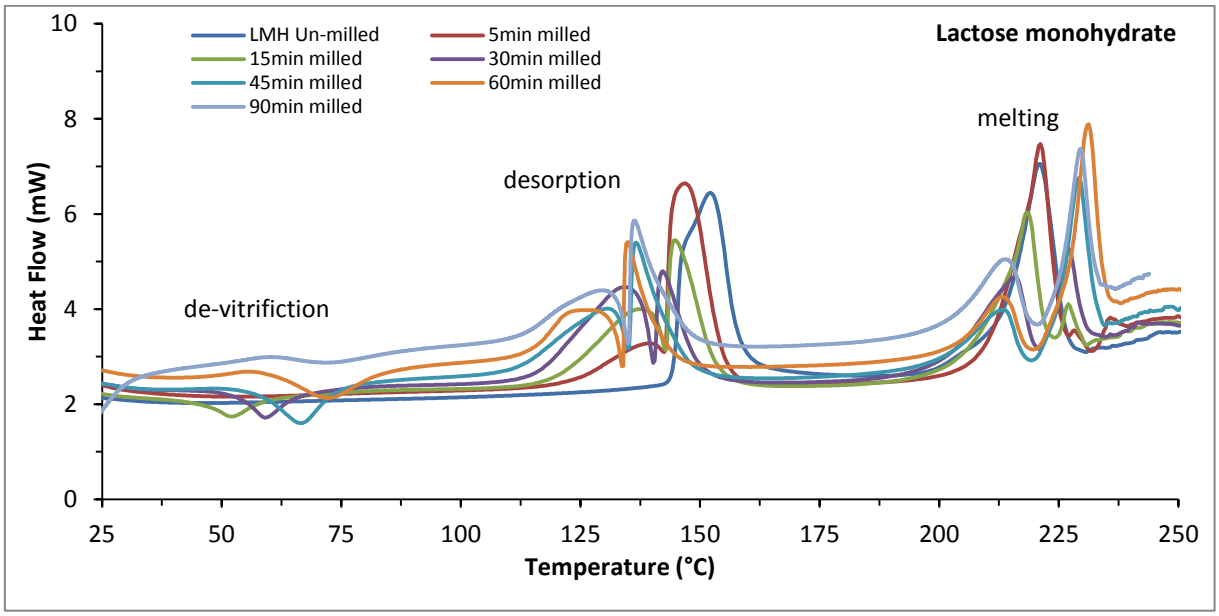

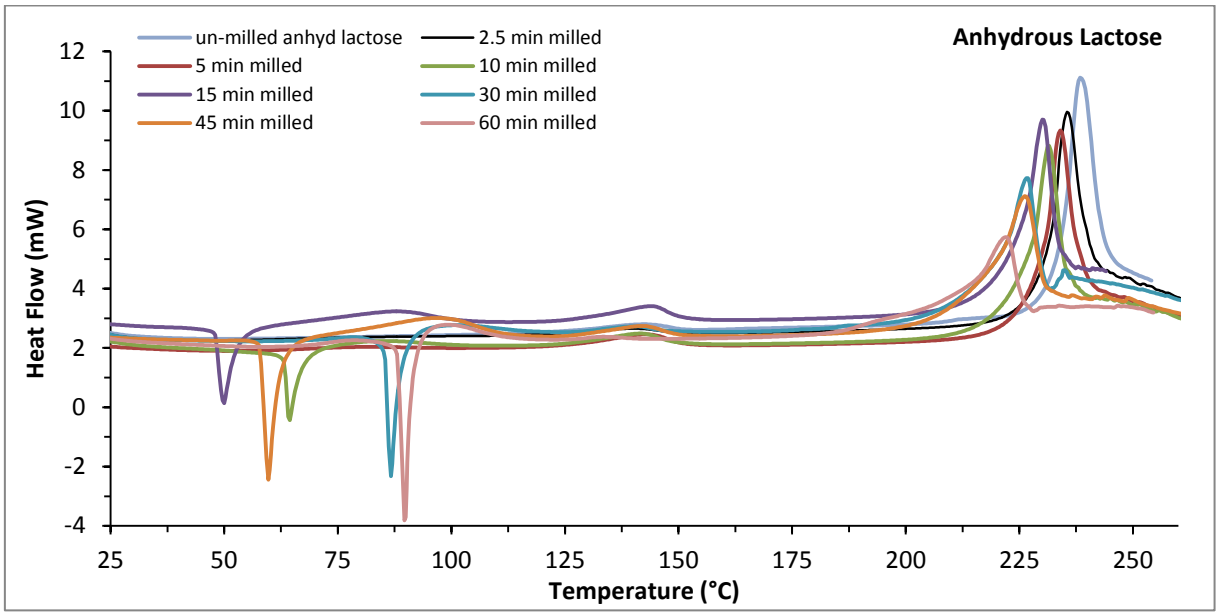

Appendix VI

THz Time domain signals and THz spectra of un-milled samples of lactose monohydrate, anhydrous lactose and Ibuprofen. The arrow heads show the characteristic peaks.

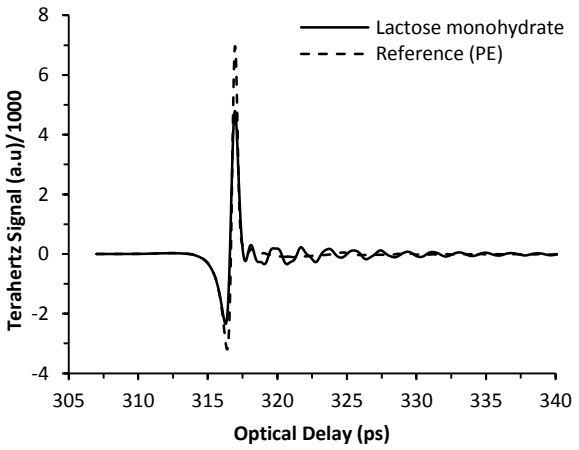

Time domain signal of LMH

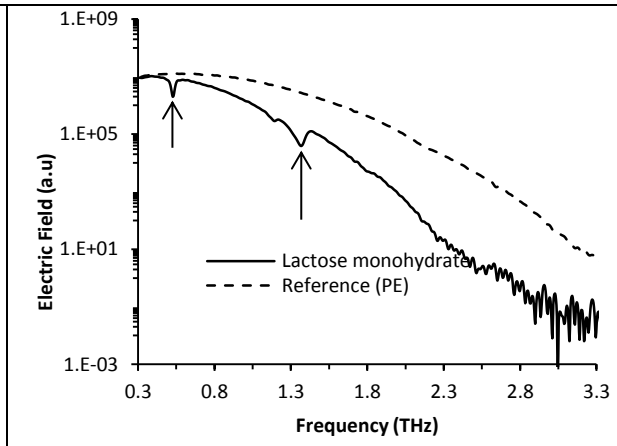

Sample spectrum of LMH

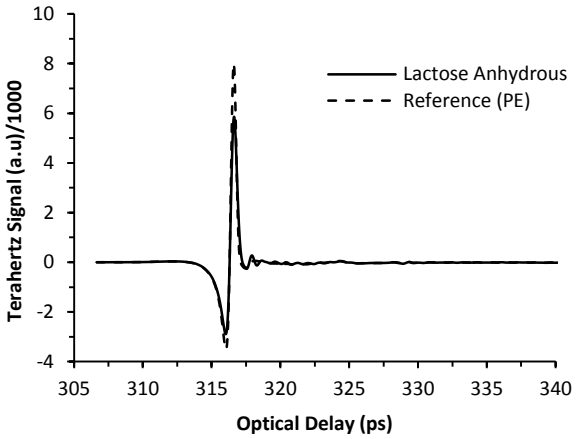

Time domain signal anhydrous lactose

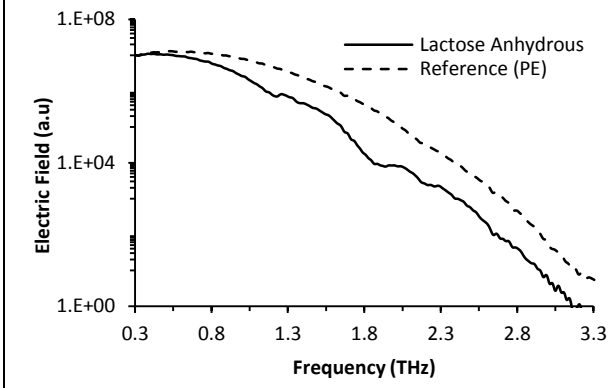

Sample spectrum anhydrous lactose

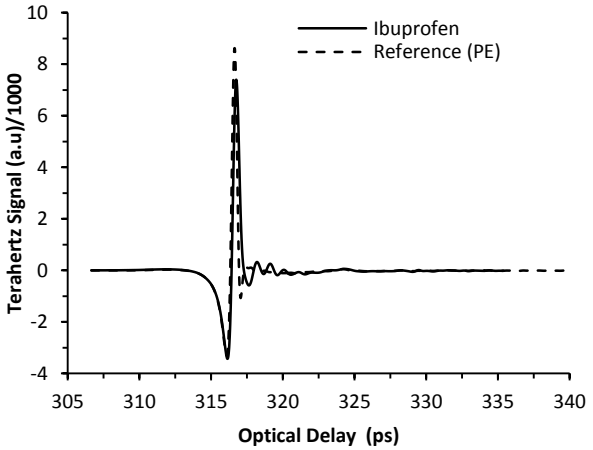

Time domain signal ibuprofen

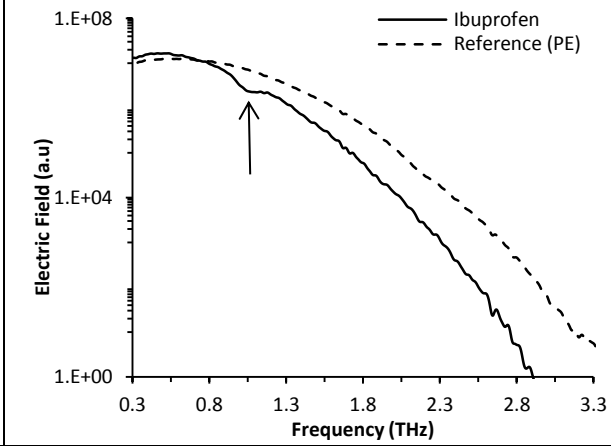

Sample spectrum ibuprofen

Appendix VII

Overlaid THz spectra of un-milled and milled samples of lactose monohydrate, anhydrous lactose and ibuprofen showing the changes in scattering and heights of the principal peaks with milling time.

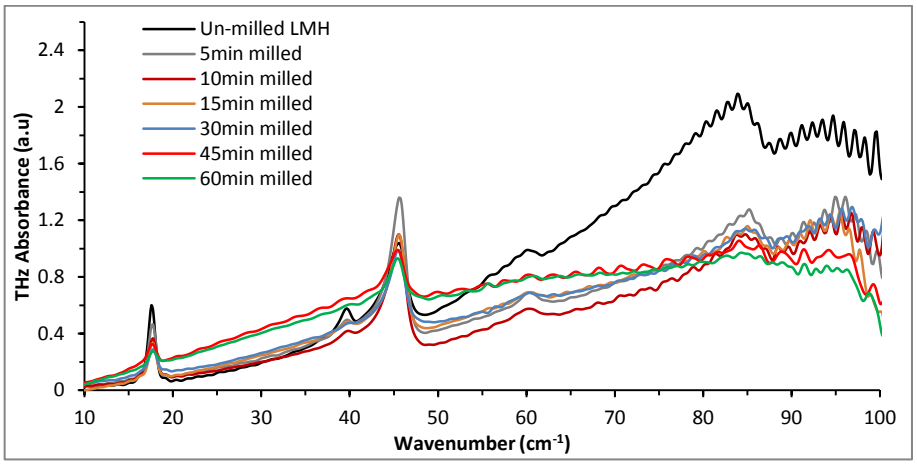

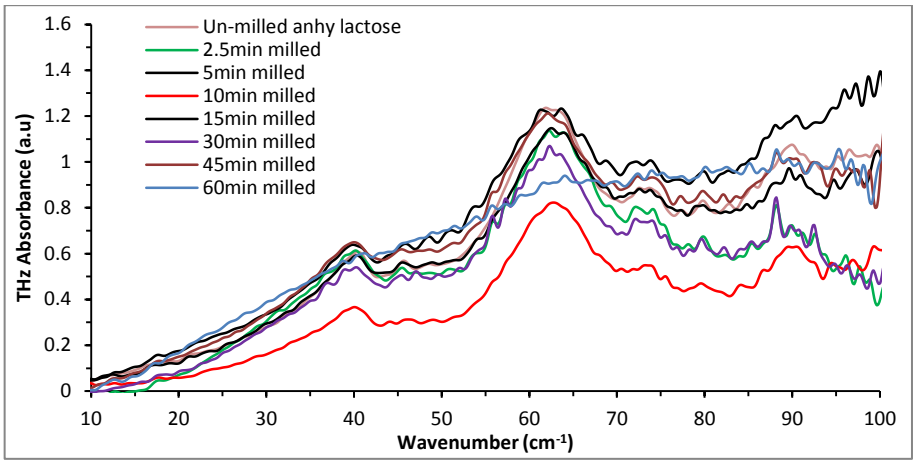

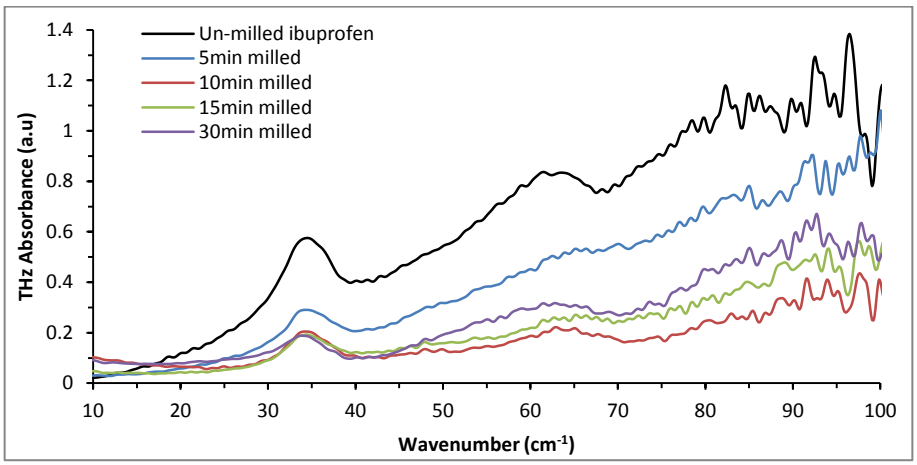

Appendix VIII

3D dielectric loss spectra of a) un-milled and b) 5min, c) 10min, d) 15min, e) 30min, f) 45min and g) 60min milled samples of anhydrous lactose showing the plots of imaginary permittivity against temperature and frequency.(measured by BDS Novocontrol Alpha-Analyser). The left Y-axis represents log frequency in Hz, while the unit of temperature is °C.

<table>
<tr><td> 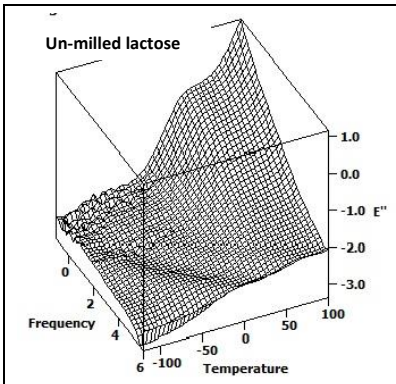
</td><td> 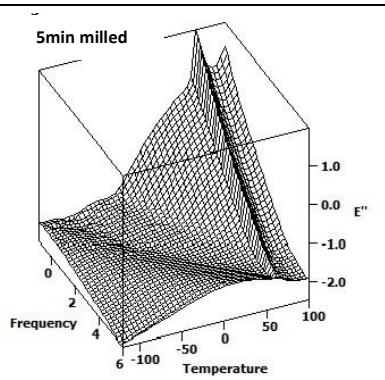
</td><td> 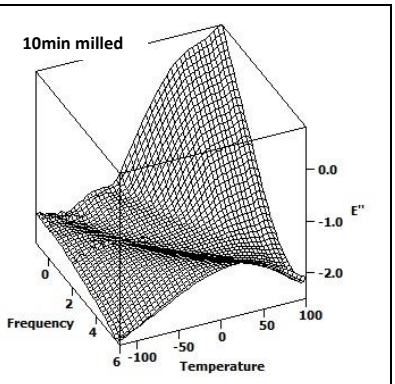
</td></tr>
<tr><td>a</td><td>b</td><td>c</td></tr>
<tr><td> 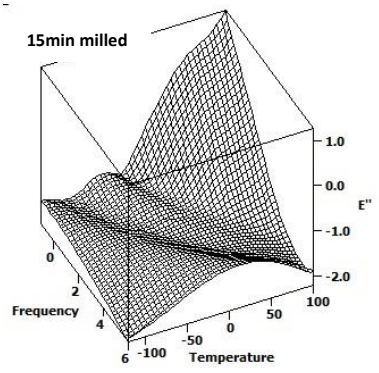
</td><td> 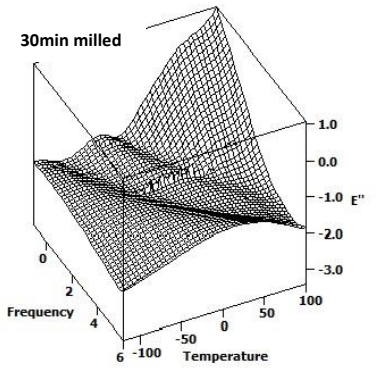
</td><td> 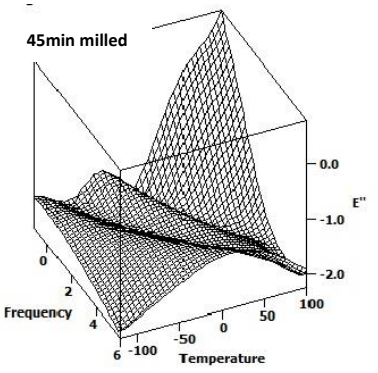
</td></tr>
<tr><td>d</td><td>e</td><td>f</td></tr>
<tr><td> 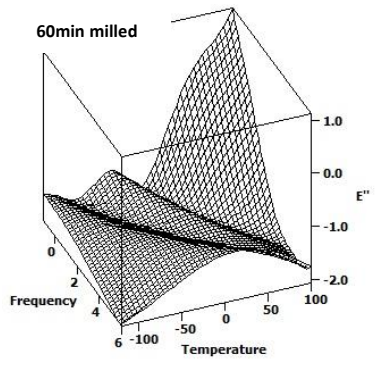
</td><td colspan="2"></td></tr>
<tr><td>g</td><td colspan="2"></td></tr>
</table>

Appendix IX

3D dielectric loss spectra of a) un-milled and b) 2.5min, c) 5min, d) 7.5min, e) 10min, f) 15min, g) 30min, h) 45min and i) 60min milled samples of Sucrose showing the plots of imaginary permittivity against temperature and frequency.(measured by BDS Novocontrol Alpha-Analyser). The left Y-axis represents log frequency in Hz, while the unit of temperature is °C.

<table>
<tr><td> 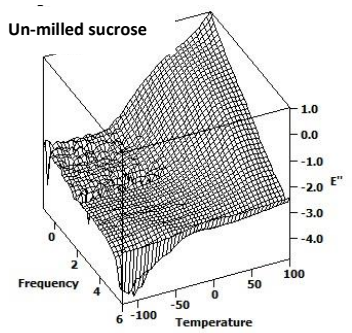
</td><td> 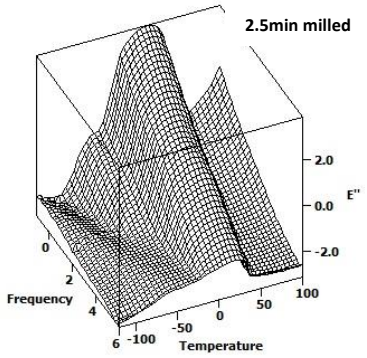
</td><td> 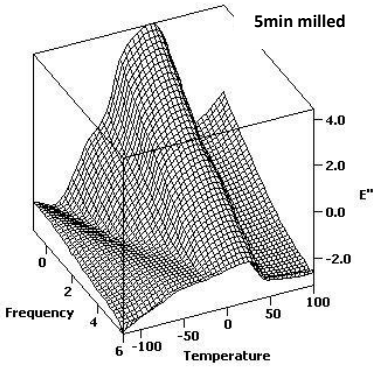
</td></tr>
<tr><td>a</td><td>b</td><td>c</td></tr>
<tr><td> 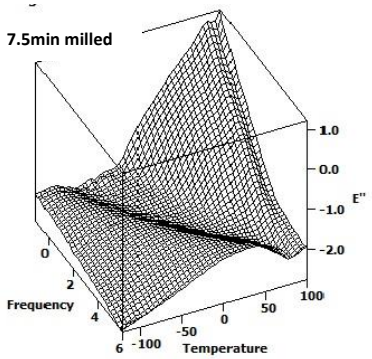
</td><td> 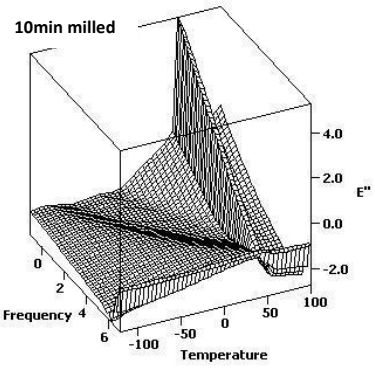
</td><td> 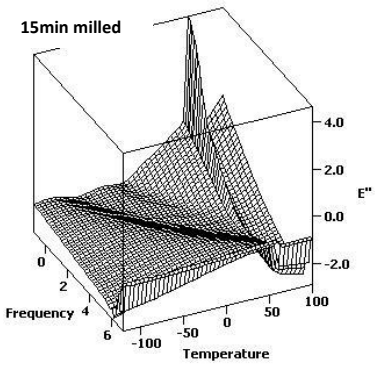
</td></tr>
<tr><td>d</td><td>e</td><td>f</td></tr>
<tr><td> 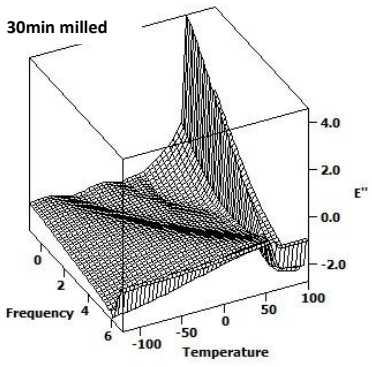
</td><td> 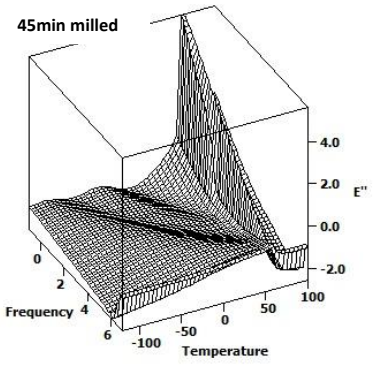
</td><td> 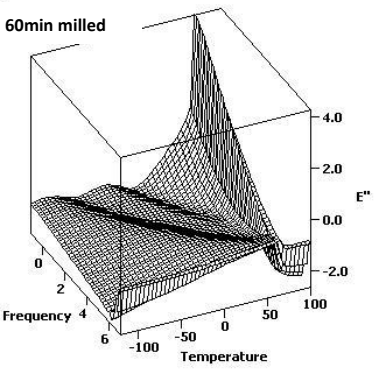
</td></tr>
<tr><td>g</td><td>h</td><td>i</td></tr>
</table>

Appendix X

Surface Percolation of Protons A Probe For The Creation of Crystal Defects In Lactose Monohydrate Following Short Time Milling

dmu.ac.uk DE MONTFORT UNIVERSITY LEICESTER

Amjad Hussain[1], I. Ermolina [1], N.I.Bukhari[2], G. Smith[1]

1 Leicester School of Pharmacy, De Montfort University, Leicester. LE1 9BH, UK.

2 University College of Pharmacy, University of the Punjab, Lahore,54000, Pakistan

APS UK PharmSci 2012, East Midland Conference Centre, University of Nottingham UK, 12 - 14 September 2012

AIM

The aim of this work is to exploit the observation of percolation processes (by broad band dielectric spectroscopy) to probe the creation of crystal defects in lactose monohydrate following short milling times.

INTRODUCTION

According to Griffith theory solid particles have structural weaknesses (flaws) that may develop into cracks under strain. The theory of milling states that the size reduction occurs through crack propagation [Lachman]. The mechanism(s) responsible for size reduction in a ball mill may include compression, attrition and impact When a crystalline solid is exposed to stress, it first deforms elastically according to Hooke's law and beyond a yield point, the elastic limit is exceeded and the solid deforms plastically and finally, at fracture point the the crystal breaks. A crystalline material usually fractures along the crystal cleavage planes while the amorphous material fractures at random.

MATERIALS AND METHODS

Lactose monohydrate (EP) was used in this study. The sieved sample (with size between 150 and 180 µm) was ball milled for various time intervals (15, 30 and 45min at 40% RH) and thermal analysis was performed using TGA and DSC after each stage of milling. Dielectric measurements were also taken immediately post milling using a Solartron 1296/1255 dielectric spectrometer across the frequency range 0.1-10^6 Hz at discrete temperatures from −80 to 100 ° C at 5° C increments (the chamber of the cryostat was maintained at 0% RH during the measurement).

RESULTS

Images from scanning electron microscopy (SEM), showed that the breakdown of crystals during milling occurs in stages, firstly, the fault lines appear on the surface of particles which are afterwards converted to cracks and then the particles break along these cracks into smaller fragments (Figure 1).

The dielectric properties for the pre-milled sample, in the frequency and temperature domains has a simple response surface with a single percolation peak (which has been ascribed previously to the percolation of protons in the hydration surface of the particles) (see Fig. 2 Arrow marked 'A'). At 15 min of milling (and beyond) a second percolation peak appears (see Fig. 2 Arrow marked 'B') at higher temperatures than the original.

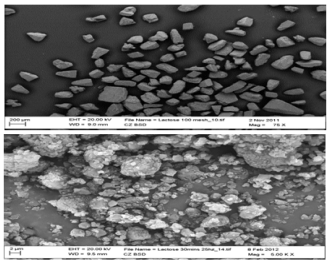

Figure 1 *SEM for un-milled and 30min milled sample showing cracks and fissures.*

At this time point, both peaks are significantly higher than that for pre-milled sample (Figure 2), presumably because water, which is released on disrupting the α-lactose monohydrate, now adsorbs onto the partially amorphized surfaces of fractured particles.

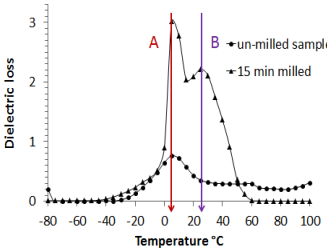

Figure 2 *Dielectric loss (at 1000 Hz) of lactose against temperature after 15 min milling*

Table 1 *Percolation temperature in different milled samples. The second percolation peak is absent in the un-milled sample, and only appears after 15-45 milling, but then disappears in the 90 min milled material*

Sample	Percolation temperature	
	1st	2nd
Un- milled LMH	5°C	-
15 min milled	5°C	30°C
45 min milled	25°C	50°C
90 min milled	35°C	-

In effect, the increased water content increases, dramatically, both the number and size of percolation induced dipoles. At 45 min, the magnitude of the percolation process has reduced again (data not shown) presumably because the high temperature of the mill has driven off much of the surface water in the sample. Both percolation peak temperatures increase up to 90 min of milling but whereas the first peak decreases thereafter, as the milling time extends beyond 90 min, the second percolation process disappears (See Table 1). This observation is co-incident with the observation that the particles are close to reaching their limiting size of 100 nm.

DISCUSSION

An increase in percolation temperature suggests an effective increase in the scale length of the percolation path (Gorbatschow, Arndt et al. 1996). It follows that the observation of the second percolation peak might be ascribed to one of two mechanisms:

(i) The creation of (more tortuous) internal paths for proton conduction that result from the creation of nano-scale defects in the crystal lattice and/or micro-scale defects such as fissures within individual particles (these are observable in SEM images at short milling times).

(ii) Milling is known to produce both an amorphous surface phase while converting a proportion of α-lactose to β-lactose (Shariare, de Matas et al. 2011). It might be the case that the effective scale length of the percolation path increases as the protons are forced to migrate through the amorphous surface domains in order to reach the grain boundaries of the particles. Given that the second percolation peak effectively disappears once the particles have been reduced to a certain limiting size, we might suggest that the origin of second percolation peak can be ascribed to mechanism (1), i.e. the creation of micron-scale defects.

CONCLUSION

Aside from the obvious increase in surface area, and hence increased dissolution rate that results from size reduction, this data presents evidence for the creation of additional contributing factors, such as defects in the crystal lattice of lactose which are manifest in the formation of amorphous surface phase and fissures within particles.

REFERENCES

[1] Gorbatschow, W., M. Arndt, et al. (1996). "Dynamics of H-bonded liquids confined to nanopores." EPL (Europhysics Letters) **35**: 719.

[2] Shariare, M. H., M. de Matas, et al. (2011). "The impact of material attributes and process parameters on the micronisation of lactose monohydrate." International Journal of Pharmaceutics **408**(1-2): 58-66.

PHARMACEUTICAL TECHNOLOGIES

Leicester School of Pharmacy

Appendix XI

A Study of The Amorphization of Lactose Monohydrate following extended Time milling

dmu.ac.uk DE MONTFORT UNIVERSITY LEICESTER

Amjad Hussain[1], I. Ermolina [1], N.I.Bukhari[2], G. Smith[1]

1 Leicester School of Pharmacy, De Montfort University, Leicester. LE1 9BH, UK.

2 University College of Pharmacy, University of the Punjab, Lahore, 54000, Pakistan

APS UK PharmSci 2012, East Midland Conference Centre, University of Nottingham UK, 12 - 14 September 2012

INTRODUCTION

Milling is known to produce both an amorphous surface phase while converting a proportion of α-lactose to β-lactose (Shariare, de Matas et al. 2011). In order to get the benefit of amorphous domain in term of solubility advantage this phase must be stabilized. For the stabilization of this amorphous surface domain we need to understand the structural or molecular dynamics or this phase and by quantification of this surface we can determine the extent to which system could be stabilized. Also the extent to which this amorphous phase convert back i.e. recrystallizes is the indicator of stability. Dielectric spectroscopy is one of the most useful technique for studying the molecular dynamics.

The aim of this work is to study the amorphous domains in milled α-lactose monohydrate.

MATERIALS AND METHODS

Lactose monohydrate (EP) was used in this study. The sieved sample (with size between 150 and 180 µm) was ball milled for extended time intervals (90, 180, 270 and 360 min) and thermal analysis was performed using TGA and DSC after each stage of milling. Dielectric measurements were undertaken in a Solartron 1296/1255 dielectric spectrometer across the frequency range 0.1-10^6 Hz at discrete temperatures from −80 to 100 ° C at 5 ° C increments.

RESULTS AND DISCUSSION

The dielectric response surface in the frequency and temperature domains for the pre-milled sample (data not shown) has a simple response surface with a single percolation peak (which has been ascribed previously to the percolation of protons in the hydration surface of the particles).

The creation of an amorphous phase is supported by the observations of a new dielectric relaxation that appears on the low temperature side of the original percolation peak (for the 45 min to 360 min samples). This dielectric relaxation process becomes more pronounced as the milling time increases, which is consistent with data obtained from TGA and DSC which show a progressive increase in amorphous content on increasing the milling time up to 180 min.

The dielectric relaxation within the amorphous component takes on a saddle-shape (See Figure 1) characteristic of that observed for ice-like water clusters in porous silica (Gutina, Antropova et al. 2003).

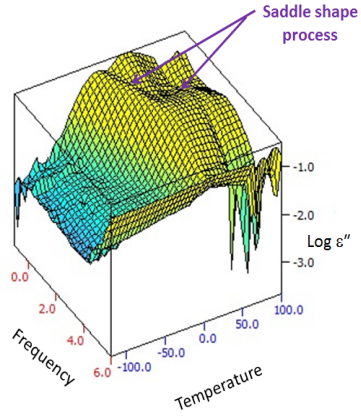

Figure 1: *Dielectric loss spectrum of 180min milled lactose monohydrate against temperature and frequency*

We hypothesize that the saddle shape could have been developed in the dielectric spectrum due to either of these processes

i. Confinement of amorphous phase within thin domains on the surface of particles OR

ii. Confinement of small water molecules in nano-porous structure of disordered lactose monohydrate.

If this saddle shape in dielectric loss spectrum is because of an amorphous phase, then the characterization of this phase present in milled sample need to be checked by conventional techniques. The amorphous phase and moisture content of this phase was determined from TGA data and by applying Gordon-Taylor equation (shown below) the value of glass transition temperature (T_g) was predicted as 43 ° C (see Table 1).

$$T_g = \frac{w1Tg1 + Kw2Tg2}{w1 + kw2}$$

Table 1 *Calculated values of glass transition temperature for milled LMH applying Gordon-Taylor equation*

Sample	Calculated T_g
90min milled	38.39
180min milled	43.08
360min milled	92.78

Now if this amorphous phase is uniformly distributed over the surface of crystalline particles in the form of thin layer, from the limiting size of these particles (measured from SEM), the thickness of this amorphous sub-surface was calculated as ~4nm. This scale length at the surface is similar to the confinement effect previously seen for polymeric glasses at scale length of tens of nanometers (Liu, Siegel et al. 2010. The T_g for this confined phase was predicted (T_g = -9° C) from the Arrhenius plot of the dielectric relaxation time by taking the value of temperature where the 'τ' equals to 100 sec. However, the measured value of glass transition from DSC (47 ° C) was close to that predicted from Gordon-Taylor equation. This implies that amorphous phase in the milled material is bulk rather than confined. So our second hypothesis about the development of saddle shape could be true and these are the small molecules of water that are confined into nano-porous structure of milled lactose monohydrate.

CONCLUSION

The molecular dynamics of lactose monohydrate on ball milling for extending times, showed a saddle shape process in dielectric loss spectra. This was due to structured water *confined* in nano-porous network in milled material. This was further checked by performing dielectric experiment on aged material stored at room conditions for few days after milling, and we observed no such process.

ACKNOWLEDGMENTS

The authors would like to thank Evgeny Polygalov for his help in applying data analysis software.

REFERENCES

[1] Shariare, M. H., M. de Matas, et al. (2011). "The impact of material attributes and process parameters on the micronisation of lactose monohydrate." International Journal of Pharmaceutics **408**(1-2): 58-66.

[2] Gutina, A., T. Antropova, et al. (2003). "Dielectric relaxation in porous glasses." Microporous and mesoporous materials **58**(3): 237-254.

[3] Liu, T., R. W. Siegel, et al. (2010). "The effect of confinement in nanoporous polymers on the glass transition temperature." Polymer **51**(2): 540-546.

PHARMACEUTICAL TECHNOLOGIES

Leicester School of Pharmacy

Appendix XII

Milling and Co-milling with various Excipients for the Improvement of Intrinsic Dissolution Rate of Ibuprofen

dmu.ac.uk DE MONTFORT UNIVERSITY LEICESTER

Amjad Hussain[1], I. Ermolina [1], N.I.Bukhari[2], K. A.Khan[1] G. Smith[1]

1 Leicester School of Pharmacy, De Montfort University, Leicester. LE1 9BH, UK.

2 University College of Pharmacy, University of the Punjab, Lahore, 54000, Pakistan

APS UK PharmSci 2013, James Watt Conference Centre, Heriot Watt University Edinburgh, Scotland, UK, 2 - 4 September 2013

AIM

The aim of this study was to improve the intrinsic dissolution rate of poor soluble drug ibuprofen.

INTRODUCTION

Milling is used to improve the dissolution rate of drugs, but it is counter-productive when milling of poor soluble drugs as the newly created surfaces are hydrophobic and have poor wettability. It means that the newly created surfaces need to be hydrophilized to improve dissolution rate with the addition of hydrophilic polymers during milling process (Rasenack and Müller 2004). This process has been called co-milling.

Ibuprofen is a poorly water soluble drug and co-milling with different hydrophilic excipients is one technique that can be employed for the improvement of solubility and dissolution rate of poorly soluble drugs (Garg et al., 2009). Soluplus® is a relatively new solubilizer which has widely been used in making solid dispersion for the improvement of dissolution rate of poorly soluble drugs (Djuric and Kolter, 2010).

MATERIALS AND METHODS

Ibuprofen and excipients (Soluplus®, HPMC, PVP, Avicel-102) in ratios of 1:1 were co-milled in a planetary ball mill. The mill was run at 25Hz for 15min. The co-milled mixtures were pressed into compacts by a 10 tons hydraulic press and coated with hard paraffin wax to cover all sides except one surface by pouring the molten wax into a cylindrical plastic mould in which compacts were placed on glass slides (Figure 1). The wax plugged compacts were attached to the basket holder of the EU dissolution apparatus and dissolution was performed in buffer solution (pH 7.4) at 37±0.4° C with the basket rotating at a speed of 50rpm. The intrinsic dissolution rate (IDR) was determined spectrophotometrically at 264 nm

Figure 1: Drug compact embedded in wax plug, exposing only one surface to dissolution medium.

RESULTS AND DISCUSSION

The observations made during intrinsic dissolution test revealed that the wax plug of hard paraffin used for embedding the tablet withstand the temperature and operating conditions (effect of medium and stirring) of the test as determined from the change in weight of same size wax plug without tablet added in dissolution medium and subjected to similar conditions . Also the dissolution medium drawn after different intervals gave absorbance almost equal to that of blank. So the interference by wax was negligible.

The change in the surface of exposed part of tablet during dissolution test was photographed by stereo zoom microscope as shown in Figure 2. It his clearly visible that tablet surface which was smooth before the test, erodes gradually and pits are formed on surface of tablet.

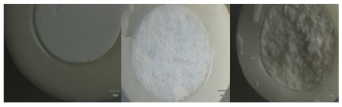

Figure 2: Pictures of wax embedded compacts taken during dissolution showing surface eroded by the dissolution medium.

The IDR of the un-milled ibuprofen compact was 0.08 mg/cm^2/min which increased to 0.30 mg/cm^2/min for the milled drug. The co-milled formulations with soluplus, HPMC, PVP and Avicel-102 gave apparent intrinsic dissolution rates of 0.26, 0.47, 0.06 and 0.14 mg/cm^2/min, respectively (Figure 3). The IDR was relatively slow for the co-milled formulations with PVP and Avicel-102 and similar to that for the un-milled drug, suggesting that a gelation effect (i.e. increased viscosity) may be retarding the release of drug. On the other hand it was high for the milled drug and even higher for the co-milled formulation with HPMC. These were probably due to increased surface area of the drug on milling and swelling and erosion action of HPMC (this was visible in micrograph pictures, Figure 2). The co-milled formulation with soluplus® appeared to have the fastest IDR with gradient of 0.58 in first 45min of dissolution which slow down afterward. The enhanced IDR is probably due in part to the of solubilization action of soluplus® (increasing the solubility of ibuprofen) and partly a consequence of the presence of micelles which scatter light at 260 nm.

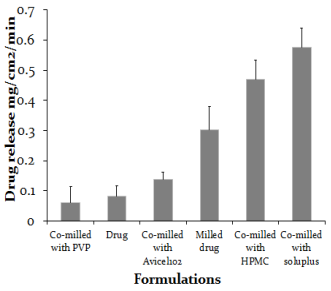

Figure 3: Drug release gradient per cm^2 for un-milled, milled drug and different co-milled formulations (n = 3) the error bars describes ± SD.

CONCLUSION

It is clear that by co-milling with HPMC it is possible to significantly increased the intrinsic dissolution rate of ibuprofen (i.e. 50% improvement over the milled drug alone). However, the apparent increase in IDR with Soluplus® requires further study by HPLC in order to establish whether this is in fact a real increase in solubility or simply the impact of micellar structures making a net contribution to the scattering of light at 260 nm.

ACKNOWLEDGEMENT

The author would like to acknowledge, University of the Punjab, Lahore, Pakistan for providing me lab facilities and funding my research project.

REFERENCES

1- Rasenack, N. and B. W. Müller (2004). "Micron-size drug particles: Common and novel micronization techniques." *Pharm. Dev. Technol*(9): 1-13.

2- Djuric, D. & Kolter, K. Bioavailability enhancement of fenofibrate and itraconazole by forming solid solutions with an innovative amphiphilic copolymer. *APV World Meeting*, 2010.

3- Garg, A., Singh, S., Rao, V., Bindu, K. & Balasubramaniam, J. 2009. Solid state interaction of raloxifene HCl with different hydrophilic carriers during co-grinding and its effect on dissolution rate. *Drug Development and Industrial Pharmacy,* 35, 455-470.

PHARMACEUTICAL TECHNOLOGIES

Leicester School of Pharmacy

Appendix XIII

Quantification of Residual Crystallinity of ball milled anhydrous lactose using DSC and terahertz spectroscopy

Amjad Hussain[1], N.I.Bukhari[2], G. Smith[1] , I. Ermolina [1]

1 Leicester School of Pharmacy, De Montfort University, Leicester. LE1 9BH, UK.

2 University College of Pharmacy, University of the Punjab, Lahore, 54000, Pakistan

ESTAC-11, August 17 - 21 , 2014, Dipoli Congress Centre, Espoo, Finland

AIM

The aim of this study is to quantify the changes in crystallinity in milled pharmaceuticals using differential scanning calorimetry (DSC) and terahertz pulsed spectroscopy (TPS)

INTRODUCTION

Milling is one of the conventional method in pharmaceutical technology for reduction of particle size and generation of amorphous from crystalline material. DSC is routinely used technique for the quantification of amorphous or residual crystallinity. THz spectroscopy has been used recently for the quantification of crystallinity [1]. Our previous study [2] on lactose monohydrate (LMH) has shown that ball milling has damaged the crystalline structure of LMH. The results of residual crystallinity determined both DSC and THz, showed a monotonic decrease in time. However quantitatively, two DSC methods overestimate the % crystallinity in comparison with the THz results, while the method based on enthalpy of α-lactose agrees with THz results.

In this study, the changes in amount of residual crystallinity on ball milling of anhydrous β-lactose (β-LA) were evaluated by DSC and terahertz pulsed spectroscopy (TPS) and compared with results of LMH.

MATERIALS AND METHODS

Anhydrous lactose was milled in a vibratory ball mill at 18 Hz for different time intervals (5, 15, 30, and 60min). DSC experiments were performed immediately after milling, using Jade DSC (Perkin Elmer, US) for the temperature range of 25 to 250 ° C at the heat flow rate of 20 ° C min^{-1}. The residual crystallinity in milled samples was calculated by

i. Subtracting the enthalpies of melting and devitrification and dividing it by enthalpy of fully crystalline lactose
ii. Enthalpies of devitrification.

The samples for THz measurement were prepared by manually mixing lactose and polyethylene (PE) at room temperature (22° C) and 40%RH. The mixture was pressed into disc shaped pellets in Gamlen tablet press and stored in desiccator until measured in transmission mode by TPS spectra 3000 (TeraView Ltd, UK). Each terahertz spectrum was obtained by averaging 900 scans, with a frequency of 30 per second and a spectral resolution of 1.2 cm^{-1}. The residual crystallinity was estimated either of following methods

i. conventional method based on the estimation of area under absorption peak.
ii. Multivariate method based on partial least square (PLS).

RESULTS AND DISCUSSION

Un-milled anhydrous lactose has shown a single melting endotherm at 237° C (β-lactose) and a tiny, broad endotherm at 140° C as similar to LMH for the desorption of crystalline water. This indicates the presence of small quantity of LMH in anhydrous lactose (Fig. 1). In milled samples, the height of melting peak decreases with milling indicating the decrease in crystallinity. The temperature of this peak also decrease and 60min milled sample shows peak at 217° C (melting of α-lactose), this mutarotation is induced during DSC experiment.

The height of desorption peak increases in early times of milling and decreases afterward (indicating the formation of MH on devitrification). The devitrification peak occurs at variable temperature and its height increase with milling time (Fig.1).

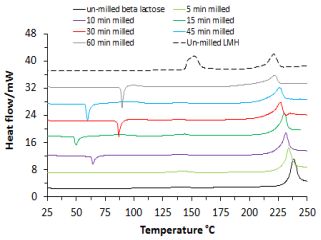

Figure 1. DSC curves of un-milled and milled (for different times) Anhydrous lactose and un-milled LMH.

THz spectrum of un-milled anhydrous lactose has shown three peaks at 39, 45 and 61cm^{-1} wavenumbers (Fig. 2). The peak at 45cm^{-1} represents the LMH, as seen by spectrum of LMH placed on top in Fig. 2, was only present in un-milled and early milled samples. Therefore the increase in LMH as seen in DSC results was only induced by de-vitrification occurring during thermal analysis, not the real effect.

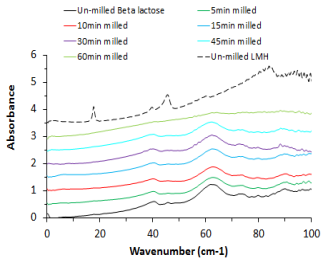

Figure 2. THz spectra milled Anhydrous β-lactose for different times and un-milled LMH.

The spectra of milled anhydrous lactose (Fig. 2) are almost similar to the un-milled one. However, the spectrum of 60min milled sample is almost flat indicating the highest amount of amorphous in this sample. This is supported by the fact that the DSC result of this sample has shown the largest devitrification peak among all milled samples and the melting of alpha form, indicating the conversion of beta to alpha by thermal effect during DSC analysis.

The results of residual crystallinity (summarized in Fig.3) have indicated that, both DSC methods show a monotonic decrease in crystallinity, although method 2, overestimates the residual crystallinity probably because this method is indirect and based on devitrification peak, and the complete devitrification is not possible at this high rate of DSC scan.

Both methods of THz have shown variable results and provide overestimates of residual crystallinity as compared with both DSC methods in milling times till 45min, while there is a rapid loss of further ~50% in next 15min. The higher estimates of residual crystallinity in short milled samples indicates the recrystallization of amorphous during sample preparation for THz measurement, as there were lot of crystallization seeds and the process was triggered by hydrophilic surfaces of PE and compression force applied during pellet preparation. For 60min milled sample there is an increase of amorphous content and reduction of crystallization seeds, therefore we observed a rapid loss in crystallinity in THz experiment which similar to results measured by DSC at long milling time.

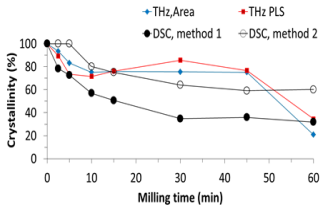

Figure 3. Changes in crystallinity of Anhydrous β-lactose

CONCLUSION

The study shows that DSC is more reliable method for measuring the crystallinity of β-LA after milling than THz, in contrary to our conclusion for LMH, where both techniques produce similar estimates for residual crystallinity on milling.

ACKNOWLEDGEMENT

A. Hussain would like to acknowledge the University of the Punjab, Lahore, Pakistan for funding his research project.

REFERENCES

1. Darkwah, J., et al., Int J. Pharm, 2013. 455(1): p. 357-364.
2. Smith, G., et al., Eur J. Pharm Biopharm, 2014 (submitted).

PHARMACEUTICAL TECHNOLOGIES
Leicester School of Pharmacy

Appendix XIV

Study of Changes in Crystallinity of Ball Milled Mefenamic Acid using Terahertz Pulsed Spectroscopy

Amjad Hussain[2], I. Ermolina [1], N.I.Bukhari[2], G. Smith[1]

1 Leicester School of Pharmacy, De Montfort University, Leicester. LE1 9BH, UK.

2 University College of Pharmacy, University of the Punjab, Lahore, 54000, Pakistan

APS UK PharmSci 2014, Weston Auditorium, Hertfordshire University, Hatfield, UK, 8 - 10 September 2014

AIM

The aim of this study is to quantify the changes in crystallinity in ball-milled mefenamic acid by terahertz pulsed spectroscopy.

INTRODUCTION

Terahertz waves are beyond the far infrared spectrum from 3.3–100 cm^{-1} (which corresponds to the frequency band 0.1–3 THz). The modes generated by THz radiation include low frequency bond vibrations, crystalline phonon vibrations, hydrogen-bonding stretches, torsion vibrations and, in gases, molecular rotations [1]. Terahertz pulsed spectroscopy (TPS) uses a femtosecond time pulses to generate the THz spectrum, and has been used to probe the crystal lattice vibrations as a way of determining the crystallinity of materials, for example amino acids [2]. In this study, TPS was applied to the determination of the reduction in crystallinity of mefenamic acid on ball milling for time period of up to 60 min and milling frequency of 18Hz.

MATERIALS AND METHODS

Mefenamic acid was milled in a vibratory ball mill at 18 Hz for different time intervals (5, 15, 30, and 60min). The samples for THz measurement were mixtures of mefenamic acid and polyethylene (PE) powder, in which the latter acts as a diluent to reduce the absorption of the incident pulse. The powders were blended geometrically to form a homogenous mixture which was then pressed into disc shaped pellets by applying the compaction force of 500 kg in Gamlen tablet press at 22° C and 40%RH.

The terahertz spectra were acquired in transmission mode by a TPS spectra 3000 (TeraView Ltd, UK). Each terahertz spectrum was obtained by averaging 900 scans, with a frequency of 30 per second and a spectral resolution of 1.2 cm^{-1}. The spectra were then analyzed (average of 3 repeat measurements on each of 3 samples, n = 9) by a conventional method based on the estimation of area under absorption peak.

The reference curve for the as-received crystalline material (over the range 4% to 12% of mefenamic acid, in a PE pellet) shows that TPS is a sensitive technique for the measurement of crystallinity of a single component system, with an LOD of ~ 1% and an LOQ of ~ 3%).

RESULTS AND DISCUSSION

The solid state THz spectrum of mefenamic acid shows three absorption peaks at 37, 43 and 73 cm^{-1} . These peaks are related to intermolecular vibrations of the hydrogen bonds in crystalline lattice.

In the case of milled mefenamic acid, the peaks of THz spectra were almost at the same position. There is systematic reduction in the height of peaks during milling. The peak near 43 cm^{-1} quickly (<10min) disappears in all milled samples. At 60 min milling the almost featureless spectrum is observed which corresponds to the amorphous phase (Figure 1).

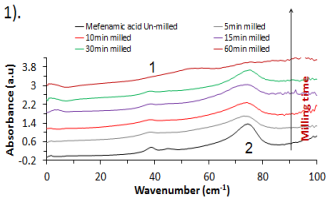

Figure 1: THz spectra of un-milled and mefenamic milled mefenamic acid for different times

The major changes in the shape of THz spectra of the milled mefenamic acid (Figure 2a) are:

i) On milling the weak absorption peak at ~37 cm^{-1} becomes broad and multi component as it contains 2-3 shoulders;

ii) The major peak at ~73 cm^{-1} becomes initially broad in 5 min milled sample and then narrows down with milling time.

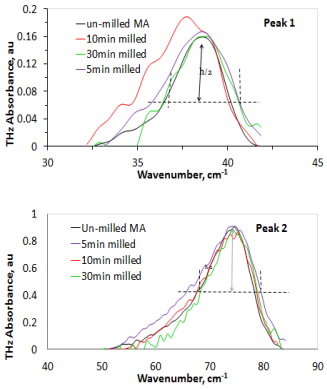

Figure 2: Master plots from THz spectra of mefenamic acid showing the change in shape of peaks 1 & 2 with milling time.

To evaluate the change in shape of peaks, first the baseline was subtracted and then the peaks were normalized to the same height (Fig. 2b). The peak width at the half height was calculated from the normalized graphs of both peaks. The results (Figure 3) indicated that width increases in early minutes of milling and then decrease for both peak 1 and peak 2.

The variation in the shape of peak in milled samples occurs probably due to the presence of the defected crystals.

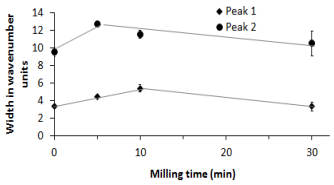

Figure 3: Change in width of half peak as calculated for THz peak1 & 2.

However what is more clear is that the quantitative analysis for the estimation of residual crystallinity based on the area under peak analysis of both peaks (37 cm^{-1} and 73 cm^{-1}) shows that there is biphasic loss in crystallinity of mefenamic acid with milling time. There is an initial loss of ~30% in first 5 min of milling followed by a gradual reduction and its value remains only ~10% in 60min milled sample (Figure 4)..

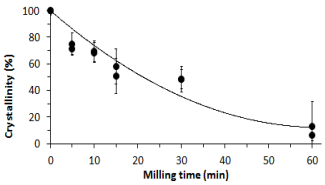

Figure 4: Changes in crystallinity of mefenamic acid with milling time (n = 9) based on the AUC of the THz absorption peak 1 & 2.

CONCLUSION

THz pulsed spectroscopy was used to establish the time dependent reduction in crystallinity on ball milling of mefenamic acid. The study shows that it is possible to achieve almost complete conversion (~ 90%) of the crystalline state to the amorphous form after 60 min of ball milling.

ACKNOWLEDGEMENT

Amjad Hussain would like to acknowledge, University of the Punjab, Lahore, Pakistan for funding my research project.

REFERENCES

1. Strachan, C.J., et al., Chemical Physics Letters, 2004. 390(1): p. 20-24.

2. Darkwah, J., et al., International Journal of Pharmaceutics, 2013. 455(1): p. 357-364.

PHARMACEUTICAL TECHNOLOGIES

Leicester School of Pharmacy